7. SITE 903[1]

Shipboard Scientific Party[2]

HOLE 903A

Date occupied: 18 June 1993

Date departed: 21 June 1993

Time on hole: 3 days, 2 hr, 45 min

Position: 38°56.298′N, 72°49.032′W

Bottom felt (rig floor; m, drill-pipe measurement): 455.5

Distance between rig floor and sea level (m): 11.1

Water depth (drill-pipe measurement from sea level, m): 444.4

Total depth (rig floor; m): 1158.3

Penetration (m): 702.8

Number of cores (including cores with no recovery): 76

Total length of cored section (m): 702.8

Total core recovered (m): 637.77

Core recovery (%): 90.6

Oldest sediment cored:
Depth (mbsf): 702.8
Nature: silty clay to claystone
Age: middle Miocene
Measured velocity (km/s): 1.7

HOLE 903B

Date occupied: 21 June 1993

Date departed: 22 June 1993

Time on hole: 10 hr

Position: 38°56.304′N, 72°49.026′W

Bottom felt (rig floor; m, drill-pipe measurement): 457.5

Distance between rig floor and sea level (m): 11.1

Water depth (drill-pipe measurement from sea level, m): 446.4

Total depth (rig floor; m): 611.5

Penetration (m): 154.0

Number of cores (including cores with no recovery): 17

Total length of cored section (m): 154.0

Total core recovered (m): 149.71

Core recovery (%): 97.2

Oldest sediment cored:
Depth (mbsf): 154.0
Nature: silty clay and clayey silt
Age: Pleistocene
Measured velocity (km/s): 1.51

HOLE 903C

Date occupied: 22 June 1993

Date departed: 30 June 1993

Time on hole: 8 days, 13 hr, 45 min

Position: 38°56.303′N, 72°49.024′W

Bottom felt (rig floor; m, drill-pipe measurement): 457.5

Distance between rig floor and sea level (m): 11.1

Water depth (drill-pipe measurement from sea level, m): 446.4

Total depth (rig floor; m): 1607.2

Penetration (m): 1149.7

Number of cores (including cores with no recovery): 60

Total length of cored section (m): 535.2

Total core recovered (m): 323.16

Core recovery (%): 60.4

Oldest sediment cored:
Depth (mbsf): 1149.7
Nature: porcellanitic chalk
Age: middle Eocene
Measured velocity (km/s): 2.4

Comments: Drilled: 0.0–485.5, 534.6–586.5, and 611.5–688.6 mbsf
Total drilled intervals: 614.5 m

HOLE 903D

Date occupied: 18 July 1993

Date departed: 20 July 1993

Time on hole: 2 days, 9 hr, 15 min

Position: 38°56.299′N, 72°49.042′W

Bottom felt (rig floor; m, drill-pipe measurement): 453.0

Distance between rig floor and sea level (m): 11.7

Water depth (drill-pipe measurement from sea level, m): 441.3

Total depth (rig floor; m): 1490.0

Penetration (m): 1037.0

Number of cores (including cores with no recovery): 25

Total length of cored section (m): 233.1

Total core recovered (m): 163.5

Core recovery (%): 70.1

Oldest sediment cored:
Depth (mbsf): 1037.0
Nature: silty claystone
Age: late Oligocene
Measured velocity (km/s): 1.87

Comments: Returned to Site 903 after Site 906; washed and drilled 0.0–774.9 and 948–977 mbsf

[1] Mountain, G.S., Miller, K.G., Blum, P., et al., 1994. *Proc. ODP, Init. Repts.*, 150: College Station, TX (Ocean Drilling Program).

[2] Shipboard Scientific Party is as given in the list of participants preceding the Table of Contents.

Principal results: Site 903 (proposed Site MAT11) was drilled in ~445 m of water on the upper continental slope offshore New Jersey, 4.4 km (2.4 nmi) upslope of Site 902. Site 903 is the shallowest of four sites on a slope transect (Sites 902–904 and 906) designed to sample post-lower Eocene sequence boundaries traced on *Maurice Ewing* Cruise 9009 (Ew9009) multichannel seismic (MCS) Line 1005 from the adjacent continental shelf. Data from these sites will be used to evaluate the effect of glacioeustatic changes on the stratigraphic record of siliciclastic passive margins.

Site 903 was selected at CDP 9140 on Cruise Ew9009 MCS Line 1005 to provide an especially thick section of lower Miocene strata. Together with Site 904, samples from Site 903 provide good representation of the lower Miocene as well. In contrast, Site 902 provides a thicker section of upper middle Miocene.

Continuous advanced hydraulic piston (APC) coring, with 97% recovery to 169.5 mbsf, sampled Holocene green muds and middle Pleistocene gray sandy silty clay at Hole 903A. We switched to the extended core barrel (XCB) and continuously cored with high recovery (89%) to a total depth of 702.8 mbsf. Excellent logs were obtained with the sonic-induction (74–604 mbsf) and porosity (0–492 mbsf) tools. Hole 903B was cored with the APC, with 97% recovery to 154 mbsf.

Hole 903C obtained spot cores from 506 to 535 mbsf and from 587 to 612 mbsf, recovering intervals lost at Hole 903A. Continuous coring began at 698 mbsf and continued to the total depth of 1149.7 mbsf with 60% recovery. Logs were obtained using the sonic-induction (975–823 mbsf) and the Quad combo tools (868–475 mbsf); hole conditions were not good because of bridges and washouts.

Hole 903D was drilled at the end of Leg 150 to sample the especially critical lower middle Miocene to upper Oligocene interval that was poorly recovered in Hole 903C. Hole 903D was drilled to 775 mbsf; coring from there to TD at 1037 mbsf was much more successful with overall recovery of 70%.

Seven lithostratigraphic units are recognized at Site 903 that can be correlated with similar units at Sites 902, 904, and 906, with the exception of Unit II, which is found only at Site 903. At all sites, the lowermost unit is predominantly carbonate, and the overlying units are predominantly siliciclastic.

Unit I (0–273.9 mbsf), middle to upper Pleistocene silty clay with fine sand layers containing a thick succession of slumps and debris flows below 221.5 mbsf.

Unit II (273.9–358.9 mbsf), middle Pleistocene nannofossil silty clay to 307.5 mbsf and middle Pleistocene and Pliocene sands below this that are glauconitic at the base.

Unit III (358.9–522.9 mbsf), upper and middle Miocene alternations of silty clays and glauconitic sands, distinguished from the unit above by abundant glauconite.

Unit IV (522.9–733.1 mbsf), middle Miocene diatomaceous silty clay to clayey silts with generally lower abundance of glauconite than above. Several slumps, debris flow deposits, and glauconitic sand layers occur in this unit.

Unit V (733.1–974.4 mbsf), lower to middle Miocene glauconitic, diatomaceous, organic-rich silty claystone distinguished from the overlying unit by higher organic content.

Unit VI (974.4–1064.1 mbsf), lowermost Miocene to upper Oligocene silty claystone, distinguished by minor glauconite, common nannofossils, and rare diatoms.

Unit VII (1064.1–1149.7 mbsf), upper Eocene clayey nannofossil chalk.

Integration of magnetic susceptibility, density, and biostratigraphic data provides a remarkably good time scale for the Pleistocene section. Preliminary correlations indicate an apparently continuous section from oxygen isotope stage 5.5 through stage 15.1 (~120–574 ka). Calcareous microfossils occur at irregular intervals in the Pliocene to upper middle Miocene, where biostratigraphic subdivision relies primarily on dinoflagellates and diatoms. Uppermost Pliocene strata appear at 358.9 mbsf (Zone NN15), whereas the first evidence for Miocene strata appears at 363 mbsf. The placement of the upper/middle Miocene boundary is uncertain; foraminiferal evidence indicates that it is as high as 510 mbsf and dinoflagellates as low as 625 mbsf. Nannofossils, diatoms, and dinoflagellates provide excellent control for the lower middle and lower Miocene section. Nannofossils and planktonic foraminifers provide good control on upper Oligocene and upper Eocene strata. Transported benthic foraminifers from the shelf are ubiquitous in the Pleistocene and common in the Miocene, whereas evidence for transport is minimal in Oligocene and Eocene benthic foraminifer assemblages. Eocene to lowermost Oligocene assemblages indicate that the paleodepth was >600 m, shallowing to 200–600 m by the Miocene. Overall shallowing and increased downslope transport of shelf sediment accompanied the seaward progradation of clinoforms observed in seismic profiles.

Determining magnetic stratigraphy at Site 903 is hampered by weak intensities of magnetization. We constructed a provisional magnetostratigraphic framework for the uppermost middle Miocene to Pleistocene at Hole 903A. Magnetization of much of the Miocene and older strata is below the detection limit of 1 mA/m for shipboard analyses of 6-cm^3 discrete samples, but above the limit of 0.1 mA/m for larger volume discrete samples to be analyzed onshore. Therefore, we are optimistic that this section will provide a magnetostratigraphic framework after shore-based studies.

Methane reaches a maximum of 602,020 ppm (60%) at 134.5 mbsf in headspace gas at Site 903. Three separate subsurface hydrocarbon gas maxima are observed. This gas is considered to be primarily biogenic because the elevated concentrations correspond with zones that are relatively enriched in organic carbon and that have generally high C_1/C_2 ratios. However, the possibility of some migrated, thermogenically generated gas contribution to the deepest gassy zone (693–1149.7 mbsf) cannot be ruled out. Minor amounts (127 ppm = ethane, 52 ppm = propane) of thermogenically produced gas are suspected to be associated with the high-salinity interstitial water and subsurface increases in sulfate, which indicate migration of fluids, possibly from local salt diapirs at depth. Organic carbon content averages 0.5% in the Pleistocene sediments. This value is considerably lower than comparable sediments at Site 902 and is probably caused by high sedimentation rates having a dilution effect. In the Miocene, organic carbon values climb to 3.5% and sulfur is in high concentrations (up to 3% ± 0.33%). These characteristics are considered to be caused by high primary productivity that induced suboxia/anoxia in the water column and sediments.

The pore-water profiles of Site 903 are similar to those at the other Leg 150 sites on the continental slope. A steep chloride (salinity) gradient occurs across the Pleistocene/Miocene boundary at Site 903. The increase in salinity is associated with a drop in pH to slightly acidic values (6.6). Several alkalinity and ammonium maxima are associated with organic-rich sediment intervals. The Ca and Mg profiles suggest that diagenetic carbonate minerals are precipitating at the alkalinity maximum.

Six physical properties units are recognized at Site 903 based on correlative trends in wet-bulk density and thermal conductivity. Significant bulk-density shifts are associated with the top of each interval and correlate very well to the predicted depths of reflectors p6 (indigo), m0.5 (Red), m1 (Tuscan), m2 (Yellow-2), m3 (Blue), m4 (Pink-2), and o1 (green-2). Intervals are subdivided by pronounced and repetitive cycles of downward increasing or decreasing average bulk density, which probably represent variations in primary depositional fabric. Additional physical properties measured at Site 903 include sub-bottom temperatures at Site 903A with the ADARA coring shoe and natural gamma-ray emissions in whole sections with the newly installed detector on the multisensor track (MST). A preliminary review indicates both devices obtained useful data; further processing is planned.

Excellent logs were obtained from Hole 903A, and preliminary synthetic seismograms constructed from log data are encouraging. Log quality was much lower at Hole 903C because of deteriorating hole conditions; however, logs obtained across the major lower and middle Miocene sequences provide sufficient log signatures to allow recognition of major sequence boundaries.

The principal result from Site 903 is that sequence boundaries traced seismically from beneath the shelf to the slope have lithostratigraphic significance and can be dated. Precise correlations for some sequence bounda-

ries will require additional shore-based studies, especially to obtain a magnetochronology for weakly magnetized lower upper Miocene and older sediments. Nevertheless, shipboard studies provide excellent correlations for several boundaries:

1. Reflector m2 (Yellow-2) is associated with a reversed magnetozone tentatively correlated to Chron C5Ar and has an age estimate of approximately 12.4 Ma.
2. We precisely dated the reflector m5 (Green) sequence boundary for the first time. This reflector correlates with an interval spanning the boundaries between the middle/lower Miocene (Zones NN4 and NN5). It has an estimated age of 16.2 Ma.
3. At Sites 902 and 903, the reflector m6 (pink-3) sequence boundary separates the lower lower Miocene from the uppermost Oligocene.
4. At Sites 902 and 903, the reflector o1 (green-2) sequence boundary separates uppermost lower Oligocene from uppermost Eocene strata.

BACKGROUND AND OBJECTIVES

Site 903 was drilled on the New Jersey continental slope 4.4 km (2.4 nmi) upslope of Site 902 (Fig. 1). It is located 141 km (77 nmi) east-southeast of Barnegat Inlet, New Jersey. Bathymetric control for this region is provided by near-bottom SeaMARC (Farre and Ryan, 1987), SeaBeam (W. Ryan and D. Twitchell, unpubl. data, 1989), and Hydrosweep data. Site 903 is in 453 m water depth on *JOIDES Resolution* precision depth recorder (PDR) profiles (see Chapter 4, this volume); it is located on *Maurice Ewing* Cruise 9009 (Ew9009) MCS Line 1005 (Figs. 1–2) 2.2 km (1.2 nmi) east-northeast of the thalweg of upper Carteret Canyon on the northeast interfluve of an unnamed slope canyon ("lower Berkeley"). This interfluve is the same as the one drilled at Site 902 (Fig. 1).

The geological background, hydrographic setting, and scientific justification for slope drilling are described in Chapters 1 and 2 (this volume). The complexity of slope stratigraphy (e.g., Poag, Watts, et al., 1987) requires drilling in several locations to assemble a composite section as free from hiatuses as possible.

The primary scientific objectives addressed at Site 903 and other slope sites are (1) to date Oligocene–Holocene "Icehouse" seismic sequences traced from the continental shelf, and (2) to evaluate correlation of these sequence boundaries with glacioeustatic age estimates obtained from the $\delta^{18}O$ record. Our secondary goals are to determine the ages of major Eocene "Doubthouse" unconformities and to test the link between sea-level change and slope failure. Although Site 902 provides the thickest upper middle to upper Miocene section, Site 903 provides the best opportunity to sample lower middle Miocene strata. Sites 903 and 904 provide the best opportunities to sample lower Miocene strata.

Site 903 is located 3 km (1.6 nmi) obliquely downdip of the AMCOR 6021 borehole, a stratigraphic test drilled in 301 m of water to a total depth of 305 mbsf (Hathaway et al., 1976). The entire section sampled at AMCOR 6021 is Pleistocene (Hathaway et al., 1976); the upper 220 m probably correlates with oxygen isotope stage 13 or younger (<about 500 ka), and the bottom of the hole may be as old as stage 15 (<about 600 ka; Groot et al., in press). Although poor recovery (~20%) limits the stratigraphic resolution at AMCOR 6021, these studies show that high sedimentation rates could be expected for the Pleistocene section at Site 903.

Based on Site 902 results and the Ew9009 seismic grid, we developed a revised time-depth relationship for predicting sub-bottom depths of seismic reflections at Site 903. Seismic profiles connecting Sites 903 and 902 (Cruise Ew9009 MCS Line 1005; Fig. 2) predicted that Site 903 would recover a thick post-reflector m1 (Tuscan of Greenlee et al., 1992) interval (680 ms; ~585 m), with truncation in the upper Neogene (upper Miocene to Pleistocene). The middle Miocene section between reflector m1 (Tuscan) and reflector m5 (Green of Greenlee et al., 1992) is locally thick (300 ms; 304 m) with a particularly expanded reflector m2 (Yellow-2 of Greenlee et al., 1992)

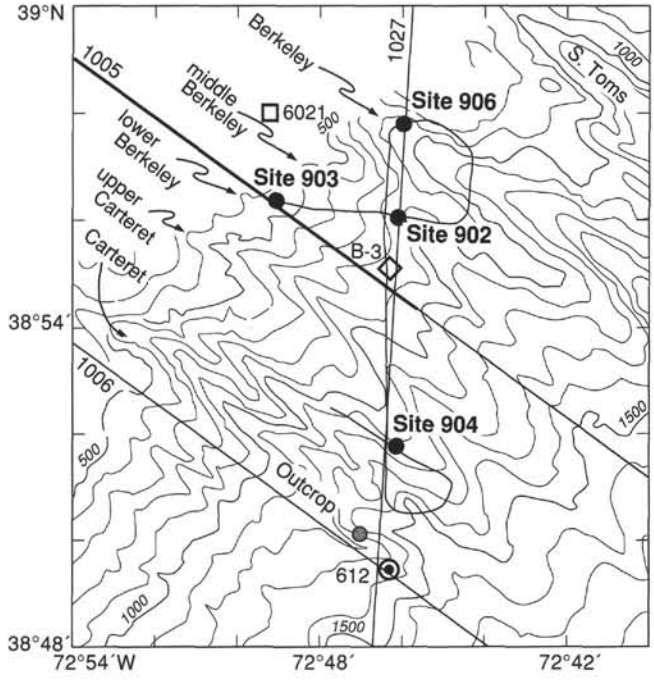

Figure 1. SeaBeam bathymetry with survey tracks near Sites 902, 903, 904, and 906. Heavy line indicates *Maurice Ewing* Cruise 9009 (Ew9009) MCS Line 1005 (shown in Fig. 2, this chapter). Canyons are indicated by arrows. The outcrop indicated near DSDP Site 612 was sampled using the *Alvin* in 1989.

to reflector m3 (Blue of Greenlee et al., 1992) interval (105 ms; 109 m; middle middle Miocene). This site provided a good opportunity to recover lower Miocene strata because it has a thick reflector m3 (Blue) to m5 (Green) section (~105 ms; 115 m). The Oligocene section was predicted to be thinner than at Site 902. As at Site 902, truncation of both the middle and upper Eocene section occurs between these sites and DSDP Site 612. Because of this, we placed a lower priority on reaching the top of the lower Eocene at this site than at Site 904.

OPERATIONS

Site 903 (proposed Site MAT11) is located about 2.4 nmi (4.4 km) to the west-northwest of Site 902 on the upper continental slope. Double advanced piston coring (APC) coverage and a deep rotary core barrel (RCB) penetration were the main drilling objectives.

Hole 903A

A beacon was launched at 1830 hr (Universal Time Coordinated [UTC]), 18 June 1993. Because water depth was only about 440 m, low-power acoustic beacons were used. An additional 2¼ hr was spent in refining the position of the drill site by offsetting on the reference beacon to the proper water depth with the core bit a few meters above the seafloor. The soft sediment produced no clear indication of bit contact with the seafloor. An APC core "shot" with the bit positioned at 455.5 m from driller's datum recovered over 9.3 m of core and seafloor depth was established at 455.5 m.

Continuous APC cores were taken to 169.5 mbsf. Temperature-shoe measurements were taken on Cores 150-903A-3H through -16H. Indication of incomplete stroke began with Core 150-903A-16H at about 145 mbsf and coring continued through Core 150-903A-20H by the advance-by-recovery technique. Following the switch to extended core barrel (XCB) coring, generally high core recovery was achieved to 703 mbsf (Table 1). Hole conditions were still excellent when coring was stopped for logging. The decision to terminate the

Table 1. Coring summary, Site 903.

Core no.	Date (1993)	Time (UTC)	Depth (mbsf)	Length cored (m)	Length recovered (m)	Recovery (%)
150-903A-						
1H	June 18	2115	0.0–9.5	9.5	9.33	98.2
2H	June 18	2150	9.5–19.0	9.5	9.78	103.0
3H	June 18	2250	19.0–28.5	9.5	9.50	100.0
4H	June 18	2315	28.5–38.0	9.5	9.74	102.0
5H	June 19	0000	38.0–47.5	9.5	9.26	97.5
6H	June 19	0040	47.5–57.0	9.5	10.00	105.2
7H	June 19	0120	57.0–66.5	9.5	9.16	96.4
8H	June 19	0155	66.5–76.0	9.5	9.97	105.0
9H	June 19	0245	76.0–85.5	9.5	10.25	107.9
10H	June 19	0345	85.5–95.0	9.5	10.65	112.1
11H	June 19	0430	95.0–104.5	9.5	10.75	113.1
12H	June 19	0515	104.5–114.0	9.5	10.58	111.3
13H	June 19	0600	114.0–123.5	9.5	6.18	65.0
14H	June 19	0700	123.5–133.0	9.5	9.77	103.0
15H	June 19	0800	133.0–142.5	9.5	2.73	28.7
16H	June 19	0850	142.5–149.0	6.5	6.52	100.0
17H	June 19	0930	149.0–154.0	5.0	4.72	94.4
18H	June 19	1015	154.0–160.0	6.0	5.94	99.0
19H	June 19	1045	160.0–164.5	4.5	4.53	100.0
20H	June 19	1130	164.4–169.5	5.2	5.29	103.0
21X	June 19	1230	169.5–172.8	3.3	4.71	143.0
22X	June 19	1250	172.8–182.3	9.5	6.56	69.1
23X	June 19	1320	182.3–191.9	9.6	4.41	45.9
24X	June 19	1345	191.9–201.4	9.5	7.31	76.9
25X	June 19	1415	201.4–211.0	9.6	9.29	96.8
26X	June 19	1440	211.0–220.6	9.6	9.15	95.3
27X	June 19	1520	220.6–230.3	9.7	8.34	86.0
28X	June 19	1600	230.3–240.0	9.7	7.20	74.2
29X	June 19	1640	240.0–249.7	9.7	7.43	76.6
30X	June 19	1715	249.7–259.3	9.6	5.13	53.4
31X	June 19	1745	259.3–268.9	9.6	9.17	95.5
32X	June 19	1820	268.9–278.5	9.6	7.78	81.0
33X	June 19	1840	278.5–288.2	9.7	7.15	73.7
34X	June 19	1920	288.2–297.9	9.7	10.09	104.0
35X	June 19	1950	297.9–307.5	9.6	9.60	100.0
36X	June 19	2035	307.5–317.2	9.7	9.43	97.2
37X	June 19	2100	317.2–326.7	9.5	10.46	110.1
38X	June 19	2200	326.7–336.4	9.7	9.50	97.9
39X	June 19	2230	336.4–346.0	9.6	7.04	73.3
40X	June 19	2310	346.0–355.7	9.7	6.33	65.2
41X	June 19	2345	355.7–365.4	9.7	7.25	74.7
42X	June 20	0015	365.4–374.9	9.5	9.91	104.0
43X	June 20	0035	374.9–384.6	9.7	9.07	93.5
44X	June 20	0100	384.6–394.3	9.7	10.35	106.7
45X	June 20	0130	394.3–404.0	9.7	5.47	56.4
46X	June 20	0200	404.0–413.7	9.7	10.12	109.2
47X	June 20	0230	413.7–423.3	9.6	9.62	100.0
48X	June 20	0300	423.3–433.0	9.7	9.27	95.5
49X	June 20	0330	433.0–442.7	9.7	9.88	102.0
50X	June 20	0405	442.7–452.2	9.5	8.67	91.2
51X	June 20	0430	452.2–461.9	9.7	9.90	102.0
52X	June 20	0500	461.9–471.6	9.7	9.88	102.0
53X	June 20	0530	471.6–481.3	9.7	9.54	98.3
54X	June 20	0555	481.3–490.9	9.6	8.87	92.4
55X	June 20	0625	490.9–500.6	9.7	9.67	99.7
56X	June 20	0645	500.6–510.2	9.6	5.95	62.0
57X	June 20	0715	510.2–519.9	9.7	5.45	56.2
58X	June 20	0745	519.9–529.5	9.6	5.01	52.2
59X	June 20	0825	529.5–539.2	9.7	9.68	99.8
60X	June 20	0845	539.2–548.9	9.7	9.84	101.0
61X	June 20	0910	548.9–558.5	9.6	9.92	103.0
62X	June 20	0935	558.5–567.8	9.3	9.79	105.0
63X	June 20	1000	567.8–577.5	9.7	9.85	101.0
64X	June 20	1030	577.5–587.1	9.6	9.74	101.0
65X	June 20	1100	587.1–596.8	9.7	9.32	96.1
66X	June 20	1135	596.8–606.3	9.5	0.23	2.4
67X	June 20	1205	606.3–616.0	9.7	9.68	99.8
68X	June 20	1245	616.0–625.6	9.6	9.74	101.0
69X	June 20	1310	625.6–635.2	9.6	8.73	90.9
70X	June 20	1400	635.2–644.7	9.5	9.52	100.0
71X	June 20	1430	644.7–654.4	9.7	9.80	101.0
72X	June 20	1500	654.4–664.1	9.7	8.51	87.7
73X	June 20	1535	664.1–673.8	9.7	9.92	102.0
74X	June 20	1615	683.5–693.1	9.6	9.86	103.0
75X	June 20	1650	683.5–693.1	9.6	9.43	98.2
76X	June 20	1800	693.1–702.8	9.7	9.60	98.9
Coring totals				702.8	637.77	90.6
150-903B-						
1H	June 21	2215	0.0–2.0	2.0	2.05	102.0
2H	June 21	2240	2.0–11.5	9.5	8.97	94.4
3H	June 21	2300	11.5–21.0	9.5	9.74	102.0
4H	June 21	2320	21.0–30.5	9.5	9.79	103.0
5H	June 21	2345	30.5–40.0	9.5	9.15	96.3
6H	June 21	0000	40.0–49.5	9.5	8.94	94.1
7H	June 22	0020	49.5–59.0	9.5	9.54	100.0
8H	June 22	0040	59.0–68.5	9.5	9.43	98.7
9H	June 22	0055	68.5–78.0	9.5	9.83	103.0
10H	June 22	0110	78.0–87.5	9.5	9.15	96.3
11H	June 22	0125	87.5–97.0	9.5	10.18	107.1
12H	June 22	0145	97.0–106.5	9.5	9.32	98.1
13H	June 22	0205	106.5–116.0	9.5	10.02	102.0
14H	June 22	0225	116.0–125.5	9.5	6.71	71.0
15H	June 22	0250	125.5–135.0	9.5	9.29	97.8
16H	June 22	0330	135.0–144.5	9.5	9.92	104.0
17H	June 22	0355	144.5–154.0	9.5	7.68	80.8
Coring totals				154.0	149.71	97.2
150-903C-						
*******Drilled from 0.00 to 485.5 mbsf *******						
1R	June 23	1340	485.5–489.8	4.3	0.00	0.0
2R	June 23	1535	489.8–493.8	4.0	0.00	0.0
3R	June 24	0400	493.8–500.6	6.8	0.00	0.0
4R	June 24	0445	500.6–505.6	5.0	0.00	0.0
5R	June 24	0615	505.6–510.3	4.7	2.85	60.6
6R	June 24	0715	510.3–515.3	5.0	0.69	13.8
7R	June 24	0900	515.3–525.0	9.7	8.12	83.7
8R	June 24	0950	525.0–534.6	9.6	0.11	1.1
*******Drilled from 534.6 to 586.5 mbsf *******						
9R	June 24	1400	586.5–592.1	5.6	3.95	70.5
10R	June 24	1510	592.1–601.8	9.7	7.97	82.1
11R	June 24	1610	601.8–611.5	9.7	3.04	31.3
*******Drilled from 611.5 to 688.6 mbsf *******						
12R	June 24	2045	688.6–698.2	9.6	7.11	74.0
13R	June 24	2155	698.2–707.8	9.6	4.33	45.1
14R	June 25	0015	707.8–717.2	9.4	7.72	82.1
15R	June 25	0110	717.2–727.0	9.8	5.68	57.9
16R	June 25	0210	727.0–736.8	9.8	6.38	65.1
17R	June 25	0315	736.8–746.5	9.7	7.35	75.8
18R	June 25	0430	746.5–756.2	9.7	4.58	47.2
19R	June 25	0545	756.2–765.9	9.7	6.29	64.8
20R	June 25	0645	765.9–775.5	9.6	9.88	103.0
21R	June 25	0745	775.5–785.2	9.7	9.71	100.0
22R	June 25	0915	785.2–794.9	9.7	9.56	98.0
23R	June 25	1015	794.9–804.1	9.2	9.64	105.0
24R	June 25	1120	804.1–813.8	9.7	1.95	20.1
25R	June 25	1245	813.8–823.5	9.7	4.88	50.3
26R	June 25	1345	823.5–833.1	9.6	0.05	0.5
27R	June 25	1445	833.1–842.7	9.6	1.55	16.1
28R	June 25	1535	842.7–852.4	9.7	3.69	38.0
29R	June 25	1635	852.4–862.1	9.7	8.03	82.8
30R	June 25	1725	862.1–871.7	9.6	0.00	0.0
31R	June 25	1815	871.7–881.4	9.7	3.48	35.9
32R	June 25	1915	881.4–891.1	9.7	5.11	52.7
33R	June 25	2000	891.1–900.7	9.6	9.53	99.3
34R	June 25	2130	900.7–910.4	9.7	2.36	24.3
35R	June 25	2220	910.4–920.0	9.6	10.02	104.4
36R	June 25	2310	920.0–929.7	9.7	3.64	37.5
37R	June 26	0020	929.7–939.0	9.3	9.50	102.0
38R	June 26	0115	939.0–948.6	9.6	9.38	97.7
39R	June 26	0215	948.6–958.2	9.6	9.06	94.4
40R	June 26	0315	958.2–967.5	9.3	8.15	87.6
41R	June 26	0415	967.5–977.2	9.7	7.38	76.1
42R	June 26	0510	977.2–986.8	9.6	0.00	0.0
43R	June 26	0650	986.8–996.5	9.7	0.17	1.8
44R	June 26	0825	996.5–1006.2	9.7	2.30	23.7
45R	June 26	1040	1006.2–1015.8	9.6	3.94	41.0
46R	June 26	1230	1015.8–1025.5	9.7	0.26	2.7
47R	June 26	1445	1025.5–1029.1	3.6	3.07	85.3
48R	June 26	1700	1029.1–1035.1	6.0	4.73	78.8
49R	June 26	1900	1035.1–1044.8	9.7	9.96	102.0
50R	June 26	2000	1044.8–1054.4	9.6	0.00	0.0
51R	June 26	2305	1054.4–1064.1	9.7	9.94	102.0
52R	June 27	0130	1064.1–1073.8	9.7	8.85	91.2
53R	June 27	0545	1073.8–1083.4	9.6	7.09	73.8
54R	June 27	0910	1083.4–1092.8	9.4	9.15	97.3
55R	June 27	1130	1092.8–1102.3	9.5	8.98	94.5
56R	June 27	1345	1102.3–1111.5	9.2	10.10	109.8
57R	June 27	1815	1111.5–1121.1	9.6	6.09	63.4
58R	June 27	2100	1121.1–1130.6	9.5	9.96	105.0
59R	June 27	2330	1130.6–1140.0	9.4	5.90	62.7
60R	June 28	0250	1140.0–1149.7	9.7	9.95	102.0
Coring totals				535.2	323.16	60.4
Drilled				614.5		
Total				1149.7		
150-903D-						
***** Drilled 0.00 to 774.9 mbsf *****						
1R	July 19	1110	774.9–784.5	9.6	2.20	22.9
2R	July 19	1210	784.5–794.2	9.7	3.95	40.7
3R	July 19	1300	794.2–803.8	9.6	7.08	73.7
4R	July 19	1400	803.8–813.4	9.6	9.23	96.1
5R	July 19	1450	813.4–823.1	9.7	9.94	102.0
6R	July 19	1550	823.1–832.8	9.7	9.28	95.7
7R	July 19	1640	832.8–842.4	9.6	9.84	102.0

Table 1 (continued).

Core no.	Date (1993)	Time (UTC)	Depth (mbsf)	Length cored (m)	Length recovered (m)	Recovery (%)
8R	July 19	1750	842.4–852.0	9.6	9.24	96.2
9R	July 19	1825	852.0–861.7	9.7	9.76	100.0
10R	July 19	1915	861.7–871.3	9.6	3.98	41.4
11R	July 19	1955	871.3–881.0	9.7	7.60	78.3
12R	July 19	2115	881.0–890.7	9.7	0.65	6.7
13R	July 19	2200	890.7–900.2	9.5	4.03	42.4
14R	July 19	2300	900.2–909.7	9.5	9.44	99.3
15R	July 20	0030	909.7–919.2	9.5	7.85	82.6
16R	July 20	0115	919.2–928.8	9.6	1.74	18.1
17R	July 20	0200	928.8–938.4	9.6	9.48	98.7
18R	July 20	0305	938.4–948.0	9.6	9.67	101.0
***** Drilled 948.0 to 977.0 mbsf *****						
19R	July 20	0600	977.0–986.7	9.7	6.65	68.5
20R	July 20	0700	986.7–996.3	9.6	10.14	105.6
21R	July 20	0800	996.3–1005.9	9.6	9.94	103.0
22R	July 20	0930	1005.9–1015.6	9.7	0.00	0.0
23R	July 20	1235	1015.6–1025.3	9.7	0.14	1.4
24R	July 20	1440	1025.3–1029.0	3.7	3.38	91.3
25R	July 20	1650	1029.0–1037.0	8.0	8.29	103.0
Coring totals				233.1	163.5	70.1
Drilled				803.9		
Total				1037.0		

hole at that depth in favor of the deeper RCB penetration was predicated partly on the desire to log before time and increased circulation could degrade the condition of the hole.

The initial logging attempt, without the side-entry sub (SES), was with the sonic induction–gamma ray tool string. Though the logging tool had to be "worked" past several impediments, it eventually reached a depth of 604 mbsf. A good log was recorded from that depth up to the bit at 74 mbsf. On the second log run, the lithoporosity combination string would not pass a bridge/ledge at 492 mbsf. Again, good results were obtained over the upper hole interval, which the caliper log showed to be in much better condition than the equivalent depth interval in Hole 902D. Logging operations were terminated, the hole plugged, and the bit pulled clear at 2000 hr, 21 June 1993.

Hole 903B

While the vessel was being offset 15 m to the northeast, the drill string was flushed of cement and the top drive was deployed. At 2200 hr, the APC was actuated to spud Hole 903B from 450 m. Two meters of sediment were recovered to fix seafloor depth at 457.5 m. Coring operations consisted of a series of 17 consecutive APC cores offset 5.5 m vertically from the coring intervals of Hole 903A. Cores 150-903B-9H, -16H, and -17H gave incomplete-stroke indication, but the 9.5-m advance coring mode was used to preserve stratigraphic overlap. After the flurry of 17 cores to a depth of 154 mbsf (Table 1) in 6 hr, the drill string was recovered and Hole 903B was terminated.

Hole 903C

The RCB bottom-hole assembly (BHA) and a drill-in casing (DIC) string were installed. The casing-running operation began at 0615 hr, 22 June. By 1715 hr, 11 joints of 11¾-in. casing had been assembled into a 149-m DIC string, attached to the BHA, and fitted with a reentry funnel. When the assembly had been run to the seafloor, the top drive was deployed and Hole 903C was spudded at 1830 hr, 22 June. After release of the casing, a 9⅞-in. hole was drilled ahead to 485 mbsf, where "spot" cores were taken over an interval that was incompletely recovered in Hole 903A.

No core was recovered in two coring attempts, and the drill string was tripped to find and remedy the problem. The bit core guide was found to be jammed tightly by a carbonate/sand concretion with clay and silt packed around it. The bit was removed and, while the obstruction was being cleared, radial cracks were noted around the spearpoint inserts of the bit cones. A new bit and mechanical bit release (MBR) were installed, the outer core barrel (OCB) spacing was checked, and the bit was run back to reentry depth. About 1 hr was required to position the bit over the funnel. Part of that time was spent with the bit stuck in the mud up-slope of the funnel, preventing the BHA from moving over the hole. Visibility was too poor to discern the problem. A successful reentry was made at 2400 hr, 23 June, and the vibration-isolated television (VIT) was recovered before the trip resumed.

A bridge or ledge was encountered at 452 mbsf, so the top drive was deployed to clean the hole to total depth. Coring operations then resumed with two short cores, which again had no recovery. Circulating pressure and markings on the deplugger put in place all indicated normal seating. Four additional cores (150-903C-5R to -8R) were taken to 535 mbsf with about 40% recovery in sandy sediment. Drilling continued to 689 mbsf with spot cores across the interval from 587 to 612 mbsf. Continuous coring resumed at that depth and proceeded with variable core recovery. Poorest recovery seemed to be in sand beds near intervals of presumed sequence boundary reflectors. Other factors in occasional substandard recovery were mechanical problems with the core barrels and the unavoidable lag in adjusting coring parameters to changing lithologies. Overall RCB recovery for the 60 cores attempted to total depth (including the ill-fated spot cores) was 60.4% (Table 1). Coring conditions in the chalk (from 1064 mbsf) provided excellent core quality and recovery. Scientific objectives were declared fulfilled, and coring was terminated at 1149.7 mbsf (Table 1).

While the hole was conditioned for logging, tight hole intervals were noted at 1084 and 340 mbsf. A single bridge or ledge was encountered at 823 mbsf, but the drill string passed it without circulation or rotation. Nine meters of fill were cleaned from the bottom of the hole with the top drive in the string. A second mud sweep was circulated before the bit was released for logging.

Logging operations began with the sonic induction–gamma ray tool string. Because logging with the SES would have been limited to an open-hole interval approximately equal to water depth, the SES was not deployed. The first lowering was interrupted by a mass of clay about 160 m above the end of the pipe and the tool had to be recovered. After the sediment was circulated from the pipe and a slug of heavy mud introduced to prevent back flow, the tool was lowered again. A solid obstruction was met at the end of the drill string. Indications were that the inner sleeve of the MBR had not been successfully down-shifted earlier and that the lowermost bore of the MBR top connector had become plugged with clay. Circulation was through the side "windows" of the top connector. It was necessary to punch the plug out mechanically with a core breaker on an inner barrel run on the coring line and then to run the rotary shifting tool (RST) again to shift the sleeve into place. On the third run, the logging tool string reached open hole, but stopped again on a bridge about 5 m below the pipe.

Because over 16 hr had elapsed since circulation of the hole, another wiper trip was made to total depth and the hole again was swept with mud. The drill string was pulled back only to 633 mbsf to isolate the bridge that had stopped the logging tool earlier.

The logging tools were stopped by obstructions a few meters below the pipe on the ensuing run and again with pipe at 765 mbsf. Finally, after the pipe had been lowered to 851 mbsf, the tool traversed enough open hole to record a sonic induction–gamma ray log from 975 to 823 mbsf (with the pipe raised to the limit).

As the SES was the only hope of obtaining logs over a significant section of the hole, the end of the pipe was pulled to 447 mbsf and the SES was installed. With the "Quad combo" tool string inside the pipe, drill-string weight and circulation were used to place the tools at 868 mbsf. Tight hole conditions forced the drill string to a halt about 40 m short of the depth limit imposed by the SES. Even with the aid of the

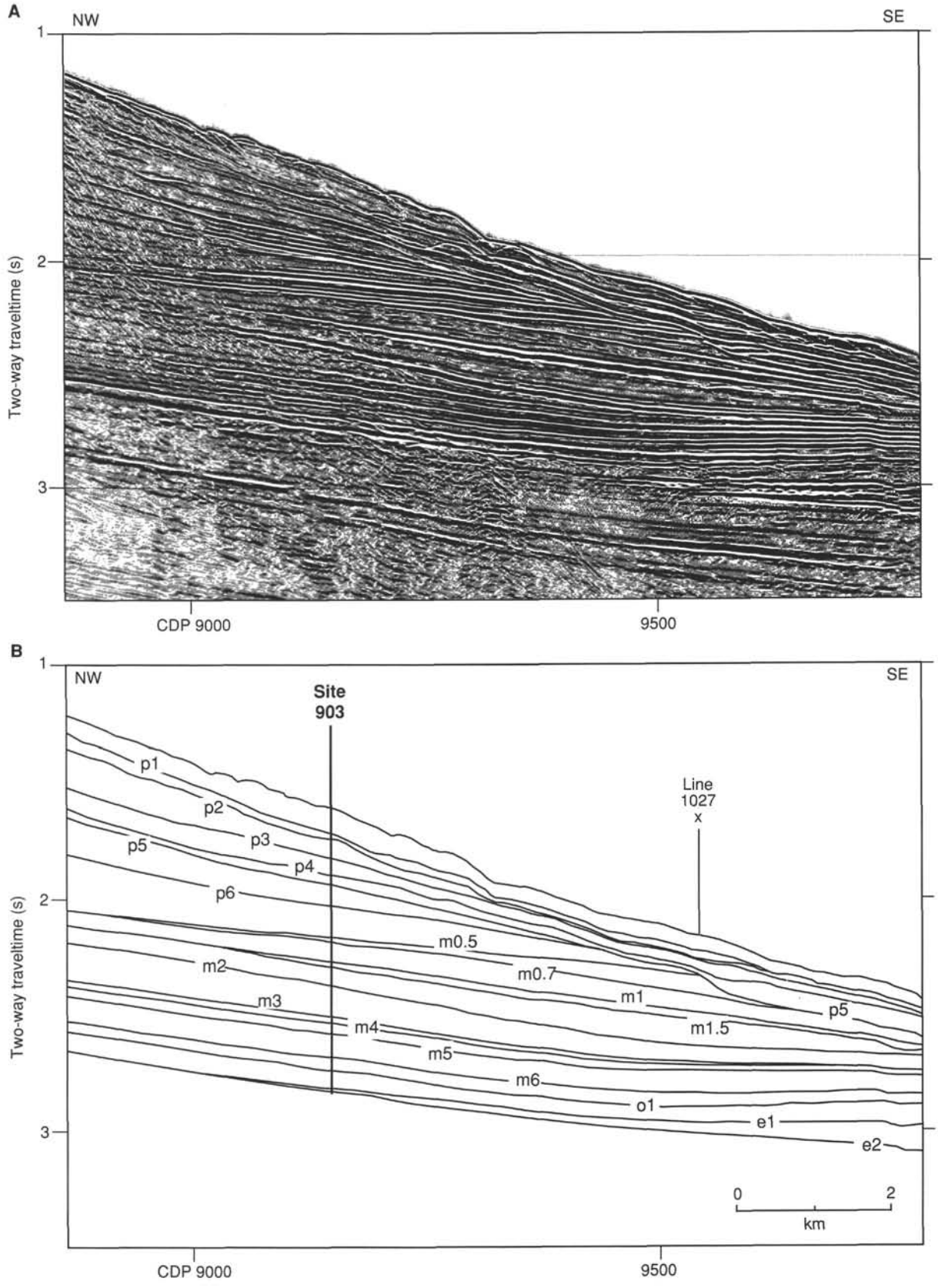

Figure 2. Ew9009 MCS Line 1005, a dip profile. **A.** Uninterpreted seismic section. **B.** Line drawing interpretation crossing Site 903. Reflectors p1 to e2 are described in the "Seismic Stratigraphy" section (this chapter). CDP = common depth point. Location of crossing with Cruise Ew9009 MCS Line 1027 (Fig. 1) is shown (x). See also Plate 1 (in back-pocket foldout).

SES, the logging operation was difficult. The logging tool became stuck at one point, and the maximum allowable pull was required to free it. Sediment packed into the top connector and on the tool apparently prevented its reentry into the pipe and 1½ hr were required to pull it inside with the help of pump circulation. The caliper log showed the hole to be in deteriorated condition, with numerous washouts and some restrictions well below bit size.

All logging equipment was rigged down, the hole plugged, the drill string recovered, the beacon recalled and retrieved, and the *JOIDES Resolution* departed Site 903 at 2000 hr, 30 June 1993.

Return to Site 903

After Site 906 was completed, insufficient operating time remained to start and complete a new site. The Shipboard Scientific Party decided to use the limited time to drill an additional hole at Site 903 (proposed Site MAT11) and to recore the inadequately recovered intervals of Hole 903C. Despite complications from shifting currents, the dynamic-positioning (DP) move of about 3 nmi from Site 906 was completed during the round trip of the drill string. A beacon had been left in operation at Site 903, but its signal was too weak to use for position referencing upon the vessel's return. Global Positioning System (GPS) and precision depth recorder (PDR) navigation were used to position over the site, and a new beacon was launched at 1545 hr on 18 July.

Because the intervals to be cored were below the XCB refusal depth at the other sites, and because polycrystalline diamond compact (PDC) bits had been highly successful in XCB coring, a RCB BHA was made up with an experimental antiwhirl PDC core bit.

Hole 903D

The PDR depth was 2–3 m shallower than that of Hole 903A; the depth for Hole 903D was 453 m below driller's datum. Hole 903D was spudded with circulation and rotation. Drilling proceeded more rapidly with the PDC bit than it had in Hole 903C with the roller-cone C-3 bit. Drilling to 775 mbsf consumed only 15½ hr, including the recovery of "wash" core barrels from 477 and 775 mbsf.

Core recovery was low on the first two cores of continuous RCB coring, though the quality of the core recovered was excellent. The third core was recovered full to the top, but with about 2.5 m missing from the bottom. It became apparent that the long, continuous core sections were so smooth that sometimes they were not being engaged by the dog-type core catchers. The contrast of RCB cores taken with the PDC bit with those of Hole 903C that were cut by the roller-cone bit was dramatic. Cores from the same section in Hole 903C were poorly recovered, broken, and "biscuited," whereas the Hole 903D cores were smooth cylinders several meters in length and often broken only during the process of removal from the core barrel. Full (99%) recovery was achieved over the next six cores in an interval that was recovered at a 35% rate in Hole 903C (Table 1). Over the next seven cores, in an interval of extra-soft mud, however, the comparison was 53% in Hole 903D vs. 51% in Hole 903C.

Two full-recovery cores then were taken before a 29-m interval was drilled to reach the next inadequately recovered portion of the Hole 903C section. Cores 150-903D-19R through -21R recovered 92% before an empty barrel was retrieved for Core 150-903D-22R. It was noted that the inner-barrel latch spring (which keeps the latch engaged under the downhole latch sleeve) was missing—apparently having broken and fallen out of its position. The lack of core recovery suggested that the inner barrel had been pushed up into the BHA by incoming core and that pieces of core probably were in the bit cavity below the float valve. A bit deplugger then was made up to an inner barrel and pumped to the bit to punch out any core fragments before the next core attempt. Core 150-903D-23R was attempted next, but the rate of penetration (ROP) was low and only 14 cm of core pieces were recovered. The entrance to the core-catcher sub was blocked by a horizontally jammed chunk of hard core. A flat surface on the bottom side of the core fragment indicated that it had spun on the bottom of the hole and prevented new core from forming. A second run then was made to clear core from the bit—this time with a chisel-shaped core breaker. The ROP remained low as a 3.7-m trial core (Core 150-903D-24R) was cut, but 3.4 m of core were recovered. Operating time ran out as Core 150-903D-25R was being cut to 1037 mbsf at the rate of 10 min per meter. The drastically lower ROP indicated a downhole problem. Full recovery length was achieved for the core, but core diameter was severely reduced over much of the length.

Because of the downhole mechanical problems and low ROP, coring had to be terminated 22 m short of the planned total depth as operating time ran out. The hole was plugged, the bit was pulled, and the positioning beacon was recalled. The vessel drifted while the drill string was recovered. At 2100 hr on 20 July, *JOIDES Resolution* departed for port at St. John's, Newfoundland.

LITHOSTRATIGRAPHY

The lithostratigraphic succession at Site 903 (Table 2 and Figs. 3–4) is the most complete of the four continental slope sites drilled on Leg 150 (Sites 902–904 and 906). Unit II is present only at Site 903 and comprises 85 m of lower Pleistocene to upper Pliocene sediment (273.9–358.9 mbsf). Unit III at Site 903 comprises 164 m of upper Miocene sediment (358.9–522.9 mbsf); it is much thinner at Site 902 (26 m) and is absent at Sites 904 and 906. An unconformity separates Units I and II, although correlations of magnetic susceptibility to the SPECMAP time scale indicate no discernible hiatus (see "Sedimentation Rates" section, this chapter). An unconformity also separates Units II and III, at which level most of the Pliocene appears to be missing (see "Seismic Stratigraphy" and "Biostratigraphy" sections, this chapter).

The lithologic units at Site 903 are 10- to 100-meter scale sediment packages, very different in character from each other. Most of these units also have an internal cyclic structure (in the sense of a systematic repetition of lithologies through the succession); these sedimentary cycles correspond to subunits as described herein. The subunit boundaries are most simply picked at the bases of coarse detrital and/or mass-transport facies packages. These subunits may be depositional sequences, as mass transport is a possible response to relative sea-level fall. However, the precise relationship of these deposits to relative sea-level change, or more directly, their precise relationship to shelfal unconformities, remains uncertain at this stage of investigation. In almost all cases at Site 903, the subunits are sharply bounded; one clear exception to this is the base of Subunit III, which is defined by a more gradational downward decrease in sand content. Subunits are not well defined in the Oligocene to lower Miocene where the problems of weak sedimentary expression are exacerbated by poor core recovery.

Unit I

Intervals: Sections 150-903A-1H-1, 0 cm, to -32X-4, 45 cm; Cores 150-903B-1H through -16H
Depth: 0–273.9 mbsf
Age: Holocene to middle Pleistocene

Subunit IA

Intervals: Sections 150-903A-1H-1, 0 cm, to -16H-1, 0 cm; Sections 150-903B-1H-1, 0 cm, to -16H-7, 87 cm
Depth: 0–144.7 mbsf (Hole 903B); 0–142.5 mbsf (Hole 903A)

Subunit IB

Interval: Sections 150-903B-17H-1, 0 cm, to 150-903A-32X-4, 45 cm
Depth: 144.9 mbsf (Hole 903B) to 273.4 mbsf (Hole 903A)

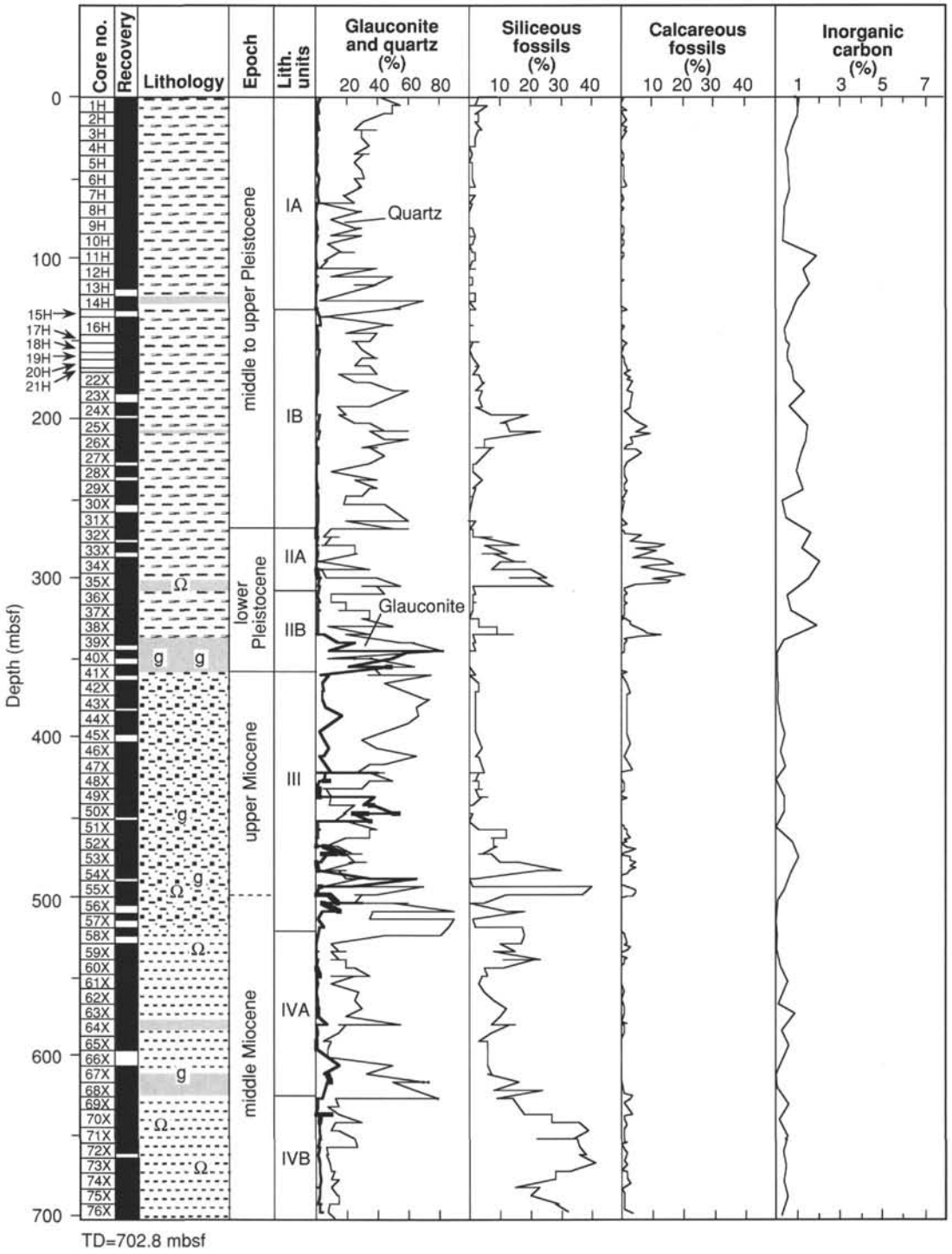

Figure 3. Generalized summary lithologic column for Holes 903A and 903C, showing glauconite and quartz, calcareous and siliceous fossil content (determined from smear slides), and inorganic carbonate (see "Organic Geochemistry" section, this chapter). Note that abundance patterns for components in Units V and VI at Hole 903C may be strongly influenced by the poor core recovery; in particular, the sharp drop in siliceous fossil content shown at around 855 mbsf is not apparent in observations from complementary cores from Hole 903D.

This unit, cored in Hole 903A and (partly) in Hole 903B, is composed predominantly of heavily bioturbated, greenish gray silty clay with very fine quartz sand. Volumetrically less important, but in striking contrast, are the intervals dominated by slump and debris–flow deposits that occur from 126 to 145 mbsf and from 222 to 274 mbsf; these mark the bases of Subunits IA and IB, respectively (Fig. 4). The uppermost 20 cm of mud recovered in Hole 903A is soupy.

Despite the close proximity of Holes 903A and 903B, approximately 15 m according to DP records, the successions recovered are somewhat different from each other. This is principally the result of incomplete, albeit complementary, core recovery. A good correlation is achieved between the two holes by matching a distinctive, thin, normally graded and sharp-based sand bed at 99.0 mbsf in Hole 903A with an identical bed at 97.8 mbsf in Hole 903B. This correlation

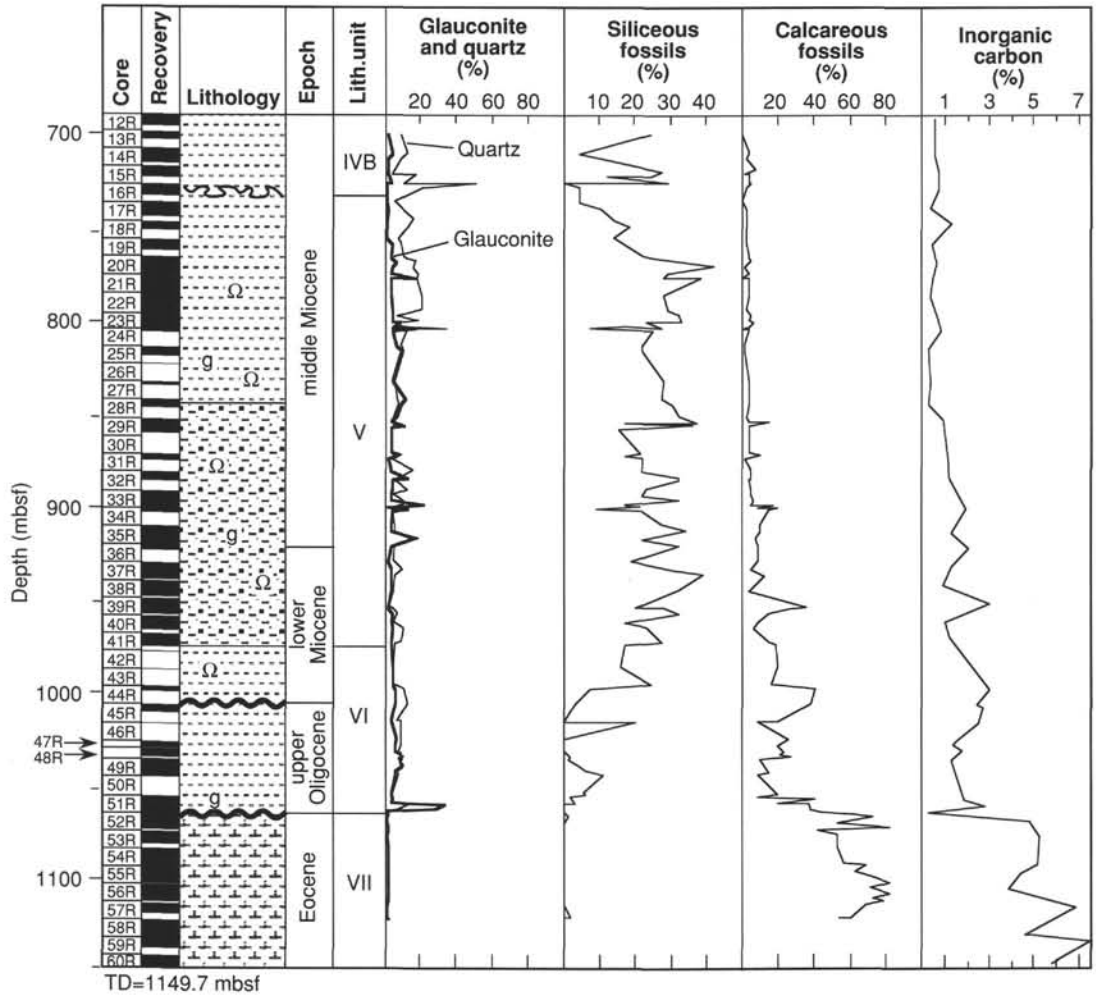

Figure 3 (continued).

suggests a "mismatch" in depth below the seafloor of only 1.2 m. Thus, it is clear that the 2.5-m-thick sand unit at 126.6–129.1 mbsf in Hole 903A was probably also present but not recovered in Hole 903B. Similarly, the sand unit at 142.2 to 144.9 mbsf in Hole 903B was probably present but not recovered in Hole 903A. It is apparent, also, that there must be some small-scale lateral changes in these units because the intervals of incomplete recovery do not correspond exactly to the sand intervals; for example, the base of the sand in Hole 903A should have been observed in Hole 903B if its thickness were constant between the holes. The sand in Hole 903A is in the middle and base of Core 150-903A-16H but is apparently unaffected by flow-in.

The silty clays that make up the bulk of the unit contain thin (<1 cm), discrete, very fine sand layers. In addition, sand is abundant in burrow fills where it has been biologically separated from the clay component. Most of this facies has a dark gray to light gray mottled appearance produced by burrowing. More restricted in their development are zones of thin color-banding (e.g., around 70 mbsf). These are light gray and dark gray with somewhat diffuse boundaries and are approximately 1 cm thick. Burrows are not evident.

Many of the thin layers of sand show slight normal grading, which suggests deposition from turbidity currents. The silty clays, which are intermixed with a moderate proportion of sand, may also have been deposited primarily from turbidity currents and related gravity-controlled flows, although indicative features are lacking.

Other products of downslope sediment transport are more complex in their structure. Two closely spaced intervals of sand occur in the middle of Unit I (the lower one defining the base of Subunit IA in Section 150-903B-16H-7, 87 cm). The upper sand 126.6–129.1 mbsf in Hole 903A) is a structureless, greenish gray, fine-to-medium sand, with numerous shell fragments and gradational upper and lower contacts. About 10 m of silty clay separates this package from the underlying sand and silty sand package (142.2 to 144.9 mbsf in Hole 903B), which is 2.8 m thick and similarly featureless at the top. However, the lower 107 cm of this lower sand package is a remarkable, gray, medium-grained, well-sorted quartz sand containing abundant light gray, subrounded mud clasts that range from 3 mm to 3 cm across and are normally graded (Fig. 5). Unfortunately, the contact with the underlying silty clay was not recovered.

A thick succession of slumps and debris flows is present in the lower part of Unit I (and the base of Subunit IB). Between 221.5 and 243.5 mbsf, at least four half-meter- to meter-scale, silty clay slumps are separated by intervals of moderately bioturbated silty clays of comparable thicknesses. Slump folds in these beds are tight, appear to be recumbent and isoclinal, and are truncated by low-angle, soft-sediment faults. It should be noted that the "herringbone" structures seen in the core photographs are produced by a combination of "biscuit"-style drilling disturbance and slump folding. A peculiar aspect of the slumps in this unit, as well as those at Site 902, is their thinly color-banded internal structure. If the color banding were a remnant primary structure, then it follows that burrowing activity upslope, from where the slumps originated, was less intense than in deeper water.

A 5-m-thick slump and debris-flow sequence sits on the basal unconformity (269–274 mbsf) and is separated from the slumps above

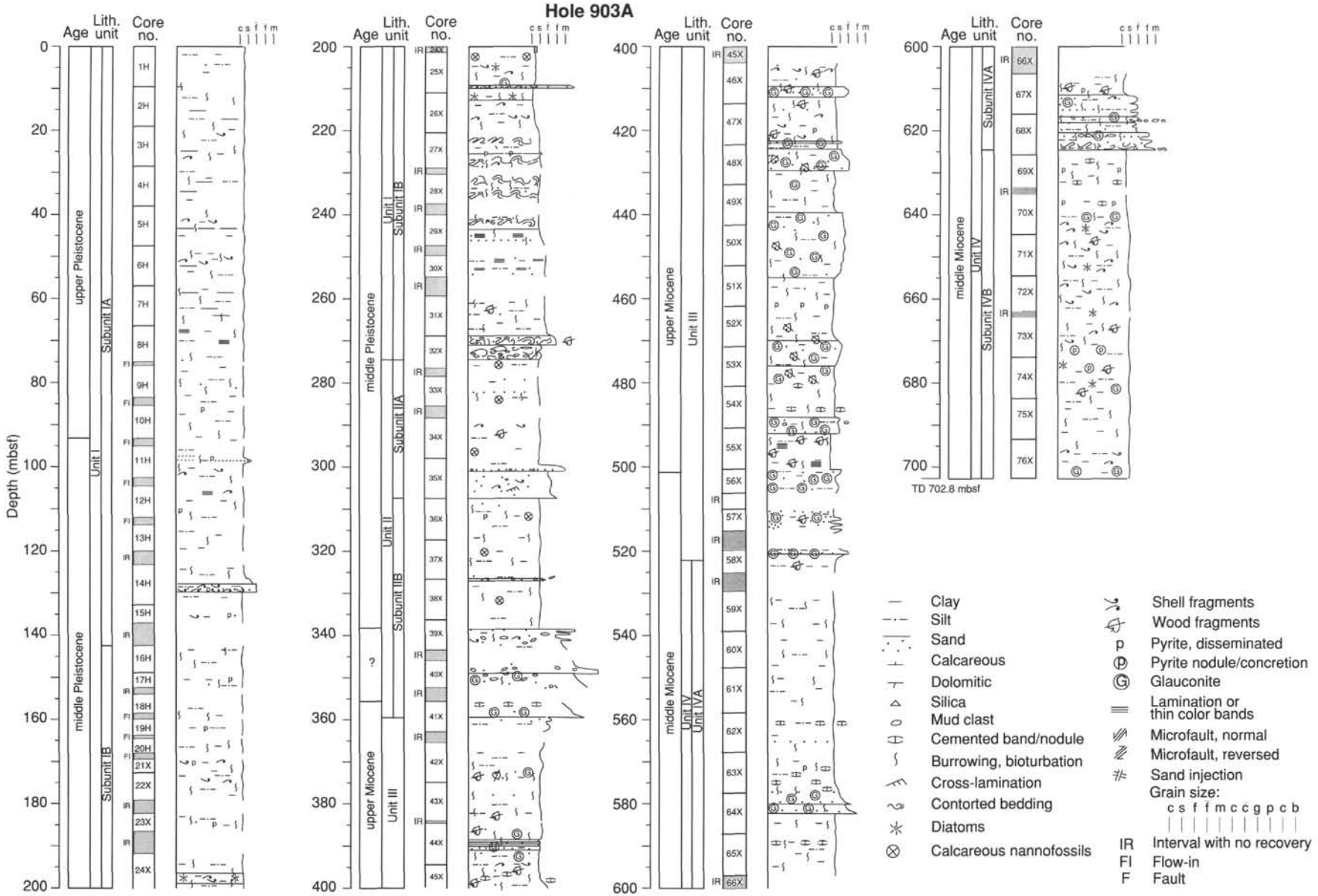

Figure 4. Detailed summary lithologic columns, Holes 903A through 903D. See also Plate 2 (in back-pocket foldout).

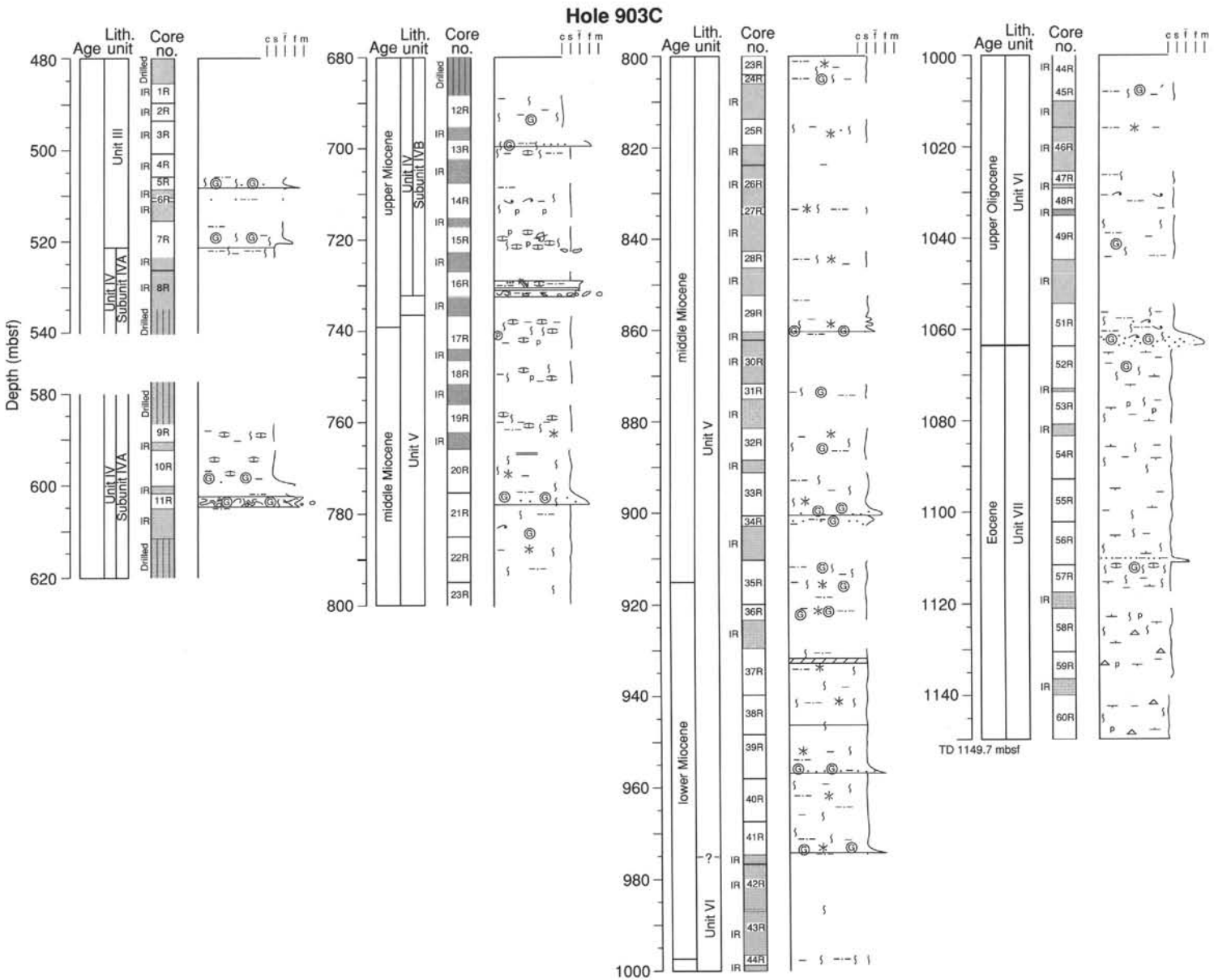

Figure 4 (continued).

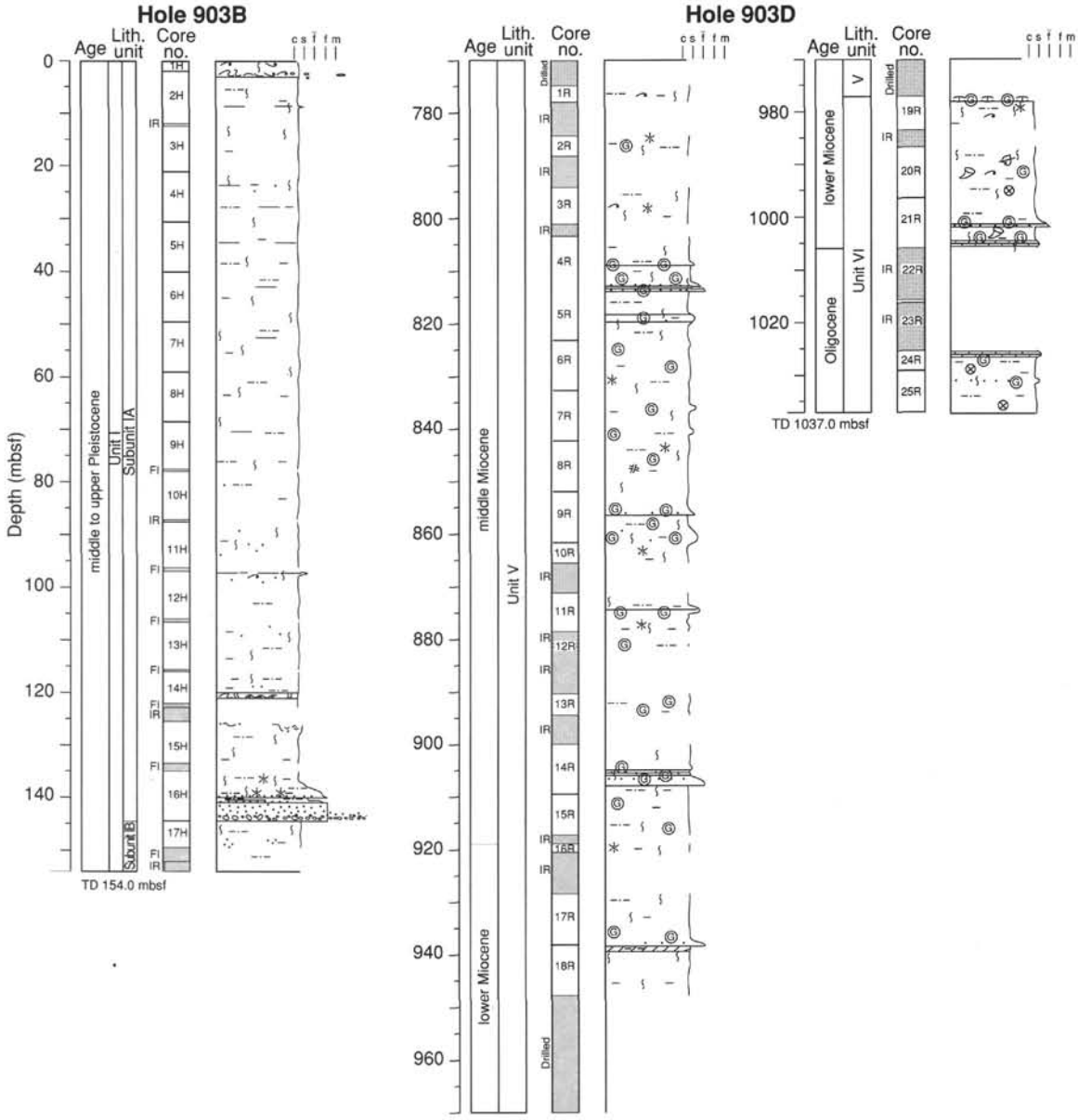

Figure 4 (continued).

by 25 m of rather homogeneous silty clay (with poor recovery). The basal slump/debris flow is significantly different from the overlying redeposited beds in that it contains abundant fine sand and woody organic detritus in the upper 110 cm of folded strata. Two sharp contacts are seen at 280.0 and 281.5 mbsf, and these may either delimit separate sedimentary events or bound cobble- or boulder-sized clasts of sandy mudstone within a larger debris flow. The underlying 1 m of silty clay contains scattered, centimeter-scale mud clasts and is probably a debris flow. Below this level there occurs a 2.45-m-thick silty clay showing very tight, soft-sediment folds and, within it, a 45-cm-thick zone containing very strongly deformed mud clasts.

Considering Unit I as a whole, smear-slide data indicate that sand content (Fig. 6) is less above 100 m at Hole 903A (~5%) than it is below (~10%). This pattern may be exaggerated because of the nature of the sand distribution through the section. Down to 100 mbsf, sand grains occur in discrete thin beds from which smear slides were not systematically made; below this level, however, the sediment has been more effectively homogenized by bioturbation and the disseminated sand grains are more likely to have been sampled. Nevertheless, peaks in sand abundance undoubtedly occur at around 10 and 210 mbsf and from 100 to 145 mbsf. The latter occurrence is clearly the major sand that defines the base of Subunit IA.

Silt-sized sediment is estimated from smear slides (Fig. 6) to range from 20% to 60% and is most abundant in the upper and lower parts of the succession, with a broad minimum in the middle (50–100 mbsf). A concomitant increase in clay content occurs through the same interval, based on smear-slide observations. The sand- and silt-sized grains are predominantly quartz and feldspar; glauconite is notably rare.

Relationships between smear-slide compositional data, X-ray diffraction (XRD) analyses (Fig. 7), and geochemical data (see "Organic Geochemistry" section, this chapter) strongly suggest that the carbonate component of Unit I is mostly detrital in origin (Fig. 8). From 0 to 220 mbsf, the general trend of the combined quartz and feldspar curve is almost identical to the curve for inorganic carbon (proportional to carbonate), except that the latter increases disproportionately between 95 and 145 mbsf. The close correlation of sand- and silt-sized siliciclastic content with carbonate implies that the carbonate was probably deposited and transported with the coarse fraction. Silt-sized carbonate

Table 2. Lithostratigraphy, Site 903.

Unit or subunit	Series	Depth (interval)	Lithology	Process
IA	Holocene to middle Pleistocene	0–144.9 mbsf (Hole 903B) (150-903B-1H-1, 0 cm, through 150-903B-16H-7, 87 cm) 0–142.5 mbsf (Hole 903A) (150-903A-1H-1, 0 cm, through 150-903A-15H-CC)	Gray silty clay, thin interbeds of very fine sand, debris flow, and slump sands and muds, particularly at base.	Hemipelagic settling, low-density turbidity current, slump, and mass flow.
IB	middle Pleistocene	144.9 mbsf–TD (Hole 903B) (150-903B-17H-1, 0 cm, through TD) 142.5–273.9 mbsf (Hole 903A) (150-903B-16H-1, 0 cm, through -32X-4, 45 cm)	Gray silty clay, thin interbeds of very fine sand, debris flow, and slump sands and muds, particularly at base.	Hemipelagic settling, low-density turbidity current, slump, and mass flow.
IIA	middle Pleistocene	273.9–307.5 mbsf (Hole 903A) (150-903A-32X-4, 45 cm, through -35X-CC, 60 cm)	Gray silty clay and coarse sand.	Hemipelagic settling, turbidity current, and sandy mass flow.
IIB	middle Pleistocene to upper Pliocene and ?upper Miocene	307.5–358.9 mbsf (150-903A-36X-1, 0 cm, through -41X-3, 20 cm)	Gray silty clay and coarse pebbly sand, glauconitic at base.	Hemipelagic settling, turbidity current, and sandy mass flow.
		Major disconformity		
III	upper to middle Miocene	358.9–522.9 mbsf (Hole 903A) (150-903A-41X-3, 20 cm, through -58X-2, 150 cm) –520.5 mbsf (Hole 903C) (150-903C-5R-1, 0 cm, through -7R-4, 70 cm)	Dark gray and green glauconitic sand and green-gray silty clay.	Hemipelagic settling and ?turbidity current or mass flow.
IVA	middle Miocene	522.9–624.6 mbsf (Hole 903A) (150-903A-58X-2, 150 cm, through -68X-6, 112 cm) 520.5– mbsf (Hole 903C) 150-903C-7R-4, 70 cm, through -11R-CC, 25 cm)	Green-gray and brown-gray silty clay, debris flow, and slump sands.	Hemipelagic and pelagic settling, slump, and debris flow.
IVB	middle Miocene	624.6 mbsf–TD (Hole 903A) (150-903A-68X-6, 112 cm, through -76X-CC, 12 cm; –733.1 mbsf (Hole 903C) 150-903C-12R-1, 0 cm, through -16R-5, 5 cm)	Green-gray and brown-gray silty clay, debris flow, and slump sands.	Hemipelagic and pelagic settling, slump, and debris flow.
V	middle to lower Miocene	733.1–974.4 mbsf (Hole 903C) (150-903C-16R-5, 5 cm, through -41R-5, 90 cm; –977.4 mbsf (Hole 903D) (150-903D-1R-1, 0 cm, through -19R-2, 7 cm)	Brown to green-gray diatom and nannofossil silty claystone and dark gray and green glauconitic sandstone.	Hemipelagic and pelagic settling and ?turbidity current.
VI	lower Miocene to upper Oligocene	974.4–1064.1 mbsf (Hole 903C) (150-903C-41R-5, 90 cm, through -51R-CC, 20 cm) 977.4 mbsf through TD (Hole 903D) (150-903D-19R-2, 7 cm, through -25R-CC, 16 cm)	Brown-gray nannofossil silty claystone and glauconitic sandstone.	Hemipelagic and pelagic settling and ?turbidity current.
		Major disconformity		
VII	upper Eocene	1064.1–1150.0 mbsf (Hole 903C) (150-903C-52R-1, 0 cm, through -60R-CC, 17 cm)	Light gray nannofossil chalk with clay and foraminifers, siliceous toward base.	Pelagic and hemipelagic settling, infrequent turbidity currents.

Note: TD = total depth.

was recognized in smear slides throughout the interval in which the carbonate curve shows a disproportionate increase (98–150 mbsf; Fig. 8). In the remainder of the section, carbonate is probably present as clay-sized particles, which, if detrital in origin, are presumably at the higher end of the clay size range; if they were significantly smaller, the abundance curve for carbonate would be expected to parallel that for clay. Below 220 mbsf, where the relationship between the detrital siliciclastic silt and sand and the carbonate content becomes inverse, the sediments quite clearly have a slumped origin. Thus, the sediment in the basal slumps may either have had a different source area or, less likely, underwent a different early diagenetic history from the rest of the unit. In this respect, they contrast strongly with the debris flow and related deposits at the base of Subunit IA.

Comparison of the abundance of the relatively minor, biogenic components of pelagic origin with percent sulfur content reveals a good correlation (Fig. 8). The sulfur is assumed to be associated principally with iron sulfide, and the relationship is compatible with more reducing, early diagenetic conditions that could be related to raised plankton productivity.

Iron sulfide is the main diagenetic phase present in Unit I and is commonly associated with burrows. It occurs possibly as a monosulfide in the upper 90 mbsf and as pyrite below this level. Well-formed pyrite nodules up to 1 cm in diameter are seen low in the unit (e.g., 226–229 mbsf). According to XRD analyses, pyrite also occurs in sandy layers and it may be partly detrital in origin (Fig. 7).

Unit II

Interval: Sections 150-903A-32X-4, 45 cm, to -41X-3, 20 cm
Depth: 273.9–358.9 mbsf
Age: middle Pleistocene to upper Pliocene

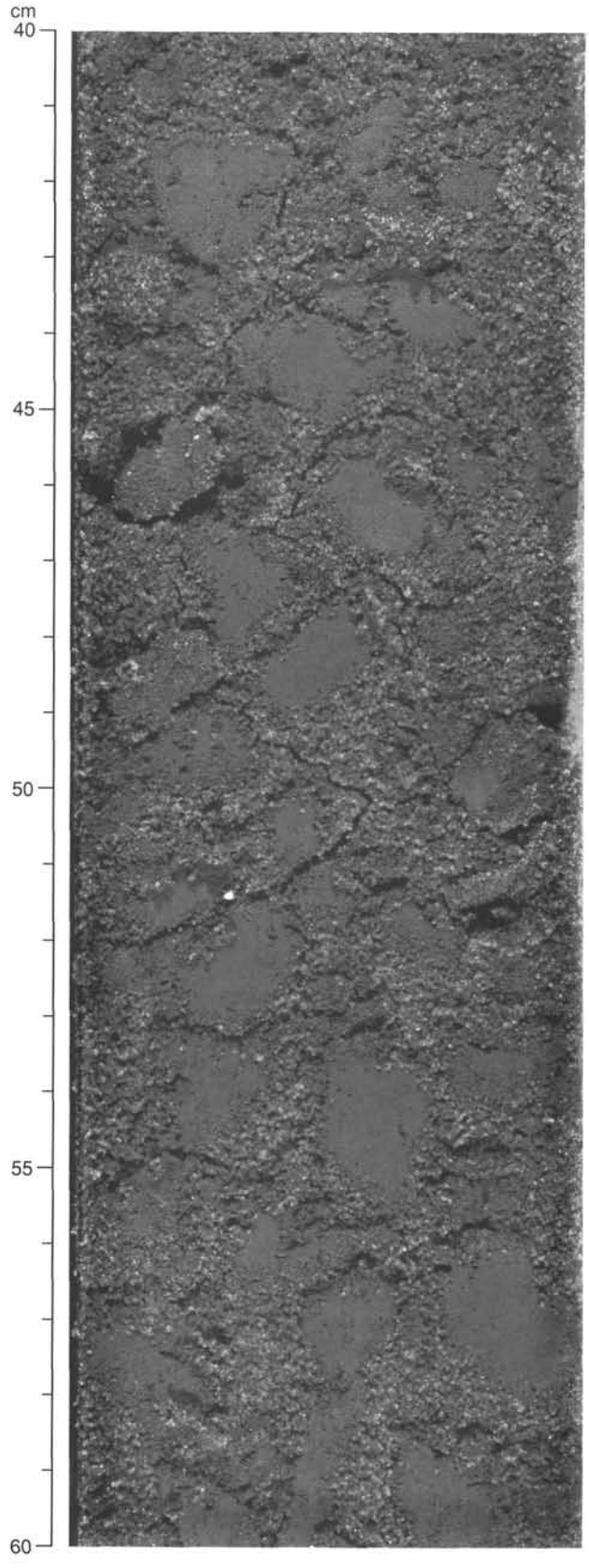

Figure 5. Detail of medium-grained, quartz sand containing subrounded mud clasts; part of a 2.5-m-thick bed at the base of Subunit IA containing normally graded mud clasts (Interval 150-903B-16H-7, 40–60 cm).

Subunit IIA

Interval: Sections 150-903A-32X-4, 45 cm, to -35X-CC
Depth: 273.9–307.5 mbsf

Subunit IIB

Interval: Sections 150-903A-35X-CC to -41X-3, 20 cm
Depth: 307.5–358.9 mbsf

Two very different facies make up Unit II: (1) greenish gray nannofossil silty clays and (2) greenish gray, fine to very coarse, poorly sorted sands, some of which are normally graded and/or contain mud clasts. Coarse-grained packages mark the bases of Subunits IIA and IIB. Overall, Unit II fines upward.

The silty clay facies, which is best developed at the top of the unit and occurs through two main intervals (273.9–298.8 and 307.5–338.2 mbsf), is bioturbated and pyritic, with limited zones containing scattered coarse-sand grains and woody fragments (e.g., 279.7–284.3 mbsf).

The two main levels at which the coarse-grained facies are developed are in the middle (298.8–307.5 mbsf) and at the base (338.2–358.9 mbsf) of the unit. A thin bed of coarse sand also occurs between these at 327.5 mbsf. The uppermost coarse interval (base of Subunit IIA) is 8.7 m thick and has a lower, ungraded portion of silty fine sand with possible climbing ripples and, rarely, centimeter-scale, matrix-supported pebbles. Above this zone is a normally graded silty, fine sand with a sharp base, which contains scattered, very coarse quartz grains. The lowermost coarse interval (base of Subunit IIB) is an impressive, 20-m-thick sand and has within it several upward-fining beds of up to 4 m thickness. These beds typically are poorly sorted and grade from granule-rich coarse sand at the base to medium or fine sand at the top; sporadic, matrix-supported mud clasts, small quartzite pebbles, and other lithic fragments are present. A strong compositional change occurs from highly glauconitic sediment at the base to weakly glauconitic sediment at the top, where abundant red mud clasts, and finer material of the same composition, lend a pink coloration to the sediment. In thin section, the glauconite grains are rounded and fragmented and are probably transported from shallower environments.

The normal grading, together with the occurrence of matrix-supported coarse grains and pebbles, has affinities of both turbidity-current and sandy mass flow (i.e., debris flow) deposition. However, the basal contact is strongly bioturbated, and burrows are recognized at several other levels within this sediment package, implying that many, perhaps all, of the normally graded beds may represent long periods of time rather than near-instantaneous depositional events.

All components in the smear slides for Unit II show abrupt vertical changes coincident with the marked facies changes. Clear trends are observed throughout the unit. Sand content ranges from negligible at the top to 80% at the base. Silt content generally varies from 20% to 40% through the unit, but is estimated at about 80% at the top and <10% at the base. The total quartz and feldspar content shows a trend similar to that of sand, although the downward increase is smoother. Glauconite is generally scarce, but comprises as much as 80% at the base of the lower coarse interval. The XRD analyses of the fine-grained facies (Fig. 7) reveal that amphibole, dolomite, and opal-A are common in Unit II, particularly at the top, down to about 300 mbsf.

Biogenic components are almost entirely calcareous nannofossils in this unit, except for an isolated diatom maximum around 300 mbsf. There are two peaks in the abundance of biogenic components within the fine-grained facies, corresponding to Subunits IIA and IIB. The upper peak is the larger of the two, with a maximum abundance of >20% at about 300 mbsf. In both peaks, there is a steady, near-exponential, downward increase with greatest abundance immediately above the coarse intervals.

Calcite cement occurs in the glauconite sand at intervals between 352 and 358 mbsf, near the base of the subunit. At 352.1 mbsf,

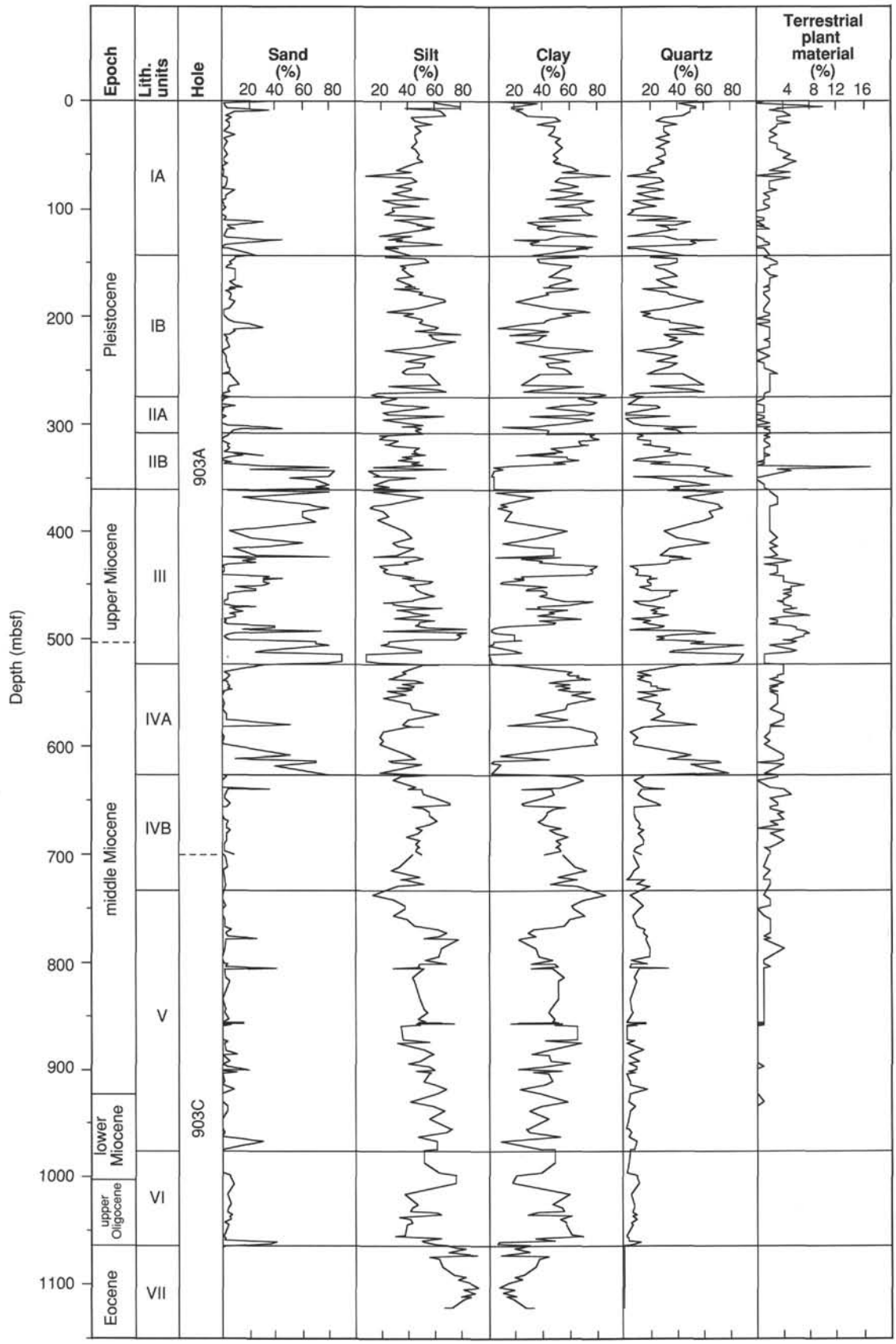

Figure 6. Visual estimates from smear slides of abundances of sand-, silt-, and clay-sized components, quartz, and terrestrial plant material.

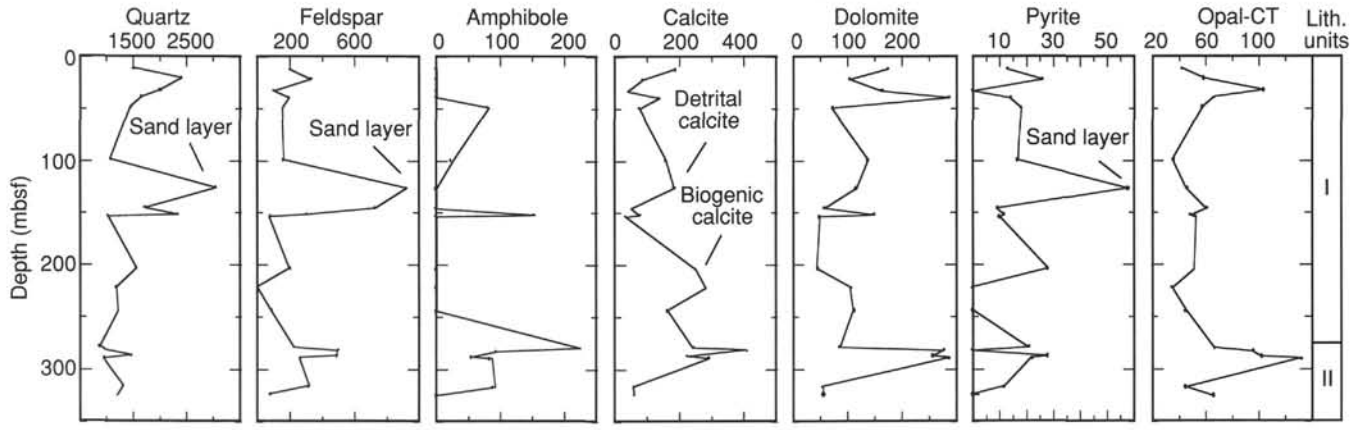

Figure 7. X-ray diffraction analyses for part of Hole 903A plotted according to the intensity of their main diffraction peak: quartz (3.33Å), feldspar (3.25Å), amphibole (8.5Å), calcite (3.03Å), dolomite (2.89Å), pyrite (2.71Å), and opal-CT (4.05Å–4.10Å).

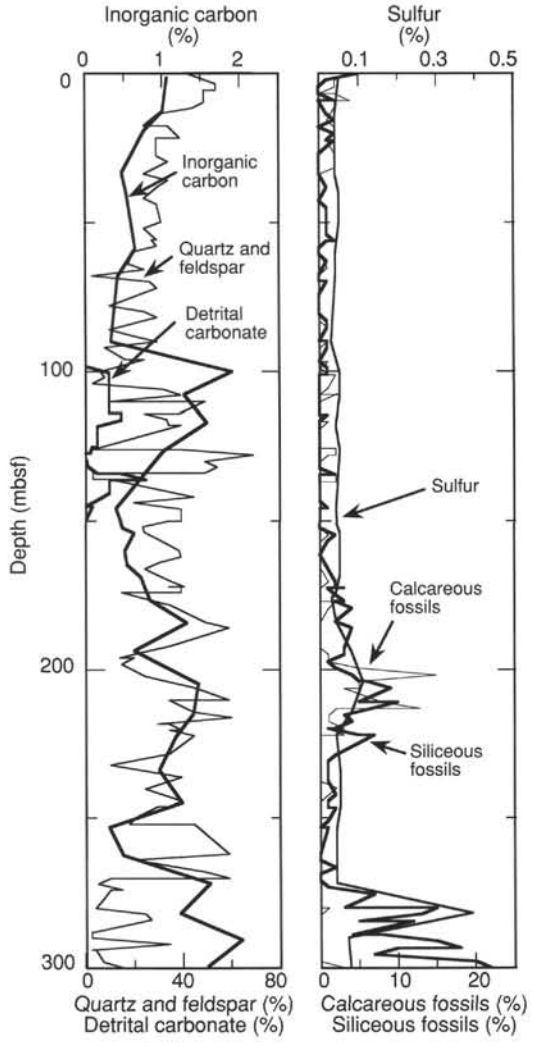

Figure 8. Relationships in Unit I between smear-slide abundance estimates for selected components, and geochemical data (see "Organic Geochemistry" section, this chapter). Inorganic carbon represents carbonate content. See text for discussion.

matrix-supported quartz and glauconite sand is cemented by microcrystalline calcite replacement of the clayey silt matrix. Grain-supported quartz and glauconite sands are similarly cemented at 356.0, 356.6, and 357.8 mbsf. This cementation appears to be precompactional. A calcite vein in the cemented zone at 356.6 mbsf has crustiform, spherulitic clusters of fibrous crystals, typical of early marine cements. An unusual feature of the cemented sands is the occurrence of isopachous calcite cement at the tops and bottoms of grains, but rarely on the sides. This pattern of pressure shadows presumably reflects an ancient stress orientation, possibly related to faulting. The glauconite is typically partially replaced and, rarely, rimmed by pyrite, which postdates the isopachous cement.

Unit III

Intervals: Sections 150-903A-41X-3, 20 cm, to -58X-2, 150 cm; Cores 150-903C-5R-1, 0 cm, to -7R-4, 70 cm
Depth: 358.9–522.9 mbsf (Hole 903A); 358.9–520.5 mbsf (Hole 903C)
Age: upper to middle Miocene

Glauconitic sand intercalated with sparsely glauconitic silty clay characterizes Unit III (Fig. 4). These lithologies are cyclic on a 1 m to >10 m scale. The arenaceous facies has a glauconite component, but quartz and feldspar are not present in all cases. Cream- to buff-colored, centimeter-scale carbonate nodules occur commonly in the silty clay.

The argillaceous facies, as exemplified by the interval from 455 to 465 mbsf, is mostly greenish gray, micaceous, moderately bioturbated silty clay containing abundant, comminuted woody plant fragments and, less commonly, shell fragments. Woody organic detritus is particularly abundant from 495 to 500 mbsf, where it forms crude laminations.

The coarse-grained facies is generally highly glauconitic and typically, though not exclusively, developed as sharp-based beds, with glauconite abundance decreasing gradationally upward from the base. Glauconitic beds are generally 1 to 10 m thick, but they reach a maximum of 16 m between 439 and 455 mbsf. The glauconitic sands are heavily bioturbated and commonly contain scattered coarse quartz sand grains or small pebbles. Plant and shell fragments may also be abundant. At the top and base of Unit III, where quartz and feldspar are more important constituents, no obvious difference is present in the facies from the bulk of the unit, apart from the composition of the relatively coarse fraction.

Smear-slide analyses reveal some clear compositional trends in Unit III. Sand content, although highly variable, is abundant at the

base and top, with a broad minimum between 425 and 475 mbsf. Seven or eight subsidiary peaks in sand abundance occur throughout the subunit and correspond to the lithologic cycles seen in the core. Silt abundance shows a broadly opposing trend to that for sand and reaches a maximum in approximately the same interval as the sand minimum; the detailed structure of the silt curve is as peaky as that of sand, and the largest of these peaks occurs at about 500 mbsf. Clay abundance is the inverse of sand content. Glauconite is highly variable in abundance and ranges as high as 50% or 60% in the middle of the unit; its abundance shows considerably greater fluctuation than that of sand or silt. This trend reflects a more steady input of quartz and feldspar as the subunit was deposited.

Biogenic components are sparse at the top of the unit and increase in abundance downward to about 500 mbsf, where they reach a maximum. This abundance pattern closely parallels that of silt content. In Unit III, diatoms are the principal biogenic component, particularly in the lower part (as much as 25%). Nannofossils comprise <5%, but their abundance curve is similar to that of the diatoms, though more subdued. A rhythmic relationship exists between the abundances of quartz and feldspar, glauconite and biogenic grains with the maximum for each component following sequentially through all of the 1-m- to 10-m-scale glauconitic sand and nonglauconitic silty clay cycles in Unit III.

Morphologic characteristics of the carbonate nodules in Unit III are highly variable. The unifying feature is that all nodules are composed predominantly of calcite, with only rare occurrences of siderite. In general, the nodules are cream to buff colored, with either diffuse or sharp margins, and are found exclusively in the greenish gray, fine-grained facies, at variable depths below the glauconitic sand facies.

The relationship between the nodules and the overlying glauconite sand is clearly observable at 429.4 mbsf, where a large calcite nodule occurs 10 cm below an intensively burrowed surface. Glauconite-filled burrows extend down to within 2 cm of the nodule, but no glauconite occurs in the nodule itself. Small burrows within the nodule are filled with peloidal micrite. Cementation apparently occurred very early and prevented the glauconite-filled burrows from extending into or through this zone. Pyrite-replaced shells and disseminated pyrite also occur in this nodule. Calcite-?dolomite nodules occur at 430.3 and 431.3 mbsf, 90 and 190 cm below the burrowed surface, and are more typical of the subunit. Their close association with the burrowed base of a glauconite sand bed, and their textural and mineralogical characteristics, suggest that accumulation of the glauconite may have been relatively slow, thereby allowing time for a well-developed diagenetic profile to become established. The calcite-pyrite nodule indicates cementation in the sulfate reduction zone, whereas the calcite-?dolomite nodules suggest formation in the carbonate-reduction zone. The XRD analyses indicate an inverse relationship between pyrite and siderite content in Unit III (Fig. 9). Also observed is an alternation of pyrite- and siderite-enriched zones.

A septarian nodule is present at 456.4 mbsf. The body of the nodule is micritic calcite, and thin veins (<1 mm), possibly siderite-filled, occur in the center but do not extend to the margins. This nodule occurs 150 cm below a gradational, heavily bioturbated contact with the overlying bed of glauconitic sand.

Unit IV

Intervals: Sections 150-903A-58X-2, 150 cm, to -76X-CC, 13 cm; Sections 150-903C-7R-4, 70 cm, to -16R-5, 5 cm
Depth: 522.9–733.1 mbsf
Age: middle Miocene

Subunit IVA

Intervals: Sections 150-903A-58X-2, 150 cm, to -68X-6, 112 cm; Sections 150-903C-7R-4, 70 cm, to -11R-CC, 25 cm
Depth: 522.9–624.6 mbsf (Hole 903A); 520.5 mbsf (Hole 903C)

Subunit IVB

Intervals: Sections 150-903A-68X-6, 112 cm, to -76X-CC, 13 cm; Sections 150-903C-12R-1, 0 cm, to -16R-5, 5 cm
Depth: 624.6 (Hole 903A) to 733.1 mbsf (Hole 903C)

Unit IV is relatively nonglauconitic, predominantly argillaceous, and strongly diatomaceous (Fig. 4). A prominent heterolithic interval, partly of slump and debris-flow origin, punctuates the middle of Unit IV (579–624.5 mbsf) defining the base of Subunit IVA. A similar, less pronounced feature is present at the base of the unit (729–733 mbsf) and floors Subunit IVB. As at Sites 902, 904, and 906, one of the main characteristics of Unit IV is the presence of common, cream- to buff-colored nodules and laminae (although these also occur abundantly in Unit III, and so are not diagnostic).

The fine-grained facies are greenish gray and brownish gray, silty clays, slightly to moderately bioturbated. *Chondrites* is common and *Planolites* less so. Carbonate shell fragments occur uncommonly in the lower half.

The heterolithic facies in the middle of Unit IV has a lithologic range from glauconitic sand to slump-folded silty clay and is broadly upward-fining. In detail, two intervals of glauconitic sand each overlie an interval of slump and debris-flow deposits with intervening muddy horizons. The glauconitic sands are present as half-meter- to meter-scale beds, the higher ones showing a gradation from strongly glauconitic sand at the base to weakly glauconitic silty clays at the top; the lower glauconitic sand package is less systematically constructed. Moderate bioturbation occurs throughout the sand, and burrowers have piped material downward into the finer sediment below. These glauconitic sands are, in essence, identical to those described from Unit III.

Several different slumps and debris flows are resolvable; the uppermost redeposited interval occurs between 602.5 and 604.5 mbsf at Hole 902C, which was spot-cored because the equivalent level was not recovered at Hole 902A. At a lower level, slump/debris-flow and burrowed, coarse sand occur between 621.0 and 624.5 mbsf in Hole 903A. The sand is poorly sorted and contains fine to coarse lithic fragments and small pebbles. Spectacular contorted strata form a basal, 1-m-thick bed of poorly sorted sand with medium- to granule-sized grains and common silty sandstone and mud clasts. These strata sit with a sharp, unburrowed contact on the underlying bioturbated silty clay and represent the base of Subunit IVA.

Redeposited strata similar to those just described occur throughout a 4-m-thick section from 729 to 733 mbsf at Hole 903C and mark the base of Unit IV and Subunit IVB. This basal package is noteworthy in that the upper half is cross-cut by many high-angle, soft-sediment faults with normal offsets of less than 1 cm (Fig. 10). The lithology is a thinly interbedded sandy silt and silty clay with abundant quartz and mica sand and minor flaky plant debris. The lower half of the package is a matrix-supported conglomerate with tabular gray-green pebbles and small cobbles of mud in a contorted matrix of clayey silt.

Smear-slide analyses indicate that sand is scarce in Unit IV, except between 600 and 625 mbsf, described above, where it reaches 80%. Silt is moderately abundant throughout, ranging from 20% to 60%. Clay content is high at the top of the unit, decreasing erratically downward to near zero at 625 mbsf; an abrupt increase occurs below this level and from there down, clay content remains high to near the base of the unit.

Biogenic components in this unit are most abundant where sand is scarce, particularly in the lower half between 625 and 700 mbsf. Below this level, biogenic component abundance drops back to nearly zero at 725–740 mbsf, coincident with the redeposited strata near the base. Diatoms are overwhelmingly the most abundant biogenic component, reaching a maximum of ~40% of all constituents from 650 to 670 mbsf. The inverse relationship between biogenic abundance and redeposition is very striking and is independent of grain size. Thus, a likely explanation is that biogenic abundance is reduced as a result of dilution

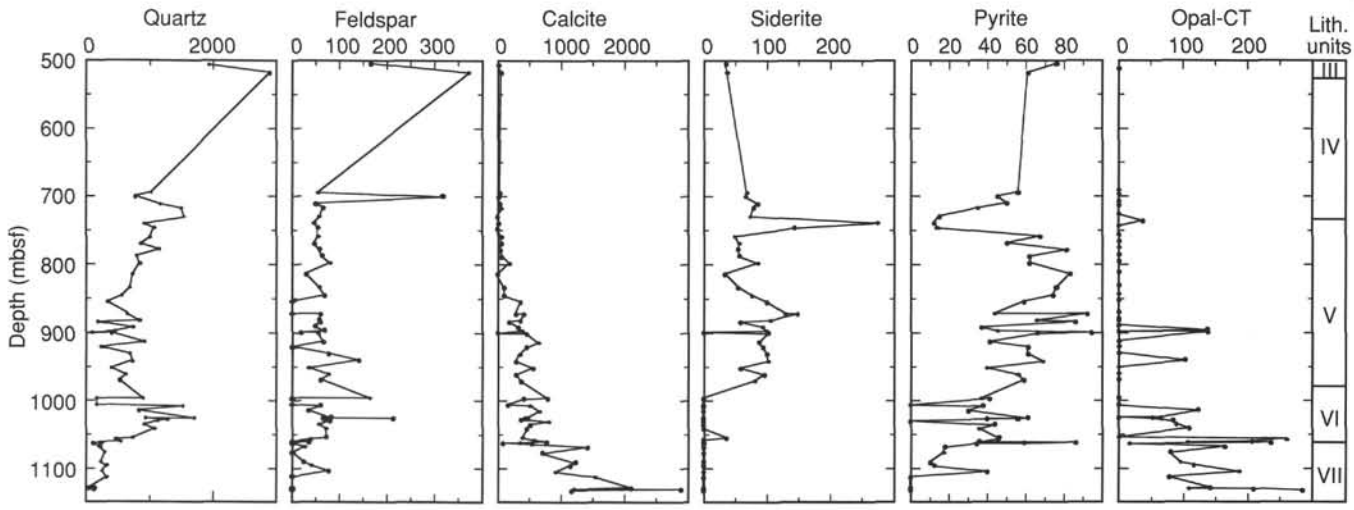

Figure 9. X-ray diffraction analyses for Hole 903C plotted according to the intensity of the mineral's main diffraction peak: quartz (3.33Å), feldspar (3.25Å), amphibole (8.5Å), calcite (3.03Å), siderite (2.8Å), pyrite (2.71Å), and opal-CT (4.05Å–4.10Å).

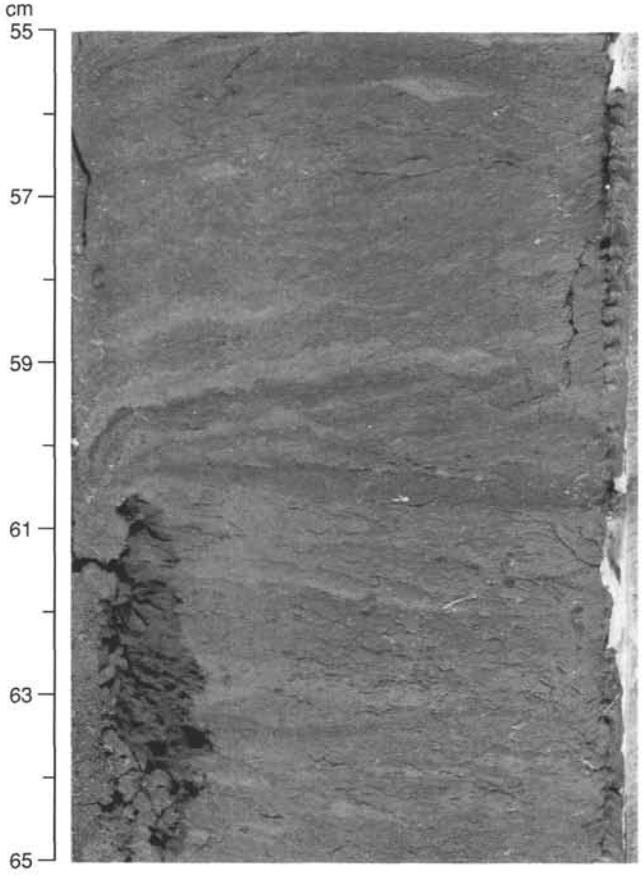

Figure 10. Microfaults with normal offsets cutting laminated silty clay and very fine sand near the base of Unit IV (Interval 150-903C-16R-3, 55–65 cm).

at the site of deposition during periods of high depositional rates (times of mass wasting) compounded by low biogenic abundance at the site from which redeposited sediment was derived.

The carbonate nodules are ~1 to 10 cm across, have either sharp or diffuse boundaries, and are cream to buff colored. They are very similar to the carbonate nodules of Unit III and presumably have a similar origin. The XRD analyses indicate an inverse relationship between pyrite and siderite content, as observed in Unit III. The XRD data from the lower part of the unit (Fig. 9) indicate the occurrence of quartz and minor feldspar and confirm the low calcite content.

Unit V

Intervals: Sections 150-903C-16R-5, 5 cm, to -41R-5, 90 cm; Sections 150-903D-1R-1, 0 cm, to -19R-2, 7 cm
Depths: 733.1–974.4 mbsf (Hole 903C); 733.1–977.5 mbsf (Hole 903D)
Age: middle to lower Miocene

Unit V is a highly diatomaceous silty clay, more glauconitic than Unit IV above and relatively organic-rich. Meter-scale glauconitic sand beds occur sporadically. Nannofossil abundance increases downsection. Core recovery over the interval of Unit V is complementary for Holes 903C and 903D, although individually they give a poor record of the stratigraphy. Correlation between these holes has been made at three horizons: (1) intervals with distinctive trace fossils in Cores 150-903C-29R and 150-903D-9R; (2) a ~1-m-thick dolomite cemented bed in Cores 150-903C-37R and 150-903D-18R; and (3) a dark green glauconitic sandstone in Cores 150-903C-41R and 150-903D-19R. These correlations, although not robust, imply that the given depths for Hole 903C are between 3 and 6 m too shallow, relative to those for Hole 903D.

Brown to greenish gray, silty claystone with slight to moderate bioturbation predominates. Highly comminuted woody plant material is visible at the top of the unit, and foraminifers occur scattered toward the base. Many burrows are well preserved and include, in rough order of abundance, *Chondrites, Planolites, Zoophycos, Thalassinoides, Teichichnus, Terebellina,* and *Phycosiphon.* Between 940 and 960 mbsf at Hole 903C (e.g., Fig. 11), a zone of interbedded dark brown and light brown silty clays shows excellently preserved trace fossils where light material has been piped into dark. Locally, near the top of the unit, thin layers are observed in which burrows are absent and no recognizable macroscopic trace fossils exist. Instead, these intervals show a fine, millimeter-scale lamination suggestive of moderately dysaerobic bottom waters (766.3–766.4 mbsf at Hole 903C). Total organic carbon (TOC) data (see "Organic Geochemistry" section, this chapter) show maximum values of 3.0% to 3.5%, somewhat lower in the succession (820–1000 mbsf at Hole 903C), where laminated facies were not recorded. However, TOC samples are widely spaced and none were taken from the thin, laminated intervals at the top of the unit. Hence, TOC values may well be high in the discrete, laminated hori-

zons. Pyrite, determined by XRD analysis, is a common mineral through this unit, but has its maximum abundance higher in the succession than does TOC.

The coarse facies comprises glauconitic silty sandstones with fine sand-sized glauconite grains arranged in upward-fining cycles. These tend to be sharp-based and very similar to those seen commonly in Unit III and sporadically in Unit IV.

Smear-slide analysis confirms that little sand-sized sediment is present in the recovered sections of Unit V; most of the quartz and feldspar are silt-sized grains (Figs. 3 and 6). The clay-sized fraction shows a steady downward decrease as the combined siliceous and calcareous biogenic components increase. Diatoms dominate the biogenic fraction, particularly in the middle of this unit; they range from 0% to 40%. Nannofossils are relatively rare at the top of the unit (<5%) but show a gentle increase downward, reaching ~20% at the base. Woody plant material persists in small amounts, down to about 855 mbsf, below which its occurrence is patchy.

Three kinds of cementation are observed in Unit V: (1) siderite + calcite, (2) dolomite/ankerite, and (3) probable calcite. The siderite + calcite nodules and laminae occur from the top of the unit to 758 mbsf in Hole 903C and are identical to the nodules in Units III and IV (see above).

Dolomite/ankerite cementation is observed mainly in the diatom-rich silty claystones, where dolomite/ankerite-cemented zones occur between 859.5 and 860.3 mbsf and between 933.1 and 934 mbsf at Hole 903C. Within the cemented zones, the clayey matrix has been replaced by clean, 50–100 µm, euhedral, rhombic dolomite/ankerite crystals, zoned from Fe^{2+}-poor cores to Fe^{2+}-rich rims. There is also a high porosity and permeability because of the open packing of the dolomite crystals. The high diatom content of this lithology is reflected as fragments of diatoms included within the dolomite crystals and in the intercrystalline voids.

Dolomite/ankerite cementation also occurs at the base of a bed of glauconitic sand at 900 mbsf at Hole 903C. A thin-section was prepared from a drilling-abraded pebble from the top of the subjacent core (Core 150-903C-34R). The silty matrix, which supports the glauconite and medium quartz sand in this bed, is replaced by zoned, rhombic dolomite/ankerite, and the siliceous fossils, diatoms, and radiolarians are incorporated and displaced. Sand-sized glauconite occurs as well-rounded and angular grains, both forms thought to be transported; the rounded grains have shrinkage cracks and alteration rims. Rare radiolarians are partly to totally replaced by light green glauconite.

A late carbonate cement occurs at the bottom of Unit V, at the bases of two upward-fining glauconitic sand cycles. The depositional characteristics of the host sediment are very similar to the dolomite/ankerite-cemented bed described above, but the cements are very different. At 957.5 mbsf in Hole 903C, and, to a lesser extent, at 974.3 mbsf in Hole 903C, glauconite sand lying directly above a burrowed contact is cemented. Neither direct thin-section observation nor staining with Alizarin Red and potassium ferricyanide were able to indicate the mineralogy conclusively; the mineral reacts sluggishly with acid. The sand grains show clear signs of compaction, such as fractured and embayed grain/grain contacts between glauconite and bedding-parallel foliations that wrap around grains.

Unit VI

Intervals: Sections 150-903C-41R-5, 90 cm, to -51R-CC, 20 cm; Sections 150-903D-19R-2, 7 cm, to -25R-CC, 16 cm
Depth: 974.4–1064.1 mbsf (Hole 903C); 977.4–1037.0 mbsf (Hole 903D)
Age: lower Miocene to upper Oligocene

Core recovery for Unit VI was generally poor, with the best between 1020.5 and 1040.5 mbsf and from 1054.5 mbsf to the base in Hole 903C, and from 978.0 to 1006.0 mbsf in Hole 903D (Fig. 4). The unit is predominantly argillaceous, except in the basal 3 m at Hole 903C, where glauconitic siltstone and sandstone are present. Sand-sized glauconite is also present in the silty claystone at about 1000.5 mbsf at Hole 903D. For the most part, the unit comprises brown gray, slightly to moderately bioturbated silty claystone with minor glauconite. Foraminifers are commonly scattered throughout and become abundant at the base. Solitary corals occur between 990 and 1005 mbsf at Hole 903D (Cores 150-903D-20R to -21R). Burrows include *Chondrites, Planolites, Thalassinoides,* and *Zoophycos.* The

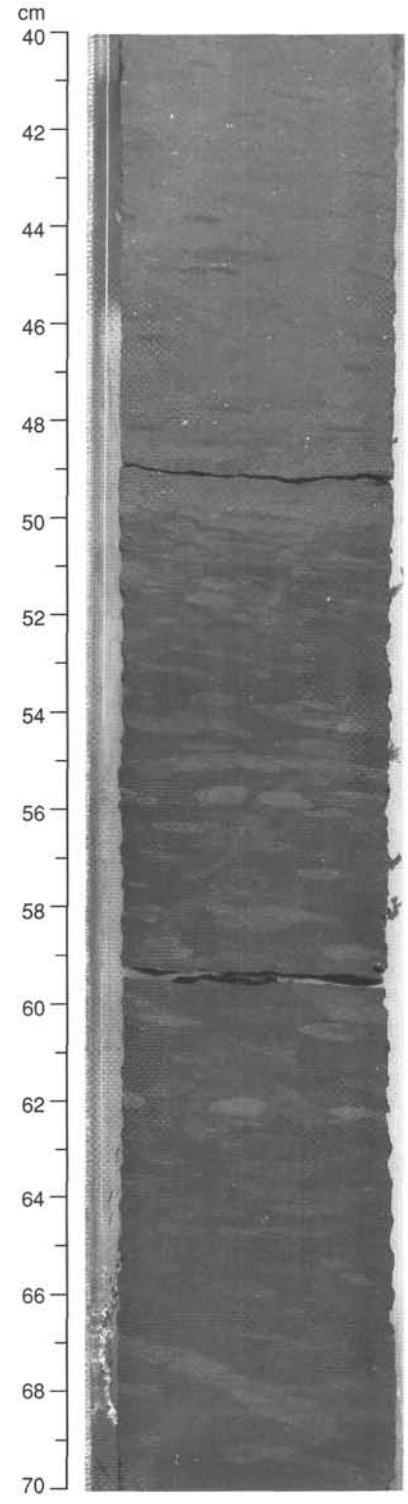

Figure 11. Light brown silty clays piped down into dark brown silty clays showing excellent preservation of *Planolites* and, at 55 cm and 67–69 cm, *Zoophycos* (Interval 150-903C-39R-5, 40–70 cm).

coarse glauconitic sand facies at the base (1061.6–1064.3 mbsf at Hole 903C) contains shell fragments and is heavily bioturbated and well cemented.

Smear slides indicate that diatoms decrease in abundance downward as they are dissolved and reprecipitated as opal-CT (Figs. 3 and 9). Calcareous nannofossils remain around 20% through the unit. Woody organic material is absent. The XRD data reveal that quartz, presumably detrital, is more abundant in this unit than in those above and below (Fig. 9).

The cementation in Unit VI is very similar to that described for Unit V, except that siderite+calcite nodules are absent. Dolomite/ankerite-cemented, slightly glauconitic silty clay occurs at 997.4 and 1006.9 mbsf in Hole 903C, and at 1006 and 1026 mbsf in Hole 903D. The basal 3 m of Unit VI is cemented as is the base of Unit V and displays similar compactional fabrics. An important difference is the presence of opal-CT, filling foraminifer tests, and possibly acting as a cement. The silica may be derived from fossils within the base of Unit VI or it may originate from silica-bearing fluids migrating from the underlying Eocene chalks.

The basal contact is an abrupt lithologic change from dark glauconitic sand above to light gray chalks below: the contact lies between cores in this hole and was not observed, but it is likely to be similar to that seen at Sites 902 and 904.

Unit VII

Interval: Cores 150-903C-52R-1, 0 cm, to -60R-CC, 17 cm
Depth: 1064.1–1150.0 mbsf
Age: upper Eocene

This unit is composed of light gray nannofossil chalk with clay and foraminifers and is porcellanitic (opal-CT) toward the base. In the middle of the unit is a complex 60-cm-thick zone of early carbonate cementation, glauconite concentration and siliciclastic deposition, suggestive of condensation (low net sediment accumulation).

The chalks are heavily bioturbated: *Chondrites* and *Planolites* are common and *Zoophycos* uncommon. *Chondrites* are picked out by having a darker gray fill of more clay-rich or pyritic sediment. Glauconite-rich sediment fills *Planolites* down to 30 cm below the top of the unit, a relationship that was not observed at the equivalent level at Site 902. Smear-slide data show that nannofossils range from 40% to 80% in the upper part of this unit, reaching a peak abundance of ~80% at ~1110 mbsf, coincident with the putative condensed section alluded to above. Below this level, nannofossil abundance decreases to about 50% or less in the zone of porcellanitic chalks. This abundance pattern may be largely diagenetic in origin and relate to dissolution.

The atypical, possibly condensed, facies occurs between 1109.3 and 1109.9 mbsf. This is most simply described in two parts: one below and one above a sharp contact at 1109.4 mbsf that has siliciclastic sediment above and carbonate below. The lithologic sequence is very similar to that recovered at Site 904 where microtektites are abundant at a horizon correlative to the contact. The lower zone is 54 cm thick and is similar to the normal chalks of this unit, except that foraminifers are unusually abundant and a 3-cm-thick carbonate nodule, ~10 cm above the base of this zone, preserves uncompacted burrows (Fig. 12). The remainder of this highly calcareous interval also has a weak nodular aspect, with localized centimeter-scale more cemented lenses resisting strong compaction. This zone is clearly bioturbated, and scattered glauconite grains occur toward the top. The contact with the overlying siliciclastic portion is disturbed by drilling. A probable burrow structure, 5 cm below the contact, contains a pyritic inner part and an orange-red outer part, a color suggestive of iron oxyhydroxide.

Above the contact, a 6-cm-thick, green-gray silt and very fine sand horizon with parallel laminations of 1 to 2 mm thickness is present. At 0.5 cm above the contact, the sediment is penetrated by a narrow (<0.5 cm diameter), cylindrical burrow, filled with speckled, medium

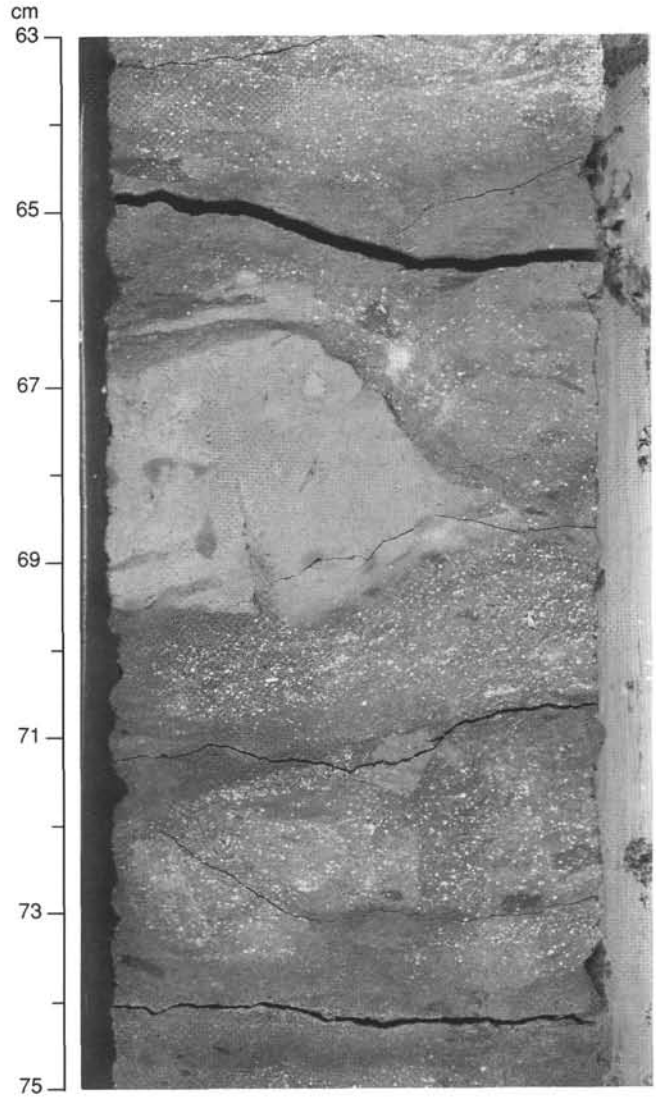

Figure 12. Early diagenetic carbonate nodule in foraminifer nannofossil clayey chalks, 40 cm below the microtektite horizon in Unit IV (Interval 150-903C-56R-6, 63–75 cm).

quartz sand identical to that yielding microtektites at Site 904 (microtektites have also been recognized tentatively from this level at Site 903). Anastomosed within the bed, between 1 and 2 cm above the contact, is a gray, fine sand in stringers, 1 to 2 mm thick, dominantly parallel to the laminae of the host sediment, but apparently truncating them locally. Relationships of this kind are commonly observed as a result of liquefaction of buried, uncompacted, and loose sediment when loaded or shocked. The top of the laminated bed is intercalated by burrowing with the overlying argillaceous chalk. Another unusual feature here, which may be unconnected with those described above, is a light gray to white, 2-cm-thick bed of poorly preserved nannofossils at 1108.7 mbsf.

In the upper 30 cm of Unit VII, petrographic observations show that the matrix is composed of euhedral to subhedral, intergrown dolomite-rhombs (30–70 μm in size). Foraminifer tests are well preserved, but they constitute less than 5%. Minor mineral components are glauconite (~4%) and pyrite (~1%).

Throughout the whole unit, the chalks are weakly to strongly silicified, as is revealed by the presence of opal-CT in the XRD

analyses (Fig. 9). Dissolution of tests of siliceous organisms (opal-A) appears to be the origin of the opal-CT (diagenetic silica). Test relics (40–100 µm and possibly diatoms) constitute 20%–30% of the sediment, and they are filled with opal-CT. Foraminifer tests are mostly well preserved, although some are etched, pitted, or fragmented. They are common (10%–20%) in the upper part of the section where their chambers are partially to completely filled by opal-CT. Increased silica diagenesis is evident downward, particularly at 1105 mbsf where an abundance of silica is present in the matrix. This increase in opal-CT corresponds to an increase in bulk density (see "Physical Properties" section, this chapter). From 1105 mbsf downward, diagenetic silica decreases slightly and sparry calcite cement becomes the dominant cement within foraminifer tests. Pyrite occurs throughout the unit in small quantities.

Microfracturing is prevalent throughout the unit, primarily subparallel to depositional bedding planes. Fractures are unmineralized, except around 1090 mbsf where they are filled with chert and, in less abundance, calcite.

BIOSTRATIGRAPHY

Summary

A 1149.7-m-thick, discontinuous middle Eocene to Pleistocene section was recovered at Site 903. Nearly 1000 m of Neogene silty clay and fine sand overlie silty diatomaceous sediment and silty claystone. The Oligocene and Eocene sediments are less than 200 m thick and consist of silty claystone overlying Eocene chalk (see "Lithostratigraphy" section, this chapter). Calcareous microfossils (foraminifers and calcareous nannofossils) are present in upper Neogene sediments (the latter group occurring more consistently), but they give way to more diatom-rich sediments in the upper Miocene. Calcareous nannofossils provide the primary age control in the upper Neogene, diatoms and dinocysts provide control for the middle Miocene and part of the upper Miocene. The latter two are sparse in the lower Miocene to Eocene and calcareous microfossils are the primary source of age data for the Oligocene and Eocene. Benthic foraminifers indicate that the region around Site 903 was at middle bathyal depths (600–1000 m) during the Eocene and Oligocene, and at upper bathyal depths (200–600 m) during much of the Neogene; this region received mixed middle and upper bathyal assemblages during the Pliocene and Pleistocene.

Four holes were drilled and cored at Site 903. Maximum penetration was achieved at Hole 903C, which reached a depth of 1149.7 mbsf. The four sites combined yielded a discontinuous Cenozoic section extending from the Holocene to the middle Eocene. Hole 903A (Cores 150-903A-1H to -76X; 0–702.8 mbsf) was terminated in the middle Miocene and Hole 903B (Cores 150-903B-1H to -17H; 0–154.0 mbsf) in the middle Pleistocene. Hole 903C was spot cored through the upper and upper middle Miocene (Cores 150-903C-5R to 150-903C-8R; 505.61–534.6 mbsf; Cores 150-903C-9R to -11R, 586.1–611.5 mbsf) and then continuously cored from Cores 150-903C-12R to -60R (688.6–1149.7 m) before terminating in the middle Eocene. Hole 903D was washed to 774.9 mbsf, continuously cored to 948 mbsf (Core 150-903D-18R), washed to 977.0 mbsf, and cored to a total depth of 1037.0 mbsf (Core 150-903D-25R).

Samples 150-903A-1H-CC to -40X-CC (0–355.7 mbsf; primarily lithologic Units I and II; see "Lithostratigraphy" section, this chapter) belong to the Pleistocene and Pliocene. This assignment is suggested by sparse diatom data (no diagnostic-age indicators but the floral aspect is modern), but the clear evidence is provided by the calcareous nannofossils. Samples 150-903A-1H-CC to -39X-CC (9.5–363.40 mbsf) belong, from youngest to oldest, to the *E. huxleyi* Acme Zone (uppermost Zone NN21), and to Zones NN21, NN20, and NN19, suggesting that a reasonably continuous uppermost Neogene section is present in this hole. This is supported by the planktonic foraminifers, which indicate that the Pleistocene extends from Samples 150-903A-1H-CC to -38X-CC (9.5–336.4 mbsf). Similarly, pollen and dinoflagellate cysts from Samples 150-903A-1H-CC to -37X-CC (9.5–326.7 mbsf) indicate a Pliocene to modern aspect for the assemblage. Upper or middle Pliocene and uppermost Miocene sediments were recovered from Core 150-903A-40X-CC to about Section 150-903A-45X-CC (352.3–399.8 mbsf). This placement is largely based on dinoflagellate cysts with support from planktonic foraminifers and calcareous nannofossils. From Samples 150-903A-47X-CC to -76X-CC (423.3–702.8 mbsf), no age-diagnostic nannofossils were recovered, and age determinations are largely derived from dinoflagellate cysts and diatoms with some contribution from planktonic foraminifers. These microfossil groups are used to assign Samples 150-903A-48X-CC to -76X-CC (433.0–702.8 mbsf) to the lowermost upper and upper middle Miocene.

Sections 150-903B-1H-CC to -17H-CC duplicated the upper 154 m of Hole 903A and cover the uppermost part of the Pleistocene. Calcareous nannofossils indicate that sediment was deposited within the past 474 k.y. (Zone NN20 and younger; younger than *P. lacunosa* LAD). Planktonic foraminifers and dinoflagellate cysts were not examined in this hole, and the diatoms, when present, are nondiagnostic.

Whereas calcareous nannofossils are generally not age-diagnostic in upper Miocene sediments of Hole 903C, dinocysts and diatoms provide useful stratigraphic controls. This is also true for middle Miocene sediments with occasional support from the planktonic foraminifers. Biostratigraphic data from the diatoms do not preclude the presence of middle Miocene hiatuses. Below the middle Miocene, the siliceous microfossil assemblages become increasingly sparse and the sediment is more carbonate rich. The increasing abundance of calcareous nannofossils downcore enhances their utility in assigning ages; they are common to abundant below Sample 150-903C-28R-CC (846.39 mbsf). Samples 150-903C-28R-CC to -44R-CC (846.39–998.8 mbsf) are assigned to the middle and lower Miocene, whereas Samples 150-903C-45R-CC to -52R-1, 3 cm (1010.2–1064.4 mbsf), can be confidently placed in the upper Oligocene. Sediments below this level to the bottom of Hole 903C (1064.4–1149.7 mbsf) are assigned to the upper and middle Eocene. A summary of zones delineated in this chapter are in Table 3.

Planktonic Foraminifers

Hole 903A penetrated a thick Pleistocene section extending downward from Sample 150-903A-1H-CC through at least -38X-CC at 336.2 mbsf. The latter sample is the stratigraphically lowest verifiable Pleistocene sample based on planktonic foraminifer evidence (co-occurrence of *Globorotalia tosaensis,* and *G. truncatulinoides*). *Globorotalia truncatulinoides* had an FAD just before the Olduvai Subchron at 1.9 Ma (BKV85). As at Site 902, the most common and persistent Pleistocene taxa include *Neogloboquadrina pachyderma* (cold-water indicator), *Globigerina bulloides,* and *Globorotalia inflata* (cool-temperate water indicators), and *Globigerinoides ruber* and *Globorotalia truncatulinoides* (warm-water indicators). Variations in the relative abundance of these three groups are used to infer glacial/interglacial patterns. Samples 150-903A-1H-CC through -8H-CC (76.0 mbsf) reflect cool-water conditions, which were preceded by a glacial interval at 85.5 mbsf in Sample 150-903A-9H-CC (Fig. 13). Alternating warm and cool faunas characterize the interval from Sample 150-903A-11H-CC through -18H-CC (104.5–160.0 mbsf), preceded by a cold interval at 164.5 mbsf in Sample 150-903A-19H-CC. Warm-water faunas at 150-903A-21X-CC and -24X-CC (172.8 and 201.4 mbsf) alternate with cool-water faunas at 150-903A-22X-CC and -27X-CC (182.3 and 230.3 mbsf). Predominantly warm-water faunas are consistently present from Section 150-903A-29X-CC at 249.7 mbsf through Section 150-903A-38X-CC at 336.4 mbsf. Full interglacial intervals are inferred at Samples 150-903A-32X-CC to -33X-CC from 278.5 through 288.2 mbsf and at Samples 150-903A-37X-CC to -38X-CC (326.7–336.4 mbsf; Fig. 13). Cool-water faunas mark Sample 150-903A-39X-CC at 346.0 mbsf, but this sample contains only long-ranging species and so cannot be unequivocally assigned to the Pleistocene.

Table 3. Biostratigraphic zonations and datum levels, Site 903.

Zone (base unless specified) and/or datum level	Code	Sample number	Depth (mbsf)
NN21	Cn	150-903A-10H-CC	95.00
NN20	Cn	150-903A-32X-CC	278.50
LO *G. truncatulinoides*	Pf	150-903A-38X-CC	336.20
NN19	Cn	150-903A-39X-CC	346.00
Pleistocene	Df	150-903A-39X-CC	
NN17–NN18	Cn	150-903A-40X-CC	355.00
N16–N17	Pf	150-903A-44X-CC	394.95
NN10	Cn	150-903A-41X-CC to 150-903A-47X-CC	362.95 to 423.32
Dinocyst Zone H	Df	150-903A-50X-CC	451.37
HO *T. grunowii*	Dm	150-903A-51X-CC	462.10
middle Miocene	Pf	150-903A-59X-CC to 150-903A-62X-CC	539.18 to 568.29
HO *D. punctata hustedtii*	Dm	150-903A-62X-CC	568.29
N6–N12	Pf	150-903A-65X-CC	596.42
Dinocyst Zone G	Df	150-903A-68X-CC	625.74
Dinocyst Zone F*	Df	150-903A-76X-CC*	702.70
middle Miocene	Pf	150-903C-5R-CC	508.45
HO *T. grunowii*	Dm	150-903C-5R-CC	
Dinocyst Zone G	Df	150-903C-10R-5, 83–88 cm	598.98
N10–N12	Pf	150-903C-14R-CC	715.52
HO *D. punctata hustedtii*	Dm	150-903C-18R-CC	751.08
N11–N12	Pf	150-903C-19R-CC	762.49
Dinocyst Zone F	Df	150-903C-22R-CC	794.76
Dinocyst Zone E	Df	150-903C-25R-CC	819.18
NN6	Cn	150-903C-12R-CC to 150-903C-27R-CC	695.71 to 834.65
Dinocyst Zone D	Df	150-903C-28R-CC	846.39
Dinocyst Zone C	Df	150-903C-32R-CC	886.51
LO *R. barboi*	Dm	150-903C-32R-CC	903.06
NN5	Cn	150-903C-28R-CC to 150-903C-34R-CC	846.39 to 903.06
HO *C. lewisianus*	Dm	150-903C-34R-CC	920.42
NN4	Cn	150-903C-36R-CC	923.64
Dinocyst Zone B	Df	150-903C-38R-CC	948.38
Dinocyst Zone A	Df	150-903C-39R-CC	957.66
NN2	Cn	150-903C-44R-CC	998.80
NN1	Cn	150-903C-43R-CC to 150-903C-44R-CC	986.97 to 998.80
Dinocyst Zone pre-A	Df	150-903C-45R-CC	1010.14
NP25	Cn	150-903C-48R-CC	1033.83
Oligocene	Df	150-903C-48R-CC	
Upper Oligocene	Pf	150-903C-47R-CC to 150-903C-51R-CC	1027.00 to 1064.34
NP23	Cn	150-903C-51R-CC	1064.34
NP19–20	Cn	150-903C-52R-1, 3 cm	1064.13
P16–P17	Pf	150-903C-52R-CC to 150-903C-55R-CC	1072.95 to 1101.78
P16	Pf	150-903C-53R-CC to 150-903C-55R-CC	1080.89 to 1101.78
P15	Pf	150-903C-56R-CC	1112.40
NP18	Cn	150-903C-57R-2, 1 cm	1113.01
NP17	Cn	150-903C-58R-CC	1131.06
NP16	Cn	150-903C-60R-CC	1149.05
P14	Pf	150-903C-57R-CC to 150-903C-60R-CC	1117.59 to 1149.95
N9–N10	Pf	150-903D-1R-CC	777.10
HO *C. lewisianus*	Dm	150-903D-7R-CC	842.64
NN6–lower NN7	Cn	150-903D-7R-CC	
N10–N11	Pf	150-903D-13R-CC	894.73
NN5	Cn	150-903D-15R-CC	917.55
NN4	Cn	150-903D-18R-CC	948.07
NN3	Cn	150-903D-20R-CC	996.84
NN2	Cn	150-903D-20R-CC	
NP25	Cn	150-903D-25R-CC	1037.29
P22	Pf	150-903D-25R-CC	

Note: An asterisk (*) means that the datum level was not reached and is below the lowest sample. Dm = diatom, Cn = calcareous nannofossil, Df = dinocyst, and Pf = planktonic foraminifer. HO = highest occurrence, LO = lowest occurrence.

Samples 150-903A-40X-CC through -42X-3, 122–124 cm (355.7–369.64 mbsf), are barren. Only a single, fragmented specimen of *Globigerinoides obliquus obliquus,* a species which ranges from Zones N8 to N19 (Bolli and Saunders, 1985), was encountered in Sample 150-903A-43X-CC at 384.6 mbsf. Age-diagnostic planktonic foraminifer assemblages were next encountered at 394.3 mbsf in Sample 150-903A-44X-CC where a modestly diverse fauna can be constrained to Zones N16–N17 based on the co-occurrence of *Globigerina nepenthes* (FAD in Chron 5; BKV85), *Neogloboquadrina pachyderma* (FAD in Zone N16; Kennett and Srinivasan, 1983), and *Globorotalia conoidea* (LAD in Zone N17; Kennett and Srinivasan, 1983). A very sparse fauna (*Globorotalia menardii* and *Globigerina bulloides*) in Sample 150-903A-46X-CC at 413.7 mbsf is not age diagnostic, and the stratigraphic interval from Sample 150-903A-47X-CC through -58X-CC (423.3–529.5 mbsf) is barren.

The section from 539.18 to 568.29 mbsf (Samples 150-903A-59X-CC, -60X-CC, -61X-7, 43–45 cm, -61X-CC, and -62X-CC) is middle Miocene (note that at Hole 903C middle Miocene planktonic foraminifers occur at 510.3 mbsf; see below). Although the assemblages in Sample 150-903A-59X-CC and -60X-CC cannot be constrained more precisely, those in the last three samples indicate Zones N10–N12. These samples contain *Globorotalia praemenardii,* which ranges in Zones N10–N12 (Bolli and Saunders, 1985), and *Globorotalia mayeri,* which has its LAD at the top of Zone N14 (BKV85). Other, longer ranging species include *Orbulina universa, Globigerina woodi, Neogloboquadrina continuosa, Sphaeroidinellopsis seminulina,* and *Globorotalia obesa.* Sample 150-903A-65X-CC at 596.42 mbsf contains an assemblage that can be constrained to the middle lower to middle middle Miocene (roughly Zones N6 to N12). Core-catcher samples from Core 150-903A-66X (606.3 mbsf) to the bottom at 702.8 mbsf are barren.

Planktonic foraminifers were not examined in sediments from Hole 903B, which resampled the Pleistocene to a depth of 154.0 mbsf.

At Hole 903C, Cores 150-903C-1R through -4R had no recovery. Sample 150-903C-5R-CC at 508.45 mbsf yielded a middle Miocene assemblage containing *Orbulina universa, Neogloboquadrina continuosa, Globigerina woodi,* and *Globorotalia miozea.* This association cannot be constrained more precisely than the interval from Zones N9 to N14. The interval from Sample 150-903C-6R-CC through -13R-CC is either barren or yielded sparse faunas of long-ranging species that do not provide precise age assignment. A more extensive planktonic foraminifer assemblage was encountered at 715.52 mbsf in Sample 150-903C-14R-CC. Assignment to the N10–N12 zonal interval is indicated by the presence of *Globorotalia praemenardii* (Kennett and Srinivasan, 1983). Other species in the sample include *Globorotalia mayeri, G. acrostoma,* and *Sphaeroidinellopsis seminulina seminulina.* Samples 150-903C-16R-CC and -17R-CC are barren. Sample 150-903C-18R-CC at 751.08 mbsf contains only longer ranging species that do not constrain the age more precisely than middle Miocene. An age-diagnostic fauna was encountered at 702.49 mbsf in Sample 150-903C-19R-CC. In addition to *Globorotalia praemenardii* and *G. acrostoma, Globorotalia fohsi fohsi* is present. The FAD of *G. fohsi fohsi* marks the boundary between Zones N11 and N12 (Blow, 1979). Zhang et al. (1993), using the recorrelation of Site 563 by Wright and Miller (1992), estimate the FAD of *G. fohsi fohsi* at 12.6 Ma.

Planktonic foraminifers are either absent or extremely sparse in Samples 150-903C-20R-CC through -46R-CC (775.78–1016 mbsf), and the assemblages are composed only of long-ranging species.

With the exception of Sample 150-903C-49R-CC (1044.8 mbsf), which is barren, the interval from Samples 150-903C-47R-CC through -51R-CC (1027.00–1064.34 mbsf) contains assemblages assignable to the upper Oligocene. Abundant species throughout this interval include *Catapsydrax unicavus, C. dissimilis, Globigerina euapertura, Globoquadrina venezuelana,* and *Globorotalia opima nana.* The last species has an LAD in middle Zone P22 (Kennett and Srinivasan, 1983; Bolli and Saunders, 1985), so its presence, along with the absence of any diagnostic early Oligocene taxa, may indicate upper Oligocene. However, Miller et al. (1989) reported its LAD in lower Miocene Zone N4. There is no planktonic foraminifer faunal evidence of lower Oligocene sediments in Hole 903C.

Rich and diverse Eocene assemblages occur downward from Sample 150-903C-52R-CC at 1072.95 mbsf to total depth at 1149.7 mbsf. Samples 150-903C-52R-CC through -55R-CC (1072.95–1101.78 mbsf) are assignable to Zones P16–P17 based on the presence of *Hantkenina* cf. *H. alabamensis* and *Globorotalia cerroazulensis cocoaensis* (both with an LAD in Chron C13 at 36.6 Ma; BKF85). Other age-diagnostic species include *Globorotalia cerroazulensis cerro-*

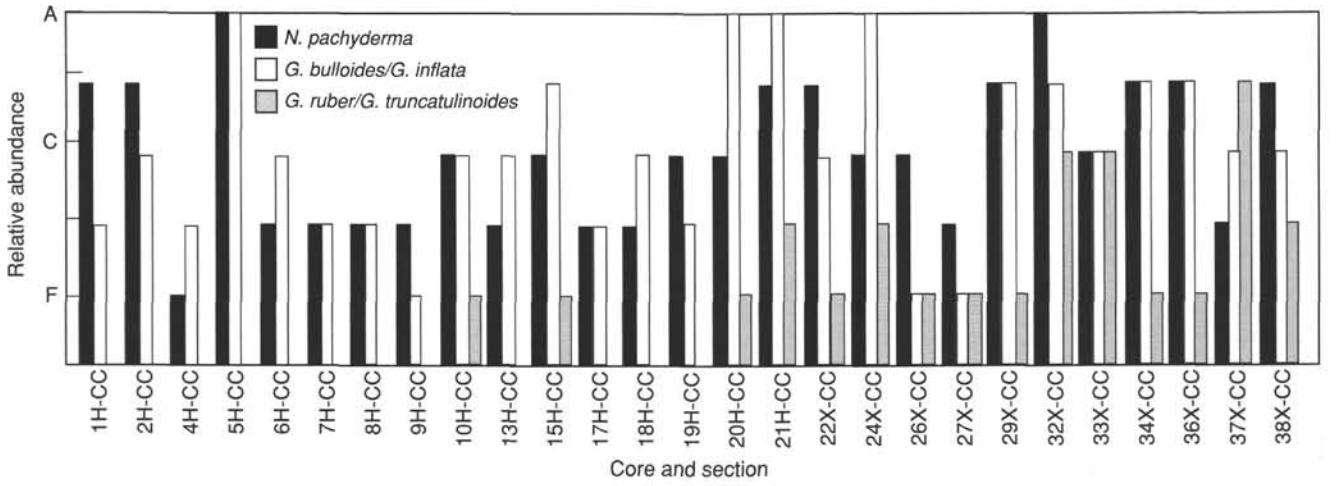

Figure 13. Relative abundances of selected groups of planktonic foraminifers indicating cold, cool temperate, and warm waters during the Pleistocene in Hole 903A. A = abundant, C = common, and F = few.

azulensis, G. cerroazulensis pomeroli, and *Globigerina corpulenta.* Numerically abundant but longer ranging taxa are *Catapsydrax unicavus, Chiloguembelina* spp., *Globigerina eocaena,* and *Pseudohastigerina micra.* The co-occurrence with this assemblage of *Globigerinatheka index,* which ranges in Zones P11 to P16 (Toumarkine and Luterbacher, 1985) suggests that Samples 150-903C-53R-CC through -55R-CC (1080.89–1101.78 mbsf) can be constrained to Zone P16. Sample 150-903C-56R-CC at 1112.4 mbsf is assigned to Zone P15 based on the presence of *Hantkenina liebusi* (with an LAD in mid P15; Stainforth et al., 1975) and the absence of *G. cerroazulensis cocoaensis* from the *Globorotalia cerroazulensis* complex. Middle Eocene sediments assignable to Zone P14 were encountered in Sample 150-903C-57R-CC at 1117.59 mbsf. Species of both *Acarinina* and *Morozovella* (LADs in Chron C17 at 40.6 Ma; BKF85) are common. Age-diagnostic species include *Acarinina bullbrooki, A. spinuloinflata, Globigerinatheka mexicana mexicana, Morozovella lehneri,* and *Truncorotaloides collactea.* Other common taxa are *Globigerinatheka index, G. mexicana barri, G. subconglobata,* and *Globorotalia cerroazulensis pomeroli.* Assemblages assignable to Zone P14 persist through Sample 150-903C-60R-CC at 1149.95 mbsf.

Hole 903D, intended to retrieve portions of the Oligocene-Miocene section poorly recovered at Hole 903C, was washed to 776.4 mbsf. The core-catcher sample from the initial core (150-903D-1R-CC at 777.1 mbsf) yielded a lower middle Miocene fauna including *Sphaeroidinellopsis seminulina, Globorotalia siakensis, G. peripheroronda,* and *Orbulina universa.* The FAD of *Orbulina universa* in Chron C5B at 15.2 Ma (BKV85; Zhang et al., 1993) and the LAD of *Globorotalia peripheroronda* in Chron C5AD at 14.6 Ma (BKV85) constrain the age of this sample to the N9–N10 zonal interval. Although some authors (Stainforth et al., 1975) recognize that *G. peripheroronda* ranges in younger zones, we consider that the assignment of this faunal association to the lower middle Miocene (N9–N11 zonal interval) is based on the absence of more advanced species of the *G. fohsi* lineage.

Samples from immediately underlying cores are either barren of planktonic foraminifers or contain sparse faunas that are not age diagnostic. Samples 150-903D-2R-CC, -4R-CC, -5R-CC, -6R-CC, -7R-CC, and -10R-CC are barren. Samples 150-903D-3R-CC (801.28 mbsf), -8R-CC (851.64 mbsf), -9R-CC (861.78 mbsf), -11R-CC (878.9 mbsf), and -12R-CC (881.65 mbsf) contain species that, at best, broadly constrain their ages to middle Miocene. Foraminifers in these samples consist almost exclusively of heavily calcified tests that are resistant to dissolution. *Globorotalia acrostoma, Sphaeroidinellopsis seminulina* (usually decorticated), and *Globorotalia miozea* are particularly prominent. Sample 150-903D-13R-CC at 894.73 mbsf contains a slightly more diverse fauna. Its assignment to the N10–N11 zonal interval is based primarily on the presence of *Globorotalia peripheroacuta* with an FAD at 14.1 Ma (Zhang et al., 1993) and an LAD in Zone N11 (Kennett and Srinivasan, 1983). Associated species in this sample include *Globigerina woodi, Globorotalia miozea, G. peripheroronda, G. continuosa,* and *Globigerinoides subquadratus.* Sample 150-903D-14R-CC at 909.6 mbsf contains a sparse fauna that cannot constrain its age more precisely than early Miocene to early middle Miocene. Samples 150-903D-15R-CC at 917.5 mbsf through -18R-CC at 948.07 mbsf are barren of planktonic foraminifers. No cores were recovered from 948.0 to 977.0 mbsf. Samples 150-903D-19R-CC at 983.7 mbsf and -20R-CC at 996.8 mbsf are barren.

Sample 150-903D-21R-CC at 1006.2 mbsf contains a few recrystallized, sediment-encrusted specimens that are difficult to identify. The presence of forms transitional from *Globorotalia opima nana* and *G. continuosa* suggests proximity to the Oligocene/Miocene boundary. However, the age may be as old as late Oligocene or as young as early Miocene. No core-catcher sample was available from Core 150-903D-22R, and the small volume of Sample 150-903D-23R-CC at 1015.6 mbsf precluded processing. The sparse fauna from Sample 150-903D-24R-CC at 1028.7 mbsf does not constrain the age more precisely than Oligocene to early Miocene. Sample 150-903D-25R-CC at 1037.29 mbsf contains an assemblage assignable to the upper Oligocene (possibly Zone P22) based on the presence of *Subbotina tripartita* and *Globorotalia opima nana.*

Benthic Foraminifers

Benthic foraminifer assemblages were used to identify episodes of transported and in situ sedimentation in the Pleistocene section. Displaced faunas dominate in Pleistocene sediments. No strictly in situ assemblages were identified, although mixed assemblages of transported and possibly in situ faunas were found. Analysis focused on the thick (~350 m) Pleistocene interval recovered at Hole 903A. Water depth at Hole 903A is 444.5 m (upper bathyal); therefore, the presence of neritic (0–200 m) benthic foraminifers in high relative abundances indicates downslope transport. Common elements of the transported faunas include shelf species such as *Buccella frigida, Cassidulina* sp., *Cibicides lobatulus, Cibicides* spp., *Elphidium* spp., *Fursenkoina* sp., *Islandiella* spp., and miliolids. Interpretation of this fauna as having been transported during glacial intervals is corroborated by the co-occurrence of cool-water planktonic foraminifer assemblages.

Deeper water (outer neritic–upper bathyal) taxa such as *Bulimina marginata, Bulimina aculeata,* and *Melonis barleeanum* occur in association with low abundances of shallower water fauna such as *Elphidium* spp. within an overall higher diversity assemblage. The

presence of *Bulimina marginata* (<30–~480 m; van Morkhoven et al., 1986) and transitional forms of *Bulimina marginata/Bulimina aculeata* (>400 m; van Morkhoven et al., 1986) may indicate in situ deposition. *Bulimina marginata* is found in greatest abundances on the western Atlantic margin in the outer shelf–upper slope regions (Miller and Lohmann, 1982). *Bulimina aculeata* is found on the western Atlantic margin at greatest relative abundances between 400 and 1000 m (Miller and Lohmann, 1982). High relative abundances of *B. marginata* may indicate in situ deposition; however, other upper bathyal species such as *Cibicidoides mundulus* are absent from the assemblage. In addition, the similarity of this fauna at Site 903 to the transported fauna at Site 902, where the water depth (811 m) is greater than the lower depth limit of *B. marginata,* is consistent with transport. Therefore, the Pleistocene assemblages at Site 903 are regarded as transported with possible in situ components, although these in situ components (e.g., *B. marginata*) do not have a paleodepth unique to the upper bathyal region. Interpretation of assemblages with low abundances of *Elphidium* spp. and other associated shelf species as interglacial is corroborated by warm planktonic foraminifer assemblages.

Glacial assemblages were differentiated from interglacial assemblages primarily by high relative abundances of *Elphidium* spp. High relative percentages of *Elphidium* spp. have long been associated with inner neritic (<30 m) depths. *Elphidium* spp. are present on the slope of the western North Atlantic (Streeter and Lavery, 1982), although not in the high abundances noted on the shelf (see "Biostratigraphy" section, "Site 902" chapter, for further discussion). This interpretation is corroborated by association with cold-water planktonic fauna. Additional support for the transported interpretation includes the presence of wood fragments, echinoid spines, glauconite, subangular to angular quartz sand grains, and high percentages of mica and the absence of in situ elements, in addition to a more diverse benthic fauna.

Samples 150-903A-47X-CC through -59X-CC (423.3–539.2 mbsf; middle Miocene) contained no benthic foraminifers.

Miocene samples examined from Cores 150-903A-60X through -66X (548.9–606.3 mbsf) are characterized by abundant *Uvigerina juncea* (up to 100%) and foraminifer tests with fair preservation. In addition to *Uvigerina juncea,* there are rare specimens of *Lagena* spp., *Lenticulina* spp., and *Planulina* spp. in Samples 150-903A-60X-CC through -63X-CC (423.3–577.5 mbsf). Faunas in Samples 150-903A-64X-CC through -66X-CC (587.1–606.3 mbsf) yielded more diverse assemblages in addition to abundant *Uvigerina juncea,* including *Bulimina elongata, Cibicidoides* spp., *Dentalina* spp., *Globobulimina* sp., *Globocassidulina subglobosa, Lagena* spp., *Lenticulina* spp., *Martinotiella* sp., *Melonis barleeanum,* miliolids, *Nonionellina* sp., *Planulina* spp., *Stilostomella* spp., and *Textularia* sp. These *Uvigerina juncea*-dominated assemblages represent transported shelf faunas. Sample 150-903A-73X-CC (673.8 mbsf) also contained a primarily transported benthic foraminifer assemblage that includes *Bulimina elongata, Cassidulina* sp., *Cibicidoides* sp., *Cibicidoides mundulus, Globobulimina* sp., *Lenticulina* spp., *Martinotiella* sp., and *Melonis barleeanum.*

Core-catcher samples from Cores 150-903A-68X, -69X, -72X, -74X, and -75X (625.6–693.1 mbsf) were either barren or contained rare benthic foraminifers with moderate preservation, including *Bulimina elongata, Lenticulina* spp., *Martinotiella* sp., and *Stilostomella* spp. Sample 150-903A-76X-CC (702.8 mbsf) yielded an in situ upper bathyal (200-600 m) benthic foraminifer fauna including *Bulimina macilenta, Bulimina* spp., *Globobulimina* sp., *Globocassidulina* sp., *Lenticulina* spp., *Oridorsalis* sp., and *Stilostomella* spp. *Cibicidoides mundulus* indicates an upper depth limit of 200 m on this sample, whereas *Cibicidoides crebbsi* places the lower paleodepth limit at 600 m.

Core-catcher samples from Cores 150-903C-6R, -10R, -11R, -25R, and -32R (515.3–891.1 mbsf) were barren. Many of the other Miocene core-catcher samples (Cores 150-903C-5R through -46R; 510.3–1025.5 mbsf) yielded impoverished benthic foraminifer faunas that contained no conclusively depth diagnostic taxa; however, paleobathymetric estimates were made for several samples in this interval based on in situ benthic foraminifers. Taxa found scattered through the Miocene section include *Bolivina* sp., *Bulimina alazanensis, Bulimina elongata, Bulimina* sp., *Cassidulina* sp., *Cassidulinoides* sp., *Chilostomella* sp., *Fissurina* sp., *Globocassidulina subglobosa, Lenticulina* spp., *Martinotiella* sp., *Nonionellina* sp., *Stilostomella* spp., *Textularia* spp., and *Uvigerina* spp. The most accurate paleodepth estimate is provided by *Cibicidoides crebbsi* in Samples 150-903C-14R-CC (717.2 mbsf) and -19R-CC (765.9 mbsf), indicating an upper bathyal depth (200–600 m; van Morkhoven et al., 1986). Other species scattered through the Miocene section that together indicate upper to middle bathyal depths include *Cibicidoides pachyderma, Cibicidoides mundulus, Hanzawaia mantaensis, Hoeglundina elegans, Plectofrondicularia parri,* and *Siphonina tenuicarinata* (van Morkhoven et al., 1986).

Benthic foraminifer preservation is fair to good in the upper Oligocene core-catcher samples examined from Hole 903C (Samples 150-903C-47R-CC to -51R-CC; 1029.1–1064.1 mbsf). These samples contained *Alabamina* spp., *Anomalinoides* spp., *Bolivina* spp., *Bulimina macilenta, Cibicidoides* spp., *Globocassidulina subglobosa, Gyroidinoides* spp., *Lenticulina* spp., *Martinotiella* sp., *Melonis barleeanum, Melonis pompilioides, Nonion havanensis, Planulina* spp., *Plectofrondicularia* spp., polymorphinids, *Pullenia bulloides, Pullenia quinqueloba,* miliolids, *Sphaeroidina bulloides, Stilostomella* spp., and *Uvigerina* spp. This fauna is consistent with the bathyal depth indicated by the presence of *Cibicidoides mundulus* and *Planulina costata.* In addition, Sample 150-903C-51R-CC (1064.1 mbsf) contains *Anomalinoides semicribratus,* indicating that the paleodepth may have been >600 m (van Morkhoven et al., 1986) in this part of the section.

Eocene benthic foraminifer assemblages contain more diverse *Cibicidoides* spp. than the overlying section, and agglutinated taxa become more diverse downhole within the Eocene section. Benthic foraminifer tests display recrystallization in this section, particularly in and below Core 150-903C-57R (1121.1 mbsf). Eocene bathyal assemblages (Samples 150-903C-52R-CC to -60R-CC; 1073.8–1149.7 mbsf) include *Alabamina* spp., *Anomalinoides* sp., *Aragonia aragonensis, Bolivinopsis* sp., *Bulimina alazanensis, Bulimina macilenta, Cibicidoides bradyi, Cibicidoides eocaenus, Cibicidoides micrus, Cibicidoides* spp., *Dentalina* spp., *Dorothia* spp., *Globobulimina* sp., *Gyroidinoides* spp., *Fissurina* spp., *Karreriella* spp., *Lagena* spp., *Lenticulina* spp., *Marginulina* spp., miliolids, *Nonion* sp., *Oridorsalis* sp., *Osangularia* sp., *Planulina costata, Plectina nuttali, Plectofrondicularia* sp., *Pleurostomella* spp., pleurostomellids, polymorphinids, *Pullenia bulloides, Pullenia quinqueloba, Pullenia eocenica, Sigmoilopsis schlumbergeri, Siphonina* sp., *Stilostomella* spp., *Textularia* sp., *Tritaxia* spp., *Uvigerina havanensis, Uvigerina* spp., and *Vulvulina* sp. *Cibicidoides truncanus* is common in the Eocene section at Hole 903C, indicating an upper depth limit of 200 m (van Morkhoven et al., 1986). In addition, occurrences of *Anomalinoides capitatus* and *Anomalinoides semicribratus* at Hole 903C indicate that the paleodepth was likely >600 m (van Morkhoven et al., 1986) during the Eocene.

Miocene core-catcher samples from Hole 903D also contained upper bathyal (200–600 m) benthic foraminifer assemblages that are similar to those described from Hole 903C. The upper bathyal indicator *Cibicidoides crebbsi* is common from Sample 150-903D-1R-CC through -18R-CC. Samples 150-903D-19R-CC and -20R-CC are barren. Below this, benthic foraminifers indicate upper to middle bathyal paleodepths.

Thus, Eocene to lowermost Oligocene assemblages indicate that the paleodepth was >600 m at Site 903. Site 903 was within the upper bathyal zone (200–600 m) by the Miocene (Samples 150-903C-19R-CC; 765.9 mbsf); however, sparse benthic foraminifer faunas and the discontinuous stratigraphic record make it difficult to estimate exactly when shallowing to the upper bathyal zone occurred. Trans-

ported benthic foraminifers from the shelf are ubiquitous in the Pleistocene and common in the Miocene, whereas evidence for transport was minimal in Oligocene and Eocene benthic foraminifer assemblages. This trend in downslope transport reflects the change in shelf morphology from an Eocene carbonate-dominated ramp-type margin (Olsson and Wise, 1987) to a Miocene siliciclastic-dominated progradational margin. Overall shallowing and increased downslope transport accompanied the change from thick, lower Miocene, progradational clinoforms that lie beneath the present-day inner shelf to more distal clinoforms that developed near the present-day shelf edge in the Pleistocene in conjunction with the canyon cutting on the slope.

Calcareous Nannofossils

Calcareous nannofossils are present intermittently in the Pleistocene through middle Miocene sediments, which consist chiefly of siliciclastic mud often with abundant diatoms and other siliceous microfossils. These sediments yielded mostly poor assemblages, often lacking marker species and consisting almost entirely of long-ranging species. Good fossil recovery was achieved from the lower Miocene, Oligocene, and upper and middle Eocene calcareous muds and clayey chalks.

Hole 903A

The cored interval at the top of Hole 903A extends from the upper Pleistocene to the middle Miocene in Core 150-903A-52X (471.6 m). Further downhole, only long-ranging Neogene species were recovered; these do not permit a definitive zonal assignment of the lower twenty cores of this hole (down to 202.6 mbsf). *Emiliania huxleyi* is the dominant species in Sample 150-903A-1H-CC (9.5 mbsf) and this level may be assigned to the *Emiliania huxleyi* Acme Zone with an age no greater than 73–85 k.y. (oxygen isotope stage 5). From Samples 150-903A-2H-CC (19 mbsf) to -10H-CC (95 mbsf), *Emiliania huxleyi* is present but in low numbers, identifying this interval as the *Emiliania huxleyi* Zone (NN21). The lower limit of this zone, the lowest occurrence of *Emiliania huxleyi* (95 mbsf), has an age of 285 k.y. (oxygen isotope stage 8). Below this level, a variety of *Gephyrocapsa* morphotypes are the most consistent element of the low-diversity assemblages. They indicate the next lower Pleistocene nannofossil zone, the *Gephyrocapsa oceanica* Zone (NN20). The lower limit of that zone corresponds to the highest occurrence of *Pseudoemiliania lacunosa* in Sample 150-903A-32X-CC (278.5 mbsf); this level has an age no older than 474 k.y. (oxygen isotope stage 12). The next lower zone, the *Pseudoemiliania lacunosa* Zone (NN19), extends downward to Sample 150-903A-39X-CC (346.0 mbsf), but its lower limit cannot be constrained owing to very poor nannofossil recovery over this interval. Sample 150-903A-38X-CC (336.4 mbsf) and within Core 150-903A-39X (336.4–346.0 mbsf) yield reworked Paleocene and Eocene taxa, indicating significant erosion and redeposition.

The zonal assignment of Sample 150-903A-40X-CC (355 mbsf) is debatable. It is assigned to Zone NN15 (middle Pliocene) by SG based on the occurrence of *Discoaster brouweri, Sphenolithus abies, Calcidiscus leptoporus, Coccolithus pelagicus, Reticulofenestra pseudoumbilicus, Helicosphaera parallela, Helicosphaera carteri, Discoaster* (6 rays), *Discoaster pentaradiatus, Discoaster variabilis,* and *Discoaster surculus.* The assemblages have been interpreted to be of mid-Pliocene age, assuming that *Helicosphaera parallela* (= *?Helicosphaera intermedia*) are redeposited or represent an undocumented morphotype; that *Sphenolithus verensis* is actually the very similar *Sphenolithus abies;* and that *Discoaster triradiatus* is an aberrant *Discoaster brouweri,* a morphotype that is encountered rarely throughout the range of the latter. This same sample is questionably assigned to Zones NN17–NN18 by MPA based on the presence of *D. brouweri, D. pentaradiatus, D. triradiatus, Pseudoemiliania lacunosa,* and *Reticulofenestra* sp. cf. *R. pseudoumbilicus.* The rare specimens of *R. pseudoumbilicus, S. neoabies, D. challengeri,* and *H.* sp. cf. *H. intermedia* in this sample are regarded as reworked.

Sample 150-903A-41X-CC (365.4 mbsf) and -47X-CC, 30–32 cm (423 mbsf) contains sporadic, diverse, but very rare nannofossil species, all suggestive of an early late Miocene age. Included among these species are *Reticulofenestra pseudoumbilicus, Discoaster brouweri, D. brouweri rutellus, D. neohamatus, D. variabilis, Discoaster* sp. cf. *D. bellus, D. challengeri,* a form very similar to *D. asymmetricus, Discoaster* sp. cf. *D. bollii, Discoaster* sp. c. *D. loeblichii,* and *Discoaster* sp. cf. *D. prepentaradiatus.* The co-occurrence of *D. brouweri* and *D. bollii* strongly suggest assignment to the *Discoaster calcaris* Zone (NN10) with an age of about 8.2 to 8.85 Ma.

From Sample 150-903A-47X-CC, 47 cm, to -76X-CC, no age-diagnostic nannofossils were recovered. Rare placoliths are present, but their generic assignment is mostly uncertain.

Hole 903B

Hole 903B duplicates the upper 154 m of Hole 903A. *Emiliania huxleyi* was recovered from Sample 150-903B-1H-CC (2 mbsf) through -11H-CC (97.0 mbsf). This is very close to the level at which the lowest occurrence of this species was observed in Hole 903A. The core-catcher samples from Cores 150-903B-12H through -17H (154 mbsf) yielded middle Pleistocene nannofossil assemblages without *Emiliania huxleyi* and without *Pseudoemiliania lacunosa,* thus indicating Zone NN20 and an age range for this interval from 275 to 474 k.y. Coring was terminated at Core 150-903B-17H (154.0 mbsf).

Hole 903C

Samples 150-903C-5R-CC (508.45 mbsf) and -7R-CC (523.42 mbsf) yielded scarce calcareous nannofossil assemblages without stratigraphic significance (with *Calcidiscus macintyrei, Helicosphaera carteri, Reticulofenestra pseudoumbilicus*), and Samples 150-903C-6R-CC (510.99 mbsf) and -8R-CC (525.11 mbsf) were barren. There is a 61.39-m gap in recovery between Cores 150-903C-8R-CC (525.11 mbsf) and -9R-CC (586.50 mbsf). Six samples from Core 150-903C-11R were barren. Sample 150-903C-10R-CC (600.07 mbsf) yielded only scarce specimens of *Reticulofenestra pseudoumbilicus.* A 77-m drilled interval separates Core 150-903C-11R from Core 150-903C-12R, resulting in a 83.84-m recovery gap between Samples 150-903C-11R-CC and -12R-1 (604.84 and 688.60 mbsf). Coring was continuous below Core 150-903C-12R (698.2 mbsf) down to the bottom of the hole.

With the exception of Samples 150-903C-16R-CC and -17R-CC (733.38 and 744.15 mbsf), which are barren, all samples taken from 150-903C-12R-CC (695.71 mbsf) to -27R-CC (834.65 mbsf) yielded rare to common, moderately preserved calcareous nannofossils. Although of low diversity, the assemblages, which yielded *Coccolithus miopelagicus, Discoaster exilis, D. sanmiguelensis, Helicosphaera carteri, Reticulofenestra floridana,* and *R. pseudoumbilicus,* suggest that the interval between Samples 150-903C-12R-CC and -27R-CC (695.71–834.65 mbsf) is middle Miocene (possibly equivalent in its lower part to Zone NN6).

Calcareous nannofossils were common to abundant below 846.39 mbsf (Sample 150-903C-28R-CC). They allow a firm biozonal subdivision of the lower part of Hole 903C (Cores 150-903C-28R to -60R; 834.65–1149.95 mbsf), except between Sample 150-903C-37R-CC and -44R-CC (939.20–998.90 mbsf). The interval between Sample 150-903C-28R-CC and -34R-CC (846.39–903.06 mbsf) belongs to Zone NN5. In addition to *Sphenolithus heteromorphus,* the assemblages yield *Coccolithus miopelagicus, Discoaster exilis, D. petaliformis, D. sanmiguelensis,* and *Reticulofenestra pseudoumbilicus.* Samples 150-903C-35R-CC (920.42 mbsf) and -36R-CC (923.64 mbsf) yielded similar assemblages with the addition of *Helicosphaera ampliaperta.* They are assigned to Zone NN4.

Samples 150-903C-37R-CC to -44R-CC (939.20–998.80 mbsf) yielded low-diversity, moderately preserved assemblages. Their stratigraphic position is difficult to determine in the absence of marker species. Samples 150-903C-38X-CC to -40R-CC (948.38–966.35 mbsf) yielded *Helicosphaera ampliaperta, H. scissura, Sphenolithus conicus,* and *S. delphix. Discoaster druggii* occurred in Samples 150-903C-40R-CC to -44R-CC (966.35–998.80 mbsf), but no specimens of *Triquetrorhabdulus carinatus* were encountered in these samples. Considering the absence of *Sphenolithus belemnos,* and the presence of *D. druggii, Sphenolithus* aff. *S. belemnos* (Sample 150-903C-44R-CC, 998.80 mbsf), and *S. capricornutus* (Sample 150-903C-43R-CC, 986.97 mbsf), the interval between Cores 150-903C-37R and -44R (939.20–998.80 mbsf) is tentatively assigned to Zone NN2 (MPA). The alternative interpretation of SG is that Samples 150-903C-43R-CC and -44R-CC belong to Zone NN1 based on the occurrence of *Dictyocoaites abisectus* and the absence of *Discoaster druggii. Sphenolithus* aff.(?) *S. belemnos* is identified as *Sphenolithus dissimilis* by SG.

Sample 150-903C-45R-CC (1010.14 mbsf) yielded a late Oligocene assemblage with *Ilselithina fusa* (rare), *Reticulofenestra abisecta* (common), *R. bisecta* (rare), *R. floridana* (abundant), *Sphenolithus ciperoensis* (very rare), and *Triquetrorhabdulus carinatus* (rare). This sample is assigned to Zone NP25, which extends down to Sample 150-903C-48R-CC (1035.1 mbsf). The interval between Samples 150-903C-49R-CC and -51R-CC (1045.06–1064.1 mbsf), is assigned to Zone NP23 based on the absence of *S. ciperoensis. Sphenolithus predistentus* is common; *S. distentus* very rare. A similar nannofossil assemblage is found in Sample 150-903C-51R-CC, 2 cm. However, the top 2 cm of Section 150-903C-52R-1 contains Oligocene sediments piped into chalk (see "Core Photographs," this chapter), and it is not certain that this level is Oligocene. Sample 150-903C-52R-1, 3 cm (1064.13 mbsf), yielded a late Eocene assemblage with *Chiasmolithus oamaruensis, Discoaster barbadiensis, D. saipanensis, Isthmolithus recurvus,* but without *Reticulofenestra reticulata.* This indicates the upper part of Zone NP19–20. The highest occurrence of *R. reticulata* is in Sample 150-903C-53R-CC (1080.89 mbsf). The lowest occurrence of *Isthmolithus recurvus* in Sample 150-903C-56R-CC (1112.40 mbsf) indicates that the NP18/NP19–20 zonal boundary occurs between this sample and Sample 150-903C-57R-1, 140 cm (1111.48 mbsf). Zone NP18 extends between this latter sample and Sample 150-903C-57R-2, 1 cm (1113.01 mbsf); Zone NP17 extends between Samples 150-903C-57R-CC and -58R-CC (1117.59–1131.06 mbsf). Zone NP16 extends between Samples 150-903C-59R-CC and -60R-CC (1136.50 and 1149.95 mbsf).

A layer thought to be correlative with the microtektite layer recovered from nearby DSDP Site 612 (Poag, Watts, et al., 1987) was encountered in Section 150-903C-56R-5 (1107.64–1109.14 mbsf) in the lower part of the upper Eocene Zone NP19–20.

Hole 903D

Except for the drilled interval between 948.0 and 977.0 mbsf (between Cores 150-903D-18R and -19R), Hole 903D duplicated the middle Miocene to upper Oligocene section that was poorly recovered from Hole 903C between 774.0 and 1037 mbsf (Core 150-903D-1R to -25R). The calcareous nannofossil zonal succession in Hole 903D is similar to that in Hole 903C. Calcareous nannofossil abundance and preservation are also similar in both holes.

Samples 150-903D-1R-CC to -7R-CC (771.10–842.64 mbsf) yield scarce assemblages with *Coccolithus miopelagicus, Discoaster exilis, D. sanmiguelensis, D. variabilis, Reticulofenestra floridana,* and *R. pseudoumbilicus.* The occurrence of *C. miopelagicus* and *D. exilis* and the absence of *D. challengeri* suggest a stratigraphic position equivalent to Zone NN6–lower part of Zone NN7. Samples 150-903D-8R-CC to -15R-CC (851.64–917.55 mbsf) yielded *Sphenolithus heteromorphus* (indicating Zone NN5). In Samples 150-903D-16R-CC to -18R-CC (920.94–948.07 mbsf), this latter species is associated with *Helicosphaera ampliaperta,* indicating Zone NN4.

The interval between Sample 150-903D-20R-CC (996.3 mbsf) and -23R-CC (1015.6 mbsf) yields low-diversity assemblages and the zonal assignment is debatable. Sample 150-903D-20R-CC (996.3 mbsf) yields *Sphenolithus belemnos,* which indicates an age not older than Zone NN3 (SG). Sample 150-903D-23R-CC (1015.6 mbsf) yields *S. delphix* and *S.* aff *S. belemnos* (regarded as a form of *S. dissimilis*) and is assigned to Zone NN1 (SG).

An alternative interpretation is proposed by MPA, who assigns Sample 150-903D-20R-CC (996.3 mbsf) to Zone NN2 (the lowest occurrences of *Helicosphaera ampliaperta* and *Sphenolithus belemnos* are in Zone NN2 [Martini, 1971; Bukry, 1973, 1975]). Samples 150-903D-21R-CC to -23R-CC (1005.9–1015.6 mbsf) yield low diversity assemblages and their zonal position is undetermined.

Samples 150-903D-24R-CC (1028.68 mbsf) and -25R-CC (1037.29 mbsf) yielded *Reticulofenestra bisecta, Sphenolithus ciperoensis,* and *Zyghrablithus bijugatus,* indicating a stratigraphic position in Zone NP25 at the level of Magnetozone 7N or lower.

Diatoms

Hole 903A

Sample 150-903A-1H-CC to -47X-CC (9.5–423.3 mbsf) are barren or have rare diatoms. Species present include *Thalassionema nitzschioides, Thalassiosira oestrupii,* and *T. gravida.* However, no age-diagnostic taxa were observed, although the sparse assemblages suggest that most of this interval is Pleistocene. However, Sample 150-903A-48X-CC (433 mbsf) contains an impoverished assemblage, which suggests that the age of the sample is older than Pliocene and younger than middle Miocene. No middle Miocene age indicators were observed; in the absence of such indicators, the presence of *D. hustedtii* suggests that the sample is lower upper Miocene. Burckle et al. (1982) note that this species disappeared from the equatorial Pacific in the middle of Chron 10. Unfortunately, the next two samples below this (150-903A-49X-CC and -50X-CC; 442.7–452.2 mbsf) contain no diatoms, so this assignment cannot be verified.

Samples 150-903A-51X-CC to -61X-CC (452.2–558.5 mbsf) are in the *Coscinodiscus yabei* Zone. Because of diatom dissolution and fragmentation in some samples, the nominate taxon was not always observed. However, heavily silicified elements of this zone, such as *Thalassiosira grunowii* and *D. hustedtii,* as well as stratigraphic position, suggest that we are essentially correct in this placement. Other forms present in this zone include *Actinocyclus ellipticus, A. ingens, Mediaria splendida, Paralia sulcata, P. sulcata* var. *coronata, Thalassiosira lineata,* and *Thalassionema nitzschioides.* We also observed the highest occurrence of *Delphineis novaecaesaraea* near the top of this zone. The presence of this species in Hole 903A is of interest because it is a zonal marker for the East Coast Diatom Zones (ECDZ) of Andrews (1988), ranging through his Zones 5, 6, and 7 and part of his Zone 3–4. Samples 150-903A-62X-CC through -76X-CC (567.8–702.8 mbsf) are provisionally placed in the *Rhizosolenia barboi* Zone. This assignment is still considered provisional because some of the samples showed severe fragmentation and/or dissolution and others did not contain the nominate taxon. Note that results from Hole 903C support assignment to this zone. Of interest is the occurrence of *Delphineis novaecaesaraea;* this species occurred in every sample, even those with extensive dissolution or breakage.

Hole 903B

Hole 903B recovered a 154-m-thick section. Diatom recovery ranged from barren to rare. The section is assumed to be Pleistocene.

Hole 903C

The first four cores (Samples 150-903C-1R to -4R; 489.8–505.6 mbsf) recovered no sediment, but Samples 150-903C-5R-CC to -8R-

CC (510.3–534.6 mbsf) penetrated into the *Coscinodiscus yabei* Zone. Also present in this interval is *Actinocyclus ingens, Actinoptychus senarius, Delphineis novaecaesaraea, Denticulopsis hustedtii, Paralia sulcata, P. sulcata* var. *coronata, Thalassionema nitzschioides,* and *Thalassiosira grunowii.* The presence of *D. hustedtii* suggests that this sediment is below the middle part of the upper Miocene. Further, the joint occurrence of *D. hustedtii* and *D. novaecaesaraea* and the absence of *Delphineis penelliptica* suggest that this interval is correlative with the upper part of East Coast Diatom Zone 6 (ECDZ 6) and all of ECDZ 7 of Andrews (1988).

According to Baldauf (1984), the next zone underlying the *C. yabei* Zone in the North Atlantic is the *Denticulopsis praedimorpha* Zone. *Denticulopsis praedimorpha,* which defines the top of the zone, was not observed in Hole 903C; either this zone is absent or, more likely, the zonal indicators of Baldauf (1984) did not extend this far south. For this reason, Samples 150-903C-9R-CC (586.5 mbsf) to -17R-CC (746.5 mbsf) are still considered part of the *C. yabei* Zone. Also found in this interval are *Actinocyclus ingens, A. tenellus, Actinoptychus senarius, Coscinodiscus temperi, Delphineis novaecaesaraea, Denticulopsis hustedtii, Paralia sulcata, P. sulcata* var. *coronata, Thalassionema nitzschioides,* and *Thalassiosira grunowii.* As with the overlying zone, the joint occurrence of *D. hustedtii* and *D. novaecaesaraea* and the absence of *Delphineis penelliptica* suggests that this interval is correlative with the upper part of ECDZ 6 and all of ECDZ 7 of Andrews (1988).

Samples 150-903C-18R-CC to -31R-CC (534–881.4 mbsf) belong to the *Rhizosolenia barboi* Zone of Baldauf (1984). The top of this zone is defined by the HO of *Denticulopsis punctata* var. *hustedtii.* Burckle et al. (1982) placed the LAD of this species in Chron 12 (= C5r) (upper middle Miocene) in sediments from the equatorial Pacific. Provisionally, we assume that the HO of this variety in this hole is correlative with the Pacific occurrence. Also found in this interval are *Actinocyclus ingens, A. tenellus, Actinoptychus senarius, Coscinodiscus temperi, Delphineis novaecaesaraea, Denticulopsis hustedtii, Mediaria splendida, Melosira westii, Paralia complexa, P. sulcata, P. sulcata* var. *coronata, Stephanogonia actinoptychus, Thalassionema nitzschioides,* and *Thalassiosira grunowii.* In Sample 150-903C-27R-CC (842.7 mbsf), we observed the HO of *Delphineis penelliptica.* In Neogene sections of the east coast of the United States, this species last occurs in the lower part of ECDZ 6 (Andrews, 1988). The occurrence of this taxon, along with *D. hustedtii* and *D. novaecaesaraea* and the absence of *Coscinodiscus lewisianus,* suggest that Samples 150-903C-27R-CC (842.7 mbsf) and -28R-CC (852.4 mbsf) are correlative with a very narrow interval in the lower part of ECDZ 6.

Samples 150-903C-32R-CC to -34R-CC (891.1–910.4 mbsf) belong to the *Denticulopsis nicobarica* Interval Zone. The top of this zone is defined by the lowest occurrence of *R. barboi* and the base is defined by the highest occurrence of *C. lewisianus.* According to Baldauf (1984), the zone is further identified by the occurrence of *D. nicobarica;* unfortunately, this latter taxon is rare in this zone. Also found in this interval is *Actinocyclus ingens, A. tenellus, Actinoptychus senarius, Cavitas jouseanus, Coscinodiscus marginatus, C. perforatus, Delphineis novaecaesaraea, Delphineis penelliptica, Denticulopsis hustedtii, Mediaria splendida, Melosira westii, Paralia complexa, P. sulcata, P. sulcata* var. *coronata, Stephanogonia actinoptychus, Thalassionema nitzschioides,* and *Thalassiosira grunowii.* The species, *D. hustedtii,* makes a first appearance toward the base of this zone. Similarly, *D. novaecaesaraea* and *D. penelliptica* also first appear at or just below the base of this zone. In the zonal scheme of Andrews (1988), *D. hustedtii* first appears in the lowermost part of ECDZ 6, *D. novaecaesaraea* first appears in the upper part of ECDZ 3–4, and *D. penelliptica* first appears at the ECDZ 2/ECDZ 3–4 boundary. In the ECDZ scheme, these latter two species co-occur with *Coscinodiscus lewisianus,* a rather widely distributed marine planktonic species. At Hole 903C, this species last occurs in Sample 150-903C-35R-CC (920 mbsf) just below the lowest occurrence of *D. novaecaesaraea* and *D. penelliptica.* The co-occurrence of four stratigraphic events near the base of the *D. nicobarica* interval zone suggests either that one or more of these datum levels are diachronous between Hole 903C and the east coast (U.S.) Neogene or that this level in Hole 903C (920 mbsf) represents a hiatus or very condensed section in middle Miocene sediments.

Samples 150-903C-35R-CC to -43R-CC (920.0–996.5 mbsf) belong to the *C. lewisianus* Zone. The top of this zone is defined by the highest occurrence of the nominate taxon; the base is not defined because, as with the study of Baldauf (1984), increasing opal dissolution downcore makes it difficult to define a base with any confidence. Other species include *Actinocyclus ingens, A. tenellus, Actinoptychus senarius, Cavitas jouseanus, Cestodiscus peplum, Coscinodiscus marginatus, C. perforatus, C. rhombicus, Craspedodiscus coscinodiscus, Mediaria splendida, Melosira westii, Paralia complexa, P. sulcata, P. sulcata* var. *coronata, Rhizosolenia praebarboi, Stephanogonia actinoptychus, Stephanopyxis lineata,* and *Thalassionema nitzschioides.* Of interest is the highest occurrence of *Sceptroneis caduceus* in Sample 150-903C-37R-CC (939 mbsf). In the zonal scheme of Andrews (1988), this species last occurs in the upper part of ECDZ 2. Of further interest is the occurrence of *Rhaphoneis* cf. *R. fossile* in Sample 150-903C-40R-CC (967.5 mbsf). Andrews (1988) found this species exclusively in his ECDZ 1. Below Sample 150-903C-43R-CC (986.8 mbsf), dissolution increases and the flora becomes increasingly impoverished. Samples 150-903C-44R-CC and 150-903C-45R-CC (1006.2–1015.8 mbsf) contain a few robust forms, which include *Stephanopyxis grossecellulata* and *S. grunowii.* The former species is considered to be upper Oligocene, but no firm data exist to support this.

In contrast to Site 902 (which was located in deeper waters of the continental slope), the shallower water Site 903 contains few diatoms in the Pleistocene. In these cases, it seems reasonable to invoke dilution by terrigenous sediment as the principle arbiter of diatom absence or occurrence. A similar comment may be made for the Pliocene, although, while a strong case may be made for the presence of Pleistocene sediments in both sites, this is not entirely true for the Pliocene. Along with benthic foraminifers, diatom occurrences in this site can be used to support a model of gradual shoaling of this region through the Neogene.

It is still too early to consider correlation between this site and the ECDZ of Andrews (1988). Some species and, presumably, some stratigraphic events occur in common between Site 903 and the Neogene of the east coast (U.S.). With additional shore-based study, it is very likely that a suitable correlation will be made. Two potential hiatuses in the interval containing stratigraphically useful diatoms are tentatively recognized. The youngest occurs around Sample 150-903C-17R-CC (746.5 mbsf); this is considered as a possible hiatus because of the absence of the *D. praedimorpha* Zone. However, as noted earlier, the floral elements making up this zone may not be present in this region. A second possible hiatus is noted at Sample 150-903C-18R-CC (756.2 mbsf); this may also be caused by the regional absence of stratigraphic markers that define the missing zones. Indeed, this seems the more likely explanation.

Hole 903D

Hole 903D was washed to a depth of 784.5 mbsf before coring began. Samples 150-903D-1R-CC to -6R-CC (784.5–832.8 mbsf) contain common to abundant diatoms and are in the *Rhizosolenia barboi* Zone. This zone occurs in the upper part of the middle Miocene. In addition to the nominate taxon, other species found in this zone include *Actinocyclus ellipticus, A. ingens, A. tenellus, Actinoptychus senarius, Coscinodiscus temperi, Cymatosira immunis, Delphineis novaecaesaraea, Denticulopsis hustedtii, D. punctata* var. *hustedtii, Mediaria splendida, Melosira westii, Paralia complexa, P.*

Table 4. Dinocyst data, Site 903.

Core, section, interval (cm)	Depth (mbsf)	Zone	Lowest occurrence	Highest occurrence
150-903A-				
37X-CC	327.66	Pleistocene		
39X-CC	343.44	Pleistocene		
40X-CC	352.33	H		*Labyrinthodinium truncatum*
41X-CC	362.95	H		*Hystrichosphaeropsos* spp.
43X-CC	383.97	H		
45X-CC	399.77	H		
47X-CC	423.32	H		
49X-CC	422.88	H		
50X-CC	451.37	H		
51X-CC	462.10	G		*Sumatradinium soucouyantae*
55X-CC	500.57	G		
60X-CC	549.04	G		
65X-CC	596.42	G		
67X-CC	615.98	G		
68X-CC	625.74	G		
69X-CC	634.33	F		*Cannosphaeropsis* sp. cf. *C. utinensis*
70X-CC	644.72	F		
71X-CC	654.50	F		
74X-CC	683.66	F		
76X-CC	702.70	F		
150-903C-				
9R-CC	590.45	G		
10R-CC	600.07	G		
10R-5, 83–88	599.00	G		
11R-CC	604.84	F		*Cannosphaeropsis* sp. cf. *C. utinensis*
15R-CC	722.88	F		
20R-CC	775.78	F		
21R-CC	785.20	F		
22R-CC	794.76	F	*Cannosphaeropsis* sp. cf. *C. utinensis*	
23R-CC	804.54	E		
24R-CC	806.05	E		
25R-CC	819.18	E		
26R-CC	823.55	D		*Systematophora* spp.
27R-CC	834.65	D		
28R-CC	846.39	D	*Habibacysta tectata*	
29R-CC	860.43	C		*Distatodinium paradoxum*
31R-CC	875.18	C		
32R-CC	886.51	C	*Labyrinthodinium truncatum*	
33R-CC	900.63	B		
34R-CC	903.06	B		
35R-CC	920.42	B		
36R-CC	923.64	B		
38R-CC	948.38	B		
39R-CC	957.66	A	*Sumatradinium soucouyantae*	*Cordosphaeridium cantharellum*
40R-CC	966.35	Pre-A		*Chiropteridium* spp.
43R-CC	986.97	Pre-A		
45R-CC	1010.14	Pre-A		
48R-CC	1033.83	Oligocene		*Thalassiphora? pansa*

sulcata, P. sulcata var. *coronata, Stephanogonia actinoptychus, Thalassionema nitzschioides,* and *Thalassiosira grunowii.* In the lower part of this zone (Sample 150-903D-6R-CC; 832.8 mbsf), *Delphineis penelliptica* has its highest occurrence. This species is a zonal marker in the East Coast Diatom Zones (ECDZ) of Andrews (1988). It consistently has its highest occurrence in the lower part of the *R. barboi* Zone in our material.

Samples from Core 150-903D-7R to -18R (842.8–948.0 mbsf) are in the *Coscinodiscus lewisianus* Zone. Baldauf (1984) places the top of this zone in the middle Miocene but indicates that it extends back to the lower Miocene. Besides the nominate taxon, this interval includes *Actinocyclus ellipticus, A. ingens, A. tenellus, Actinoptychus senarius, Cavitas jouseana, Cestodiscus peplum, Coscinodiscus temperi, Cymatosira immunis, Delphineis novaecaesaraea, D. penelliptica, Denticulopsis hustedtii, D. nicobarica, D. punctata* var. *hustedtii, Mediaria splendida, Melosira westii, Paralia complexa, P. sulcata, P. sulcata* var. *coronata, Rhizosolenia barboi, R. praebarboi, Stephanogonia actinoptychus, Thalassionema nitzschioides,* and *Thalassiosira grunowii.* This zone also yields the lowest occurrences of *Delphineis novaecaesaraea* and *D. penelliptica,* the former in Sample 150-903D-10R-CC (871.3 mbsf) and the latter in Sample 150-903D-13R (900 mbsf). Diatoms in Samples 150-903D-19R-CC to -20R-CC (986.7–996.3 mbsf) show increasing signs of breakage and dissolution. This interval is very likely still in the *C. lewisianus* Zone, but the zonal markers could not be found. Samples 150-903D-20R-CC to -25R-CC (996.3–1037 mbsf) are barren of diatoms or have few broken specimens.

Dinoflagellate Cysts

Palynological studies at Site 903 were restricted mainly to the Miocene section and undertaken only for Holes 903A and 903C. The biostratigraphic zonation and datum levels are given in Tables 3 and 4.

Hole 903A

Sample 150-903A-37X-CC (327.6 mbsf) contains a lean assemblage dominated by pristine grains of *Pinus* and *Picea* pollen.

The dinocyst assemblage indicates an age of late Pliocene or younger, based on the occurrence of *Bitectatodinium tepikiense.* This species, *Algidasphaeridium*? *minutum,* and *Protoperidinium conicoides* are the most common elements of the assemblage. Rare specimens of the *Systematophora ancyrea/placacantha* complex, reworked from the middle Miocene or older, are present. Sample 150-903C-39X-CC (343.4 mbsf) contains very little organic matter and a dinocyst assemblage characterized by reworked late Paleogene taxa, including *Cordosphaeridium cantharellum* and *Deflandrea phosphoritica.* No age-diagnostic taxa were recorded.

The interval from Samples 150-903A-40X-CC to -50X-CC (352–451 mbsf) contains assemblages indicative of dinocyst Zone H. The

highest observed occurrence of *Hystrichosphaeropsis obscura* is in Sample 150-903A-41X-CC (362 mbsf), but the assemblage from 150-903A-40X-CC contains *Labyrinthodinium truncatum,* a species which has its highest stratigraphic occurrence within Zone H. Assemblages within this zone at Site 903 are diverse and well preserved and yield the same taxa as at Site 902. At the base of the zone, the dinocyst flora becomes restricted and the assemblage is dominated by an unidentified, thick-walled, spherical algal cyst type.

Zone G occurs from Samples 150-903A-51X-CC to -68X-CC (462–624.7 mbsf). The top of this zone is recognized by the highest occurrence of *Sumatradinium soucouyantiae* in Sample 150-903A-51X-CC. The base of Zone G is placed above the highest occurrence of *Cannosphaeropsis* sp. cf. *C. utinensis,* which is at 634 mbsf in Sample 150-903A-69X-CC. This record marks the top of Zone F, which extends down to the bottom of the hole at 702.7 mbsf. *Cannosphaeropsis* sp. cf. *C. utinensis* occurs in each of five samples analyzed in this interval (Samples 150-903A-69X-CC, -70X-CC, -71X-CC, -74X-CC, and -76X-CC). Assemblages within this interval do not differ significantly from their counterparts at Site 902.

Hole 903C

Samples 150-903C-9R-CC and -10R-CC (590.4 and 600 mbsf) contain an assemblage that indicates Zone G based on the occurrence of *S. soucouyantiae* and superposition with respect to Zone F. The top of Zone F is above Sample 150-903C-11R-CC (604.8 mbsf) on the basis of the highest occurrence of *Cannosphaeropsis* sp. cf. *C. utinensis.* The lowest occurrence of *C.* sp. cf. *C. utinensis* in Sample 150-903C-22R-CC (794.7 mbsf) marks the base of this zone. Sediments between Samples 150-903C-23R-CC (804.5 mbsf) and -25R-CC (823.6 mbsf) belong to Zone E. This is based on the absence within this interval of *C.* sp. cf. *C. utinensis* and *Systematophora* spp., and stratigraphic position with respect to Zones F and D.

Zone D is recognized in Samples 150-903C-26R-CC, -27R-CC, and -28R-CC (823.5, 834.6, and 846.4 mbsf, respectively) based on the occurrence of specimens of the *Systematophora ancyrea/placacantha* complex and *Habibacysta tectata* in each sample, together with the absence of *Distatodinium paradoxum.* Sample 150-903C-29R-CC (860.4 mbsf) belongs to Zone C. It contains the zonal species *Distatodinium paradoxum* and overlies samples containing *L. truncatum.* The lowest recorded occurrence of this latter species at Site 903 is in Sample 150-903C-32R-CC (886.5 mbsf) and delineates the Zone C/Zone B boundary. Samples 150-903C-33R-CC and -34R-CC (900.6 and 903.6 mbsf) contain an assemblage typical of the upper part of Zone B. These include *Hystrichokolpoma*? sp. 1 (= Dinocyst sp. 6 of Manum et al., 1989), *Aptiodinium spiridoides, Spiniferites pseudofurcatus,* and *Operculodinium longispinigerum.* Samples 150-903C-35R-CC, -36R-CC, and -38R-CC (902.4, 923.6, and 948.4 mbsf) contain an assemblage essentially the same as those typically found in Zone A. *Operculodinium* sp. 1 of Manum 1976, *Cribroperidinium tenutabulata, Saturnodinium* sp. cf. *S. perforata, Dinopterygium cladoides* sensu Morgenroth (1966), and undescribed species of *Lingulodinium, Cerebrocysta,* and *Sumatradinium* are all characteristic of this assemblage. However, *Cordosphaeridium cantharellum* was not recorded from these samples, and they thus belong to Zone B.

The only sample examined that can be assigned unequivocally to Zone A is Sample 150-903C-39R-CC (957.6 mbsf). The boundary between Zones A and Pre-A is between this sample and Sample 150-903C-40R-CC (966.3 mbsf). The latter contains *Chiropteridium lobospinosum, Hystrichokolpoma truncana, H. cinctum, Deflandrea phosphoritica, Membranophoridium aspinatum,* and *Distatodinium biffii.* Samples 150-903C-43R-CC and -45R-CC (986.9 and 1010.1 mbsf) contain the same assemblage and belong to Zone Pre-A. The final sample examined was Sample 150-903C-48R-CC (1033.8 mbsf). The presence of *Thalassiphora*? *pansa* indicates an age of middle late Oligocene for this level.

PALEOMAGNETISM

Procedures

Paleomagnetic measurements of whole sections and discrete 6-cm^3 samples were made for the purpose of constructing a magnetostratigraphy at Site 903. Pass-through and pilot discrete sampling was conducted in the upper part of Hole 903A (0–490 mbsf) and in Hole 903B. Farther downhole (490–702.5 mbsf) and for most of Hole 903C, the pass-through method seemed no longer reasonable because of drilling disturbance and secondary magnetic overprints, which we suspected were not being removed by alternating-field (AF) demagnetization to 15 mT. Discrete samples from these intervals were AF demagnetized to 70 or 90 mT. A total of 246 discrete shipboard samples were studied at Site 903. In each sample, progressive demagnetization was analyzed using orthogonal projections, which allowed us to determine the point at which a characteristic remanent magnetization was reached. Magnetic susceptibility was also measured in each discrete sample as a check on the routine susceptibility measurements on whole cores.

Results and Discussion

At Site 903, the intensities of the natural remanent magnetization (NRM) range from 10^{-1} mA/m to several 10 mA/m in Holes 903A and 903C, respectively (Fig. 14). The NRM intensities approach the noise level of the cryogenic magnetometer (see Chapter 3, this volume) in the lower half of Hole 903A and throughout Hole 903C. Thus, only a minor portion of the data set was suitable for shipboard construction of a magnetic polarity stratigraphy. A correlation of Holes 903A and 903C within about 1 m is possible using magnetic susceptibility acquired with the multisensor track (MST) system (Fig. 15). The range of susceptibility values at Site 903 is 1 to 250×10^{-5} SI, and the downhole trends in the intensity of remanent magnetization and susceptibility parallel one another.

We note a distinct intensity decrease within the upper 10 m in Hole 903A from about 30 mA/m to an average 3 mA/m (Fig. 14). This change could be related to alteration of magnetic minerals by diagenetic reduction in the sediment. The origin of the wide-ranging remanence intensities in the interval between 150 and 750 mbsf in Site 903 is as yet uncertain. However, intensity peaks always seem to match more or less drastic changes in lithology, such as interbedded turbidites or slump structures. A shift to more scattered, but generally steep, inclinations between 150 and 330 mbsf in Hole 903A suggests a slightly stronger drilling-induced magnetization overprint incompletely removed at 15 mT. Nevertheless, magnetic polarity remained interpretable in this interval. Unfortunately, the sediments in Hole 903A below 330 mbsf and, for the most part, sediments in Hole 903C are weakly magnetized and often unstable to AF demagnetization.

Paleomagnetic measurements at Site 903 yield a uniform zone of normal polarity in the upper 336.3 ± 4 m in Hole 903A, which is confirmed by paleomagnetic measurements in Hole 903B. Between 336.3 and 348.0 mbsf, we identify a short reversed polarity interval (Fig. 14 and Table 5). Unfortunately, at this stage of the study, the polarity of the interval (348–370 mbsf) further downhole is uninterpretable because of weak intensities and scattered inclinations. Shipboard paleontology suggests the occurrence of nannofossils diagnostic of Zone NN19 between about 278.4 and 336.4 mbsf in Hole 903A (see "Biostratigraphy" section, this chapter). Thus, we identify the normal polarity zone between 0 and 336.3 mbsf as a record of the Brunhes Chron (Chron C1n). However, interpretation of the reversed polarity zone below (336.3–348.0 mbsf) is less straightforward because of discontinuous sedimentation. An unconformity likely occurs between the level at which the last direct measurement of Chron C1n was made (332.56 mbsf) and the level at which Pliocene sediments were identified (352.33 mbsf; see "Biostratigraphy" section, this chapter). In addition, the identification of upper Miocene sediments

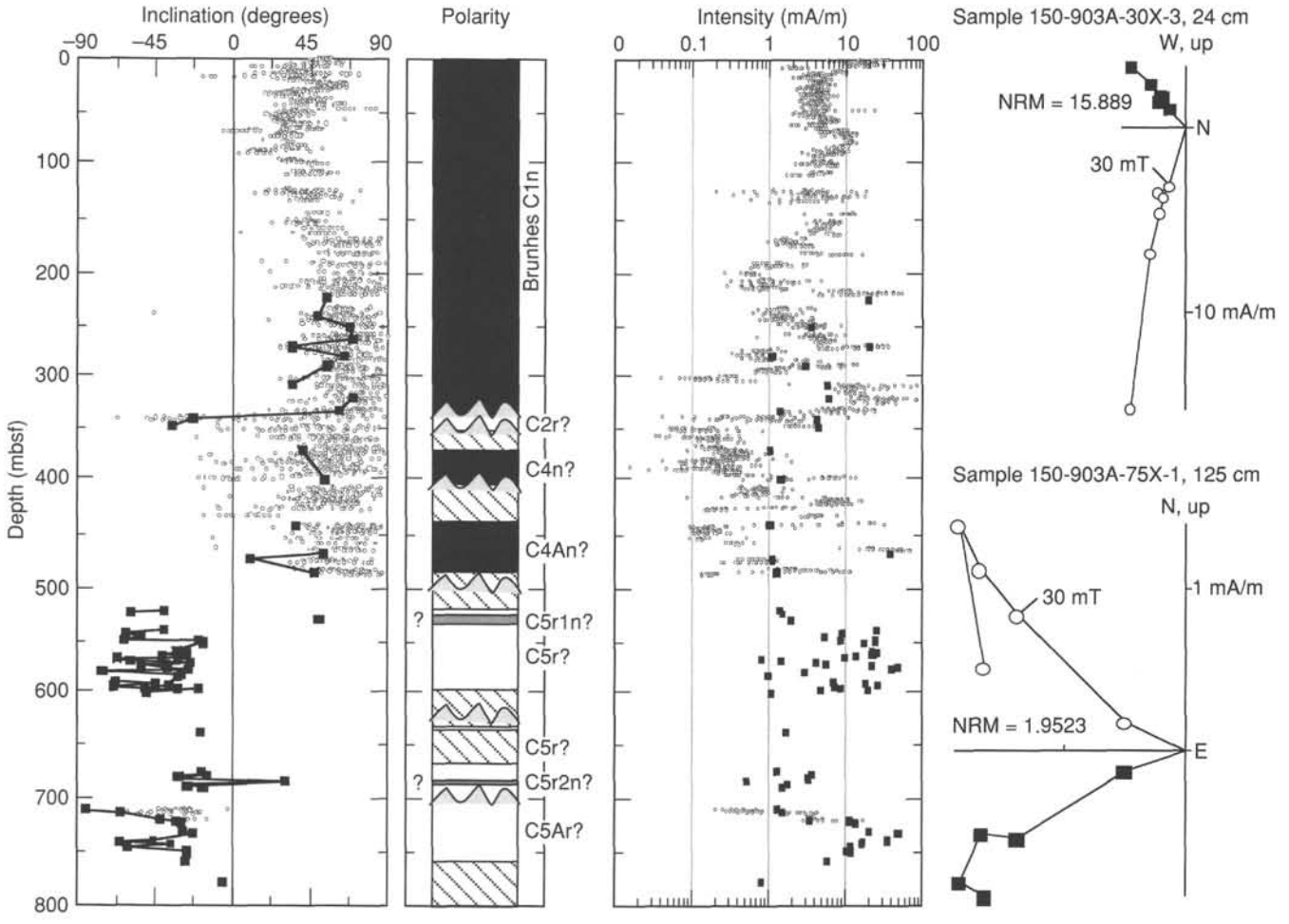

Figure 14. Tentative magnetostratigraphic framework in the Pleistocene and late to middle Miocene sections at Site 903. Inclination and intensity data represent a combination of two demagnetized discrete samples and pass-through measurements from Holes 903A and 903C. In the polarity column, black = normal polarity, white = reversed polarity, cross-hatched = uninterpretable, and gray = normal likely (based on only one sample). Orthogonal projection of representative demagnetization of discrete samples also shown (open and closed symbols = vertical and longitudinal projection, respectively).

at 365.4 mbsf suggests a second unconformity somewhere between 352.33 and 365.4 mbsf. The presence of Zone NN15 or NN17–NN18 at 352.33 mbsf (see "Biostratigraphy" section, this chapter) allows alternative correlations of the reversed polarity zone between 336.3 and 348.0 mbsf to either Chrons C1r or C2r (Fig. 14). However, identification of glacial stage 14 (~550 ka) at about 325 mbsf and possibly stage 15.1 (~574 ka) at 335 mbsf suggests the lower part of Chron C1n may be missing in Hole 903A (see "Sedimentation Rates" section, this chapter). Therefore, a possible third unconformity lies above at 336.3 mbsf, separating a partial record of Chron C1n from reversed polarity sediments below. According to Site 903 shipboard lithologic descriptions and velocity logs, several surfaces are suggested over the interval from 330 to 360 mbsf, including candidate reflector p6 (indigo) in the vicinity of 338 mbsf (see "Lithostratigraphy" and "Downhole Measurements" sections, this chapter).

Construction of magnetostratigraphy in the bottom half of Hole 903A is hampered by the low amount of reliable paleomagnetic data in this section. In addition, the presence of several candidate sequence boundaries over this interval, representing potentially significant stratigraphic gaps at Site 903, prohibits us from delineating polarity zone, even where the paleomagnetic data are interpretable. However, in accordance with the preliminary shipboard biostratigraphic dating (see "Biostratigraphy" section, this chapter) and assuming a relatively constant sedimentation rate (see "Sedimentation Rates" section, this chapter), we can attempt a tentative correlation of the polarity zones in Hole 903A to the time scale of BKV85 and CK92. An interval of normal polarity between 370 and 400 mbsf may correlate to early Miocene Chron C4n (Fig. 14), as is suggested by planktonic foraminifers and nannofossil stratigraphy. As the first occurrence of *Denticulopsis hustedtii* at 430 mbsf suggests an age of about 8–8.3 Ma (see "Biostratigraphy" section, this chapter), the section of normal polarity between 438 and 485 mbsf (Fig. 14) may represent Chron C4An. This may imply that the ~40-m-thick uninterpretable zone between 400 and 438 mbsf corresponds to Chron C4r. Given the estimated duration of Chrons C4n and C4An (CK92), a stratigraphic gap or a drastic decrease in sedimentation rate within this magnetically uninterpretable zone would be implied. This interval of possible lower sedimentation rates is associated with reflector p7 (yellow) at 405 mbsf (see "Seismic Stratigraphy" section, this chapter).

The remainder of Hole 903A between 485 and 700 mbsf contains discontinuous intervals of mainly reversed polarity. The presence of candidate sequence boundary m0.5 (Red) at 500 mbsf (see "Seismic Stratigraphy" section, this chapter) and the preliminary shipboard biostratigraphy (see "Biostratigraphy" section, this chapter) suggest a stratigraphic gap at this level. The presence of planktonic foraminifer diagnostic fossils *Globorotalia praemenardii* and *Paragloborotalia mayeri* (see "Biostratigraphy" section, this chapter) suggests that the lower part of Hole 903A is middle Miocene. Assuming a relatively constant sedimentation rate in this interval (see "Sedimentation Rates" section, this chapter), the interpretable sections of re-

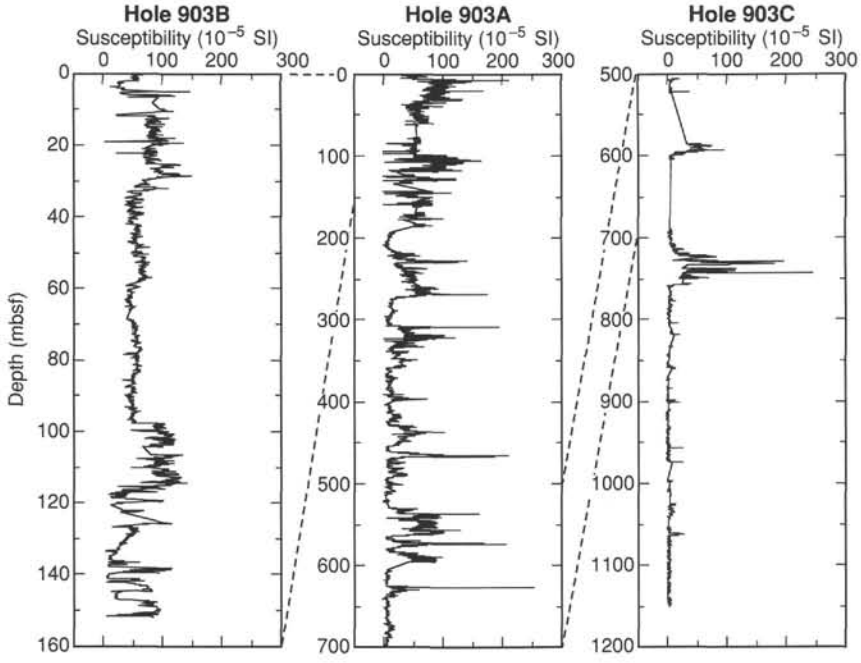

Figure 15. Downhole behavior of volume susceptibility, Holes 903A, 903B, and 903C. Note differences in depth scale.

versed polarity between 520 mbsf and the bottom of Hole 903A at 700 mbsf may correlate to Chron C5r. Two minor sections of possibly normal polarity at 526 and 680 mbsf may be correlative to Subchrons C5r.1n and C5r.2n, although future shore-based work is needed to characterize these zones.

Although recovery was low at the top of Hole 903C, susceptibility can be used to correlate Holes 903A and 903C. Based on major trends in susceptibility, the bottom 200 m of Hole 903A correlate with the interval 500–700 mbsf in Hole 903C within about 1 m (Fig. 15). Hole 903C is characterized by reversed polarity wherever magnetostratigraphic interpretation is possible. At the present state of the investigation, it is likely that several normal polarity intervals are absent in Hole 903C despite the numerous intervals with uninterpretable magnetic signals; thus, the paleomagnetic results may only be used as an auxiliary means for interpreting the stratigraphy of Hole 903C. The thin zone of reversed polarity recovered at the top of Hole 903C between 580 and 600 mbsf confirms the results obtained in the middle Miocene section of Hole 903A. A zone of reversed polarity between 709 and 757 mbsf may correlate to Chron C5Ar (according to the preliminary paleontology; see "Biostratigraphy" section, this chapter), which would therefore indicate a possible stratigraphic gap at the candidate sequence boundary m2 (Yellow) at 700 mbsf (see "Seismic Stratigraphy" section, this chapter).

Coring with the RCB in Hole 903D (775–1040 mbsf) provided cores at a high recovery rate and in excellent condition, yet intensities of magnetization in the green silty clays are unfortunately very weak and difficult to interpret. Alternating-field demagnetization to 10 or 15 mT reduces NRM intensities on the order of 0.1 mA/m by more than 50% to generally below measurement capabilities (see Chapter 3, this volume). However two thin intervals at the top and at the bottom of Hole 903D (775–788 and 1025–1037 mbsf, respectively) with slightly higher intensities may represent zones of normal polarity. Shipboard paleontology suggests a middle Miocene age for the upper interval (Zone NN6; see "Biostratigraphy" section, this chapter). Given a constant sedimentation rate over this interval (see "Sedimentation Rates" section, this chapter), the normal polarity zone between 775 and 788 mbsf could correlate to either Chrons C5ABn or C5ACn. The normal polarity zone between 1025 and 1037 mbsf occurs within a stratigraphic interval identified as Zone NP25 (see "Biostratigraphy" section, this chapter) and likely correlates with any of the normal subchrons within Chrons C6Cn through C8n.

Susceptibility is constantly low throughout Hole 903D, with an average value of less than 10×10^{-5} SI. Despite little if any distinct features in susceptibility, one is worth mentioning. As observed in Hole 903C, susceptibility tends to increase slightly at the top and at the bottom of the cored interval, enclosing a zone of mainly diamagnetic sediments between about 850 and 1000 mbsf.

Shore-based studies are planned for confirmation and expansion of the preliminary Site 903 magnetostratigraphy presented here.

SEDIMENTATION RATES

A 1149.7-m-thick middle Eocene to Pleistocene section was recovered at Site 903 from four holes (see "Operations" section, this chapter). Hole 903A was terminated at 702.8 mbsf (Section 150-903A-76R-CC), whereas Hole 903B was cored with the APC to refusal depth of 154 m (Core 150-903B-17H). Hole 903C was washed to 485.5 mbsf, spot-cored and drilled to 688.60 mbsf, then continuously cored to 1149.95 mbsf. Hole 903D was cored between 774.9 and 948 mbsf and between 977.0 and 1030.0 mbsf.

The section consists of 346.4 to 348.0 m (see below) of Pleistocene silty clay and fine sands (lithologic Unit I and the greater part of lithologic Unit II; see "Lithostratigraphy" section, this chapter); ~10 to 15 m of possibly mixed middle or upper Pliocene and older (Paleocene, Eocene, Miocene) coarse sands, which constitute the lower part of lithologic Unit II (Fig. 16; see "Lithostratigraphy" section, this chapter); ~160 m of upper Miocene glauconitic sands (most of lithologic Unit III; see "Lithostratigraphy" section, this chapter); ~405 m of middle Miocene diatomaceous muds (lower part of Unit III through the greater part of Unit V); ~80 m of lower Miocene diatomaceous muds and glauconitic sands (lower part of lithologic Unit V and uppermost part of lithologic Unit VI (see "Lithostratigraphy" section, this chapter); ~70 m of upper Oligocene nannofossil muds and glauconitic sands (lithologic Unit VI; see "Lithostratigraphy" section, this chapter); and ~135 m of upper and middle Eocene clayey chalk (lithologic Unit VII; see "Lithostratigraphy" section, this chapter).

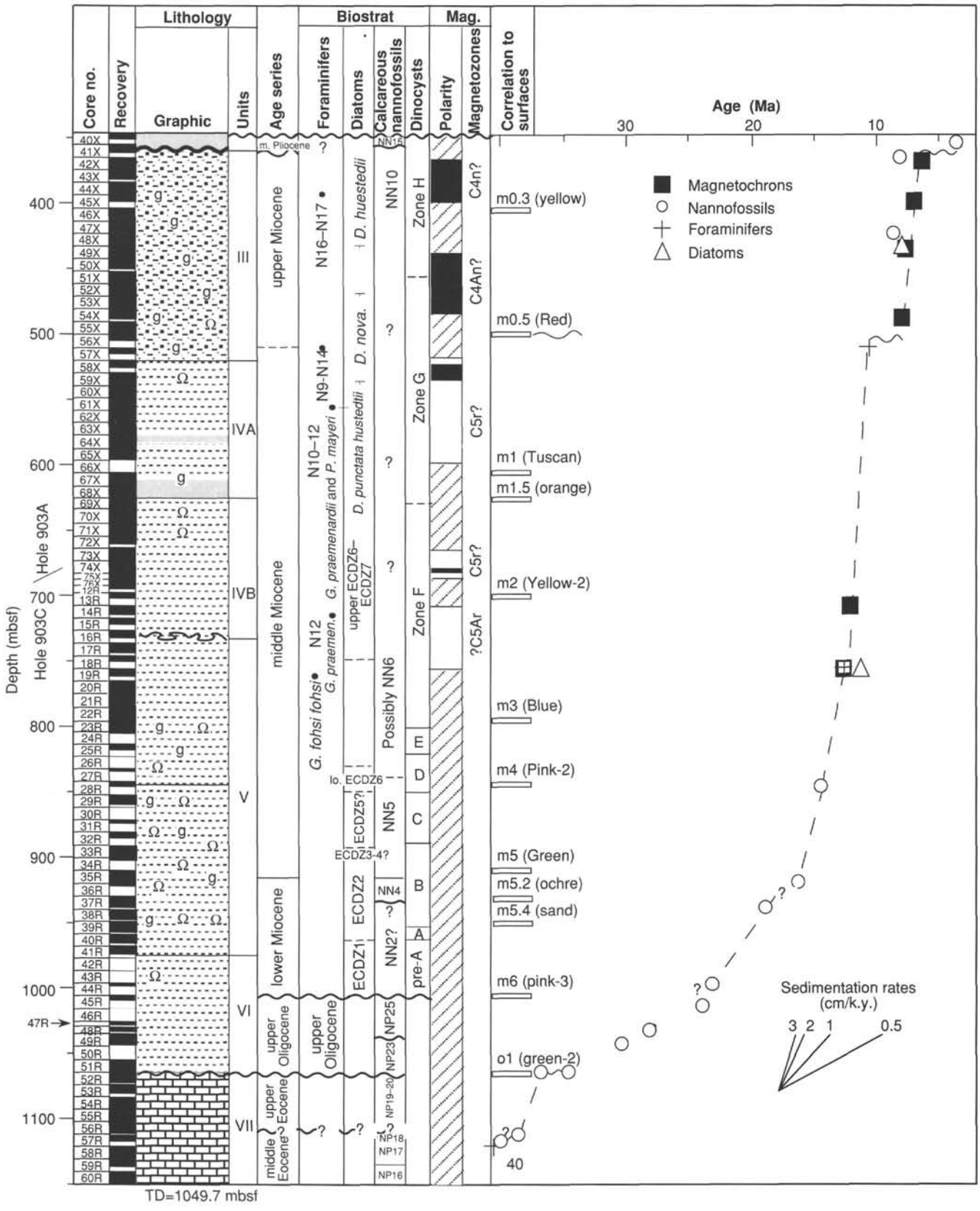

Figure 16. Age-depth diagram for Holes 903A and 903C showing lithostratigraphic units, age interpretation, biostratigraphy, magnetostratigraphy (black = normal polarities, white = reversed, cross hatch = uncertain), and seismic reflectors. Wavy lines indicate hiatuses and/or unconformities noted in the borehole. Note that the age scale is from 2 to 41 Ma. TD = total depth.

Calcareous nannofossils provided a fine stratigraphic control for the Pleistocene-Holocene interval (between 0 and 339.40 mbsf). Together with the planktonic foraminifers, they allowed a good stratigraphic resolution for the lower middle Miocene to middle Eocene section (Sections 150-903C-27R-CC to -60R-CC; 834.65–1149.95 mbsf). Diatoms and dinoflagellates provide biostratigraphic controls for the upper middle to upper Miocene, with additional, but spotty information derived from the planktonic foraminifers.

A thick Pleistocene interval was recovered at Site 903. The Pleistocene section extends from 0 to 336.4 mbsf at Hole 903A, corresponding to lithologic Unit I and most of lithologic Unit II (see "Lithostratigraphy" section, this chapter). Nannofossils show that the section from 0.2 to 278.5 mbsf at Hole 903A lies between the *E. huxleyi* abundance datum and the LAD of *P. lacunosa.* This establishes that this part of the section is older than 80 ka and younger than 474 ka (from oxygen isotope stage 5 to stage 12; terminology of Imbrie et al., 1984). Hole 903B duplicated the upper 154 m (Cores 150-903B-1H to -17H) of Hole 903A.

The base of the Pleistocene is truncated at Hole 903A. The lowest appearance of *G. truncatulinoides* (FAD, 1.9 Ma; BKFV85) is at 336.4 mbsf in an interval of uncertain polarity between the Brunhes magnetozone (lowest sample at 332.56 mbsf) and a reversed magnetozone (340.07–348 mbsf). This suggests that this lowest occurrence is truncated (i.e., it occurs within or immediately below the Brunhes). Sample 150-903A-40X-CC (352.33 mbsf) is assigned to Zone NN15 or NN17–NN18 (middle or upper Pliocene), suggesting that the reversed magnetozone from 340.07 to 348 mbsf may be either Chron C1r (0.73–0.91 Ma) or C2r (1.88–2.47 Ma). Sample 150-903A-41X-CC (362.95 mbsf) is upper Miocene. Thus, at least two and perhaps three disconformities are present in the interval between 336.4 and 362.95 mbsf: (1) at the base of the Brunhes (between 332.56 and 340.08 mbsf); (2) between the base of the reversed magnetozone at 348 mbsf and the Pliocene at 352.33 mbsf; and (3) between the Pliocene at 352.33 mbsf and the upper Miocene at 362.95 mbsf. Lithostratigraphy and velocity logs also indicate three potential surfaces in this section. We conclude that further study is needed to refine the position and ages of these stratal discontinuities.

Pleistocene sedimentation rates based on three calcareous nannofossil datums indicate rapid deposition. The *Emiliania huxleyi* acme (~73–85 ka) occurs at 0.2 mbsf (Section 150-903A-1H-1, 20 cm), indicating that Holocene drape overlies a truncated Pleistocene section. *E. huxleyi* has its lowest occurrence (FAD ~285 ka in stage 8) at 95 mbsf (Section 150-903A-10H-CC), indicating a minimum sedimentation rate of about 50 cm/k.y. The highest occurrence of *Pseudoemiliania lacunosa* (474 ka) is at 276.68 mbsf (Sample 150-903A-32X-CC), indicating a sedimentation rate of about 100 cm/k.y. from this level to the lowest occurrence of *E. huxleyi.* These rates are two to three times the rates at Site 902.

Site 902 sedimentation rates were determined successfully by correlating density changes (GRAPE and gravimetric) to the SPECMAP time scale of Imbrie et al. (1984) (see Fig. 19 in Chapter 6, this volume). However, the GRAPE data at Site 903A are discontinuous, requiring splicing from Hole 903B. Instead, we used magnetic susceptibility to recognize glacial-interglacial changes and to correlate to oxygen isotope stages and the SPECMAP time scale. Susceptibility has been used successfully as a proxy for glacial-interglacial changes (e.g., Bloemendal et al., 1993). Susceptibility is proportional to magnetic mineral concentration and potentially mimics terrigenous input. In this case, increased detrital content is interpreted as glacial in origin. Interglacial intervals display more biogenic influence (see below). Glacial-interglacial changes are often expressed in physical properties data (including susceptibility, density, and thermal conductivity) as a result of sedimentation changes. The susceptibility records at Sites 902 through 904 mimic the GRAPE density data (e.g., see Fig. 21 in Chapter 8, this volume).

Magnetic susceptibility results for Hole 903A are discontinuous because of gas voids and minor coring gaps. Therefore, a composite susceptibility section was constructed by splicing the susceptibility record from Hole 903B into the record at Hole 903A at an equivalent sub-bottom depth. We correlated the composite susceptibility section to oxygen isotope stages (Fig. 17), with minor gaps remaining in the record below the depth of Hole 903B (between 160 and 190 m), rendering the correlation of substages within 9 and 10 uncertain.

An excellent match occurs between major peaks in susceptibility and glacial intervals, with stages 6, 8, 10, 12, and 14 clearly represented (Fig. 17; note that the scale on susceptibility has been inverted to mimic the SPECMAP scale). Calcareous nannofossil datums (see above) constrain correlation of the section between 0.2 and 278 mbsf to stages 5.5 and 12 (474 ka), confirming the susceptibility correlations. Smear-slide data, indicating interglacial (increased biogenic sedimentation) and glacial (increased terrigenous sedimentation), and benthic (transported; in situ) and planktonic foraminifer (warm-water; cool-water) assemblages agree well with the interpretation.

Like any ordinal correlation tool, susceptibility and density data cannot be used alone to recognize stratigraphic breaks. The apparent continuity of the middle Pleistocene record is remarkable given the presence of five reflectors in the Pleistocene section (Fig. 17) and gaps may remain undetected. However, we suggest that these gaps, if present, are very minor. Although the section above reflector p6 (indigo) thickens toward the shelf, little evidence exists for seismic truncation landward, consistent with the apparent continuity of the record. Still, minor gaps are suggested by reduced sedimentation rates near the stage 9/8 transition, that encompasses reflector p2 (blue; Fig. 17) and perhaps near the stage 13/12 transition (reflector p5 [orange]).

Mean sedimentation rates between stages 5.5 and 15.1 were 73 cm/k.y. (Fig. 18). Identification of substages in the SPECMAP time scale are tentative (see Fig. 19 in Chapter 6, this volume); therefore, we estimated the following sedimentation rates between the major glacial-interglacial stages (Fig. 16): stages 6.2–7.1 = 98 cm/k.y.; stages 7.1–7.5 = 71 cm/k.y.; stages 7.5–8.5 = 57 cm/k.y.; stages 8.5–10.2 = 85 cm/k.y.; stages 10.2–11.1 = 79 cm/k.y.; stages 11.1–12.2 = 102 cm/k.y.; stages 12.2–13.11 = 56 cm/k.y.; stages 13.11–14.2 = 80 cm/k.y.; and stages 14.2–15.1 = 58 cm/k.y. These estimates minimize glacial/interglacial changes in sedimentation rate because they average rates across transitions. The most prominent mass-flow deposits are generally associated with glacials or interglacial-glacial transitions: (1) a sand unit from 126.5 to 144.5 mbsf is correlated with the stage 9/8 transition; (2) four slumps between 221.5 and 243.5 mbsf are correlated with glacial stage 12; (3) slumps and debris flows between 269 and 274 mbsf are correlated to the stage 13/12 transition; and (4) a thin sand bed at 327.5 mbsf correlates with the stage 15/14 transition (see "Lithostratigraphy" section, this chapter). The exception to this correlation with glacial stages is a sand unit from 298.8 to 307.5 mbsf that correlates with a transition from glacial stage to interglacial stage 13. Shore-based studies will attempt to make finer substage correlations, to estimate glacial vs. interglacial fluxes of sedimentary components, and to relate these to processes of sedimentation.

As noted above, unconformities separate the middle Pleistocene from the Pliocene and the Pliocene from the upper Miocene. Although a comprehensive interpretation of the Pleistocene and lower middle Miocene to middle Eocene intervals recovered at Site 903 is possible based on the integration of calcareous plankton stratigraphies, interpretation of the upper and middle Miocene section requires extensive onshore studies. The age of the upper part of the Miocene at Site 903 is uncertain, although it is possible that the normal magnetozones at 365–400 mbsf and 438–485 mbsf correlate with Chrons C4n and C4An, respectively (Fig. 16). Because of the discontinuous calcareous microfossil records in Holes 903A and 903B and the uncertain position of the *C. yabei* and *R. barboi* diatom zones, the interpretations presented (Fig. 16) for the upper middle Miocene must be considered tentative. The middle/upper Miocene boundary is tentatively placed at ~510 mbsf based on the highest occurrence of a middle Miocene planktonic foraminifer assemblage. This apparently contradicts the dinoflagellate assignment to Zone G, previously thought to

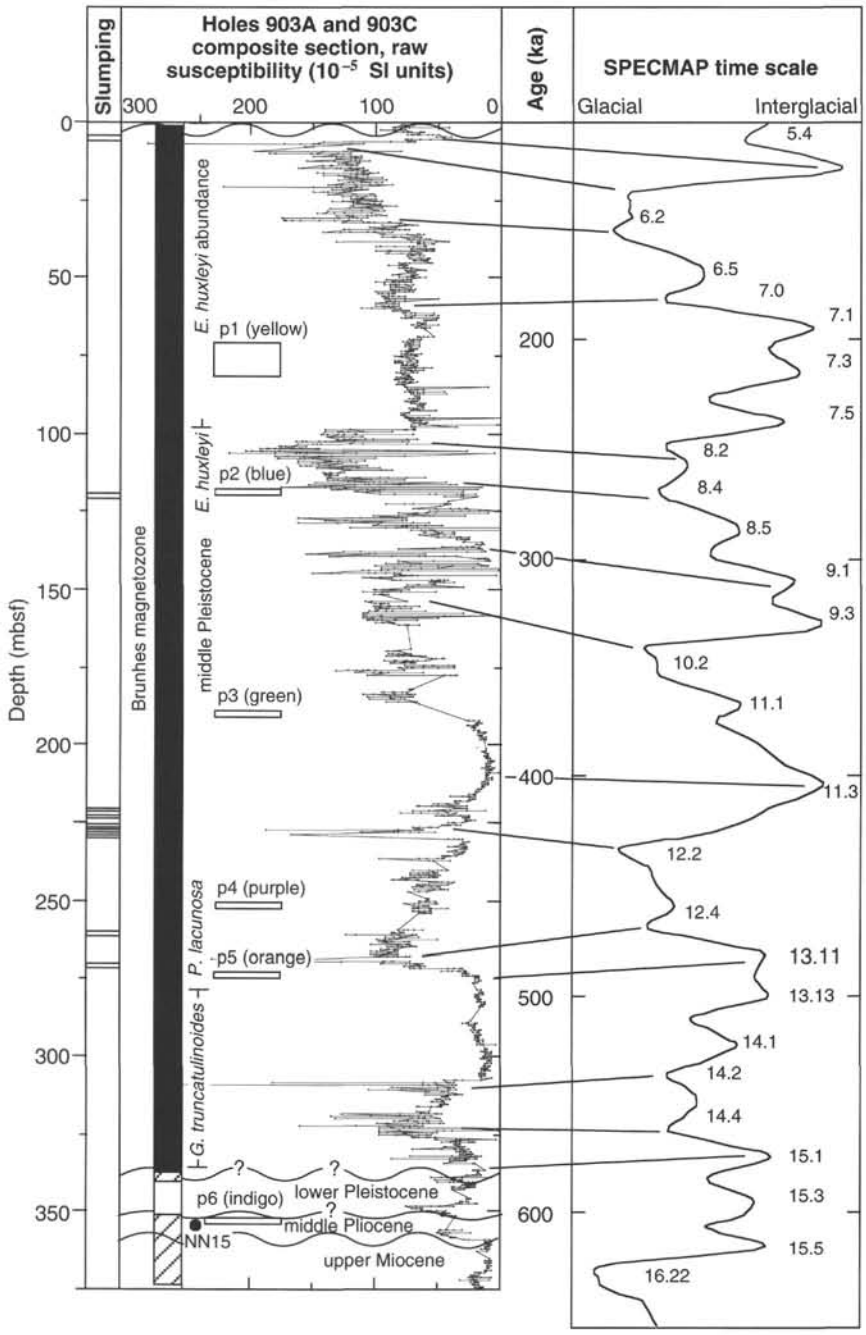

Figure 17. Correlations in Holes 903A and 903C between slumped sediment, seismic reflectors, magnetozones, susceptibility data, and the SPECMAP time scale (from Imbrie et al., 1984). Oxygen isotopic substages are noted along the latter. The susceptibility scale has been inverted to match trends in the SPECMAP curve.

be upper Miocene. The problem is further compounded by the identification of lower middle to middle middle Miocene Zones N10–N12 in sediments assigned to Zone G.

One way to reconcile the data is as follows. At Site 905, Zone G is clearly associated with upper middle Miocene Zones N14 and NN7 (see "Biostratigraphy" section in Chapter 9, this volume) indicating that the middle/upper Miocene boundary occurs within Zone G. The assignment to planktonic foraminifer Zone N10–N12 is based not on primary zonal criteria (which are absent from this interval), but on the presence of *Globorotalia praemenardii*. Kennett and Srinivasan (1983) have suggested that this taxon last appears in Zone N12, although this LAD is not calibrated to the geomagnetic polarity time scale (GPTS). The sole occurrence of the zonal marker for the base of Zone N12 (*Globorotalia fohsi fohsi*) is in Sample 150-903C-14R-CC (715.52 mbsf), whereas the stratigraphically highest occurrence of *Paragloborotalia mayeri* (= criteria for base of Zone N14) is in Sample 150-903A-61X-CC (558.82 mbsf). By assuming that the latter is a LAD, the magnetostratigraphy can be correlated to the GPTS (see below).

Although the Pleistocene interval appears to be mostly continuous, the lower middle Miocene to middle Eocene is riddled with unconformities. At least five unconformities occur. The youngest separates the upper Miocene (Chron C4An?) from the lowermost upper Miocene (Chron C5r?) at the reflector m0.5 (Red) sequence boundary (500 mbsf). Dramatic seismic truncation is associated with this reflector at Site 903. The next youngest separates a lower middle

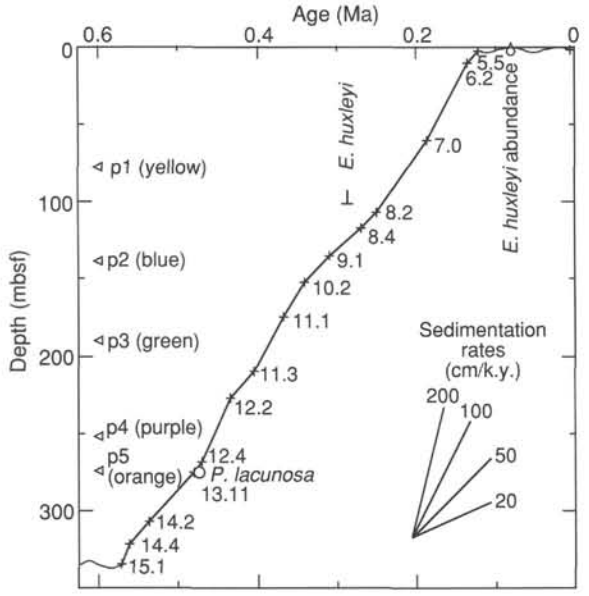

Figure 18. Age-depth diagram for the Pleistocene of Hole 903A based on the oxygen isotope substage correlations established using susceptibility data (Fig. 17, this chapter). p1–p5 are correlations of seismic reflectors. Numbers adjacent to crosses on curve are substages.

Miocene allostratigraphic unit (Sections 150-903C-27R-CC to -36R-CC; 834.55–923.64 mbsf) from a lower Miocene unit (Sections 150-903C-37R-CC to -44R-CC; 939.20–998.80 mbsf). The Oligocene/Miocene contact (1064.12 mbsf) is unconformable, as indicated by the juxtaposition of the lower part of calcareous nannofossil Zone NP25 with Zone NN1 or Zone NN2. Because Zone NP24 was not delineated, there may be an intra-Oligocene unconformity, separating the upper lower Oligocene from the upper upper Oligocene; however, there is a 9.5-m sample gap and characterization of this possible unconformity requires shore-based studies. An unconformity occurs clearly between Core 150-903C-51R-CC (1064.12 mbsf) and core 150-903C-52R-1H, 0 cm (at 1064.1 mbsf). It corresponds to the contact between lithologic Units VI and VII and to a stratigraphic gap encompassing the lower Oligocene. There may be one or more unconformities in the upper and middle Eocene, as suggested by the reduced thickness of calcareous nannofossil Zones NP18 and NP17. However, detailed stratigraphic analysis of closely spaced samples is required to document such eventual stratigraphic gaps.

Because of the numerous truncations in the middle Eocene to lower middle Miocene section, the difficulty in interpreting its middle and upper Miocene record, and in the absence of reliable magnetostratigraphy, it is not possible to establish firm sedimentation rate estimates for the Eocene to Miocene section recovered at Site 903. Figure 16 is provided only with the intent to document apparent variations in sedimentation rates, assuming that the magnetic reversals have been correctly identified based on their relations with the planktonic foraminifer stratigraphy. In addition, in comparing Eocene-Miocene sedimentation rates with Pleistocene rates, we have not accounted for compaction. One point is clearly illustrated in Figure 16: sedimentation rates were very high in the late middle Miocene (over 250 m between ca. 12–10 Ma; minimum sedimentation rates of 12.5 cm/k.y.). This figure also shows that the upper Miocene magnetostratigraphic interpretation yields an apparently constant sedimentation rate that is consistent with several biostratigraphic datum level and possible hiatuses associated with reflectors m0.5 (Red), m5 (green; = Zone NN4/Zone NN5 boundary), m5.2 (ochre; = Zone NN4/Zone NN2 boundary), and o1 (green-2; Zone NP23/NP19–20 boundary).

Table 5. Reversal boundary depths, Site 903.

Depth (mbsf)	Polarity	Interpreted polarity zone
Hole 903A:		
0.0–336.0	N	C1n
336.0–348.0	R	C2r?
348.0–370.0	?	No zonation
370.0–400.0	N	C4n?
400.0–438.0	?	No zonation
438.0–485.0	N	C4An?
485.0–520.0	?	No zonation
520.0–526.0	R	C5r composite?
526.0–534.0	N?	C5r1n?
534.0–596.0	R	C5r composite?
596.0–636.0	?	No zonation
636.0–637.0	R?	C5r composite?
637.0–672.0	?	No zonation
672.0–680.0	R	C5r composite?
680.0–682.0	N?	C5r2n?
682.0–700.0	R	C5r composite?
Hole 903C:		
588.0–599.0	R	C5r?
599.0–709.0	R?	No zonation
709.0–757.0	R	C5Ar?
757.0–1146.0	?	No zonation
Hole 903D:		
775.0–788.0	N?	C5ABn or C5ACn?
788.0–1025.0	?	No zonation
1025.0–1037.0	N?	C6n? through C8n?

Note: N = normal, R = reversed, and ? = uncertain.

ORGANIC GEOCHEMISTRY

Shipboard organic geochemical studies of sediments from Holes 903A, 903B, 903C, and 903D included volatile hydrocarbon and nonhydrocarbon gas, Rock-Eval, and elemental analyses. The instrumentation, operating conditions, and procedures are summarized in Chapter 3 (this volume).

Volatile Gases from Sediments

Volatile gases released from the sediments recovered at Site 903 were continuously measured as part of the shipboard safety and pollution monitoring program. Expansion voids occurred in the cores recovered between 30 and 141 mbsf, and gas in these voids was sampled using an evacuated vacutainer. The vacutainer gas was injected directly on to the Hewlett Packard 5890II gas chromatograph (Table 6). Headspace samples were obtained from every core by taking a 5-cm^3 plug of sediment from an unsplit section end, placing it in a septum sealed vial, then thermally desorbing the gas by heating to 70°C for 30 min. The liberated gas was injected onto the Hach Carle gas chromatograph (HC), which is routinely used for close monitoring of hydrocarbon gases during deep-sea drilling because of its short (8 min) analysis time.

Headspace methane concentrations were found at similar levels to those measured at Site 902, reaching a maximum value of 602,020 ppm at 134.5 mbsf in Hole 903A (Table 7). Methane concentration in vacutainer samples reached a maximum at 904,488 ppm at 146.7 mbsf (Table 6). The difference in absolute values between the two methods is assumed to be caused by the different sample preparation and collection procedures, as discussed by Behrmann et al. (1992). At Site 903, headspace methane appears at increased concentrations in three separate subsurface zones. Methane has two possible origins in these sediments: (1) biologic generation as a metabolic end product of organic matter oxidation through a series of oxidation, or (2) reduction reactions involving several species of microorganisms (Claypool and Kaplan, 1974). Interstitial water alkalinity values also tend to become elevated where biological organic degradation takes place by the reaction

$$2HCO_3^- + 4H_2 \leftrightarrow CH_4 + CO_3^{2-} + 3H_2O,$$

Table 6. Vacutainer gas composition from sediments at Site 903.

Core, section, interval (cm)	Depth (mbsf)	O_2	N_2	CO_2	C_1	C_2	C_3
150-903A-							
4H-2, 30–33	30.30	36269	119390	116794	245630	0	0
5H-1, 145–147	39.45	53695	225770	454338	653508	0	0
10H-7, 50–53	95.05	5235	21353	5564	854552	0	0
11H-2, 60–70	97.10	7883	29581	6338	853453	0	0
12H-3, 134–136	108.84	8636	60676	7117	830030	0	0
13H-2, 84–86	116.34	34865	115938	8567	848981	0	0
14H-4, 74–76	128.74	13592	40303	9849	876657	0	0
15H-1, 127–128	134.27	30347	100095	533960	823652	0	0
16H-3, 124–126	146.74	4118	10208	4314	904488	0	0
18H-2, 131–132	156.81	131342	433581	27258	430288	0	0
19H-2, 140–141	162.90	37173	125572	3561	892590	0	0
21X-3, 33–34	172.83	16056	48699	7194	892156	0	0
22X-2, 108–109	175.38	72656	235718	438972	676283	0	0
23X-2, 33–34	184.13	48603	154359	7309	878513	0	0
24X-4, 109–110	197.49	45936	145366	32030	898490	146	0
25X-3, 120–121	205.60	92406	296426	26380	901195	150	0
29X-2, 38–39	241.88	518977	99	104101	5242.19	99	0
31X-6, 55–56	267.35	163460	564136	59510	85671	0	0
32X-1, 60–61	269.50	150608	510604	26804	40064	0	0
35X-5, 13–14	304.03	114431	376461	388065	576702	127	0
37X-5, 100–120	323.29	165783	63216	43771	63215	0	0
42X-7, 40–43	374.80	29949	368318	160979	137	137	9
44X-3, 124–127	388.84	28706	92107	510318	750516	289	28
61X-3, 35–36	552.25	0	0	0	4566	0	0
64X-6, 10–11	585.10	106967	351764	0	134612	129	0
68X-6, 2–3	623.52	0	0	1772	4376	0	0
70X-5, 33–34	641.53	38691	119538	315604	509450	645	12
150-903B-							
11H-6, 100–102	96.00	31899	95248	148027	361671	0	0
12H-4, 116–117	102.66	49326	154804	37392	110059	0	0
13H-3, 94–96	110.44	30553	91279	150550	0	0	0
14H-2, 65–67	118.15	44910	143111	106430	259156	0	0
15H-6, 75–80	133.75	54293	171215	28074	87926	0	0
16H-4, 115–117	140.65	137590	461199	186524	244216	85	0
17H-5, 71–73	151.21	175692	618505	2174	324	0	0

Note: Volatile gas concentrations given in parts per million (ppm).

in which a mole of carbonate is produced for every mole of methane (Nissenbaum et al., 1972). Alternatively, subsurface methane may have been generated thermogenically when deeply buried sediments reached temperatures (>50°C) sufficient to crack polycondensed sediment organic matter and liberate free hydrocarbons. In this latter process, high-molecular-weight gases (C_{2+}) would also be liberated in increasingly larger quantities as the organic matter continued to be thermally degraded. This allows the C_1/C_2 ratio to be used as an indicator of gas source. The methane in this shallow zone at Site 903 is considered to be of biogenic origin because of the very high C_1/C_2 ratios (C_2 was detected in trace levels in only two samples from this interval). Methanogenic bacteria depend on hydrogen for their energy but are unable to compete successfully with sulfate reducers for hydrogen (Claypool and Kaplan, 1974). Consequently, methanogens normally become active only beneath the zone of sulfate reduction. This is reflected in the top 15 mbsf of Hole 903 sediments, where sulfate declines dramatically to minimal levels (see "Inorganic Geochemistry" section, this chapter), whereas methane concentrations begin to increase at 14 mbsf (Fig. 19). An interesting correlation occurs between methane concentration and carbonate as percentage by weight in the interval from 100 to 150 mbsf. This interval of lithologic Unit I contains several intervals of redeposited sediments (see "Lithostratigraphy" section, this chapter). Although the total organic carbon does not increase in this interval (Fig. 20), sediment emplacement by mass-transport processes, may optimize conditions necessary for high organic-matter preservation, thus increasing the amount of substrate available for bacterial utilization and, coincidentally, sediment methane concentrations.

Between 205 and 380 mbsf, methane levels drop to less than 10,000 ppm (<1%). A second subsurface enrichment of gas occurs within lithologic Unit III (380–520 mbsf), and methane levels reach 380,333 ppm at 513 mbsf, accompanied by minor amounts of C_2 and C_3 hydrocarbons. This latter gaseous zone occurs in especially sandy clay at the base of Unit III (see "Lithostratigraphy" section, this chapter). The increased gas concentrations correspond to, and are presumably produced by, a concomitant increase in organic matter content (see "Elemental Analysis," this section, and Fig. 20), which is being bacterially degraded in situ at and below the boundary. C_1/C_2 ratios vary irregularly in lithologic Subunit IIB between 1×10^3 and 29×10^3. These high ratios, coupled with corresponding total organic carbon (TOC) and alkalinity increases (see "Inorganic Geochemistry" section, this chapter), suggest that this subsurface pocket of gas is of biogenic origin.

The deepest gassy zone at Site 903 occurs from 693 mbsf to the base of Hole 903C (1149.7 mbsf). The upper limit appears to be associated with the lithostratigraphic boundary between lithologic Units IV and V (733 mbsf), where a further increase downsection occurs in TOC values (Fig. 20). A significant minimum in the gas concentrations occurs in the interval between 940.2 and 962.7 mbsf. The reason for this decline is unclear; however, a corresponding decline in carbonate values also takes place.

The C_2 and C_3 values reach significant amounts (C_2: 127 ppm, C_3: 52 ppm; Table 7) at 1028.4 mbsf and the C_1/C_2 ratios plummet to <100 in occasional samples. However, the very low C_1/C_2 ratios were calculated on samples that contained <0.1% methane; these ratios do not show the exponential decrease with depth that is characteristic for thermogenically generated methane. In fact, C_1/C_2 values from consecutive cores at the base of the hole actually showed a gradual increase with depth. These data, together with the shallow penetration depth, Rock-Eval T_{max} values indicative of organic-matter immaturity, and the correlation of the gas-enriched zone with increased TOC, lead to the assumption that the gas was primarily generated biologically, rather than thermogenically in situ. The possibility that some migrated, thermally generated gas has contributed to the deeper gas zone cannot be unequivocally ruled out. The concentrations of C_2 and C_3 hydrocarbons present are most likely generated by means of biological organic-matter degradation. Alternatively, these concentrations could be associated with high-salinity interstitial waters (see "Inorganic Geochemistry" section, this chapter), which indicates migration of fluids from local salt diapirs at greater depth.

Elemental Analysis

Elemental analysis, inorganic carbon (IC), and total organic carbon (TOC) were determined on 144 samples from Site 903; sample frequency was one sample per core (Table 8). The IC concentration was measured by coulometry and translated to $CaCO_3$ (wt%), assuming that most of the IC exists within calcite. Within the Pleistocene sediments at Site 903 (0–350 mbsf), inorganic carbon (lithologic Units I and II) values range from 0.6% to 16.9% and the profile appears to be strongly controlled by detrital sedimentation (see "Lithostratigraphy" section, this chapter). The effect of the Pleistocene/Pliocene unconformity is clearly reflected in the carbonate data at 340 mbsf; carbonate values drop from 16 wt% at 10 m above the boundary to 0.3 wt% directly below it (Fig. 19). In the upper and middle Miocene section (340–844 mbsf), carbonate concentrations remain below 10 wt% $CaCO_3$; as at Site 902, this low value is considered to be caused by dissolution reactions resulting from low pH values (see "Inorganic Geochemistry" section, this chapter). Below 844 mbsf (the boundary of lithologic Subunits IVA and IVB in the lower Miocene), $CaCO_3$ values gradually increase from 2 wt% up to 25.1 wt% at 998.0 mbsf. This increase coincides with an increased abundance of calcareous microfossils (see "Lithostratigraphy" section, this chapter). Values decrease once more to 10.7 wt% in Oligocene muds before a dramatic increase to 50+ wt% at the top of the Eocene chalks. At 1063 mbsf, the carbonate content is anomalously low (2.3 wt% $CaCO_3$) compared with the general trend of the profile because this sample was taken from a glauconitic sand unit present at the Oligocene/Eocene boundary.

In the Pleistocene part of the section at Site 903 (lithologic Units I and II, 0–359 mbsf), organic carbon values are significantly lower than those measured for the same interval at Site 902 (average of 0.5% vs. 2.0%, respectively). Sedimentation rates were almost two times higher at Site 903 than at Site 902 (see "Sedimentation Rates" section

Table 7. Headspace gas composition from sediments at Site 903.

Core, section, interval (cm)	Depth (mbsf)	C_1	$C_{2=}$	C_2	C_3	C_1/C_2	C_1/C_{2+}
150-903A-							
1H-2, 0–5	1.50	1	0	0	0		
2H-4, 0–5	14.00	74494	0	0	0		
3H-4, 0–5	23.50	174485	0	0	0		
4H-5, 0–5	34.50	175280	0	0	0		
5H-4, 0–5	42.50	132215	0	0	0		
6H-4, 0–5	52.00	116674	0	0	0		
7H-4, 0–5	61.50	125347	0	0	0		
8H-4, 0–5	71.00	117911	0	0	0		
9H-4, 0–5	80.50	164431	0	0	0		
10H-4, 0–5	90.05	321226	0	0	0		
11H-4, 0–5	99.50	124079	0	0	0		
12H-4, 0–5	109.00	67370	0	0	0		
13H-3, 0–5	117.00	521916	0	0	0		
14H-4, 0–5	128.00	460503	0	0	0		
15H-2, 0–5	134.50	602020	0	1	0	602020	
16H-3, 0–5	145.50	262977	0	1	0	262977	
17H-3, 0–5	152.00	8965	0	0	0		
18H-2, 0–5	155.50	67098	0	0	0		
19H-3, 0–5	163.00	21620	0	0	0		
21X-2, 0–5	171.00	6950	0	0	0		
22X-2, 0–5	174.30	40	0	0	0		
23X-2, 0–5	183.80	9596	0	0	0		
24X-4, 0–5	196.40	144	0	0	0		
25X-4, 0–5	205.90	36814	1	1	0	36814	18407
26X-4, 0–5	215.50	7572	0	0	0		
27X-4, 0–5	225.10	103	0	0	0		
28X-3, 0–5	233.30	7079	0	0	0		
29X-2, 0–5	241.50	6588	0	0	0		
30X-2, 0–5	251.20	6704	0	0	0		
31X-2, 0–5	260.80	10272	0	0	0		
32X-3, 0–5	271.90	9333	0	0	0		
33X-3, 0–5	281.25	7699	0	0	0		
34X-5, 0–5	293.20	8827	1	1	0	8827	
35X-4, 0–5	302.40	7703	0	0	0		
36X-4, 0–5	312.00	8839	0	1	0	8839	
37X-4, 0–5	320.79	10325	0	1	0	10325	
38X-4, 0–5	331.20	9349	0	0	0		
39X-4, 0–5	340.90	6585	0	0	0		
40X-3, 0–5	349.00	14200	0	1	1	14200	7100
41X-4, 0–5	360.20	7445	0	1	0	7445	
42X-4, 0–5	369.90	8703	0	2	2	4352	2176
43X-4, 0–5	379.40	89801	1	3	2	29934	14967
44X-3, 0–5	387.60	44315	1	3	2	14772	7386
45X-3, 0–5	397.30	8194	0	2	2	4097	2049
46X-6, 145–150	412.45	29064	0	5	4	5813	3229
47X-4, 0–5	418.20	7525	0	2	2	3763	1881
48X-4, 0–5	427.80	95140	0	4	3	23785	13591
49X-4, 0–5	437.50	82122	0	7	3	11732	8212
50X-4, 0–5	447.20	8038	0	3	2	2679	1608
51X-4, 0–5	456.70	40262	0	8	3	5033	3660
52X-4, 0–5	466.40	101381	0	10	3	10138	7799
53X-4, 0–5	476.10	169787	1	12	6	14149	8936
54X-4, 0–5	485.80	51652	0	7	2	7379	5739
55X-3, 0–5	493.90	8963	1	9	2	996	747
56X-2, 0–5	502.10	9961	1	9	0	1107	996
57X-3, 0–5	513.20	380333	2	13	3	29256	21130
58X-2, 0–5	521.40	27074	0	6	0	4512	4512
59X-4, 0–5	534.00	9959	0	9	0	1107	1107
60X-4, 0–5	543.70	7149	0	3	0	2383	2383
61X-4, 0–5	553.40	8942	0	5	0	1788	1788
62X-4, 0–5	563.00	10087	0	7	0	1441	1441
63X-4, 0–5	572.30	6024	0	4	0	1506	1506
64X-4, 0–5	582.00	32721	2	21	3	1558	1259
65X-4, 0–5	591.60	21269	1	9	0	2363	2127
67X-4, 0–5	610.80	73	0	0	0		
68X-4, 0–5	620.50	9592	0	10	1	959	872
69X-4, 0–5	630.10	3963	0	3	0	1321	1321
70X-4, 0–5	639.70	8953	1	11	2	814	640
71X-4, 0–5	649.20	9336	0	10	1	934	849
72X-4, 0–5	658.90	7934	0	5	0	1587	1587
73X-4, 0–5	668.60	155	0	1	0	155	155
74X-4, 0–5	678.30	17798	1	19	2	937	809
75X-4, 0–5	688.00	7293	1	9	0	810	729
76X-4, 0–5	697.60	3	0	0	0		
150-903B-							
1H-2, 0–5	1.50	1	0	0	0		
2H-4, 0–5	5.23	1	0	0	0		
3H-4, 0–5	16.00	113273	0	0	0		
4H-4, 0–5	25.50	128577	0	0	0		
5H-4, 0–5	35.00	152281	0	0	0		
6H-4, 0–5	44.50	143238	0	0	0		
7H-4, 0–5	54.00	451240	0	0	0		
8H-4, 0–5	63.50	446733	0	1	1	446733	223367
9H-4, 0–5	73.00	375465	0	1	1	375465	187733
10H-3, 0–5	81.00	159704	0	0	0		
11H-4, 0–5	92.00	74660	0	0	0		
12H-4, 0–5	101.50	174287	0	0	0		
13H-4, 0–5	111.00	17377	0	0	0		
14H-3, 0–5	119.00	36355	0	0	0		
15H-3, 0–5	128.50	36617	0	0	0		
16H-4, 0–5	139.50	5093	0	0	0		
17H-4, 0–5	149.00	154477	0	1	0		
150-903C-							
5R-2, 0–5	507.10	66744	1	12	1	5562	4767
6R-1, 50–54	510.80	36865	0	3	0	12288	12288
7R-4, 0–5	519.80	36301	2	14	2	2593	2017
9R-2, 0–5	588.00	10100	1	7	0	1443	1263
10R-4, 0–5	596.60	36429	0	10	0	3643	3643
11R-2, 0–5	603.30	4953	2	4	1	1238	708
12R-4, 0–5	693.10	154510	1	41	3	3769	3434
13R-2, 0–5	699.70	63407	1	25	2	2536	2265
14R-4, 0–5	712.30	170134	1	56	5	3038	2744
15R-3, 0–5	720.20	8832	1	10	1	883	736
16R-3, 0–5	730.00	25097	0	9	0	2789	2789
17R-4, 0–5	741.30	6325	0	3	0	2108	2108
18R-2, 0–5	747.13	9841	1	17	2	579	492
19R-3, 0–5	759.20	25241	1	30	3	841	742
20R-5, 0–5	770.61	70926	1	78	7	909	825
21R-2, 0–5	776.58	8442	0	15	3	563	469
22R-4, 0–5	789.70	47897	1	46	5	1041	921
23R-4, 0–5	799.40	230	0	6	2	38	29
24R-1, 0–5	804.10	3275	0	72	0	45	45
25R-2, 0–5	815.30	951	1	12	4	79	56
26R-CC, 0–5	823.50	7619	1	34	6	224	190
27R-1, 0–5	833.10	9103	1	47	6	194	169
28R-2, 0–5	844.20	56773	1	94	9	604	546
29R-4, 0–5	856.90	8990	1	41	6	219	187
31R-1, 0–5	871.70	95921	0	105	3	914	888
32R-2, 0–5	882.90	8855	0	46	5	193	174
33R-4, 0–5	895.60	68628	0	95	7	722	673
34R-2, 0–5	902.20	99909	0	145	23	689	595
35R-4, 0–5	913.81	69212	1	132	24	524	441
36R-3, 0–5	923.00	72540	0	104	10	698	636
37R-4, 0–5	934.20	45322	1	122	24	371	308
38R-2, 0–5	940.15	8489	0	43	6	197	173
39R-4, 0–5	953.10	7843	0	27	4	290	253
40R-4, 0–5	962.70	5924	0	19	2	312	282
41R-4, 0–5	972.00	84021	1	103	15	816	706
43R-CC, 0–5	986.80	174978	0	134	22	1306	1122
44R-2, 0–5	998.00	181160	1	121	37	1497	1139
45R-2, 0–5	—	68981	1	117	37	590	445
46R-1, 0–5	—	120124	1	126	31	953	760
47R-2, 137–142	—	53277	2	127	52	420	294
48R-1, 0–5	—	60652	0	102	20	595	497
49R-4, 0–5	—	111725	0	116	28	963	776
51R-2, 135–140	—	131509	0	113	19	1164	996
52R-4, 0–5	—	64695	0	35	4	1848	1659
53R-3, 0–5	—	92129	0	63	6	1462	1335
54R-5, 0–5	—	37894	0	25	3	1516	1353
55R-4, 0–5	—	131599	0	98	7	1343	1253
56R-4, 0–5	—	68596	0	41	5	1673	1491
57R-2, 0–5	—	189	0	3	0	63	63
58R-5, 0–5	—	42002	0	12	1	3500	3231
60R-3, 0–5	—	103344	0	28	4	3691	3230
150-903D-							
1R-1, 0–5	774.9	12682		13	0	975.54	975.54
2R-2, 0–5	786	1167		0	0	0	0
3R-1, 0–5	794.2	11385		41	3	277.68	258.75
4R-2, 0–5	805.3	6098		11	3	554.36	435.57
5R-4, 0–5	816.81	8435		14	3	602.5	496.18
6R-4, 0–5	827.6	33237		151	3	220.11	215.82
7R-4, 0–5	837.3	39614		191	4	207.4	203.15
8R-4, 0–5	846.9	9907		102	4	97.13	93.46
9R-4, 0–5	856.5	28045		141	3	198.9	194.76
10R-3, 0–5	864.7	2319		7	0	331.29	331.29
11R-4, 0–5	875.8	17884		107	3	167.14	162.58
12R-1, 0–5	881	55415		206	7	269	260.16
13R-3, 0–5	893.7	46590		142	3	328.1	321.31
14R-3, 0–5	903.2	11139		32	4	348.09	309.42
15R-2, 0–5	911.2	41014		333	9	123.17	119.92
16R-2, 0–5	920.2	31169		198	6	157.42	152.79
17R-3, 0–5	931.8	9856		15	0	657.07	657.07
18R-4, 0–5	942.9	31478		167	5	188.49	183.01
19R-3, 0–5	978.83	22380		119	5	188.07	180.48
20R-3, 0–5	988.51	74079		417	13	177.65	172.28
21R-5, 0–5	1000.96	84499		417	13	202.64	196.51
24R-2, 0–5	1026.8	3415		120	11	28.46	26.07
25R-2, 0–5	1030.5	8548		227	12	37.66	35.77

Note: Volatile gas concentrations given in parts per million (ppm).

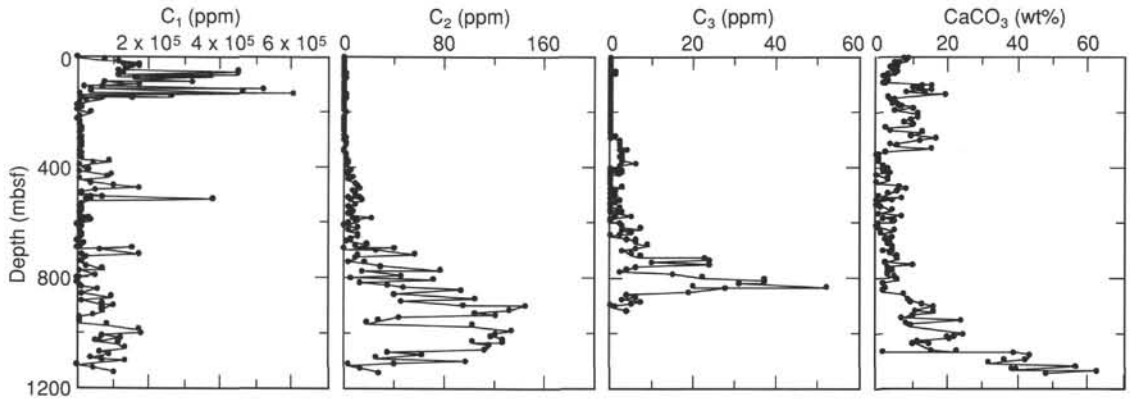

Figure 19. Headspace volatile hydrocarbon composition and carbonate concentration (calculated as $CaCO_3$) vs. depth for sediment samples from Site 903.

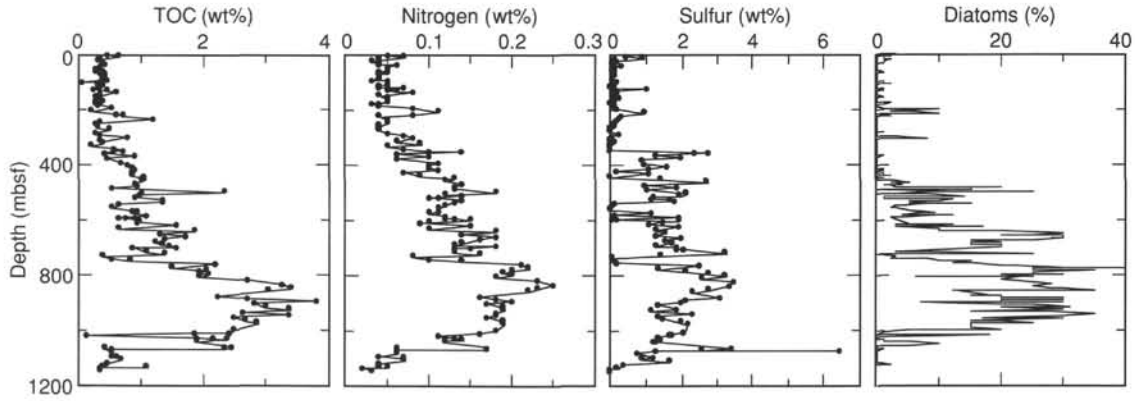

Figure 20. Total organic carbon (TOC), nitrogen, sulfur, and diatom abundance vs. depth for sediment samples from Site 903.

in this chapter as well as "Sedimentation Rates" section in Chapter 6 [this volume]) and are thought to have had a clastic dilution effect on sediment organic matter. Mass accumulation rates for carbon (MAR [TOC]) were calculated for the two sites according to van Andel et al. (1975) with physical properties and sediment rate data by

$$MAR(TOC) = (TOC/100) \cdot LSR\ [WBD - 1.024\ (Po/100)],$$

where

MAR = mass accumulation rate ($g/cm^2/1000$ yr),
TOC = total organic carbon (wt%),
LSR = linear sedimentation rates (cm/1000 yr),
WBD = wet-bulk density (g/cm^3), and
Po = porosity (%).

The following parameters were used:

Site 902	Site 903
Po = 51	Po = 45.5
WBD = 1.93	WBD = 2.03
LSR= 29 cm/1000 yr	LSR = 73 cm/1000 yr
TOC = 0.85%	TOC = 0.38%

The MAR (TOC) average value obtained for the Pleistocene sediments at Site 903 is 0.43 g cm^{-2} $k.y.^{-1}$, which is approximately 25% higher than the organic carbon accumulation rate calculated at Site 902 (0.35 g cm^{-2} $k.y.^{-1}$). This suggests that although organic-matter concentrations in Pleistocene sediments at Site 903 are smaller than at Site 902, organic-carbon mass accumulation rates were similar at Sites 902 and 903 during the Pleistocene. Below the Pleistocene/Miocene boundary, TOC values (Fig. 20) steadily increase throughout the upper and middle Miocene (0.5% to almost 2.0%), and intervals with increased organic carbon appear to correlate with plant fragments observed in smear-slide analyses (see "Lithostratigraphy" section, this chapter). The lower middle and lower Miocene sections (800–1000 mbsf; Fig. 20) have the highest TOC values of the section, which average 3.0%. These values, which occur in more pelagic facies, are significantly higher than values obtained higher in the section where transported sediments predominate (see "Lithostratigraphy" section, this chapter), in which abundant woody detritus was observed. The TOC data shows that the preservation of marine organic matter controls the profile to a greater extent than more refractory terrestrial organic matter, which tends to be deposited in more oxygenated conditions in canyon outlets and mass-flow units (Hülsemann and Emery, 1961; Summerhayes, 1981).

During periods of upwelling along the shelf edge, nutrient-laden bottom waters are brought to the photic zone and are able to support high levels of marine primary productivity. Oxygen demands by the recycling of dead organisms can be greater than supply, leading to low oxygen conditions in ocean bottom waters and sediments. In the lower middle and lower Miocene at Site 903 (759–1061 mbsf), TOC values of 2.0%–3.4% and the correlation of the TOC profile with that of total sulfur, total nitrogen, and diatom-rich intervals (Fig. 20) support the suggestion that localized oxygen depletion impinged on the continental slope during this time and was caused by upwelling. Conditions of oxygenation are considered to be either dysoxic to completely anoxic owing to burrow-free, laminated zone observed at 766 mbsf (see "Lithostratigraphy" section, this chapter). The oxygen depletion has permitted the development of a reducing sedimentary environment, which allows high preservation of organic carbon. High amounts of sulfur occur (up to 6.4%); however, the origin of this sulfur is unclear.

Sulfur may be present as a variety of species: organosulfur compounds, hydrogen sulfide, polysulfide ions, pyrite, and elemental sulfur. In the same respect, nitrogen (maximum at 0.25 wt% at 833.9 mbsf), may be organically bound, having been preserved from planktonic proteins or incorporated into organic polymers during diagenesis. Alternatively, nitrogen may exist as ammonium, associated with clay minerals. The downhole trend of nitrogen mimics that of TOC (Fig. 20), implying that regardless of its present speciation, it probably originated from organic compounds.

Characterization of Organic Matter

At Site 903, the character and maturity of the sediment organic matter was determined by Rock-Eval and C/N ratios. Rock-Eval data were obtained from 27 samples taken from various intervals in Holes 903A and 903C (Fig. 21 and Table 9). Most of the samples have T_{max} values of <435, indicating that the organic matter is immature. A few of the samples have T_{max} values >435, but these values are probably caused by mineral-matrix effects as TOC is correspondingly low (<0.5%). Organic matter encountered in such shallow sediments could not have reached temperature and pressure conditions suitable for in situ maturation. The samples with T_{max} values of >435 and TOC >0.5% may indicate that the mature organic matter has been eroded and transported from elsewhere; however, further analyses are needed to verify this. On the van Krevelen-type diagram, values for the samples analyzed from Hole 903A plot with a large amount of scatter and show no clear trend vs. depth (Fig. 21). Most of the shallow samples from this site plot between the type II and type III kerogen evolutionary pathways in an area that suggests these samples contain a mixture of immature terrestrial and marine-derived organic matter. Most of the deep samples analyzed from Hole 903C plot in a field of higher hydrogen indexes (>300 mg HC/g TOC) and low oxygen indexes (<100 mg HC/g TOC), which indicates that the organic matter is made up of predominantly phytoplankton, zooplankton, and bacteria. This subtle shallow vs. deep contrast is consistent with a marine-influenced slope environment in the early Miocene.

The composition of terrestrial higher plants contains significantly more carbon than do marine organisms. This high carbon content gives plants their structural rigidity in the form of cellulose and lignified tissues, whereas nitrogen content is lower because of low levels of proteinaceous material. These characteristics allow C/N ratios to be used as indicators of organic matter provenance. Generally, the C/N ratios of zooplankton, phytoplankton, and bacteria are between 5 and 10, whereas values between 20 and 100 are indicative of terrestrial species. At Site 903, the C/N ratios varied between 1 and 22 (Table 8 and Fig. 22). Values <5 cannot be used to determine the origin of the organic matter because such low values are artifacts of the sample having a very low TOC and inorganic ammonium present in clays affecting the ratio (Müller, 1977). The ratios from the seafloor to 750 mbsf at Site 903 are variable, but generally have values less than 10. Higher values occur sporadically and are apparently attributable to samples that contain more plant-derived organic matter contained in sediment slumps and debris.

At depths greater than 750 mbsf, C/N ratios are consistently higher and range from 10 to 20. This is inconsistent with Rock-Eval data, which suggest a more marine-influenced origin for the organic matter throughout the lower Miocene section. The higher values are considered to be a function of organic-matter diagenesis (in which organic nitrogen is preferentially mineralized as organic carbon with depth) and similar values have been observed in other deep-sea sediments (Summerhayes, 1983). This phenomenon calls into question the use of C/N ratios as reliable indicators of organic matter source (Müller, 1977). The results from this cruise at Sites 902 and 903, together with data from a wide variety of other environments (de Lange, 1992), indicate that TOC content and C/N ratios are positively correlated. Apparently, in deep-sea sediments, TOC and diagenesis exert a strong control over the C/N ratio, which in many cases obliterates the ratio that is provided by the organic matter.

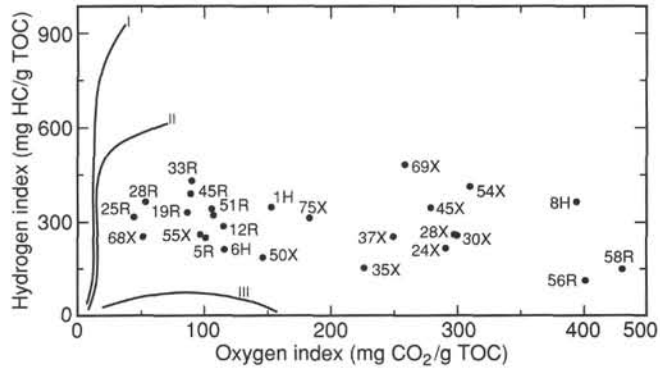

Figure 21. Van Krevelen-type diagram of sediment samples from Site 903. The numbers and letters adjacent to the data points (solid dots) identify core numbers.

INORGANIC GEOCHEMISTRY

Forty-nine interstitial water samples were collected from Site 903: 33 from Hole 903A and 16 from Hole 903C. Sample depths range from 1.5 to 1113 mbsf; every third core was sampled, except in Hole 903A, where every core taken from the upper 100 mbsf was sampled. Samples from Holes 903A and 903C are plotted together (Table 10 and Fig. 23).

Bacterial degradation of organic matter results in the rapid removal of sulfate ions and concentrations approach zero by 14 mbsf (Table 10). Site 903 has the shallowest sulfate-reduction zone of all Leg 150 sites and reflects the high Pleistocene sedimentation rates at this site (see "Sedimentation Rates" section, this chapter). Sulfate remains low at greater depths and methane increases, indicating the transition from predominantly sulfate-reducing to methanogenic bacteria (see "Organic Geochemistry" section, this chapter). The degradation of organic matter in the rapidly deposited (>250 m in 0.4 m.y.), organic-rich (>0.5 wt% TOC) Pleistocene sediment results in a rapid increase in titration alkalinity, ammonium ion, and phosphate ion (Fig. 23).

High alkalinity values result from the production of CO_2 by bacteria during organic-matter degradation. In general, high alkalinity corresponds to intervals of organic-rich (>0.5 wt%), diatomaceous sediment (see "Organic Geochemistry" section, this chapter). Three principal alkalinity maxima occur: 16 mM at 14 mbsf, 32 mM at 196 mbsf, and 39 mM at 486 mbsf (Fig. 23). The shallowest alkalinity maximum corresponds to the base of the current sulfate-reduction zone. Alkalinity then decreases to 6 mM at 71 mbsf before increasing to the broad second maximum of 18 to 32 mM between 128 and 196 mbsf. Alkalinity decreases to 7.5 mM by 253 mbsf and then rapidly increases to a maximum of 39 mM by 486 mbsf. Alkalinity remains fairly constant at around 35 mM to 720 mbsf and then decreases steadily to 19 mM by 1023 mbsf.

Ammonium (NH_4^+) is a by-product of organic-matter degradation and has three maxima that coincide with or occur somewhat deeper than the alkalinity maxima (Fig. 23). The first ammonium maximum of 6.5 mM occurs at 43 mbsf. Ammonium decreases to 4 mM at 71 mbsf before increasing to 10–11 mM from 128 to 196 mbsf. Ammonium decreases to 5.5 mM by 397 mbsf before increasing to a broad, sporadic maximum of 16 mM centered around 720–747 mbsf. Ammonium decreases from 15 to 6 mM between 883 and 1113 mbsf.

Phosphate is another by-product of organic-matter degradation that usually occurs at shallower burial depths than ammonium and alkalinity maxima because bacteria preferentially metabolize phosphorus-rich organic matter (Gieskes, 1981). Phosphate ion increases to a maximum of 115 µM at 14 mbsf and 125 µM at 196 mbsf (Fig.

Table 8. Inorganic carbon, organic carbon, and elemental analysis data from sediments at Site 903.

Core, section, interval (cm)	Depth (mbsf)	Total carbon (wt%)	Inorganic carbon (wt%)	Total organic carbon (wt%)	$CaCO_3$ (wt%)	Nitrogen (wt%)	Sulfur (wt%)	C/N	C/S
150-903A-									
1H-2, 20–22	1.70	1.52	1.08	0.44	9.00	0.05	0.45	9	1
2H-3, 45–47	12.95	1.35	1.03	0.32	8.60	0.04	0.14	8	2
3H-1, 70–72	19.70	1.12	0.77	0.35	6.40	0.04	0.19	9	2
4H-4, 67–69	33.67	0.92	0.50	0.42	4.20	0.04	0.13	10	3
5H-2, 60–62	40.10	0.90	0.56	0.34	4.70	0.05	0.12	7	3
6H-2, 70–72	49.70	0.96	0.62	0.34	5.20	0.05	0.11	7	3
7H-2, 71–73	59.21	0.93	0.67	0.26	5.60	0.04	0.09	7	3
8H-2, 68–70	68.68	0.76	0.42	0.34	3.50	0.04	0.15	9	2
10H-4, 10–12	90.15	0.75	0.35	0.40	2.90	0.03	0.16	13	3
11H-4, 76–77	100.26	1.93	1.90	0.03	15.80	0.05	0.09	1	0
12H-3, 68–70	108.18	1.67	1.29	0.38	10.70	0.05	0.02	8	19
13H-3, 56–58	117.56	1.90	1.58	0.32	13.20	0.04	0.11	8	3
14H-3, 65–67	127.15	1.24	1.02	0.22	8.50	0.05	0.20	4	1
16H-3, 72–74	146.22	0.75	0.40	0.35	3.30	0.04	0.11	9	3
17H-3, 63–64	152.63	0.76	0.49	0.27	4.10	0.05	0.22	1	4
18H-1, 66–67	154.66	0.93	0.63	0.30	5.20	0.05	0.09	6	3
19H-1, 69–71	160.69	0.86	0.53	0.33	4.40	0.05	0.13	7	3
20H-1, 73–75	165.23	0.82	0.55	0.27	4.60	0.05	0.06	5	5
20H-4, 6–7	168.99	1.08	0.72	0.36	6.00	0.05	0.00	7	—
21X-3, 72–73	173.22	1.05	0.77	0.28	6.40	0.04	0.12	7	2
22X-3, 90–92	176.70	1.17	0.85	0.32	7.10	0.03	0.08	10	4
23X-2, 59–61	184.39	1.62	1.31	0.31	10.90	0.04	0.12	8	3
24X-2, 68–70	194.08	1.17	0.64	0.53	5.30	0.08	0.18	7	3
25X-3, 60–62	205.00	1.67	1.47	0.20	12.20	0.11	0.95	2	0
26X-3, 76–78	214.76	1.99	1.39	0.60	11.60	0.08	0.31	8	2
27X-2, 80–82	222.90	1.88	1.17	0.71	9.70	0.04	0.27	18	3
28X-3, 68–71	233.98	2.15	0.96	1.19	8.00	0.05	0.18	24	7
29X-4, 76–78	245.26	1.58	1.26	0.32	10.50	0.05	0.15	6	2
30X-3, 50–52	253.20	0.59	0.31	0.28	2.60	0.04	0.12	7	2
31X-3, 74–75	263.04	0.78	0.48	0.30	4.00	0.04	0.00	8	—
32X-3, 59–60	272.49	2.08	1.61	0.47	13.40	0.04	0.00	12	—
33X-3, 79–80	282.04	1.49	1.22	0.27	10.20	0.05	0.22	1	1
34X-3, 70–72	290.90	2.36	2.03	0.33	16.90	0.07	0.05	5	7
35X-3, 60–61	301.50	2.28	1.51	0.77	12.60	0.08	0.02	10	38
36X-3, 69–71	311.19	0.86	0.52	0.34	4.30	0.06	0.09	6	4
37X-4, 70–71	321.49	1.06	0.70	0.36	5.80	0.09	0.02	4	18
38X-3, 68–69	330.38	2.08	1.90	0.18	15.80	0.05	0.00	4	—
39X-3, 60–62	340.00	0.93	0.36	0.57	3.00	0.07	0.02	8	28
40X–2, 95–97	348.45	0.73	0.04	0.69	0.30	0.10	2.40	7	0
40X-3, 64–66	349.64	0.63	0.06	0.57	0.50	0.14	2.78	4	0
41X-3, 127–129	359.97	0.47	0.07	0.40	0.60	0.06	1.25	1	0
42X-2, 63–64	367.53	1.01	0.13	0.88	1.10	0.10	2.02	9	0
43X-2, 84–85	377.24	0.53	0.10	0.43	0.80	0.06	0.89	7	1
44X-4, 94–96	390.04	0.91	0.24	0.67	2.00	0.11	0.99	6	1
45X-3, 80–82	398.10	1.19	0.42	0.77	3.50	0.10	1.61	8	1
46X-4, 62–64	408.62	1.06	0.22	0.84	1.80	0.10	1.08	8	1
47X-4, 64–66	418.84	1.36	0.47	0.89	3.90	0.11	0.17	8	5
48X-3, 70–71	427.00	0.86	0.01	0.85	0.10	0.07	1.10	12	1
49X-3, 69–70	436.69	1.25	0.41	0.84	3.40	0.09	0.00	9	—
50X-3, 76–77	446.46	1.45	0.40	1.05	3.30	0.13	1.43	8	1
51X-3, 79–80	455.99	1.05	0.03	1.02	0.20	0.12	2.73	9	0
52X-3, 78–81	465.68	1.66	0.78	0.88	6.50	0.14	0.96	6	1
53X-3, 76–79	475.36	1.98	1.04	0.94	8.70	0.13	1.89	7	1
54X-3, 60–63	484.90	1.22	0.70	0.52	5.80	0.13	1.01	4	1
55X-3, 62–64	494.52	2.73	0.41	2.32	3.40	0.18	2.15	13	1
56X-2, 71–72	502.81	1.12	0.12	1.00	1.00	0.12	1.96	8	1
57X-4, 28–29	514.98	0.93	0.02	0.91	0.20	0.10	1.13	9	1
58X-3, 70–71	523.60	1.38	0.06	1.32	0.50	0.14	1.81	9	1
59X-3, 70–71	533.20	1.37	0.05	1.32	0.40	0.13	0.11	10	12
60X-3, 89–91	543.09	0.85	0.21	0.64	1.70	0.12	0.03	5	21
61X-3, 89–91	552.79	1.07	0.54	0.53	4.50	0.11	0.01	5	53
62X-6, 63–65	566.63	1.06	0.13	0.93	1.10	0.11	1.17	8	1
63X-4, 54–56	572.84	1.72	0.88	0.84	7.30	0.10	0.11	8	8
64X-4, 69–71	582.69	1.36	0.27	1.09	2.20	0.12	1.93	9	1
65X-4, 68–70	592.28	1.36	0.62	0.74	5.20	0.13	0.04	6	18
67X-3, 83–85	610.13	0.97	0.03	0.94	0.20	0.09	1.09	10	1
68X-2, 67–68	618.17	1.61	0.07	1.54	0.60	0.15	1.90	10	1
69X-3, 77–79	629.37	1.24	0.61	0.63	5.10	0.10	1.28	6	1
70X-3, 92–94	639.12	2.02	0.17	1.85	1.40	0.18	1.57	10	1
71X-3, 80–81	648.50	1.85	0.55	1.30	4.60	0.14	1.28	9	1
72X-3, 79–80	658.19	2.05	0.35	1.70	2.90	0.18	1.98	9	1
73X-3, 80–81	667.90	1.86	0.49	1.37	4.10	0.16	1.52	9	1
74X-3, 80–81	677.60	1.60	0.37	1.23	3.10	0.14	1.73	9	1
75X-3, 56–59	687.06	1.87	0.54	1.33	4.50	0.13	1.27	10	1
76X-4, 68–71	698.28	1.86	0.29	1.57	2.40	0.15	1.85	10	1
150-903B-									
2H-3, 58–59	4.31	1.57	0.94	0.63	7.80	0.07	0.91	9	1
3H-6, 58–59	19.58	0.92	0.63	0.29	5.20	0.03	0.06	10	5
4H-3, 58–59	24.58	1.02	0.65	0.37	5.40	0.04	0.08	9	5
5H-3, 58–59	34.08	1.12	0.72	0.40	6.00	0.06	0.29	7	1
6H-3, 58–59	43.58	0.97	0.64	0.33	5.30	0.05	0.05	7	7
7H-3, 58–59	53.08	0.94	0.68	0.26	5.70	0.05	0.03	5	9
8H-3, 58–59	62.58	0.79	0.42	0.37	3.50	0.05	0.10	7	4
9H-3, 58–59	72.08	0.66	0.24	0.42	2.00	0.04	0.12	11	4
10H-3, 58–59	81.58	0.76	0.37	0.39	3.10	0.04	0.08	10	5

Table 8 (continued).

Core, section, interval (cm)	Depth (mbsf)	Total carbon (wt%)	Inorganic carbon (wt%)	Total organic carbon (wt%)	$CaCO_3$ (wt%)	Nitrogen (wt%)	Sulfur (wt%)	C/N	C/S
11H-5, 60–62	94.10	0.72	0.29	0.43	2.40	0.05	0.09	9	5
12H-3, 60–61	100.60	1.95	1.60	0.35	13.30	0.05	0.07	7	5
13H-3, 48–49	109.98	1.73	1.44	0.29	12.00	0.04	0.07	7	4
14H-2, 21–23	117.71	2.23	1.90	0.33	15.80	0.07	1.00	5	0
15H-3, 56–58	129.06	2.08	1.63	0.45	13.60	0.06	0.13	8	4
16H-1, 37–39	135.37	2.97	2.36	0.61	19.70	0.08	0.20	8	3
150-903C-									
5R-2, 74–76	507.84	1.83	0.88	0.95	7.30	0.14	1.23	7	1
7R-3, 15–16	518.45	1.50	0.59	0.91	4.90	0.11	1.69	8	1
9R-3, 72–73	590.22	1.26	0.63	0.63	5.20	0.12	0.20	5	3
10R-3, 68–70	595.78	1.50	0.59	0.91	4.90	0.15	1.93	6	1
11R-1, 95–96	602.75	1.06	0.10	0.96	0.80	0.10	1.48	10	1
12R-3, 70–72	692.30	1.97	0.54	1.43	4.50	0.18	1.86	8	1
13R-1, 120–122	699.40	1.44	0.57	0.87	4.70	0.13	2.06	7	0
14R-3, 62–64	711.42	1.59	0.52	1.07	4.30	0.13	3.25	8	0
15R-3, 20–21	720.40	2.11	0.75	1.36	6.20	0.16	1.43	9	1
16R-3, 56–57	730.56	1.09	0.73	0.36	6.10	0.08	0.08	5	5
17R-3, 80–82	740.60	0.88	0.35	0.53	2.90	0.10	0.14	5	4
18R-2, 69–71	747.82	2.10	1.30	0.80	10.80	0.14	0.17	6	5
19R-3, 79–81	759.99	2.61	0.42	2.19	3.50	0.21	2.52	10	1
20R-4, 80–81	769.91	2.09	0.59	1.50	4.90	0.22	1.33	1	1
21R-3, 81–83	778.89	2.41	0.38	2.03	3.20	0.20	2.11	10	1
22R-3, 35–37	788.55	2.30	0.37	1.93	3.10	0.19	2.77	10	1
23R-2, 77–78	797.17	2.72	0.65	2.07	5.40	0.20	3.24	10	1
24R-2, 9–10	805.69	2.70	0.76	1.94	6.30	0.18	2.56	11	1
25R-2, 73–74	816.03	2.94	0.23	2.71	1.90	0.23	3.46	12	1
27R-1, 80–81	833.90	3.59	0.31	3.28	2.60	0.25	3.35	13	1
28R-2, 45–46	844.65	3.63	0.23	3.40	1.90	0.23	2.79	15	1
29R-2, 40–43	854.30	3.96	0.93	3.03	7.70	0.22	2.34	14	1
31R-2, 40–41	873.60	3.33	1.12	2.21	9.30	0.16	3.07	14	1
32R-3, 108–109	885.48	3.90	1.20	2.70	10.00	0.18	2.12	15	1
33R-2, 61–62	893.21	5.35	1.55	3.80	12.90	0.20	2.01	19	2
34R-1, 43–44	901.13	4.75	1.94	2.81	16.20	0.17	1.34	17	2
35R-4, 66–67	914.47	4.31	1.32	2.99	11.00	0.19	1.89	16	2
36R-2, 76–77	922.26	5.40	2.01	3.39	16.70	0.19	1.15	18	3
37R-2, 78–79	931.98	3.91	1.27	2.64	10.60	0.18	2.34	15	1
38R-3, 70–71	942.35	4.29	0.91	3.38	7.60	0.18	1.34	19	3
39R-3, 72–73	952.32	5.43	2.95	2.48	24.60	0.17	1.45	15	2
40R-3, 70–72	961.90	3.69	1.01	2.68	8.40	0.19	1.97	14	1
41R-3, 65–67	971.15	4.04	1.18	2.86	9.80	0.19	2.19	15	1
44R-1, 146–148	997.96	5.49	3.01	2.48	25.10	0.18	2.09	14	1
45R-1, 43–44	1006.60	4.83	2.41	2.42	20.10	0.16	1.65	15	2
45R-2, 79–80	1008.50	4.57	2.70	1.87	22.50	0.16	1.75	12	1
46R-1, 9–10	1015.90	2.62	2.51	0.11	20.90	0.11	1.33	1	0
47R-1, 59–60	1026.10	3.38	1.47	1.91	12.20	0.13	1.36	15	1
47R-2, 70–71	1027.70	3.76	1.40	2.36	11.70	0.14	1.38	17	2
48R-2, 79–80	1031.40	3.95	1.79	2.16	14.90	0.12	1.29	18	2
49R-2, 71–72	1036.00	3.18	1.28	1.90	10.70	0.12	1.21	16	2
51R-4, 72–73	1058.30	4.32	1.87	2.45	15.60	0.17	3.42	14	1
51R-6, 72–73	1061.30	5.06	2.74	2.32	22.80	0.17	2.56	14	1
51R-7, 120–123	1063.30	0.68	0.28	0.40	2.30	0.06	6.44	7	0
52R-4, 64–66	1069.20	5.26	4.74	0.52	39.50	0.06	1.30	9	0
53R-3, 92–93	1077.70	5.81	5.29	0.52	44.10	0.06	0.77	9	1
54R-6, 48–49	1091.40	5.64	5.13	0.51	42.70	0.04	1.20	13	0
55R-3, 61–62	1096.40	5.02	4.41	0.61	36.70	0.07	0.90	9	1
56R-3, 44–45	1105.10	4.52	3.86	0.66	32.20	0.07	1.65	9	0
57R-3, 77–78	1115.30	7.32	6.86	0.46	57.10	0.04	0.38	11	1
58R-7, 76–77	1129.50	5.01	4.62	0.39	38.50	0.04	0.20	10	2
58R-8, 27–28	1130.50	5.92	4.83	1.09	40.20	0.05	0.17	22	6
59R-3, 47–48	1133.00	7.86	7.54	0.32	62.80	0.02	0.00	16	—
60R-4, 74–75	1144.00	6.12	5.78	0.34	48.10	0.03	0.00	11	—

23). Phosphate ranges from 3 to 26 µM from 225 to 698 mbsf. Below 720 mbsf, phosphate is essentially zero.

The trends of phosphate, alkalinity, and ammonium maxima with increasing sediment depth is similar to that commonly observed in organic-rich marine sediments (Gieskes, 1981). However, it is less common to observe more than one subsurface maximum. The high organic-carbon contents of these sediments, combined with the fact that alkalinity, ammonium, and phosphate decrease below ~700 mbsf, suggests that they are produced primarily from local organic-matter degradation. The possibility that they were derived from greater burial depths by the thermal degradation of organic matter, then migrated to shallower depths in association with high-salinity pore waters (see below) appears unlikely.

Similar to Site 902, salinity and chloride increase rapidly below the Pleistocene/Miocene contact and correspond to a drop in pH to slightly acidic values (Fig. 23). The maximum salinity of 57.8‰ at Site 903 is slightly higher than the maximum salinity reported from ODP Site 902 (54‰) or DSDP Site 612 (53‰) (Poag, Watts, et al., 1987). Salinity initially decreases from 35.5‰ to 33.0‰ from 1.5 to 43 mbsf and remains uniform to 172 mbsf (Fig. 23). The lower salinity reflects the loss of sulfate by means of sulfate reduction, as well as the loss of calcium and magnesium ions from diagenetic carbonate precipitation (see below). Salinity increases to 36.2‰ by 341 mbsf, followed by a rapid increase to 51‰ by 544 mbsf. Salinity increases in a stepwise fashion to a maximum of 57.8‰ between 883 and 972 mbsf and then decreases somewhat to 55.8‰ by 1113 mbsf.

The chloride profile largely parallels the salinity profile (Fig. 23). The chloride profile results from the diffusion of Cl from a Cl-rich brine below, which appears to have an asymptotic Cl concentration of around 960 to 980 mM, and from the accumulation of sediment above with a Cl concentration of seawater (559 mM). Chloride shows an inverted exponential increase from the sediment/seawater interface

Table 9. Results of Rock-Eval pyrolysis, Site 903.

Core, section, interval (cm)	Depth (mbsf)	T_{max} (°C)	S_1 (mg/g)	S_2 (mg/g)	S_3 (mg/g)	TOC (wt%)	HI	OI	PI	S_2/S_3
150-903A-										
1H-2, 20–22	1.70	391	1.04	2.23	1.03	0.65	343	158	0.32	2.16
6H-2, 70–72	49.70	573	0.08	0.67	1.30	0.31	216	419	0.11	0.51
8H-2, 68–70	68.68	ND	0.07	1.55	1.43	0.39	397	366	0.04	1.08
24X-2, 68–70	194.08	ND	0.24	1.15	1.57	0.55	209	285	0.17	0.73
28X-3, 68–71	233.98	452	0.06	1.13	1.15	0.39	250	294	0.05	0.98
30X-3, 50–52	253.20	ND	0.06	0.65	0.78	0.26	250	300	0.09	0.83
35X-3, 60–61	301.50	415	0.24	1.13	1.61	0.70	161	230	0.18	0.70
37X-4, 70–71	321.49	395	0.14	1.14	1.14	0.45	253	253	0.11	1.00
45X-3, 80–82	398.10	443	0.32	3.31	2.63	0.94	352	279	0.09	1.25
50X-3, 76–77	446.46	421	0.23	1.42	1.76	0.96	147	183	0.14	0.80
54X-3, 60–63	484.90	591	0.17	3.23	2.49	0.79	408	315	0.05	1.29
55X-3, 62–64	494.52	417	0.84	6.4	2.35	2.44	262	96	0.12	2.72
68X-2, 67–68	618.17	412	0.63	4.39	0.97	1.70	258	57	0.13	4.52
69X-3, 77–79	629.37	544	0.18	3.79	2.05	0.78	485	262	0.05	1.84
75X-3, 56–59	687.06	421	0.37	5.25	2.93	1.70	308	172	0.07	1.79
150-903C-										
5R-2, 74–76	507.84	423	0.46	4.58	1.91	1.81	253	105	0.09	2.39
12R-3, 70–72	692.30	418	0.45	4.39	1.79	1.51	290	118	0.09	2.45
15R-3, 20–21	720.40	414	0.48	4.35	3.41	1.53	284	222	0.10	1.27
19R-3, 79–81	759.99	418	0.69	7.51	2.02	2.34	320	86	0.08	3.71
25R-2, 73–74	816.03	417	0.63	8.47	1.31	2.79	303	46	0.07	6.46
28R-2, 45–46	844.65	405	1.13	12.77	2.03	3.48	366	58	0.08	6.29
33R-2, 61–62	893.21	404	1.89	15.36	3.20	3.64	421	87	0.11	4.80
45R-2, 43–44	1006.63	423	0.45	10.6	2.51	2.77	382	90	0.04	4.22
51R-6, 72–73	1058.34	420	0.27	8.07	2.64	2.41	334	109	0.03	3.05
56R-3, 44–45	1105.12	408	0.1	0.79	2.72	0.67	117	405	0.11	0.29
58R-8, 27–28	1115.27	416	0.03	0.43	1.52	0.33	130	460	0.07	0.28

Note: TOC = total organic carbon, HI = hydrogen index, OI = oxygen index, and PI = production index, and ND = no data.

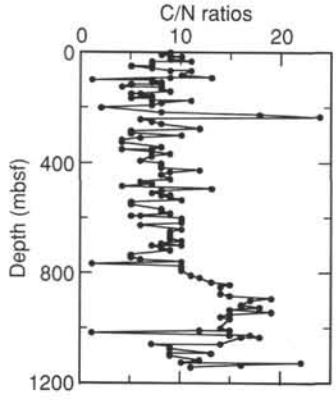

Figure 22. Organic C/N atomic ratios vs. depth for sediment samples from Site 903.

down to 507 mbsf, a depth that corresponds to the approximate predicted depth of the m0.5 (Red) seismic reflector. Chloride concentrations are close to the seawater value of 559 mM from 0 to 225 mbsf. Chloride increases gradually from 564 mM at 225 mbsf to 575 mM at 253 mbsf. This low chloride gradient is associated with sedimentation rates greater than 60 cm/k.y. (see "Biostratigraphy" section, this chapter). A change in chloride gradient occurs between 253 and 283 mbsf, within the depth predicted for the p5 (Orange) seismic reflector. The chloride gradient steepens somewhat with concentrations reaching 618 mM by 341 mbsf. A change in chloride gradient occurs between 341 and 370 mbsf, within the depth predicted for the p6 (indigo) seismic reflector. The chloride gradient becomes increasingly steep with a concentration of 753 mM by 457 mbsf. The gradient is steepest where it reaches a concentration of 847 mM by 507 mbsf (predicted depth of seismic reflector m0.5 [Red] is near 500 mbsf). Chloride shows a second inverted exponential increase from 826 at 513 mbsf to 883 mM at 611 mbsf; the latter corresponds to the approximate depth predicted for the m1 (Tuscan) seismic reflectors. The steep chloride gradient at this site corresponds with the gradient observed at Site 902; both occur between the upper Pleistocene/upper Miocene boundary and the upper Miocene/middle Miocene boundary. From 640 to 777 mbsf, chloride shows a slight broad maximum centered within the middle Miocene. Chloride has a second broad maximum centered around the lower Miocene/lower middle Miocene boundary, increasing from 886 to 975 mM between 777 and 940 mbsf (a depth range predicted to contain the m5 (Green) seismic reflector). The maximum chloride content of 986 mM occurs in upper Eocene rocks at 1089 mbsf. The calculated sodium profile parallels the chloride trends discussed above (Fig. 23). The high salinity, chloride, and sodium values indicate the migration or diffusion of a salt brine from greater depths. The brine may originate from dissolution of deeply buried Jurassic salt; diapirs have been observed in profiles beneath the outer continental shelf (Grow et al., 1988).

An exponential decrease in pH corresponds to the steep increase in salinity and chloride and may explain the scarcity of Miocene calcareous fossils in these sediments. The pH initially decreases downward to 7.4 by 14 mbsf; below this level, pH tends to increase from 7.4 to 7.8 by 341 mbsf (upper Pleistocene sediment) (Fig. 23). The relatively high pH values from 100 to 350 mbsf correspond to relatively high carbonate contents of 10 to 20 wt% (see "Organic Geochemistry" section, this chapter). Below 341 mbsf, pH decreases exponentially from 7.8 to 6.6. The steep pH drop to slightly acidic values corresponds to low bulk sediment carbonate contents of <5 wt% from 350 to 850 mbsf. However, the lowest pH values (<6.7) occur in carbonate-rich sediments (10–60 wt%) below 850 mbsf. These low pH values should be buffered by the dissolution of carbonate minerals.

The Ca, Sr, and Mg profiles are important for evaluating the diagenesis of carbonate minerals. Diagenetic dolomite and siderite are common at Site 903 (see "Lithostratigraphy" section, this chapter) and may form at the expense of biogenic carbonate. The decrease in Ca, Mg, and Sr between 100 and 200 mbsf suggests precipitation of diagenetic carbonate promoted by the associated increase in alkalinity. The high Mg/Ca ratios of 7 to 11 in this depth interval indicate that dolomite precipitation is favored over calcite precipitation. Ca decreases from 9.7 to 3.3 mM between 1.5 and 152 mbsf and then increases to a near-seawater value by 400 mbsf (Fig. 23). Ca remains nearly constant from 397 to 513 mbsf and then increases to a maxi-

Table 10. Interstitial-water data, Site 903.

Core, section, interval (cm)	Depth (mbsf)	IW (mL)	pH	Alkalinity (mM)	Salinity (‰)	Cl^- (tit) (mM)	Cl^- (chr) (mM)	SO_4^{2-} (µM)	NH_4^+ (µM)	PO_4^{3-} (µM)	SiO_2 (µM)	Sr (µM)	Mn (µM)	Fe (µM)	Na^+ (calc) (mM)	Na^+ (chr) (mM)	K^+ (AA) (mM)	K^+ (chr) (mM)	Mg^{2+} (tit) (mM)	Mg^{2+} (chr) (mM)	Ca^{2+} (tit) (mM)	Ca^{2+} (chr) (mM)
150-903A-1H-1, 145–150	1.48	43	7.52	7.88	35.5	564	542	25.5	0.3	36	605	78	4	6	481	496	11.37	12.29	52.65	51.36	9.68	9.30
150-903A-2H-3, 145–150	14.0	32	7.42	15.97	33.5	565	533	0.2	3.5	115	616	65	2	27	471	477	10.29	10.10	39.63	37.52	3.61	3.37
150-903A-3H-3, 145–150	23.5	40	7.40	12.13	33.2	560	538	0.0	4.6	62	654	67	2	NM	463	466	9.72	9.53	37.59	37.10	3.97	3.92
150-903A-4H-4, 145–150	34.5	38	7.43	10.25	33.8	562	538	0.3	4.7	24	367	71	3	49	467	463	9.96	9.32	37.11	35.80	4.44	4.07
150-903A-5H-3, 145–150	42.5	36	7.46	7.71	33.0	565	544	0.4	6.5	29	440	72	3	50	468	479	9.65	8.92	35.34	35.22	4.33	4.53
150-903A-6H-3, 145–150	52.0	36	7.50	7.59	33.5	566	546	0.2	5.2	24	435	72	3	54	470	501	9.23	8.98	33.88	35.39	4.32	4.37
150-903A-7H-3, 145–150	61.5	42	7.46	7.83	33.5	563	547	0.1	4.9	19	460	72	3	45	470	477	8.94	8.38	34.41	34.88	4.42	4.43
150-903A-8H-3, 145–150	71.0	44	7.49	6.31	33.0	564	598	0.0	4.3	10	495	72	3	44	462	484	8.91	8.92	33.50	31.29	4.69	4.61
150-903A-9H-3, 145–150	80.5	46	7.52	6.62	33.5	560	541	0.2	4.5	13	460	70	3	44	469	467	8.33	8.08	33.36	33.77	4.84	4.67
150-903A-10H-3, 150–155	90.0	43	7.49	6.88	33.0	559	535	0.5	5.2	13	381	67	3	37	467	486	8.56	8.61	32.22	33.69	4.30	4.38
150-903A-11H-3, 145–150	99.5	26	7.58	10.57	33.0	557	565	0.3	7.3	37	695	62	3	14	472	475	5.59	8.54	31.30	32.77	3.95	4.02
150-903A-12H-3, 145–150	109.0	22	7.49	13.09	33.0	558	554	0.7	9.4	62	656	60	2	24	474	448	8.67	8.26	31.29	31.55	3.76	3.77
150-903A-14H-3, 143–150	128.0	12	7.72	17.96	33.5	558	531	0.3	11.3	36	509	58	NM	2	474	448	8.27	9.24	32.46	31.83	4.06	3.98
150-903A-17H-2, 140–150	152.0	44	7.76	17.96	33.0	565	545	0.3	8.7	23	253	52	1	3	486	468	11.90	9.45	28.64	28.91	3.26	3.32
150-903A-21X-2, 145–150	172.0	30	7.61	12.25	33.0	556	552	0.4	10.4	50	526	59	2	10	474	462	9.83	9.48	27.80	27.93	3.68	3.72
150-903A-24X-3, 145–150	196.0	24	7.60	31.78	34.5	556	560	1.0	10.3	125	770	68	3	5	483	444	9.97	10.02	32.79	32.80	4.35	4.02
150-903A-27X-3, 140–150	225.0	30	7.78	16.45	34.0	564	537	0.0	8.7	18	528	59	2	8	484	449	9.13	8.84	30.06	30.10	3.94	3.54
150-903A-30X-2, 140–150	253.0	26	7.65	7.51	33.5	575	557	0.7	8.0	8	358	67	2	NM	495	454	7.81	7.18	29.08	29.44	5.13	5.10
150-903A-33X-3, 140–150	283.0	34	7.62	14.38	35.0	581	812	0.3	6.8	26	700	86	5	9	505	509	8.08	7.00	30.98	29.31	6.59	6.71
150-903A-36X-3, 140–150	312.0	36	7.75	10.15	35.5	598	629	0.3	7.5	6	335	104	2	6	516	501	8.21	7.29	31.11	31.98	6.25	6.14
150-903A-39X-3, 140–150	341.0	19	7.70	12.83	36.2	618	613	0.0	8.6	16	279	124	NM	NM	531	528	7.59	9.39	33.69	33.84	7.24	6.48
150-903A-42X-3, 140–150	370.0	22	7.25	27.85	40.0	658	648	0.1	6.3	24	588	149	NM	6	573	567	9.80	11.43	39.91	39.40	9.41	8.53
150-903A-45X-2, 140–150	397.0	26	7.12	32.45	42.0	687	680	0.1	5.5	10	628	154	3	9	604	576	11.84	11.39	42.17	40.79	10.72	10.11
150-903A-48X-3, 140–150	428.0	28	7.74	34.35	44.0	727	699	0.3	7.1	5	861	154	2	NM	644	623	11.70	12.73	41.68	41.68	9.95	11.07
150-903A-51X-3, 140–150	457.0	15	6.99	34.56	46.0	753	754	0.5	7.3	11	916	166	2	14	669	696	9.94	11.68	44.49	45.03	10.07	12.10
150-903A-54X-3, 140–150	486.0	33	6.92	38.56	46.5	815	788	0.2	9.5	6	1109	203	2	15	732	707	12.46	12.87	45.69	44.44	11.81	11.69
150-903C-5R-1, 145–150	507.0	16	6.93	38.01	50.0	847	972	0.0	11.3	17	1089	216	NM	NM	762	673	12.03	12.43	47.16	45.94	14.13	13.45
150-903A-57X-2, 140–150	513.0	22	7.01	35.62	50.0	826	797	0.3	13.2	25	1103	222	3	16	736	725	11.92	12.80	45.23	44.83	10.80	NM
150-903A-60X-3, 140–150	544.0	22	7.59	36.31	51.0	830	888	0.1	10.2	3	1150	236	3	NM	682	709	9.44	11.97	45.54	44.07	13.44	NM
150-903A-63X-3, 140–150	572.0	22	7.52	36.03	49.0	836	899	0.0	10.9	17	1160	253	3	NM	641	739	13.03	11.96	47.96	44.05	14.37	NM
150-903C-9R-1, 140–150	588.0	20	6.93	37.03	50.5	848	986	0.2	11.5	5	1174	248	2	72	761	703	10.54	12.00	48.49	47.27	15.10	14.49
150-903A-67X-3, 140–150	611.0	18	7.66	37.68	50.0	876	933	0.0	16.6	7	1190	253	3	NM	719	747	9.83	12.39	46.90	45.30	15.22	12.94
150-903A-70X-3, 140–150	640.0	26	6.84	34.99	53.8	883	971	0.0	12.3	19	1162	282	4	NM	787	777	11.28	12.39	48.36	45.65	16.48	11.17
150-903A-73X-3, 140–150	669.0	26	6.79	36.73	54.5	908	958	0.0	13.2	3	1251	297	3	21	812	772	10.66	13.26	49.36	46.41	17.17	18.45
150-903C-12R-3, 140–150	693.0	30	6.74	35.23	54.0	885	1055	2.5	12.5	15	1282	310	3	NM	799	728	10.71	13.15	48.91	47.85	17.83	17.14
150-903A-76X-3, 140–150	698.0	40	6.80	36.43	54.5	908	969	0.0	12.8	21	1350	274	3	31	814	769	12.70	12.53	48.39	46.55	17.30	18.51
150-903C-15R-2, 140–150	720.0	40	6.77	34.17	54.5	897	1052	2.9	15.5	0	1218	329	2	75	809	758	9.49	13.16	47.92	47.85	18.40	17.49
150-903C-18R-1, 53–63	747.0	30	6.73	32.75	54.2	896	1067	0.8	15.8	0	1230	276	2	32	802	715	11.34	12.28	46.25	48.28	17.76	18.42
150-903C-21R-1, 98–108	777.0	36	6.77	31.69	54.0	886	1057	1.7	13.0	5	1230	347	3	23	795	732	11.24	12.73	47.83	47.50	19.11	18.78
150-903C-25R-2, 140–150	817.0	29	6.78	30.32	56.0	933	1108	0.5	12.1	5	1303	433	3	50	842	748	11.64	12.59	47.47	47.24	21.36	20.98
150-903C-29R-3, 140–150	857.0	34	6.62	27.05	56.5	941	1157	0.0	12.8	5	1447	519	2	24	843	784	14.01	13.92	45.60	46.18	22.40	21.42
150-903C-32R-1, 140–150	883.0	29	6.66	27.66	57.8	963	1180	0.3	14.9	0	1492	607	2	12	869	756	11.71	13.29	45.77	45.75	24.75	24.12
150-903C-35R-3, 140–150	915.0	40	6.60	25.92	57.8	956	1143	0.4	12.4	5	1480	695	2	59	867	747	12.85	12.88	45.71	43.33	26.90	25.76
150-903C-38R-1, 105–115	940.0	30	6.64	22.71	57.8	975	1219	0.1	13.7	5	1464	763	1	21	881	772	12.19	13.41	43.05	43.72	27.26	27.10
150-903C-41R-3, 140–150	972.0	34	6.61	22.81	57.8	958	1175	0.9	12.6	3	1376	778	2	32	867	730	12.26	12.58	44.66	44.20	28.38	28.44
150-903C-47R-2, 142–152	1028.0	9	6.66	19.32	56.2	945	1147	1.0	10.9	0	780	849	2	NM	853	750	11.39	11.40	44.56	44.81	28.47	28.37
150-903C-51R-3, 140–150	1059.0	0.1	NM	NM	NM	947	NM	NM	0.0	NM	NM	NM	NM	NM	NM	NM	NM	NM	NM	NM	NM	NM
150-903C-54R-4, 140–150	1089.0	1	NM	NM	NM	986	1233	0.0	0.0	0	NM	NM	NM	NM	NM	754	NM	9.26	47.21	47.21	33.28	33.28
150-903C-57R-1, 140–150	1113.0	2.5	NM	NM	55.8	935	NM	NM	6.4	0	587	1138	NM	NM	NM	732	10.23	10.02	48.44	48.88	27.74	26.90

Notes: NM = not measured, tit = titration, chr = chromatography, and AA = atomic absorption.

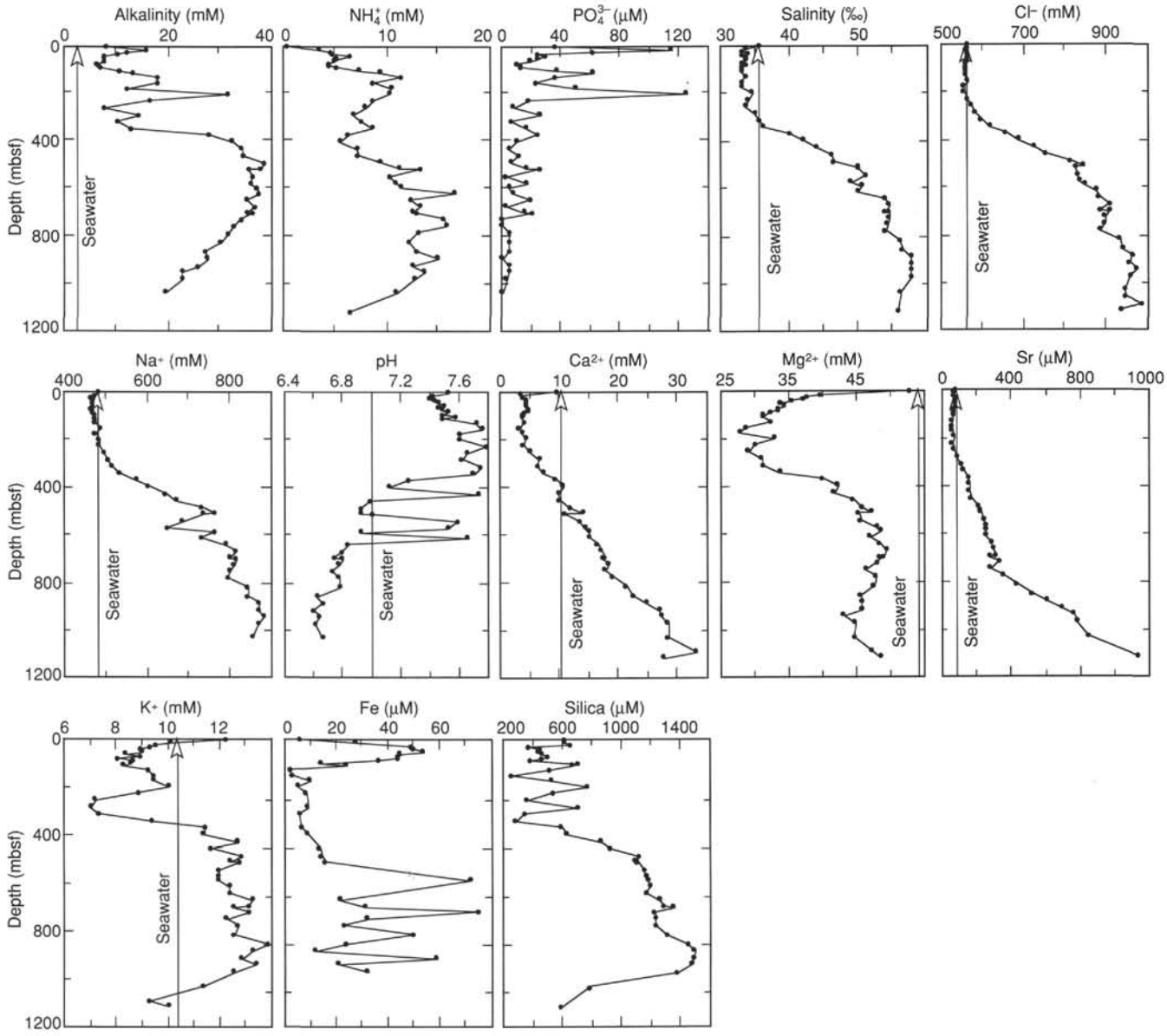

Figure 23. Interstitial-water geochemical data vs. depth, Site 903.

mum of 33.3 mM by 1089 mbsf. Strontium decreases to a minimum of 52 μM by 152 mbsf, increases to 329 μM by 720 mbsf, and then increases more rapidly to a maximum of 1138 μM by 1113 mbsf (Figs. 23–24). The increase in Ca with depth is associated with the increase in chloride and suggests a possible association of Ca and SO_4^{2-} with the diffusion of the salt brine because salt diapirs commonly have an anhydrite cap. The sulfate would be reduced to sulfide and may help to explain the high abundance of pyrite in these sediments. Alternatively, the increase in Ca may reflect the dissolution of carbonate-rich rocks resulting from the low pH values.

The Sr profile is similar to the Ca profile and suggests Sr uptake during the precipitation of diagenetic carbonates (Ca uptake) and Sr release during recrystallization or dissolution of relatively Sr-rich biogenic carbonate at greater depths. Mg ion decreases to a minimum concentration of 27.8 mM by 172 mbsf (Fig. 23). Mg then progressively increases to a maximum value of 49.4 mM by 669 mbsf. Mg decreases to a local minimum of 43 mM at 940 mbsf and then increases to 48.4 mM by 1113 mbsf. A dolomite-cemented bed occurs at 960 mbsf, which corresponds to a local Mg minimum and to a decreased Ca and Sr gradient (Fig. 23).

Potassium and iron profiles can provide clues to the diagenetic history of glauconite, a mineral that is commonly interpreted to represent condensed intervals. Key questions concerning the abundant glauconite in these sediments include the following: (1) Is the glauconite authigenic or detrital? (2) Is the glauconite stable or is it undergoing dissolution? K concentrations initially decrease downward to 8.1 mM at 80.5 mbsf, increase to a near-seawater value near 196 mbsf, and then decrease to a minimum of 7 mM near 283 mbsf (Fig. 23). K increases rapidly to 12.7 mM by 428 mbsf and then remains at values greater than those of seawater, up to a maximum of 13.9 mM at 857 mbsf. K drops back to a near-seawater value by 1113 mbsf. K normally decreases with increasing burial depth at deep-sea sites because of its uptake in the alteration of volcanic sediment and underlying basalt (Gieskes, 1981). No volcanic material or basalt is known to be associated with these sediments; therefore, the cause of the decrease in K in the uppermost 300 mbsf at Site 903 is unclear. The high K values at Site 903 between 350 and 1000 mbsf are associated with glauconite-rich sediment intervals (see "Lithostratigraphy" section, this chapter). This association may indicate the equilibrium K concentration of the pore water with glauconite, or it may indicate solu-

tion or recrystallization of the glauconite. The increase in K may also be explained by the temperature-of-squeezing effect, which has been observed to cause an increase in K concentration (Waterman, 1973).

Variations in the Fe concentration may be related to both pyrite and glauconite abundance. Fe increases to a maximum of 54 µM at 52 mbsf and then decreases to 2 µM by 128 mbsf (Fig. 23). Fe remains low from 128 to 513 mbsf and then increases rapidly to 72 µM by 588 mbsf. Fe fluctuates between 10 and 70 µM to 972 mbsf. The first occurrence of pyrite is at 85 mbsf and corresponds to the rapid decrease in the first Fe maximum at 52 mbsf, a depth at which the sediment contains reddish/gray bands (see "Lithostratigraphy" section, this chapter). Pyrite at greater depths also tends to occur with major drops in Fe concentration and suggests that Fe is being removed by the formation of pyrite. The source of the sulfur for the precipitation of pyrite may be from the diffusion of sulfate from the brine below as well as from organic sulfur released during organic-matter degradation. In addition to pyrite, Fe-rich illite (glauconite) and Fe-rich carbonate (siderite) occur in the high-Fe interval between 500 and 1000 mbsf. Replacement of some of the glauconite by pyrite would explain the high Fe and K values.

The high silica concentrations correspond to diatomaceous intervals and result from the high solubility of amorphous, biogenic silica (opal-A). Silica varies sporadically between 250 and 800 µM in the top 350 mbsf and then increases rapidly to around 1200 µM by 486 mbsf (Fig. 23). Silica increases more gradually to a maximum value of 1492 µM by 883 mbsf and then decreases to 587 µM by 1113 mbsf.

PHYSICAL PROPERTIES

Introduction

Physical properties measured at Site 903 included multisensor track (MST) measurements of magnetic susceptibility, GRAPE wet-bulk density, natural gamma-ray emission, and compressional-wave velocity (PWL). Also measured were index properties (wet-bulk density, water content, porosity, and grain density), thermal conductivity, longitudinal velocity, and compressional strength. Correlations were found among the measured properties and are described herein after a review of the procedures of data acquisition.

Sampling Procedures

All but 14 badly deformed sections of the 205 cores recovered at Site 903 were processed through the multisensor track (MST), although the *P*-wave logger (PWL) and natural gamma-ray (NGR) instruments were inoperative over most intervals. Below Cores 150-903A-6H (57 mbsf) and 150-903B-3H (21 mbsf), PWL signals were highly attenuated by gassy sediments; subsequent tests showed that the PWL velocities probably represented the traveltime of the plastic core liner, and hence the PWL was deactivated. We confirmed the ineffectiveness of the PWL by checking its signal strength and sonic velocity during every third to fourth core thereafter. The newly installed MST NGR detection tool was first tested at Holes 903A and 903C, and operated continuously in its spectral mode at Hole 903D. Test results are discussed in more detail in the next section.

Index property samples for pycnometer measurements were taken at a frequency of two to four samples per core in all holes of Site 903 at regularly spaced intervals, 1.5 to 2.0 m apart. Some exceptions to this routine were necessitated by drilling "biscuits" and other coring-induced sediment deformation in the XCB cores of Hole 903A and the RCB cores at Hole 903C.

Our onboard examination of Site 902 index properties data resulted in the addition of the "dry volume method" (see Chapter 3, this volume) of measuring grain density. During coring operations at Site 902, calculated grain densities appeared too high (2.9 g/cm^3 average) for the mostly clay-rich sediments. Several causes were examined including inadequate or over-drying of clays, gas expulsion before sampling, pycnometer inaccuracies, variable iron sulfide and carbonate fractions, fluid density, and potential bugs in the new index properties database program. Because we found no unequivocal reason for the higher than expected grain densities, we added the "dry method" routine as an independent check to several sections of Hole 903A and to all sections of Holes 903B and 903C. "Dry method" measurements were reduced to once per core at Hole 903D after an analysis of initial results indicated a linear relationship between the two methods. Dry-method grain densities were found to be more reasonable (see Figs. 25–28); however, the cause of aberrant grain densities calculated from "wet" volume measurements was not isolated.

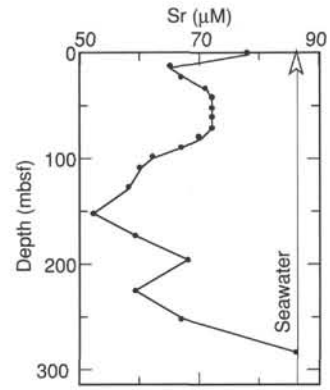

Figure 24. Detail of strontium ion data vs. depth (0–300 mbsf).

Approximately 25 APC cores from Holes 903A and 903B, and 16 XCB cores from Hole 903A experienced moderate to significant expansion within the core liner before being processed through the MST. Expansion resulted either in extruded sediments that were subsequently bagged or in gas voids within the core liner. Although the size and frequency of such gaps were highly variable, most ranged from 5 to 20 cm in length and occurred up to seven or more times per core. Coring gaps are routinely closed by technicians after MST processing and splitting if possible, and before sampling by the scientific party; discrepancies of up to 1 m are therefore expected among correlations of MST data, properties measured from half-core samples, and downhole log data.

Gas expansion, coring-related deformation, and sediment induration all affected thermal conductivity measurements. As gas expansion and coring deformation badly segmented some cores, thermal needle probes often experienced boundary effects that were recognized and deleted during raw-data processing. Below 700 mbsf, cores fractured when thermal probes were inserted and, thus, our sampling frequency dropped to zero. We considered an alternative, "half-space" method but, because the sediments were too brittle for polishing, decided it was not plausible.

We measured compressional velocities with the Digital Sediment Velocimeter (DSV) and Hamilton Frame devices, and compressional strength at a frequency of approximately two measurements per core through intervals with valid signals and strength. Our sampling intervals and procedures were similar to those described in the "Physical Properties" section of Chapter 6 (this volume).

Results

Physical properties measurements are grouped into 6 units and 16 subunits on the basis of variable trends in wet-bulk density records from both GRAPE and mass-volume (MV) methods. Summary figures of the physical properties data are provided as Figures 25 through 28; these represent Holes 903A, 903B, 903C, and 903D, respectively.

Distinct units and subunits are evident in bulk-density records from all four holes. A typical subunit consists of repetitive, small increases or decreases of bulk densities that are bounded by abrupt, significant changes. Subunits are based on trends of increasing or decreasing average bulk densities with respect to depth. This ap-

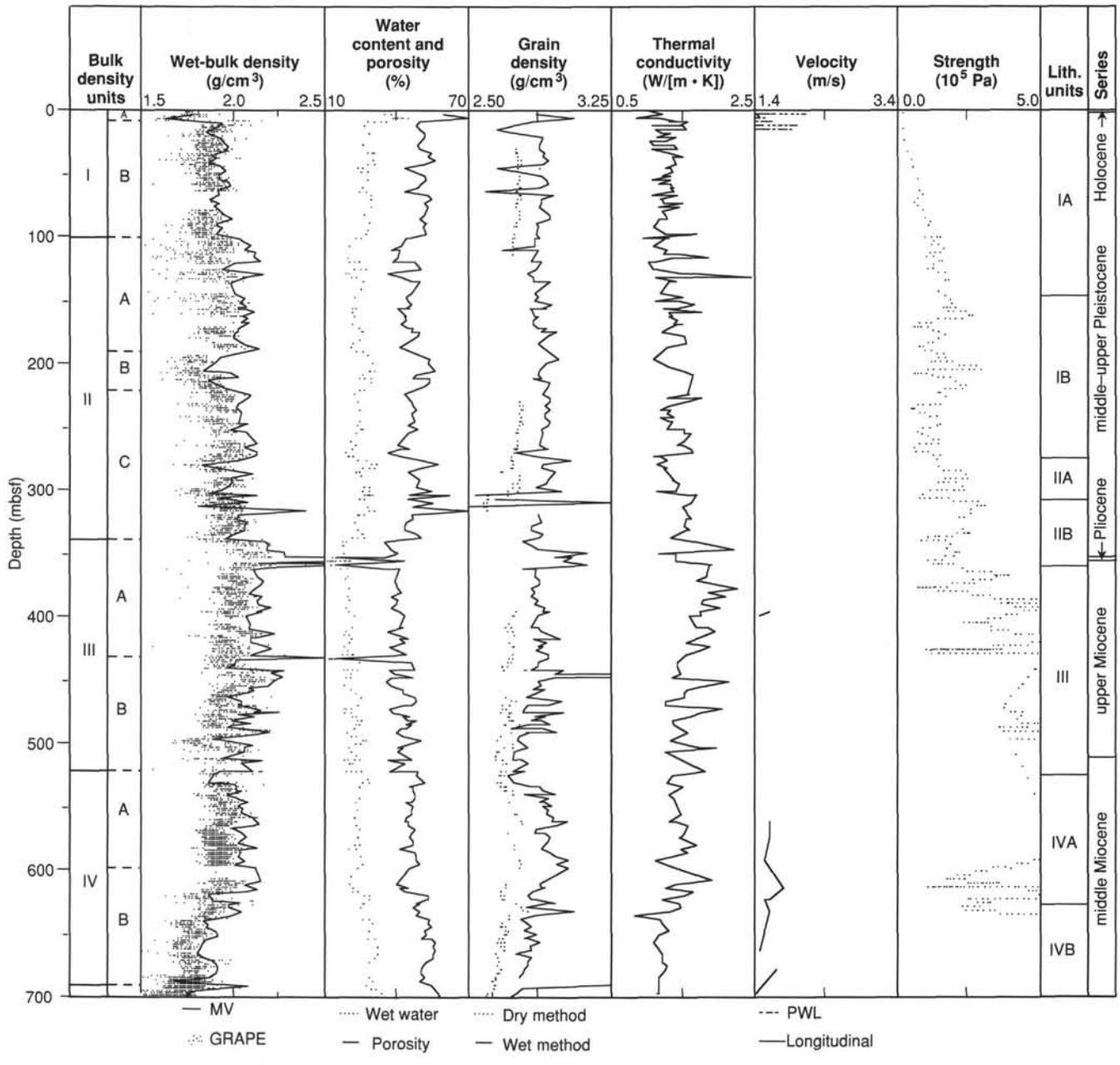

Figure 25. Physical properties results (wet-bulk density, water content and porosity, grain density, thermal conductivity, compressional velocity, and penetrometer readings), Hole 903A. Penetrometer readings exceeding the instrument scale of 4.5×10^5 Pa are plotted at 5×10^5 Pa. MV = mass-volume method.

proach works extremely well below 350 mbsf at Site 903; however, through the upper 350 m (approximately the Pleistocene section) of Holes 903A and 903B, density trends are ill defined and units are subdivided solely on large-amplitude changes in bulk density. The lowermost unit of Hole 903A and uppermost units of Holes 903C and 903D are subdivided assuming that the Hole 903C record is an approximate continuation of the Hole 903A data. Initial correlations of GRAPE density data indicate that this approximation is valid.

Unit I (0–100 mbsf)

All physical properties measured through Unit I, with the exception of compressional strength, show large variations through the upper 100 mbsf of Holes 903A and 903B. Although wet-bulk density and thermal conductivity both show marked increases, compressional velocity is undetectable below 25 to 30 mbsf. A marked, 0.3 g/cm^3 increase in wet-bulk density at 8 mbsf forms the basis for subdividing Unit I into upper (IA) and lower (IB) cycles. This unit is middle Pleistocene (stage 7) to Holocene.

Few data are available to characterize Subunit IA; however, Subunit IB is characterized by its low wet-bulk densities (1.9 g/cm^3 average) and thermal conductivities that vary proportionately between 1.0 and 1.55 W/(m · K). Velocities measured through the upper portion of Subunit IB range from 1.5 to 1.6 km/s; gassy sediments preclude compressional velocity measurements at greater depths. Compressional strength was below the lowest measurable levels until 30 mbsf when a rise of 0.75 10^5 Pa/m began and continued until 160 mbsf. Water content and porosity average 20% and 60%, respectively. Grain

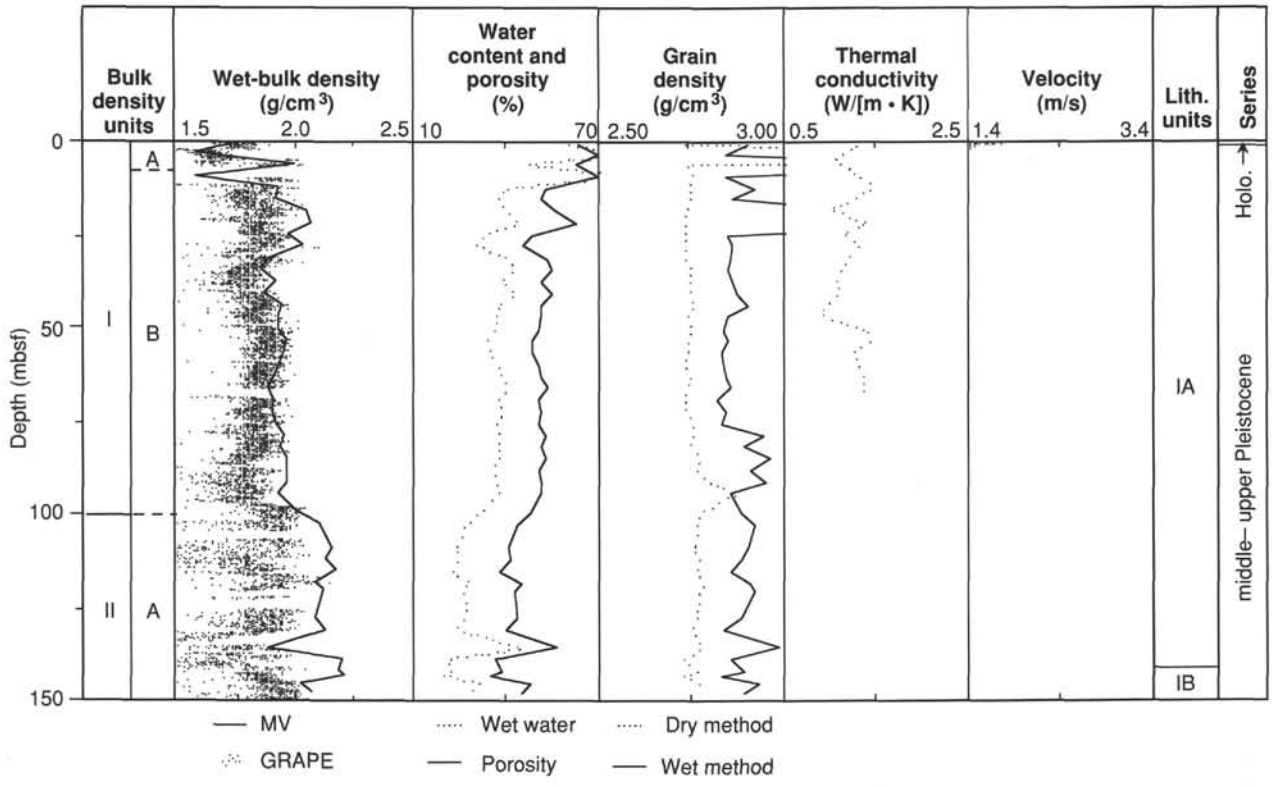

Figure 26. Physical properties results (wet-bulk density, water content and porosity, grain density, thermal conductivity, and compressional velocity), Hole 903B. MV = mass-volume method.

densities calculated from bulk densities average 2.87 g/cm^3 using the "wet volume method," and 2.75 g/cm^3 when calculated directly using the "dry volume method."

Unit II (100–340 mbsf)

Unit II is marked by a 0.2 g/cm^3 increase in bulk density at its upper contact and 0.5 g/cm^3 at its lower contact. We divided this unit into three subunits (IIA, IIB, and IIC) based on lower average bulk densities (1.88 g/cm^3) between 190 and 220 mbsf as well as correlations to lower thermal conductivities and increased compressional strength. This unit is primarily middle Pleistocene, although it may be lower Pleistocene at its base.

The following trends are evident in Unit II:

1. Water content and porosity reflect the increased bulk density of Unit II and are slightly (10%) lower than in Unit I.
2. Grain densities, measured from 250 to 325 mbsf, are similar to those in Unit I.
3. Thermal conductivity shows several large spikes of up to 2 W/(m · K) between 100 and 150 mbsf, which correspond to increased percentages of sand.
4. Penetrometer data, although possibly affected by the switch from APC to XCB coring methods, reflect overall changes to lower compressional strength below 160 mbsf.

Unit III (340–520 mbsf)

Unit III includes two subunits (Fig. 25) that exhibit decreasing average bulk density. Subunit IIIA begins at 340 mbsf with bulk densities of 2.65 g/cm^3, the highest recorded at Site 903, and ends in a thin, low density (1.85 g/cm^3) section at 430 mbsf. The upper contact of Subunit IIIB is marked by the abrupt downhole increase of bulk density by 0.15 g/cm^3 and a gradual decrease (0.1 g/cm^3) over the next 80 m. Scattered values (±0.3 g/cm^3) throughout Subunit IIIB might allow further division or necessitate minor revisions of depths to subunit boundaries.

Downhole changes in thermal conductivity, compressional strength, water content, and porosity all coincide with the boundaries of Unit III. Thermal conductivities of 1.0 to 2.4 W/(m · K) vary proportionately to bulk density throughout Subunit IIIA, and possibly show higher order bulk-density values in Subunit IIIB. Compressional strength increases steadily through Unit III from 1.0 to over 4.5 10^5 Pa, the maximum strength detected. Water content and porosity drop to their lowest values, averaging 15% and 40%, respectively. This unit spans the lower Pleistocene to uppermost middle Miocene.

Three velocity measurements were made at 350 and 430 mbsf in calcite-cemented sediment. The velocity (4.65 km/s) at 350 m could not reasonably be displayed (Fig. 25) as it was three times the average of all other measurements. Some of the indurated intervals occupy the entire width of the core and may represent thin (~10 cm) layers. Others are more fragmentary. All may therefore be nodules of limited lateral extent.

Unit IV (520–690 mbsf)

Unit IV consists of two subunits bounded by sections of low (1.85 and 1.89 g/cm^3) bulk density (Fig. 25). The upper subunit (IVA) is poorly defined by the present data, but it is clearly distinct from the lower subunit (IVB), which is an excellent example of a subunit defined by bulk densities decreasing downhole. Bulk densities in Subunit IVB decrease from 2.15 to 1.82 g/cm^3 between its upper (600 mbsf) and lower (690 mbsf) boundaries. Unit IV is middle Miocene.

Unit IV physical properties trends are as follows:

1. Thermal conductivity again varies proportionally with bulk density and confirms the choice of subunit divisions.
2. Water content and porosity average 15% and 45%, respectively, in Subunit IVA and increase to 20% and 50% in Subunit IVB.

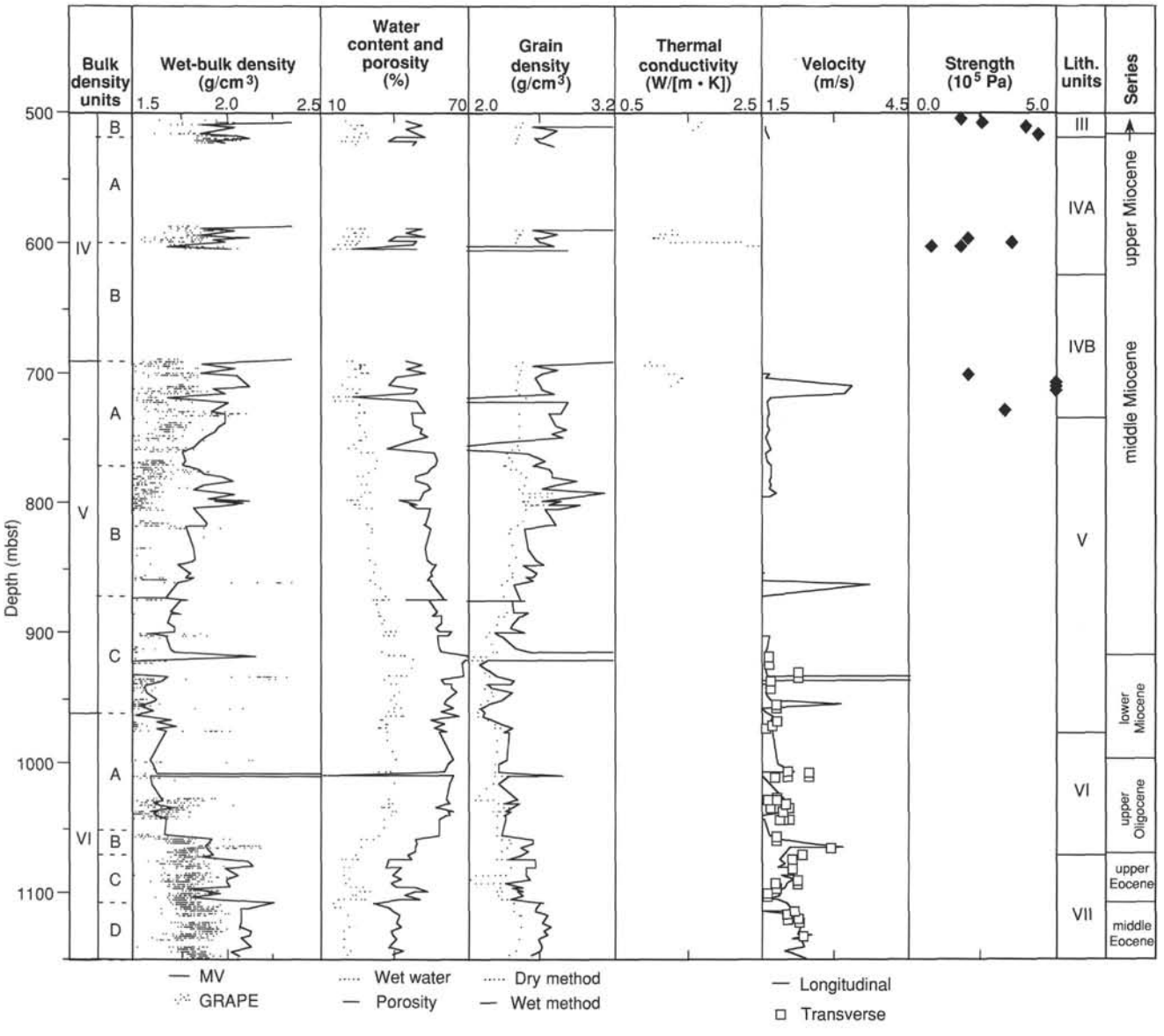

Figure 27. Physical properties results (wet-bulk density, water content and porosity, grain density, thermal conductivity, compressional velocity, and penetrometer readings), Hole 903C. Bulk-density unit and subunit interpretations assume that Holes 903A and 903C are contiguous. Penetrometer readings exceeding the instrument scale at 4.5×10^5 Pa are plotted at 5×10^5 Pa. MV = mass-volume method.

3. Sediment strength in most sections exceeds the range of our penetrometer; however, a weak section exists between 580 and 630 mbsf and corresponds to an increase in sand content.

4. Reasonable signal strengths were obtained and compressional velocities measured with the Hamilton Frame between 540 and 650 mbsf. Velocities were generally difficult to obtain from the mud and claystones and low (1.5–1.6 km/s) velocities were common.

Three cores from the base of Unit IV were run through the NGR detector on the MST system as a test of its capabilities. During the test, total MST NGR counts were summed over a test period of 5 min, once per core. The results were adjusted and compared to the natural gamma-ray curve of the downhole logging tool. Although the two data sets overlapped for only 12 m, a rough correlation was observed (Fig. 29A) (see Chapter 5, this volume).

Unit V (690–960 mbsf)

Unit V displays decreasing bulk density with respect to increasing depth. There are at least three well-formed subunits (VA, VB, and VC). The base of this unit consists of diatomaceous mudstones and glauconitic sands and possesses the lowest bulk densities seen at Site 903. Several well-indurated beds and many nodules of iron carbonate, only a fraction of which were large enough to be sampled, also exist throughout this section. They were recorded as very high bulk-density spikes in GRAPE and, in two instances, MV wet-bulk densities. This unit is middle to lower Miocene.

Other physical properties results include:

1. Increased induration and severe coring disturbances limited our measurement of thermal conductivity and compressional strength so that data were collected only over a small interval at the top of Subunit VA and were not used for investigating trends.

2. Water content and porosity steadily increase from 15% and 50% at 710 mbsf to 45% and 65% at 920 mbsf. This unusual phenomenon is probably related to increased intra-particle porosity associated with a high biogenic content (see "Lithostratigraphy" section, this chapter); this tenet is supported by Thein and von Rad (1987), whose work on nearby DSDP Site 612 indicated that the internal

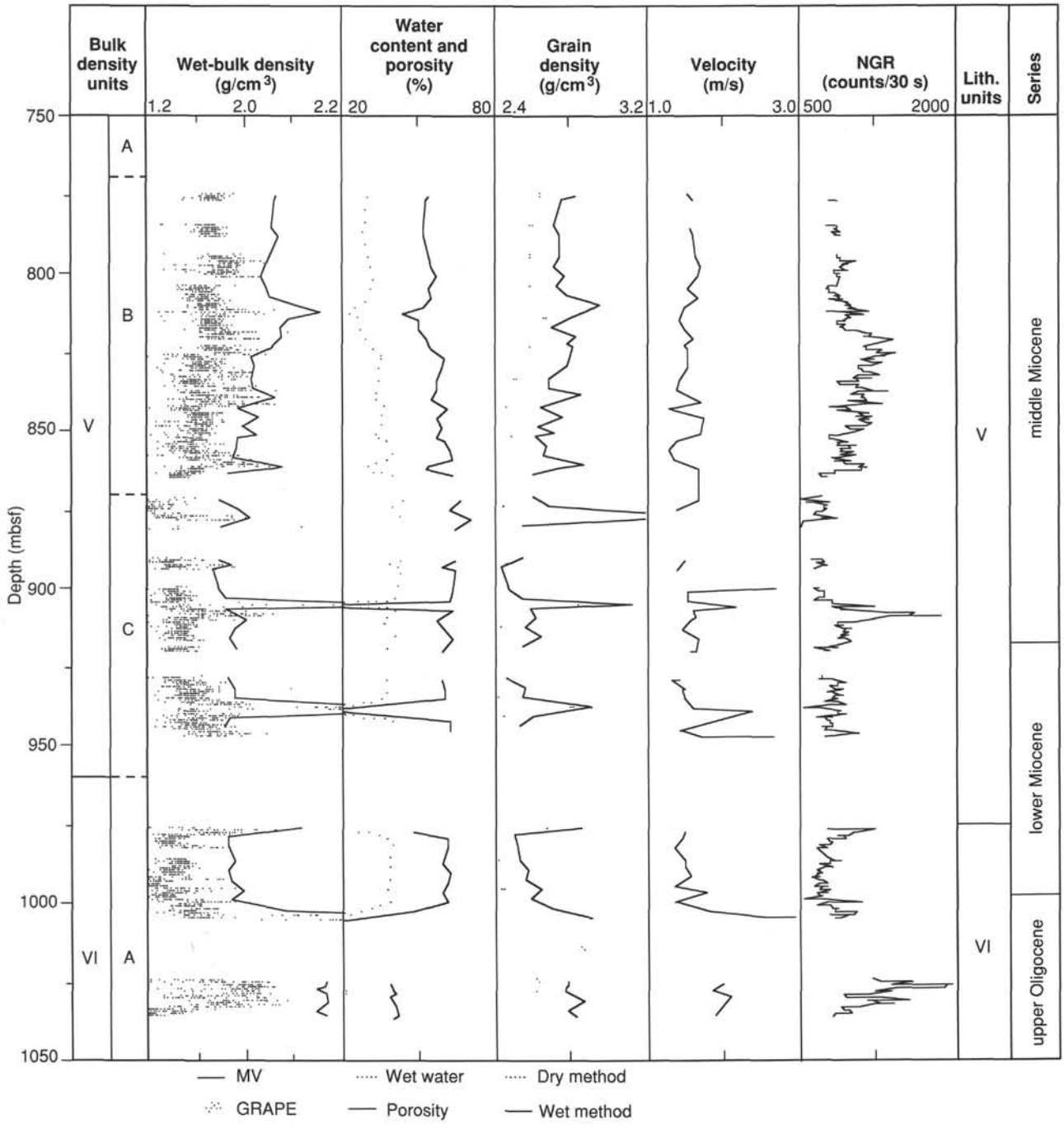

Figure 28. Physical properties results (wet-bulk density, water content and porosity, grain density, and compressional velocity), Hole 903D. Note addition of multisensor track (MST) natural gamma-ray log. MV = mass-volume method.

porosity of microfossils above the silica-diagenesis front, which occurs at 1105 mbsf (lithologic Unit VII) at Site 903 (see "Lithostratigraphy" section, this chapter), remains largely intact.

3. Although punctuated by thin intervals of high velocity (>3.0 km/s) caused by authigenic carbonate nodules, compressional velocities in Unit V are mainly low, averaging 1.6 km/s.

Two tests of NGR measurements on the MST began in this unit. During the first test at Hole 903C, gamma-ray collection times were reduced to 1 min. Good total-count variability exists in the data, implying that it is a viable log-core correlation tool (Fig. 29B). However, as poor core recovery plagued this hole and the tool is not calibrated to the API units used by downhole gamma-ray logs, the test was not used to correlate core to downhole logs at Hole 903C.

Spectral natural gamma radiation (SGR) was measured every 40 cm on the whole cores of Hole 903D. As with the MST NGR, further calibration and processing is necessary before these data can be used.

Unit VI (960–1146 mbsf)

Although Unit VI incorporates a major lithologic change from claystone to chalk and an associated 0.6-g/cm^3 bulk-density increase, the upper boundary of the unit begins approximately 100 m above lithologic Unit VII (Eocene chalk). This is because bulk-density

increases begin in the claystone in lithologic Unit V and continue through lithologic Unit VII and the remaining cored depth of Site 903. There are four subunits within Unit VI: two (VIA and VIB) in the claystone and two (VIC and VID) in the chalk.

Water content and porosity both show a sharp contact at the chalk boundary and decrease by about 10% to 20% each. DSV and Hamilton Frame velocities are about 1.6 km/s in the claystones of Subunits VIA and VIB. Average velocities in the chalk are 2.2 km/s, although variations correlative to bulk-density changes are evident.

Synthesis

As the range of typical velocities measured in the PWL, DSV, and Hamilton Frame at Site 903 is relatively small (approximately 0.2 and 0.6 km/s), correlation with seismic reflectors is dependent on bulk-density variations. We scanned our bulk-density record for large-scale (>0.2 g/cm^3) shifts and estimated the depths of major seismic reflectors (see "Seismic Stratigraphy" section, this chapter).

In Hole 903A, major bulk-density changes predict the presence of p1 (yellow-1), p3 (green), p6 (indigo), and m1 (Tuscan) sequence boundaries to within 40 m of pre-site estimated depths. A significant bulk-density change of 0.25 g/cm^3 also occurs within 40 m of seismic reflector m0.5 (Red); however, the bed thickness associated with this change is only 10 m and its ability to produce a major seismic reflection is questionable. Many smaller bulk-density variations exist in our record and may support the predicted depths of p4 (purple), m0.3 (yellow), and m1.5 (orange). However, because of the large number of small scale changes, the depths of these sequence boundaries cannot be uniquely defined using the physical properties data.

At Holes 903C and 903D, major bulk-density shifts support the depths of m2 (Yellow-2), m6 (pink-2), and o1 (green-2). The density change at m5 (Green) is quite small and no other large-scale density shifts occur nearby. As downhole geophysical logs indicate that infrequent, large-scale shifts in sonic velocity are possible (see "Downhole Measurements" section, this chapter), we speculate that m5 (Green) may be such a feature, but we were unable to sample it in the laboratory.

Finally, density shifts of greater than 0.5 g/cm^3 exist between claystones and horizons with iron carbonate nodules in Units IV through VI. The GRAPE data and visual descriptions indicate that these zones are less than 1 m thick and, although they may possess great reflectivity potential, we cannot predict their influence on the seismic record.

APC Downhole Temperature (ADARA) Measurements

A total of 14 ADARA measurements were taken at Hole 903A, from Cores 150-903A-3H to -16H. Depths of measurements, estimates of depth error, averaged thermal conductivity values, the temperature tool used for each station, and tentative, calculated temperature estimates are listed in Table 11. General information on tool calibration, deployment, processing, and error estimates is given in Chapter 3 (this volume).

Data from Cores 150-903A-12H, -14H, -15H, and -16H (lowermost 4 out of 14 cores at this site) display "classic" smooth decay curves, with single spikes at insertion and removal of the tool, although some of them are slightly noisy (Fig. 30). Records from Cores 150-903A-3H, -5H, -6H, -7H, 8H, and -10H display either double insertion, "shoulders" in the cooling curves, or considerable noise but are still useful. These features are likely related to the shallow water depth at this site, where heave may not have been compensated completely. Of the remaining stations, Cores 150-903C-4H, -9H, and -13H have unusual shapes or are very noisy, probably because of multiple penetrations or significant movement during deployment. The record from Core 150-903A-11H was too noisy to use.

The lowermost seven measurements show a gradient of about 4.0°C per 100 m, close to that measured at Site 902 (Fig. 31). The uppermost measurements suggest that a 30- to 40-m-thick zone that is located between 35 and 75 mbsf is at least isothermal, and quite probably thermally inverted.

DOWNHOLE LOGGING

Logging was performed with the sonic-induction and porosity tool strings at Hole 903A and with the sonic-induction and Quad combo tool strings at Hole 903C. Hole conditions prevented complete coverage of the drilled intervals of each hole (Table 12). Below we describe the acquisition and preliminary interpretations of log data completed at sea. Additional processing and display were conducted onshore by the Borehole Research Group, and their results are presented at the end of this chapter and on the CD-ROM disk in the back pocket of this volume.

Hole 903A

Introduction

The seafloor at Hole 903A was at 456 m below rig floor, and the sonic-induction and porosity tool strings were run. The LDEO temperature tool was attached to the bottom of both tool strings. For a description of the tool combinations and logging runs, see Table 12.

The first run was made after the hole had been drilled to 703 mbsf. Logging could only be performed above 605 mbsf as swelling clays created a bridge that the tools could not pass. In this first run, logging continued up through the drill pipe to record natural gamma ray values across the seafloor to permit correlation of logging depth with driller's depth. For control of tool performance, a duplicate run from 144 to 62 mbsf was made before entering the pipe.

The second logging run was made directly after the first one. The hole condition was good and no extra wiper trip was needed. However, the light weight of the porosity tool string prevented it from descending as deep as the first tool string, and the log was run uphole from 492 mbsf. Before entering the pipe, a duplicate run was made over an interval of approximately 75 m. After logging was completed, the hole was plugged and abandoned and the ship moved to drill Hole 903B.

Log Quality

Because the borehole was in good condition, all logging data from Hole 903A are generally of good quality. The temperature readings were also good, perhaps because of the uniform pace of the tool string's upward motion. The two repeated sections correspond well with the main runs. The logging heave compensator was used during the second run as a precaution, despite calm seas.

Depth Shifting

Total natural gamma-ray data were recorded on both runs, and the log has been used for depth correcting the different curves. Even without the gamma-ray log, it would have been possible to depth shift the two runs as good correlation exists between the various logs.

Logging Results

Two major log units can be distinguished in Hole 903A. The boundary between them can be seen on all the log curves (Fig. 32). Within these main log units, several subunits can be described. Log Unit 1 extends from 68 to 361 mbsf, and log Unit 2 comprises the rest of the logged interval. The boundary between these two log units approximately corresponds with that between lithologic Units II and III, the unconformable Pliocene–Pleistocene and Miocene contact (see "Lithostratigraphy" section, this chapter).

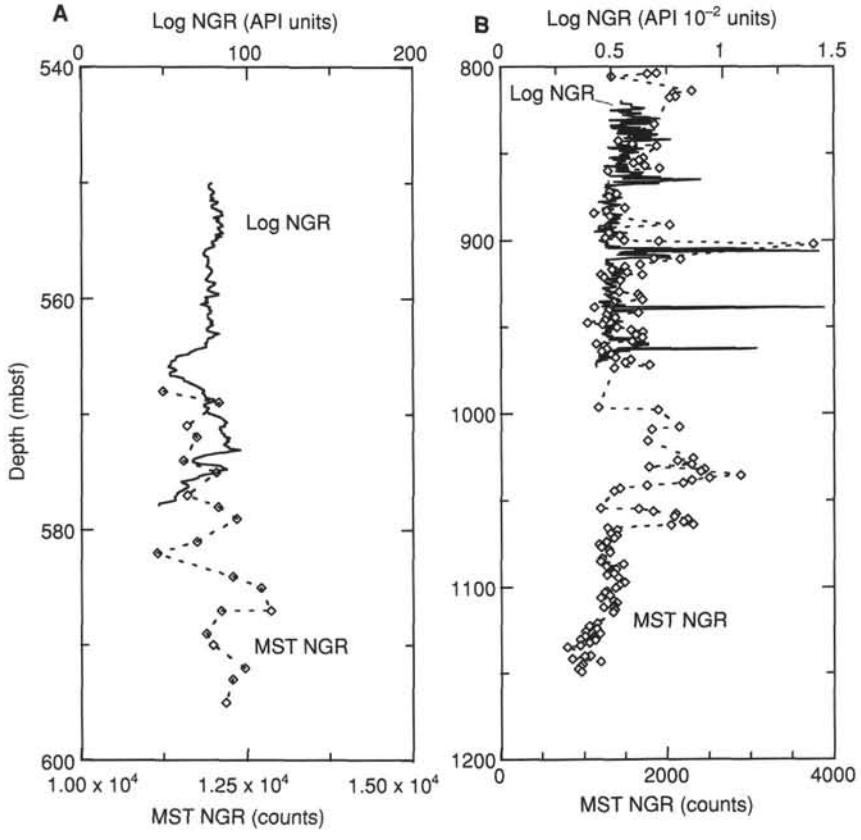

Figure 29. **A.** Multisensor track natural gamma-ray (MST NGR) and Schlumberger spectral gamma-ray logs plotted without depth corrections for Hole 903A. Measurements are plotted at different scales to show similar relative ranges in gamma radioactivity. MST NGR measured once per section for 5 min. **B.** MST NGR log for Hole 903C. Data are plotted similarly to Figure 29A. MST NGR measurements were taken every 40 cm for 30 s each.

Log Unit 1

Log Unit 1 extends from 68 mbsf (lowest pipe position) to 361 mbsf, and corresponds to post-Miocene lithologic Units I and II. The diameter of most of Hole 903A was close to the bit size (10 1/8 in.). There were, however, exceptions where the diameter increased to 19 in. or more (Fig. 32). These intervals can all be correlated to variations in lithology. There were also intervals (325–330 mbsf) where the diameter was less than bit size, indicating "swelling material." Changes in gamma-ray log values correlate well with those of the caliper log. Zones of variable hole diameter can also clearly be seen on other logs.

Log Unit 1 is characterized by a resistivity that varies between 1 and 2 Ωm. The major resistivity variations occur in the intervals with increased borehole diameter. Within this unit, velocity increases with depth. The lowest value, 1550 m/s, is recorded just below the pipe. In the lower part of Unit 1, velocity readings vary between 1840 and 2200 m/s. The neutron porosity is almost constant (48%–49%) throughout the unit except in the intervals with enlarged diameter, where the porosity log shows erroneously high porosity values. A minor decrease in porosity occurs in the lower part of the unit, however. Density is almost constant, with a small increase with depth and, in general, variations in density readings match those of the porosity log. As with porosity, the density curve changes abruptly, with low-density readings in intervals with enlarged hole diameter.

Several distinct intervals can be seen within log Unit 1. The interval from 68 to 99 mbsf is characterized by nearly constant values of density, caliper, neutron porosity, and resistivity. Both the gamma-ray and velocity curve show a small increase with depth. The interval from 220 to 252 mbsf shows constant log values for all the recorded parameters, whereas below this interval the curves either decrease or increase depending on the registered parameter. This interval of the hole is described in the "Lithostratigraphy" section (this chapter) as an interval with slump material. The upper part is bounded by an interval with enlarged borehole diameter.

Log Unit 2

Log Unit 2 (below 361 mbsf) is characterized by a decrease in resistivity. Below 532 mbsf, resistivity is nearly constant at 1 Ωm (Fig. 32). The velocity in log Unit 2 varies around 1900 m/s. Porosity shows a minor increase with depth and density a decrease with depth. As in log Unit 1, the different logs show variations at the same levels. The influence of hole diameter is noted on all the curves.

Several intervals with different log characteristics can be seen. The interval between 361 and 412 mbsf shows constant values compared with the rest of the unit. Hole diameter is very close to bit size in this interval. Density is approximately 2.2 g/cm^3. Porosity and velocity are also more or less constant with readings of 46% and 2025 m/s, respectively. This unit is middle to upper Miocene.

Log values within the interval from 412 to 532 mbsf show more variations, possibly because of variations in hole diameter. The interval between 440 and 455 mbsf, however, consists of coarse glauconitic sand, suggesting that abrupt changes in lithology may also contribute to the variable log character.

Only the sonic-induction tool reached below 532 mbsf; therefore, only three logs were recorded in this interval. Most characteristic of this interval are the nearly constant resistivity readings of 1 Ωm. The

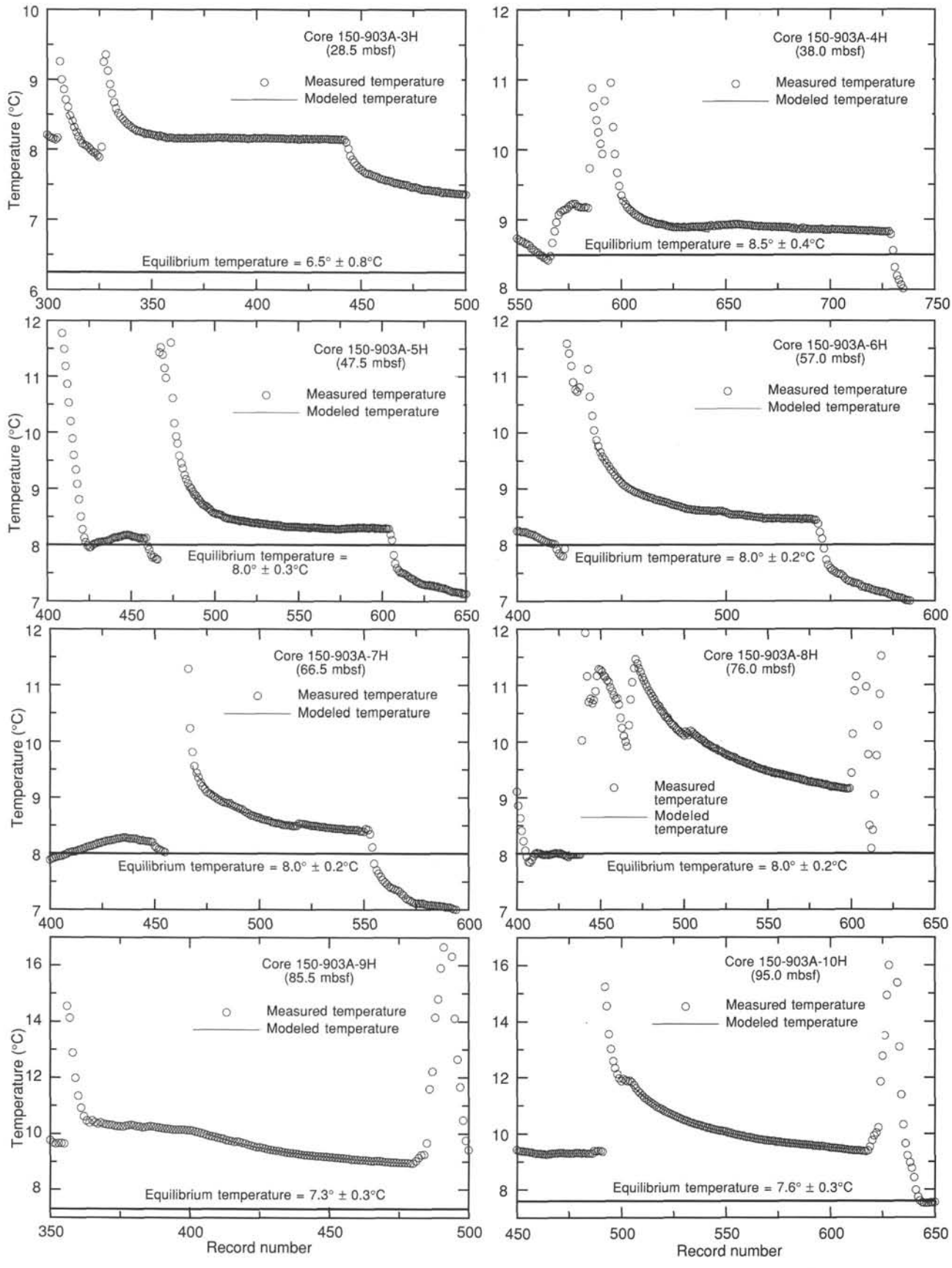

Figure 30. Plots of measured temperatures, modeled temperature equilibrium curves, and calculated equilibrium temperatures, from 14 APC cores at Hole 903A. Data based on measurements with the ADARA tool.

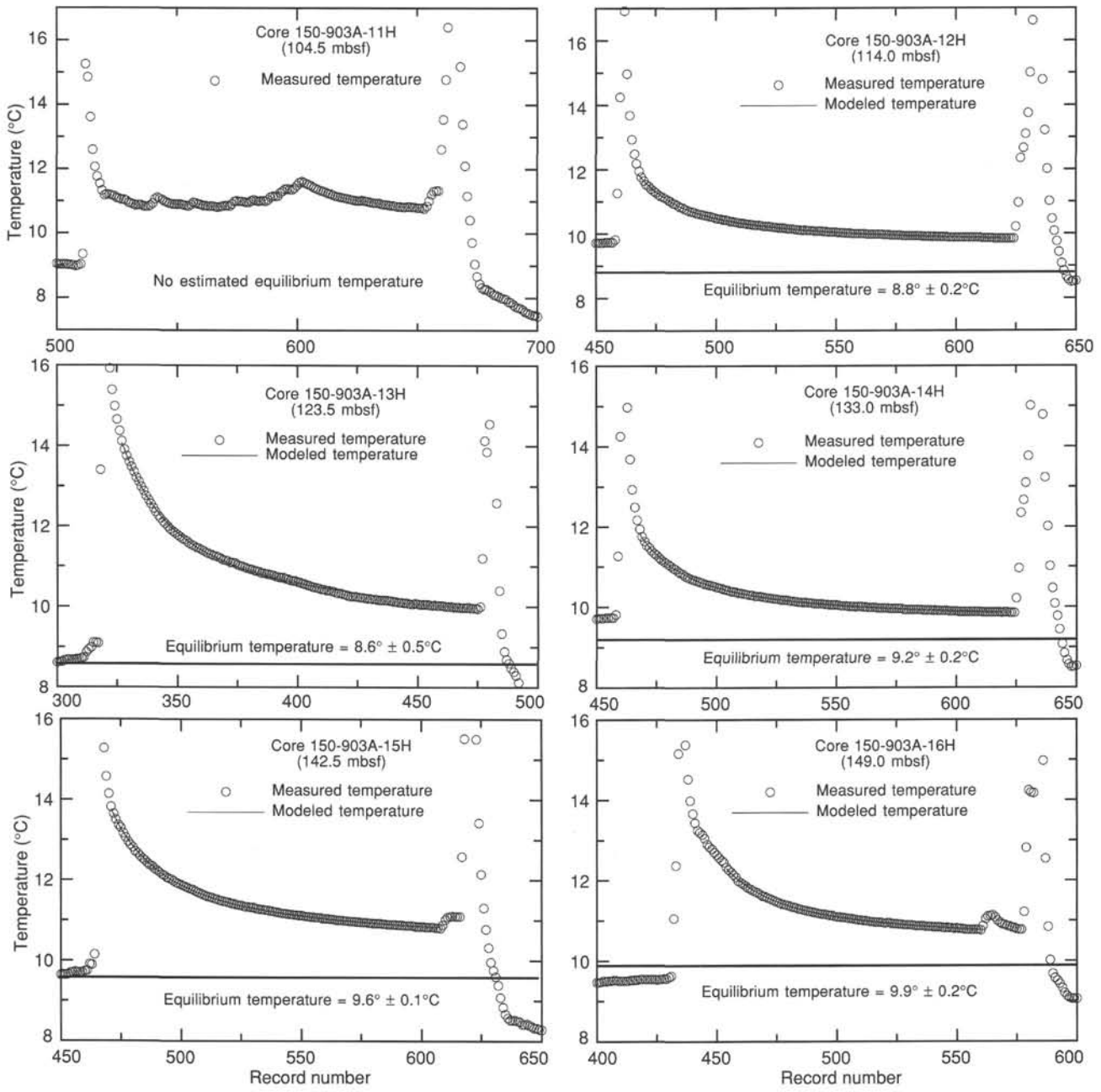

Figure 30 (continued).

gamma-ray curve shows lower readings in the upper part of this interval, corresponding to velocity values (~1955 m/s) that are more variable than below. Unfortunately, there are no caliper data below 480 mbsf, so it is possible that the variations are caused by irregular borehole size.

Hole 903C

Introduction

Seafloor at Hole 903C was at 457 m below rig floor. The sonic-induction tool string and a combination of sonic-induction and porosity tool strings (Quad combo) constitute the two runs made (see Chapter 3 [this volume] for descriptions of the tools). The Quad combo tool string was not normally used on Leg 150, but the condition of Hole 903C mandated its use. Table 12 summarizes the tool combinations and logging runs in Hole 903C.

Logging started after Hole 903C was drilled (to a total depth of 1150 mbsf) and conditioned for logging (see "Operations" section, this chapter, for additional discussion). Logging Hole 903C encountered several problems. The first logging attempt was made in an open hole without the sidewall-entry sub (SES). There were several intervals where the sediment swelled and constricted the hole and, in attempts to break through some of these, the cable was damaged and the string had to be retrieved so the cable head could be replaced. The tool was then lowered to 973 mbsf where it was stopped by a constriction. Logging run 1, with the sonic-induction tool, began at this depth up and continued with difficulty to the bottom of the pipe at 793 mbsf.

Because the first logging run had encountered so many problems with hole conditions, the second logging run was performed with the

Table 11. APC downhole temperature measurements, Hole 903A, using the ADARA tool.

Core no.	Depth (mbsf)	Depth error (m)	Thermal conductivity (W/[m · K])	Probe no.	Calculated Temperature (C°)
150-903A-					
3H	28.5	1.0	1.20	17	6.5 ± 0.8
4H	38.0	1.0	1.35	18	8.5 ± 0.4
5H	47.5	1.0	1.30	12	8.0 ± 0.3
6H	57.0	1.0	1.35	17	8.0 ± 0.2
7H	66.5	1.0	1.30	18	8.0 ± 0.2
8H	76.0	1.0	1.25	12	7.5 ± 0.5
9H	85.5	1.0	1.25	18	7.3 ± 0.3
10H	95.0	1.0	1.30	12	7.6 ± 0.3
11H	104.5	1.0	—	18	—
12H	114.0	1.0	1.30	12	8.8 ± 0.2
13H	123.5	1.0	1.20	18	8.6 ± 0.5
14H	133.0	1.0	1.40	12	9.2 ± 0.2
15H	142.5	1.0	1.40	18	9.6 ± 0.1
16H	149.0	1.0	1.40	12	9.9 ± 0.2

Notes: The bottom of the drilled interval of a core is used as the measurement depth and is given in meters below seafloor. Thermal conductivity values are based on a 4-m box car average (±2 m from depth of measurements). See Chapter 3 (this volume) for information regarding the probe numbers.

Table 12. Total drilling depth, SES, tool configuration, logging interval, and logging speed at Holes 903A and 903C.

Total depth (mbsf)	SES	Tools (string and combination)	Logging interval (mbsf)	Logging speed (m/hr)
Hole 903A:				
703	No	Sonic-induction tool string NGT/SDT/MCD/DIT/LDEO temperature	~24 to 605	275
703	No	Porosity tool string NGT/CNT/HLDT/LDEO temperature	56 to 492	275
Hole 903C:				
1151	No	Sonic-induction tool string NGT/SDT/MCD/DIT/LDEO temperature	793 to 973	275
1151	Yes	Quadombo tool string NGT/CNT/HLDT/SDT/DIT	433 to 766	275

Note: SES = side-entry sub.

SES. Water depth at Hole 903C was less than the maximum sub-bottom depth, so the SES could only be used in part of the borehole. Furthermore, the drill pipe could not be lowered to the maximum depth of the SES, because of a tight zone at 766 mbsf. The second logging run began at this depth. The condition of the borehole deteriorated after each run; therefore, it was decided to run the Quad combo to save one run, even though the quality of the readings would suffer. After logging was completed up to 433 mbsf, the hole was plugged and abandoned and the ship moved to Site 904.

Log Quality

Because of deteriorating hole conditions, the quality of log data from Hole 903C is not as good as from the other sites. Because of poor hole conditions, no duplicate run was made. However, sections where the diameter of the hole is within a reasonable range show good, reliable readings.

During attempts to break through swelling parts of the hole, the tool string was often stationary. As the porosity tool uses radioactive sources, the formation is irradiated while the tool is in the hole, and readings of gamma ray, density, and porosity in these intervals can be affected. Some of the logs (e.g., dual induction) were recorded in both runs, giving two curves in the overlapping interval. In Figure 33, these logs have been merged to one curve.

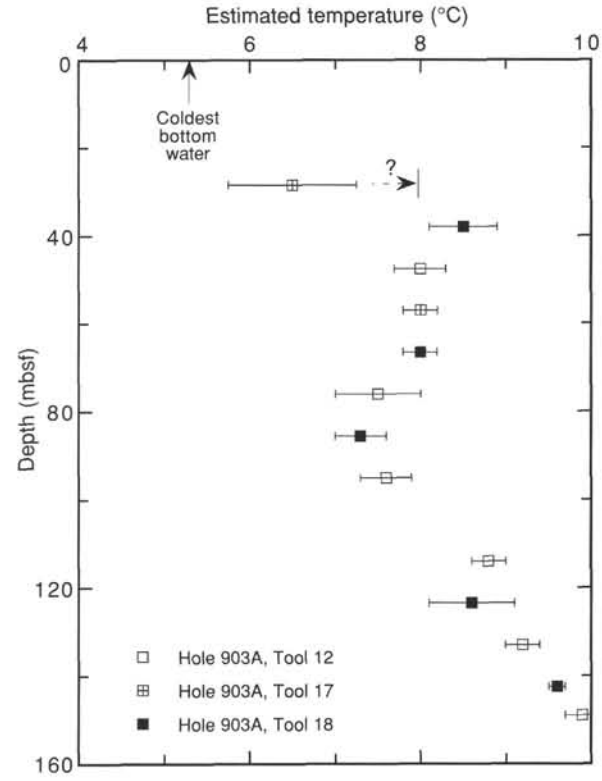

Figure 31. Depth vs. calculated equilibrium temperatures from APC cores at Hole 903A. Data based on measurements with the ADARA tool.

Depth Shifting

Total gamma-ray data were recorded on both runs and have been used for depth shifting to match sub-bottom depths of both logging runs.

Logging Results

As mentioned above, the condition of Hole 903C was very poor. Several tight spots were encountered where the tool string had severe difficulty passing. Between 786 and 796 mbsf, the arm of the caliper on the lithodensity tool had to be closed to let the tool string pass this section. Between 722 and 765 mbsf, some log data are missing because the tools came too close to the drill pipe that was moving ahead of the tool string.

It is difficult to distinguish separate log units in Hole 903C. Several sections are present, however, where minor variations in the various logs can be seen. The major change in the logged part of Hole 903C is seen at 626 mbsf. This level also corresponds to seismic reflector m1.5 (orange) and to the boundary between middle Miocene lithologic Subunits IVA and IVB. The section from 626 to 678 mbsf is characterized by minor variations in log values. Resistivity is approximately 0.7 Ωm, velocity 1750 m/s, porosity 57%, and density 1.75 g/cm^3. Below 678 mbsf, density decreases to 1.3 g/cm^3, whereas porosity increases slightly to 60%–65%, but this increase is probably an effect of the hole diameter.

The other interval that differs from the major trend is below 852 mbsf. Only the sonic-induction tool was run in this part of the hole. Lacking caliper measurements, there is no information about hole condition. The quality of the sonic velocity is greatly improved below 852 mbsf, with values almost constant at 1860 m/s. Resistivity of approximately 0.4 Ωm is more constant than it is above this level. Gamma-ray readings are mostly lower than above 852 mbsf. Uranium content, however, increases between 909 and 923 mbsf, with a

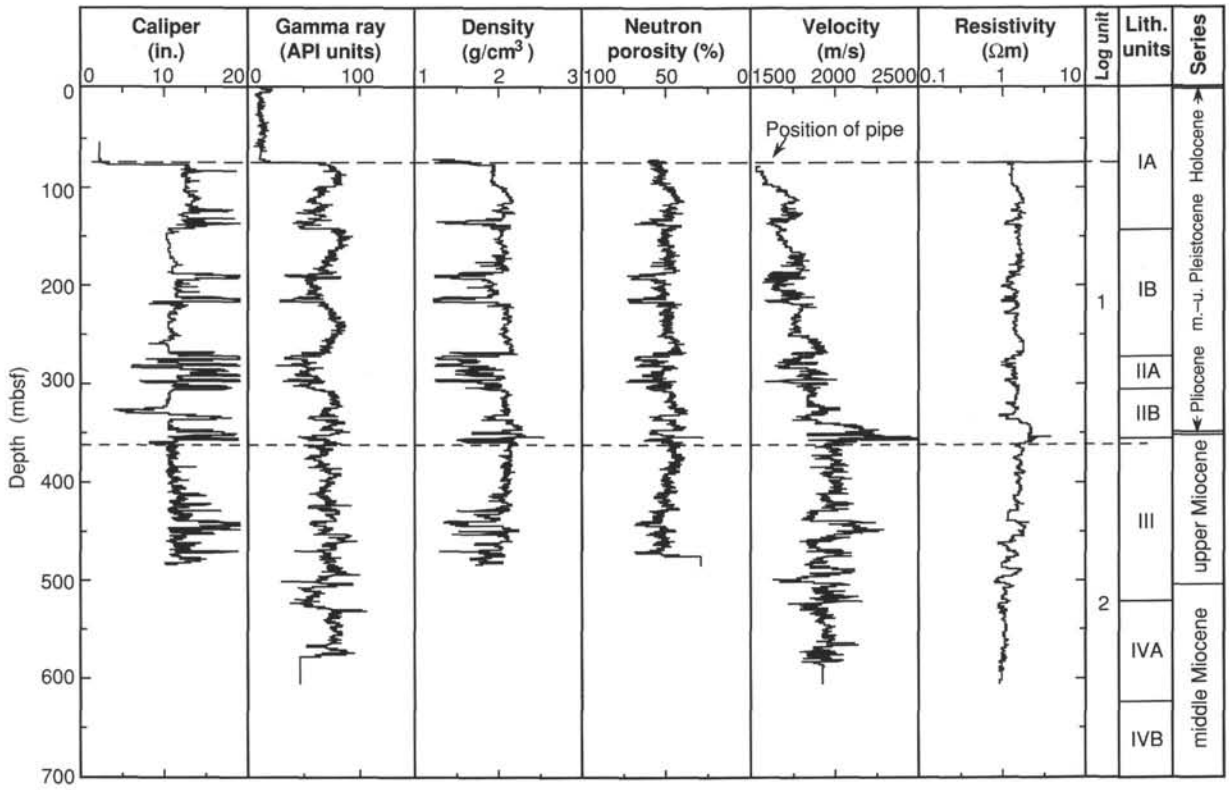

Figure 32. Preliminary logging results based on caliper, gamma-ray, density, neutron porosity, sonic velocity, and deep resistivity logs run in Hole 903A. Results of shore-based processing are shown at the end of this chapter and on the enclosed CD-ROM disk.

peak between 909 and 911 mbsf where it increases from an average of 4 ppm to a maximum of 18 ppm. Unfortunately, core recovery at this level was not complete in Hole 903C, and the source of the increased uranium content has not yet been determined. Samples from the peak between 909 and 911 mbsf may have been recovered in Hole 903D, although this latter hole was not logged.

Synthetic Seismograms from the Logs

Despite the difficulties encountered during the logging operations, it was possible to combine the different logs in Holes 903A and 903C to produce a synthetic seismogram from the logging data for this site. The densities and sonic velocities used for this purpose were from Hole 903A for the interval from 77 to 500 mbsf, and from Hole 903C between 500 and 900 mbsf. The series of reflection coefficients produced was convolved with a theoretical wavelet, and the resulting seismogram is compared with a section of Cruise Ew9009 MCS Line 1005 between CDP 9125 and CDP 9155 (Fig. 34).

Most of the main synthetic reflectors can be correlated to changes in lithology observed in the cores. The highest amplitude is produced by p6 (indigo), at 420 ms (TWT) from the seafloor, and corresponds to a depth of 357 mbsf, which is the boundary between lithologic Units II and III. Among the other significant signatures, p5 (orange), at 330 ms or 272 mbsf, corresponds to the boundary between lithologic Units I and II; m0.5 (Red), at 575 ms or 507 mbsf, may correspond to the boundary between lithologic Units III and IV; and m1 (Tuscan), at 680 ms or 601 mbsf, can be correlated with the top of the slump/coarse sands section in the lower part of lithologic Subunit IVA. The slight differences (<8 m) between these depths and the values obtained from the core analysis (see Table 2, "Lithostratigraphy" section; and Table 13, "Seismic Stratigraphy" section, this chapter) are considered insignificant at this stage of analysis.

Downhole Temperature Measurements

The Lamont-Doherty temperature tool was used during run 1 in Hole 903A. The temperature tool was also attached to the tool string during the second run, but no temperature measurements were made. The tool with its lower bull nose was simply used to protect the logging string when attempting to pass obstructions in the pipe and borehole. Temperature measurements were recorded during the first run in Hole 903C. The temperature tool was not attached to the tool string during the second run.

Because of the multiple attempts to pass through bridges and difficulties encountered while trying to exit the pipe, most of the readings on the way down in Hole 903C were meaningless. However, the profiles in Figure 35, obtained from the first run in Hole 903A, and from the first run in Hole 903C, will allow an evaluation of the thermal regime at this site after processing. Further processing of the recorded temperature data together with operational data should also explain the apparent anomaly in the lower part of the curve from Hole 903C. The two profiles yield a first estimate of the average temperature gradient of 20°C/km, which is an underestimate of the true equilibrium gradient.

SEISMIC STRATIGRAPHY

Introduction

Seismic stratigraphic interpretation at Site 903 is based are based primarily on the grid of Ew9009 and Exxon seismic data that provides direct ties from the slope to the adjacent continental shelf (see Chapter 2, this volume). In particular, the location and interpretation of Site 903 is based on Cruise Ew9009 MCS Lines 1027 (Fig. 1) and 1005 (Fig. 2 in Chapter 6, this volume).

Most reflectors that we identified within the Pleistocene section at Site 903 are associated with slump/mass flow deposits, consistent with their typically irregular and occasionally downcutting seismic

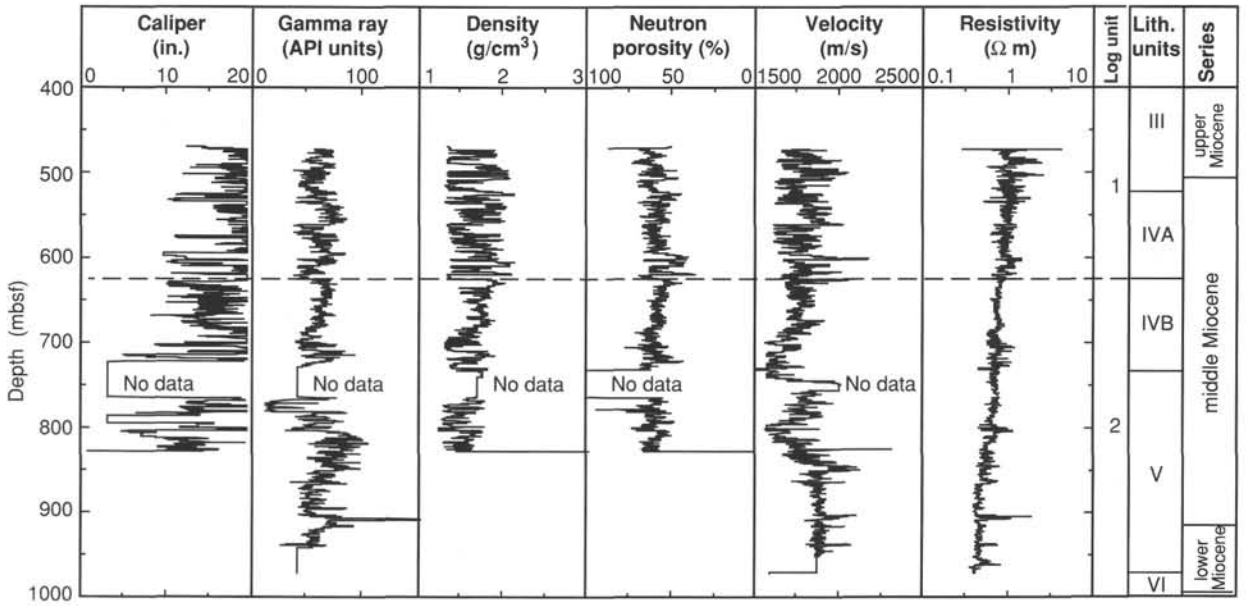

Figure 33. Preliminary logging results based on caliper, gamma-ray, density, neutron porosity, sonic velocity, and deep resistivity logs run in Hole 903C. Results of shore-based processing are shown at the end of this chapter and on the enclosed CD-ROM disk.

character. These can be traced with available seismic profiles to the outer shelf where the geometric relationships used (see Chapter 3, this volume) indicate these reflectors at Site 903 are likely correlatives to sequence boundaries.

In contrast, pre-Pleistocene reflectors that we identified at Site 903 are generally higher amplitude and more nearly smooth and continuous. Erosional relationships are apparent, but less common than in the Pleistocene section. Acoustic character between these major reflectors is typically useful for inferring depositional processes in those cases where reflectors are more than 40 ms apart. Several Oligocene-Miocene reflectors identified as sequence boundaries by Greenlee et al. (1992) were traced from the continental shelf using the Ew9009 seismic grid (see Chapter 2, this volume). These included the following: Red, Tuscan, Yellow-2, Pink-2, and Green. Additional reflectors identified as potential sequence boundaries (G.S. Mountain, K.G. Miller, and N. Christie-Blick, unpubl. data, 1990) have been traced to Site 903 using these same data, and include the Eocene-Miocene reflectors ochre, sand, true blue, pink-3, green-2, and red-3. However, uncertainties are present in some correlations of the shelf reflections because of downlapping, erosion, and masking of reflectors. Therefore, we established a local alphanumeric scheme (Fig. 36 and Table 13) that is tentatively correlated with the shelf reflections.

Time-depth relationships for correlation of seismic profiles to the boreholes were derived from seismic-borehole correlations made at Site 902 (see "Seismic Stratigraphy" section in Chapter 6, this volume). We plotted the two-way traveltimes (TWT) and depth (mbsf) of the most prominent reflectors identified at Site 902 against their respective depths (mbsf) (see Table 16 in Chapter 6, this volume) and fit a second-order polynomial to these data. This polynomial function was used to predict the sub-bottom depth of reflectors traced to Site 903 (Table 13 and Figs. 36–37). The predicted sub-bottom depths appear to have been remarkably accurate, because we found no evidence (based on log, physical properties, lithostratigraphic, or biostratigraphic gaps) to compel us to adjust depth correlations by more than ±3% (Figs. 36–37).

Pleistocene Sequences

We penetrated six Pleistocene seismic reflectors observed in profiles that cross or pass near Site 903 and that are informally named p1 through p6 (Fig. 2). The shallowest four can be traced to Sites 902 and 904 where they have similar lithostratigraphic and chronostratigraphic significance (see "Seismic Stratigraphy" section in Chapters 6 and 8, this volume). The Pleistocene interval is thickest at Site 903 for two reasons: (1) most intervals between reflectors thicken towards this, the most upslope location of Leg 150 sites, and (2) the reflector p4–p6 interval is present only at Site 903.

Reflector p1 (yellow) is difficult to distinguish from the higher amplitude reflector p2 near CDP 9300 on Cruise Ew9009 MCS Line 1005 (Fig. 2). Hence, there is some uncertainty in tracing p1 from Site 902 upslope to Site 903. Reflector p1 is between 85 and 125 ms TWT at Site 903 on Line 1005; our best estimate is that it is at 105 ms with a predicted depth of 83 mbsf (Table 13 and Fig. 36). Based on the patterns shown in the magnetic susceptibility measurements, this reflector correlates to a minor glacial interval within interglacial stage 7 (see Fig. 18, "Sedimentation Rates" section, this chapter). This contrasts with correlation of this reflector with the oxygen isotope stage 7/stage 6 transition at Site 902. However, on *JOIDES Resolution* Line 2 (see "Background and Objectives" section in Chapter 8, this volume), this reflector apparently lies at about 90 ms with a predicted depth of 72 mbsf, closer to the transition from stages 7 to 6. Higher resolution seismic data that image the upper 200 ms are needed to resolve this problem.

Reflector p2 (blue) lies at about 170 ms at Site 903 with a predicted depth of 134 mbsf (Table 13 and Fig. 36). This is immediately above a local density low and velocity high at 138 mbsf noted on the geophysical logs (Fig. 36). This level correlates with the transition from oxygen isotope stage 9 to stage 8 (see "Sedimentation Rates" section, this chapter), as it does at Site 902. It is associated with a major sand bed in Core 150-903B-16H.

Reflector p3 (green) is at 235 ms with a predicted depth of 186 mbsf immediately above a log density trough and velocity peak at 190 mbsf (Table 13 and Fig. 36). This level is correlated with the transition from oxygen isotope stage 11 to stage 10; at Site 902, it is correlated with a possible hiatus in stage 10.

Reflector p4 (purple) lies at 305 ms at Site 903 with a predicted depth of 244 mbsf (Table 13 and Fig. 36). We correlate this reflector with a log velocity peak at 252 mbsf (Fig. 36) that places it about 10 m above the highest occurrence of *Pseudoemiliania lacunosa,* in association with glacial stage 12 (see "Sedimentation Rates" section, this

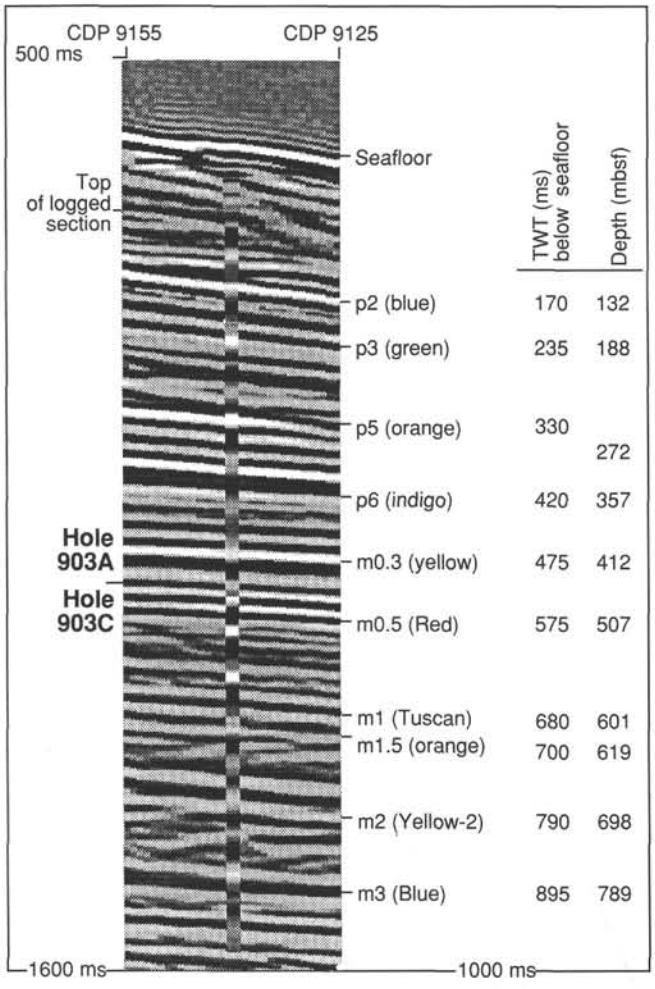

Figure 34. Synthetic seismogram resulting from the density and sonic logs at Site 903. The seismogram is compared with Cruise Ew9009 MCS Line 1005 between CDP 9155 and CDP 9125.

chapter). At Site 902, this reflector occurs near the transition from stages 13 to 12 at the HO of *P. lacunosa*. This minor disagreement can be explained by the uncertainty in distinguishing reflector p4 from the underlying reflector p5 (orange) along the seismic tie from Site 902 to 903 (see Fig. 2 in Chapter 6, this volume; see also Fig. 2, this chapter). At Site 903, reflector p5 lies at 330 ms with a predicted depth of 265 mbsf. We correlate this reflector with a log density and velocity peak and a slump deposit at 274 mbsf (Fig. 36), with the stage 13/12 transition, and with the HO of *P. lacunosa*.

Reflector p6 (indigo) lies at 420 ms with a predicted depth of 343 mbsf. It is best matched with velocity and density increases that peak at 353 mbsf related to a debris flow deposit; this correlation yields a reasonable interval velocity between reflectors p5 and p6 (1756 m/s; Table 13 and Fig. 36). Reflector p6 could correlate with the disconformable base of the Pleistocene. Most of the section between reflectors p5 (orange) and p6 (indigo) correlates to the interval between stages 13 and 14 (~475–600 ka). Alternatively, reflector p6 could be placed at the base of the very thin Pliocene section. Only one sample of Pliocene strata (Zone NN15 or Zones NN17–NN18) was found in shipboard studies (352.33 mbsf); the next sample (362.95 mbsf) is upper Miocene Zone NN10. The magnetostratigraphy (see "Paleomagnetism" section, this chapter) infers another unconformity within the Pleistocene at 336 mbsf that further complicates the interpretation of this section. A lithologic change at 358.9 mbsf from lithologic Unit II to III may correlate with this reflector and the disconformable Pliocene/Miocene contact.

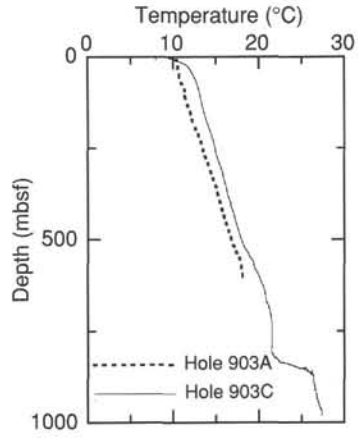

Figure 35. Temperature profiles based on Lamont-Doherty temperature tool, before processing, for Holes 903A and 903C.

Thus, we have been able to identify six middle-upper Pleistocene (less than ~600 ka) sequences at Site 903, bounded by 6 reflectors tied to the cores and/or the downhole logs. Reflectors p2, p3, and p5 are associated with transitions into glacial stages 8, 10, and 12, respectively (i.e., with glacioeustatic lowerings), and as at Site 902, mass-transport deposits are usually associated with the base of these sequences.

Miocene and Older Sequences

A major disconformity at 358.9 mbsf separates the Pliocene from the upper Miocene section at Site 903, corresponding to the contact between lithologic Units II and III. The first Miocene reflector observed, m0.3 (yellow), lies at 475 ms with a predicted depth of 392 mbsf. No discontinuities were noted at this depth on the logs or in the lithologic descriptions. Based on maintaining reasonable interval velocities with the overlying and underlying reflectors, m0.3 lies at 405 mbsf. This is immediately below the base of a normal magnetozone tentatively correlated to Chron C4An (~8.5 Ma; Fig. 36). The several reflectors at or adjacent to the level of m0.3 (Fig. 2) are that much more puzzling because of the unusually featureless log character between 358 and 430 mbsf (see "Downhole Logging" section, this chapter). The fact that these seismic events are generally level despite the wedge-shaped boundaries defined by the underlying reflector m0.5 and the overlying reflector p6 suggests that they are not internal reverberations ("peg-leg multiples"). Their explanation awaits more detailed study.

Reflector m0.5 (Red) lies at 575 ms with a predicted depth of 484 mbsf (Table 13 and Fig. 36). It apparently correlates with a velocity change and major sand bed at 500 mbsf; no density log is available for this section. Much of the section between reflectors m0.3 and m0.5 that is represented at Site 903 has been truncated at Site 902, whereas the section between reflector m0.5 and the underlying m0.7 that is represented at Site 902 is missing at Site 903. At Site 903, reflector m0.5 lies below a normal magnetozone tentatively correlated to Chron C4An (older than about 8.2 Ma) and below the LO of *Denticulopsis hustedtii* (LAD about 8.0–8.2 Ma; Burckle et al., 1982). Thus, as at Site 902, this reflector is about 8.0 Ma, consistent with the correlation of Greenlee et al. (1992) of the Red reflector on the continental shelf to the 8.2 Ma sequence boundary of Haq et al. (1987).

Reflector m1 (Tuscan of Greenlee et al., 1992) is at 680 ms with a predicted depth of 585 mbsf (Table 13 and Fig. 36), closely overlying reflector m1.5 (orange) at 700 ms (predicted depth, 601 mbsf). We match this pair of stratal boundaries with an interval of slumps at 602.5–624.5 mbsf. These correlations are supported by log velocity peaks at these depths in Hole 902C (see Fig. 36 in Chapter 6, this volume), although log quality is poor. Based on interval velocities of

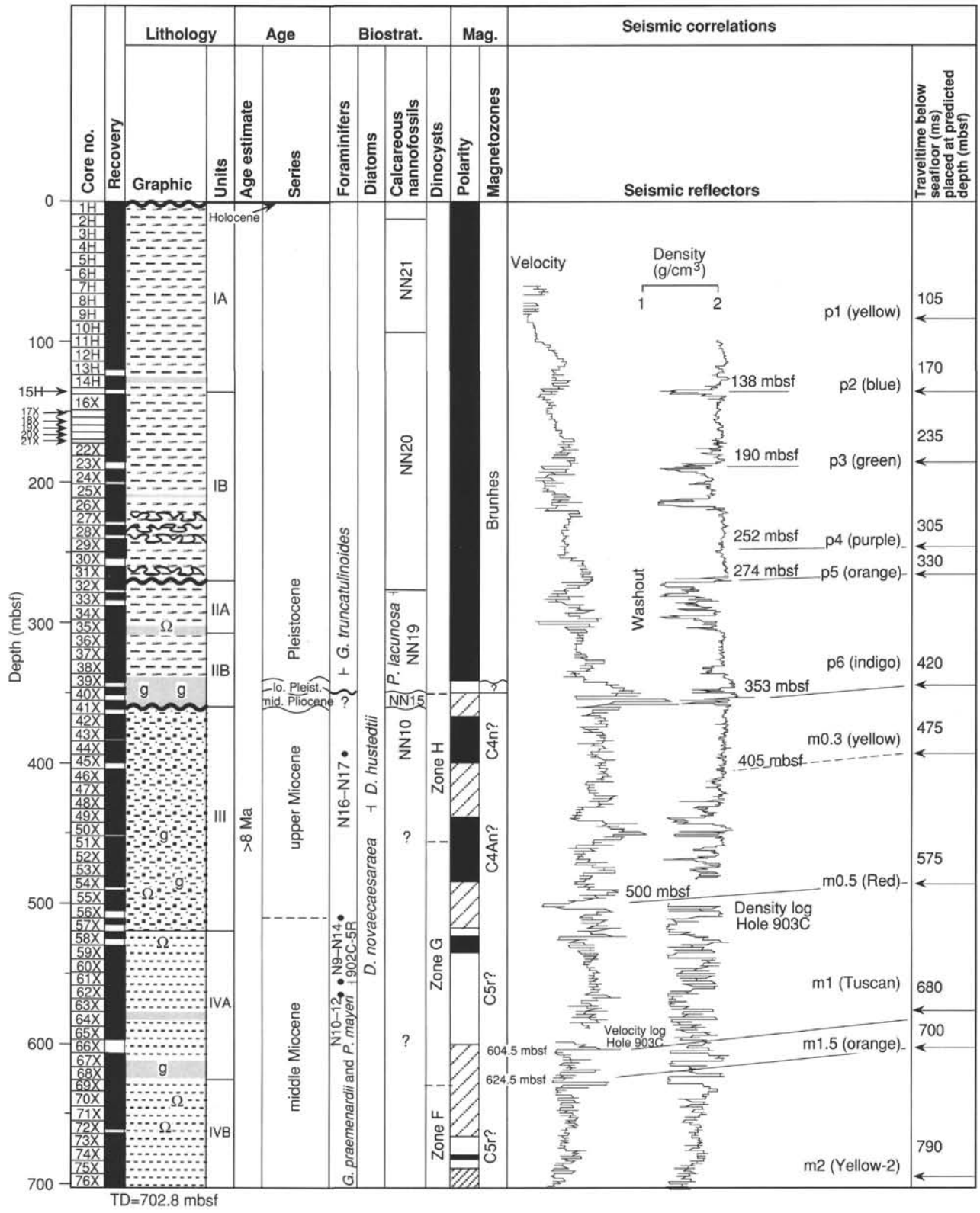

Figure 36. Seismic-core correlations for Hole 903A showing lithology, age, biostratigraphic zones, magnetozones, and seismic reflections discussed in text. Note that the velocity log below 600 mbsf and the density log below 500 mbsf are from Hole 903C.

Table 13. Seismic reflectors identified at Site 903.

Name	Color	Two-way traveltime (ms)	Depth (mbsf)	Calculated velocities (m/s)		Correlation to borehole
				Interval	Average	
p1	yellow	105	83	1581	1581	??
p2	blue	170	138	1692	1624	Log density minimum; major sand bed.
p3	green	235	190	1600	1617	Log density minimum.
p4	purple	305	252	1771	1652	Log velocity maximum.
p5	orange	330	274	1760	1661	Density minimum; slump.
p6	indigo	420	353	1756	1681	Log velocity maximum, density minimum; debris flow.
m0.3	yellow	475	405	1891	1705	Picked on interval velocity.
m0.5	Red*	575	500	1900	1739	Log velocity kick; major sand bed.
m1	Tuscan*	680	604.5	1990	1778	Base of slump.
m1.5	orange**	700	624.5	2000	1784	Base of slump/debris flow.
m2	Yellow-2*	790	700	1678	1772	Below density maximum, at velocity maximum.
m3	Blue*	895	796	1829	1779	At core density maximum.
m4	Pink-2*	935	845	2450	1807	Log velocity peak.
m5	Green*	980	900	2444	1837	Minor log velocity increase; sand bed.
m5.2	ochre**	1020	940	2000	1843	Break NN2/NN4?
m5.4	sand**	1040	960	2000	1846	? cemented sand bed.
m6	pink-3**	1080	1010	2500	1870	Core density maximum; ?cemented sand bed.
o1	green-2**	1120	1064.1	2705	1900	Top of chalks; major sand bed.
e2	red-3**	1215	—	—		Not reached.

Notes: Single asterisk (*) = possibly equivalent to the shelf reflectors of this color (Greenlee et al., 1992), whereas double asterisk (**) = possibly equivalent to the shelf reflectors of this color (G.S. Mountain, K.G. Miller, and N. Christie-Blick, unpubl. data, 1990).

1900–2000 m/s, we correlate reflector m1 to the base of slumps at 604.5 mbsf and m1.5 to the base of slumps at 624.5 mbsf (Table 13). The age of reflector m1 (and, by superposition, m1.5) is slightly older than we estimated at Site 902. At Site 903, reflector m1 lies immediately below a reversed magnetozone tentatively correlated with part of Chron C5r.2 (<~11 Ma; Figs. 36–37). Although this is consistent with the age estimate of 9–11 Ma of Greenlee et al. (1992), it is slightly older than the age of 9.7 ± 0.7 Ma estimated at Site 902. Biostratigraphic evidence also points to an older age estimate for reflector m1 than estimated previously. Planktonic foraminifers indicate correlation to Zone N10–N12 undifferentiated above reflector m1 based on the presence of *Globorotalia praemenardii*. It is possible that the last appearance of this taxon is somewhat younger based on previous correlations of reflector m1 (Greenlee et al., 1992). If we assume that the highest occurrence of *Paragloborotalia mayeri* at Site 903 is its LAD, then the foraminifer data would indicate that reflector m1 is slightly older than this datum (10.4 Ma). This is supported by the association of reflector m1 with the last occurrence of *P. mayeri* in shelf wells (Greenlee et al., 1992).

Reflector m2 (= Yellow-2 of Greenlee et al., 1992) is at 790 ms (694 mbsf predicted depth; Fig. 37). This reflector could correlate either with a core density peak at 690 mbsf or a log velocity peak at 700 mbsf; we chose the latter because it yields a reasonable interval velocity of 1678 m/s (vs. 690 mbsf, which yields an interval velocity <1500 m/s; Table 13). This reflector is middle middle Miocene, occurring immediately above a sample with *Globorotalia fohsi fohsi* (12.1 to ~12.9 Ma; Zhang et al., 1993), within East Coast Diatom Zone (ECDZ) 7 to upper ECDZ 6 (~12.5–13.5 Ma; Sugarman et al., 1993), and immediately above a reversed magnetozone tentatively correlated with C5Ar (less than about 12.46 Ma). This dates reflector m2 as ~12.4 Ma, consistent with the broad age estimate at Site 902 (11.5–12.5 Ma?) and with an age estimate of 11.2–12.2 Ma for Yellow-2 of Greenlee et al. (1992).

Reflector m3 (= Blue of Greenlee et al., 1992) crosses Site 903 at 895 ms (803 mbsf predicted); it is apparently associated with a wet-bulk density peak at 796 mbsf (Fig. 37). No obvious peak is noted on the density log, although the quality of this log suffered from poor hole conditions. This correlation yields a reasonable interval velocity of 1829 m/s (Table 13). The age of reflector m3 can be estimated as middle middle Miocene (~13.5 Ma), within ECDZ 6 (~13.5–13.0 Ma; Sugarman et al., 1993) and probably within Zone NN6 (14.4–13.2 Ma), in agreement with the estimate by Greenlee et al. (1992) of 13.5 ± 0.7 Ma.

Reflector m4 (= Pink-2 of Greenlee et al., 1992) lies at 935 ms with a predicted depth of 835 mbsf (Fig. 37). We correlate this reflector with a velocity kick at 845 mbsf (Fig. 36) that lies in the middle middle Miocene within the upper part of Zone NN5 (~14.4 Ma) and near the base of ECDZ 6 (14–13 Ma). This differs from the biostratigraphic correlation of this reflector with the base of ECDZ 3–4 at Site 902 (~15.5 Ma), perhaps because of the diachrony of the benthic diatom zone (see "Biostratigraphy" section, this chapter).

The position of reflector m5 (Green of Greenlee et al., 1992) occurs at 980 ms (889 mbsf predicted depth; Fig. 37). Based on interval velocities (Table 13), this reflector best correlates with a log velocity peak and sand bed at 900 mbsf, 15 m above a wet-bulk density peak (Fig. 36). We date this reflector relatively precisely at Site 903 because it lies in the lowermost part of Zone NN5 at Hole 903D with an age of slightly less than 16.2 Ma. This reflector occurs near the middle/lower Miocene boundary. This is consistent with diatom correlations to the upper part of ECDZ 2 (see Fig. 36 in Chapter 6, this volume).

Reflectors m5.2 (ochre) and m5.4 (sand) lie at 1020 and 1040 ms, respectively (932 and 954 mbsf; Fig. 37). No velocity or density logs are available. Based on maintaining reasonable interval velocities, these reflectors correlate with about 940 and 960 mbsf, respectively. They are both lower Miocene. Reflector m5.2 may correlate with a possible break between Zones NN2 and NN4. At Site 902, m5.2 matches the downhole reappearance of calcareous nannofossils; at Site 903, a similarly marked increase in nannofossils is observed (Fig. 3B). Reflector m5.4 may be associated with a cemented sand bed.

Reflector m6 (pink-3) crosses Site 903 at 1080 ms and we correlate it with dolomite-cemented glauconitic silty claystone at 1006 mbsf (Fig. 36). Logging did not reach this depth. A sharp increase in wet-bulk density and a cemented sand bed at the base of 150-903D-21R suggests the top of a substantially thicker bed could extend one or more meters downwards into the poorly recovered interval beneath this core. This correlation places reflector m6 within lithologic Unit VI, at or near the unconformable Miocene/Oligocene boundary.

Reflector o1 (green-2) lies at 1120 ms with a predicted depth of 1049 mbsf (Fig. 37). As at Site 902, this reflector correlates with the contact between Oligocene siliciclastics and upper Eocene chalks at 1064.1 mbsf, the contact between lithologic Units VI and VII, a major

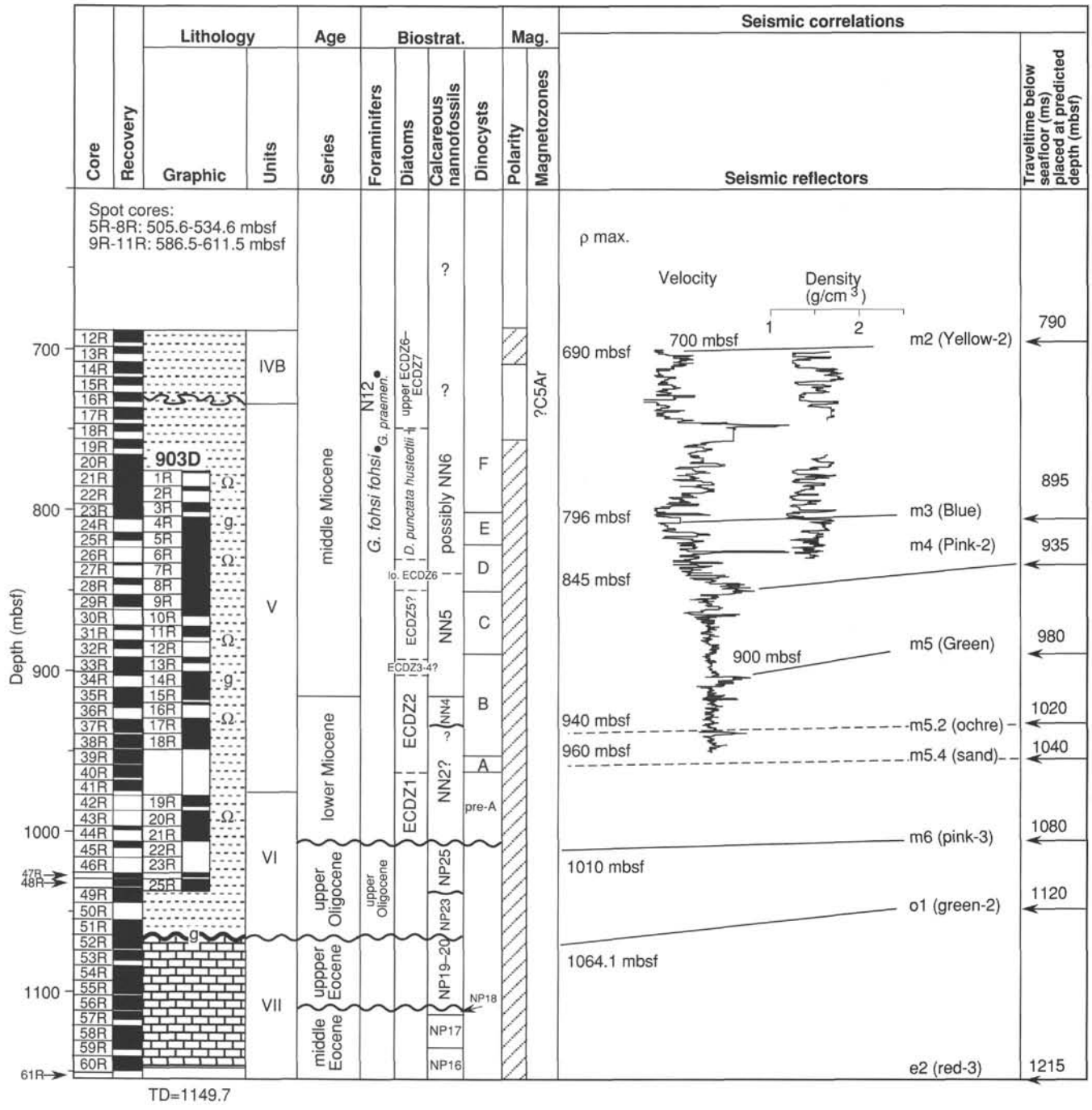

Figure 37. Seismic-core correlations for Holes 903C and 903D showing lithology, age, biostratigraphic zones, magnetozones, and seismic reflections discussed in text.

sand bed, and a disconformity separating the uppermost lower Oligocene (Zone NP23) from uppermost Eocene (Zone NP19–20).

Summary

Based on correlation to the SPECMAP time scale, three Pleistocene reflectors (p2, p3, and p5) at Site 903 are correlated with glacioeustatic lowerings associated with transitions from interglacial to glacial intervals; two others (p1 and p6) are consistent with correlation to glacioeustatic lowerings. Reflectors p2, p5, and p6 match slump/mass transport deposits.

Correlations of the Miocene and older reflectors are based on depths predicted by the Site 902 time-depth function and interval velocities. These correlations are adjusted up- or down-section less than several per cent to match reasonable surfaces in the hole based on lithologic log or physical properties character. Reflectors m0.5, m1, m1.5, m5, m5.4, m6, and o1 are all associated with mass transported sediments. These stratal surfaces are typically rich in quartz and/or glauconite; those towards the bottom of the hole are cemented as well. The ages of Miocene and older reflectors are tentative at present. The ages of sequence boundaries traced from the adjacent shelf are: m0.5 (Red) = 8 Ma; m1 (Tuscan) = ~11 Ma, m2 (Yellow-2) = 12.4 Ma, m3

(Blue) = ~13.5 Ma, m4 (Pink-2) = ~15.5 Ma , and m5 (Green) = 16.2 Ma. These ages are consistent with those at Site 902. However, those for reflectors m1, m4, and m5 are best defined at Site 903.

SUMMARY AND CONCLUSIONS

Site 903 recovered an upper slope (444 m water depth) section that is complimentary to middle slope Site 902 (811 m). A thicker Pleistocene section (336 m) was recovered than at Site 902, which permitted extension of the slope record back to oxygen isotope stage 15 (~575 ka). As at Site 902, a moderately thick upper Miocene section (~135 m) was recovered at Site 903; however, this section is younger than most of the upper Miocene recovered at Site 902. Thick middle Miocene (>450 m) and moderately thick lower Miocene (>100 m) sections were also recovered at Site 903 and provide the best opportunity to date reflectors that can be traced seaward to Site 903 from sequence boundaries beneath the modern shelf. The upper Oligocene, upper Eocene, and middle Eocene sections recovered contain unconformities that correlate with those at the more complete sections at Sites 902 and 904.

Deposition of middle to late Eocene pelagic carbonate was followed by widespread erosion and/or nondeposition on the slope in the early Oligocene. This hiatus correlates with two inferred glacioeustatic sea-level lowerings at around 35.8 and 32.5 Ma (Oi1 and Oi2 of Miller et al., 1991). As observed at Site 902, a switch to siliciclastic deposition of silty clays occurred sometime in the early Oligocene. Another intra-Oligocene hiatus may occur at Site 903 (i.e., Zone NP24 was not identified), which potentially correlates with an inferred glacioeustatic lowering at 28.4 Ma (Oi2b of Miller et al., 1991). A hiatus across the Oligocene/Miocene boundary at Sites 902 and 903 correlates with an inferred glacioeustatic lowering at 25.5 Ma (Mi1 of Miller et al., 1991). Shallowing occurred at Sites 902 and 903 from the late Eocene (>600 m) to the early Miocene (upper bathyal; 200–600 m).

At Sites 902 and 903, early to early middle Miocene sedimentation was dominated by organic-rich (>1%), diatomaceous, glauconitic silty clays with occasional sand interbeds. These sediments suggest that high surface-water productivity began in the early Miocene; intervals of laminated sediments, high organic content, and common pyrite indicate possible intermittent suboxic/anoxic conditions. A probable hiatus in the early Miocene may correlate with an inferred glacioeustatic lowering at 18.1 Ma (Mib of Miller et al., 1991).

During the late middle Miocene, there was a change to increased downslope transport of sediments in the form of intermittent mass-transport deposits. Late Miocene deposition was dominated by glauconite sand and mass-transport deposition. As at Site 902, this transition to increased sedimentation rate and downslope transport in the middle to late Miocene probably reflects the seaward progradation of clinoforms from a position beneath the modern middle shelf to the outer shelf.

A late Miocene to Pliocene hiatus at Site 903 was followed by deposition of a thin Pliocene graded sand unit. This was followed by a hiatus and then by rapid deposition (~70 cm/k.y.) of middle Pleistocene to Holocene hemipelagic silty clays to clayey silts punctuated by mass-transport deposits. Integration of magnetic susceptibility, density, and biostratigraphic data permit correlation of these deposits to the SPECMAP time scale for the Pleistocene (Imbrie et al., 1984). As at Site 902, mass-transport deposits were prevalent during glacial stages, although downslope transport of sediment apparently occurred fairly continuously throughout the Pleistocene.

The principal result from Site 903 is that sequence boundaries identified beneath the modern shelf on seismic data, and traced to the slope, can be recognized as stratal surfaces in the section and confidently dated. Although additional shore-based studies are needed, shipboard analyses provide excellent correlations for several boundaries:

1. Reflector m2 (Yellow-2) is associated with a reversed magnetozone tentatively correlated to Chron C5Ar. It has an age estimate of approximately 12.4 Ma.
2. We have precisely dated the reflector m5 (Green) sequence boundary for the first time. This surface correlates with an interval spanning the boundaries between the middle/lower Miocene (Zones NN4 and NN5) and has an estimated age of 16.2 Ma.
3. At Sites 902 and 903, the reflector m6 (Pink-3) sequence boundary separates the lower lower Miocene from the uppermost Oligocene.
4. At Sites 902 and 903, the o1 (green-2) sequence boundary separates uppermost lower Oligocene from uppermost Eocene strata.

Ms 150IR-107

NOTE: For all sites drilled, core-description forms ("barrel sheets") and core photographs can be found in Section 4, beginning on page 369. Forms containing smear-slide data can be found in Section 5, beginning on page 833. Thin-section data are given in Section 6, beginning on page 875.

SHORE-BASED LOG PROCESSING

Hole 903A

Bottom felt: 455.5 mbrf (used for depth shift to seafloor)
Total penetration: 702.8 mbsf
Total core recovered: 637.77 m (90.6%)

Logging Runs

Logging string 1: DIT/SDT/NGT (upper and lower sections)
Logging string 2: HLDT/CNTG/NGT (upper and lower sections)

Drill Pipe

The following drill-pipe depths are as they appear on the logs after differential depth shift (see **Depth shift** section) and depth shift to the seafloor. As such, there might be a discrepancy with the original depths given by the drillers on board. Possible reasons for depth discrepancies are ship heave and drill-string and/or wireline stretch.

DIT/SDT/NGT: Bottom of drill pipe at ~77 mbsf (on merged data)
HLDT/CNTG/NGT: Bottom of drill pipe at ~72.5 mbsf (on merged data)

Processing

Depth shift: All logs have been interactively depth shifted with reference to NGT from DIT/SDT/NGT runs, and to the seafloor (–457 m). The amount of depth shift to seafloor differs from the bottom-felt depth because logs show the mud line at 457 mbsf.
Gamma-ray processing: NGT data were processed to correct for borehole size and type of drilling fluid.
Acoustic data processing: The sonic logs have been processed to eliminate some of the noise and cycle skipping experienced during recording.

Quality Control

Hole diameter was recorded by the hydraulic caliper on the HLDT tool (CALI).
Invalid gamma-ray readings were detected from 61 to 71 mbsf (DIT/SDT/NGT run) and from 64 to 68 mbsf (HLDT/CNTG/NGT run).

Hole 903A: Resistivity-Velocity-Natural Gamma Ray Log Summary

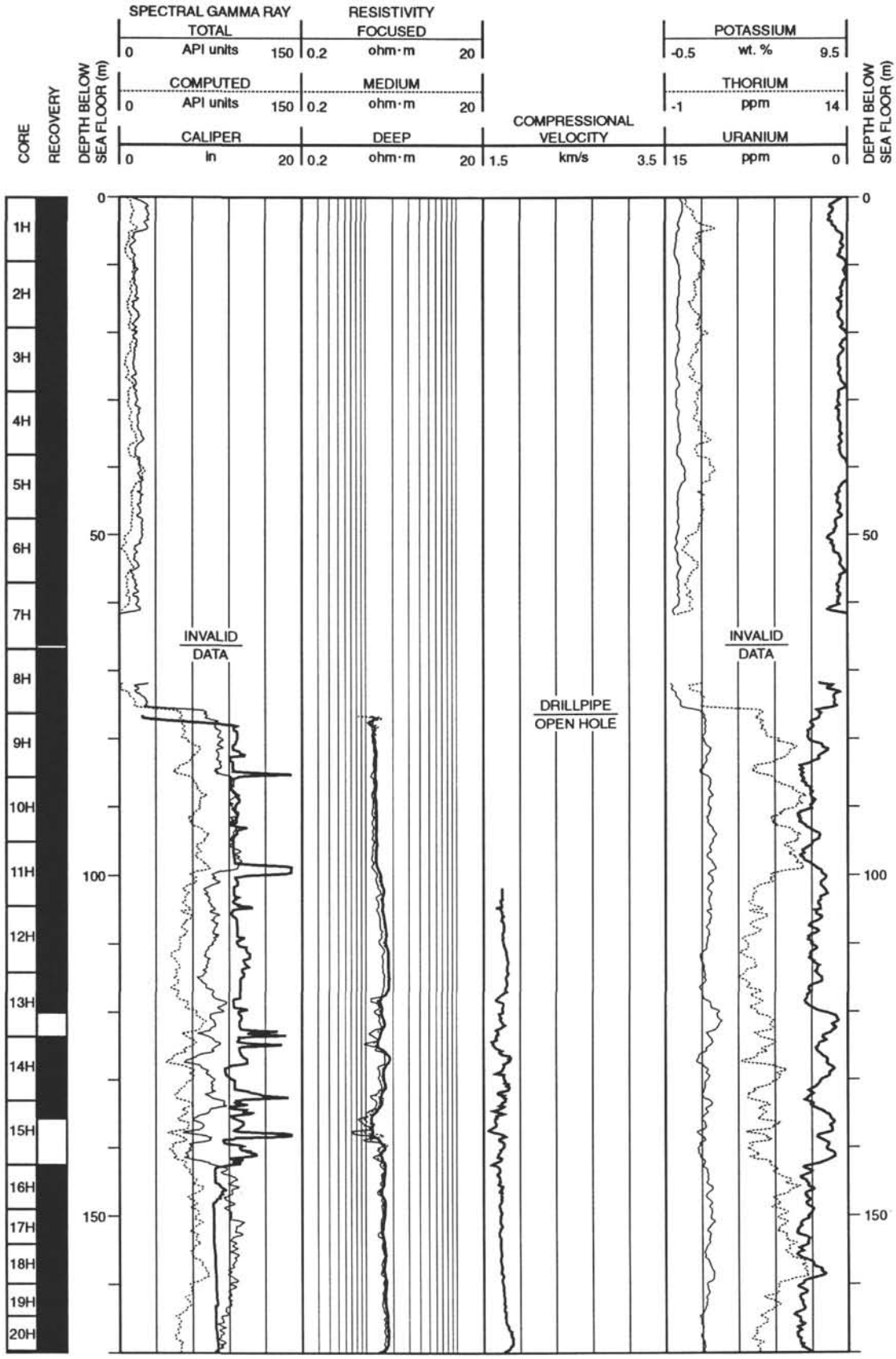

Hole 903A: Resistivity-Velocity-Natural Gamma Ray Log Summary (continued)

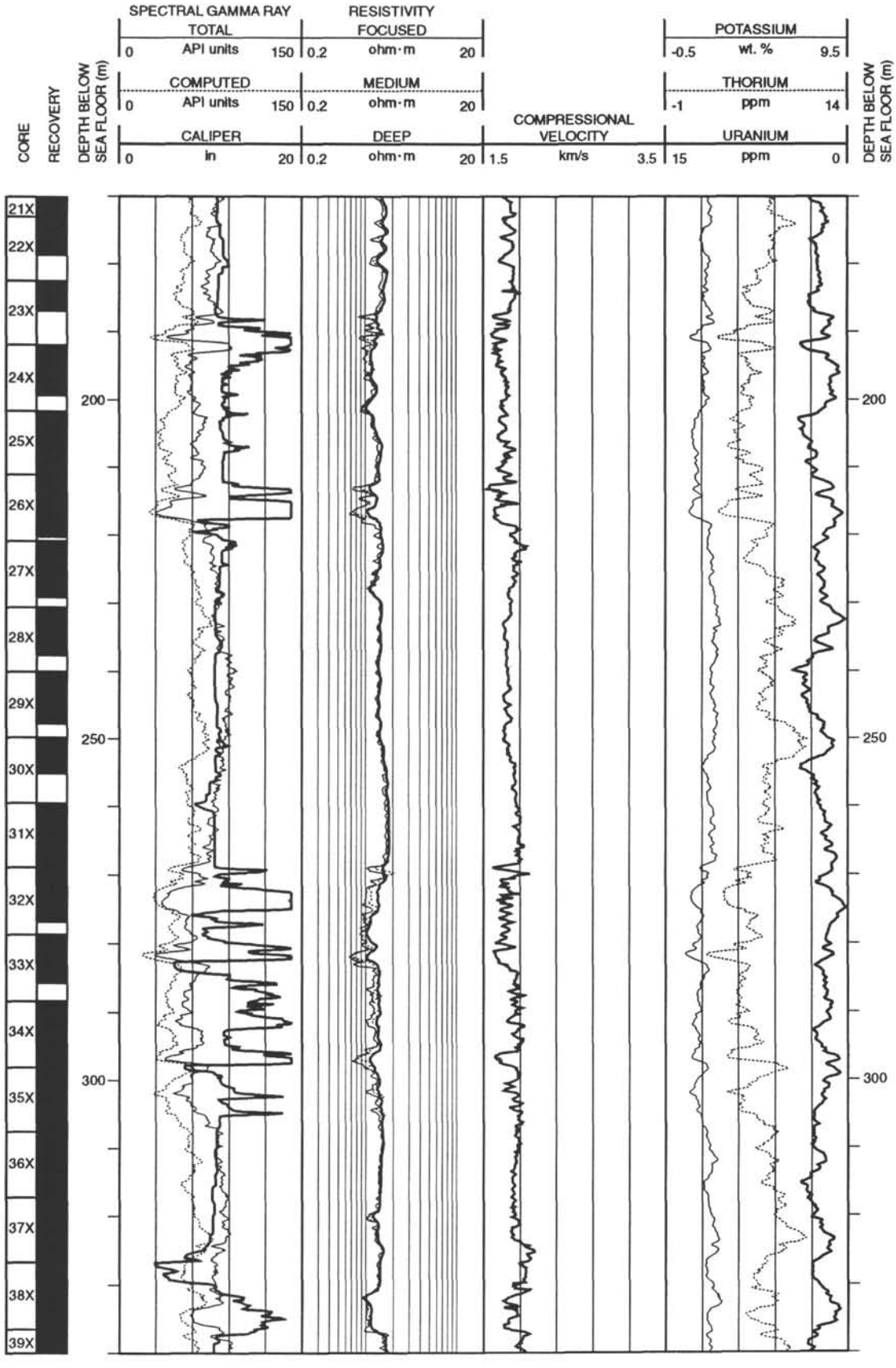

Hole 903A: Resistivity-Velocity-Natural Gamma Ray Log Summary (continued)

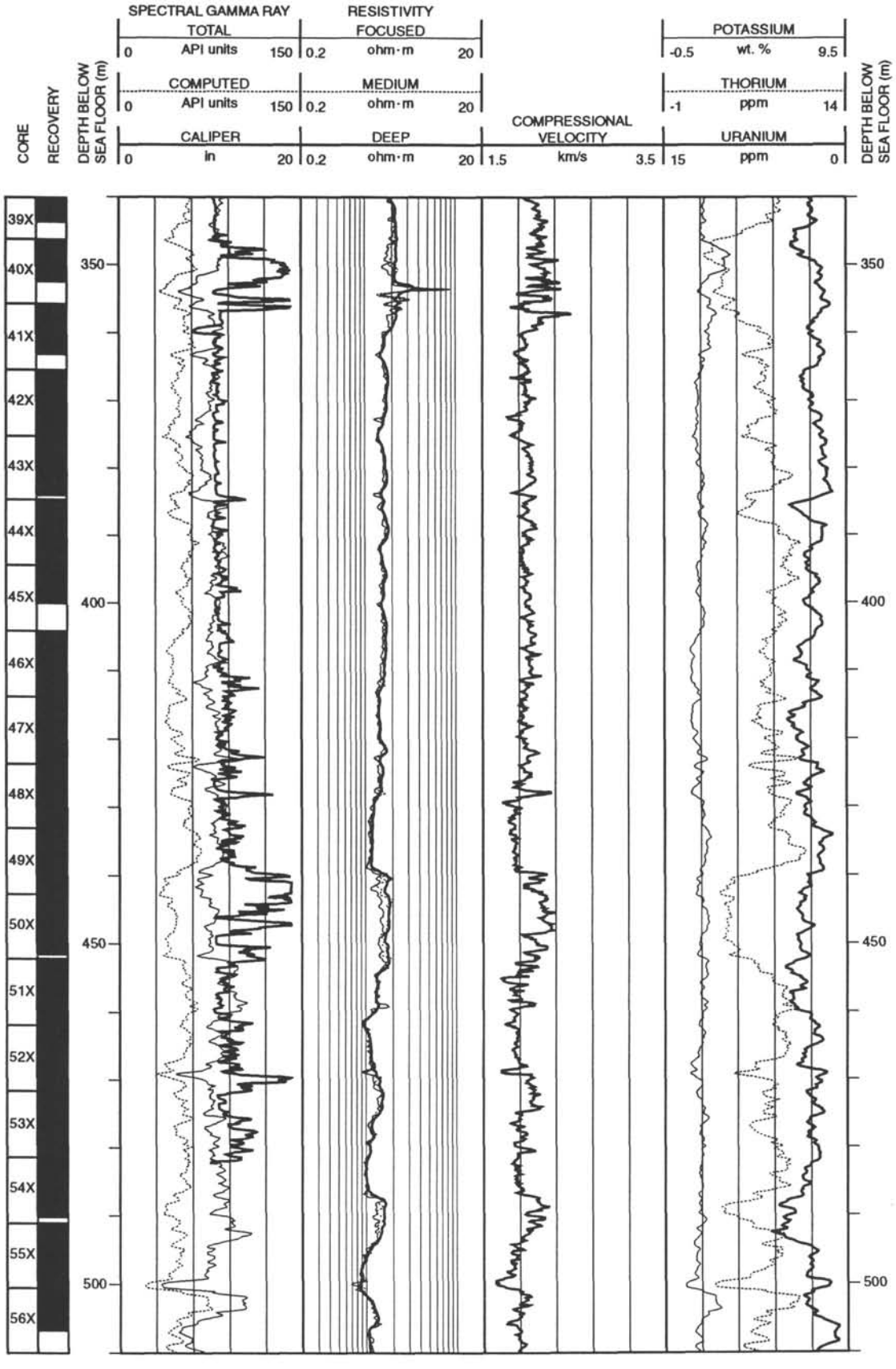

Hole 903A: Resistivity-Velocity-Natural Gamma Ray Log Summary (continued)

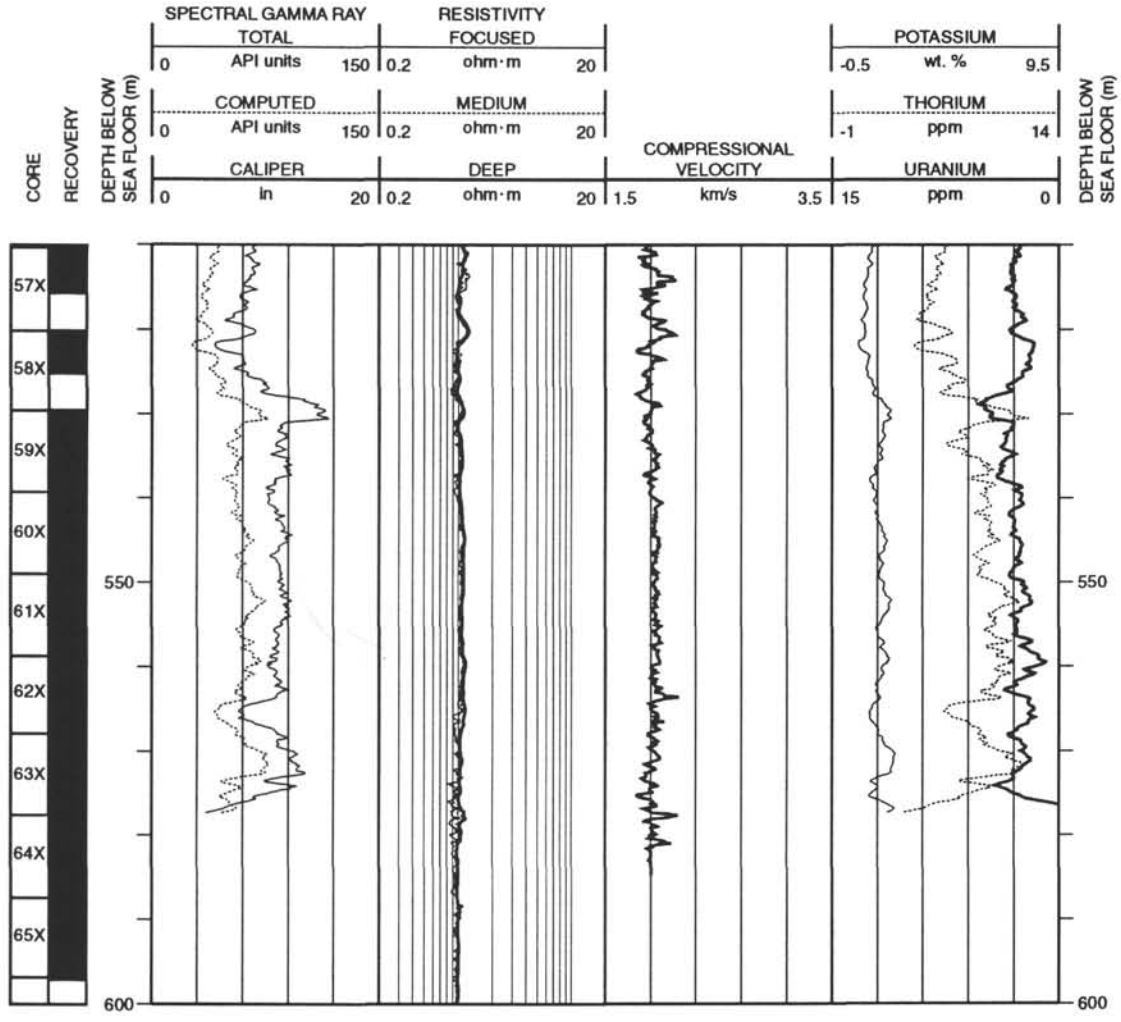

Hole 903A: Density-Porosity-Natural Gamma Ray Log Summary

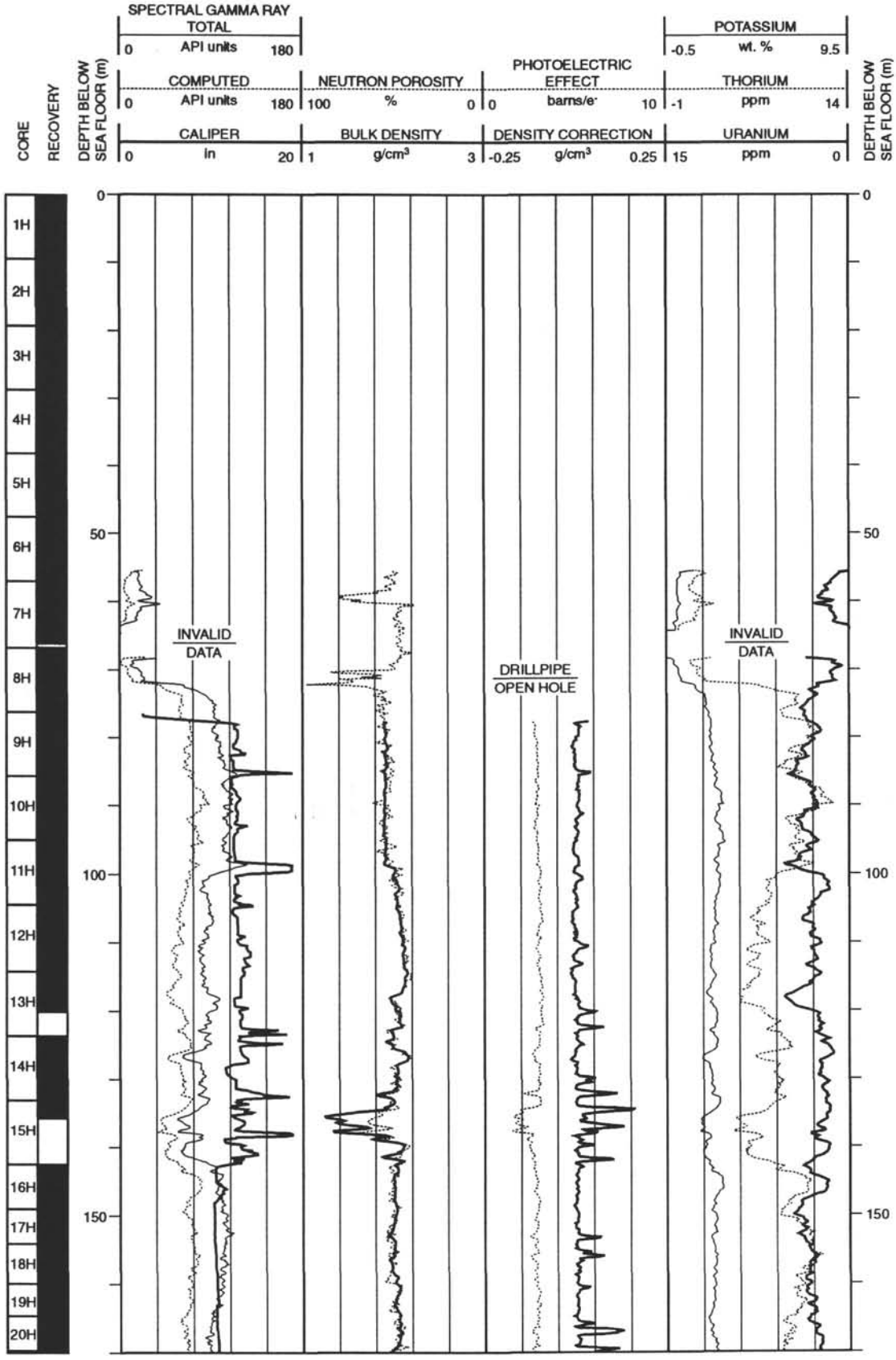

Hole 903A: Density-Porosity-Natural Gamma Ray Log Summary (continued)

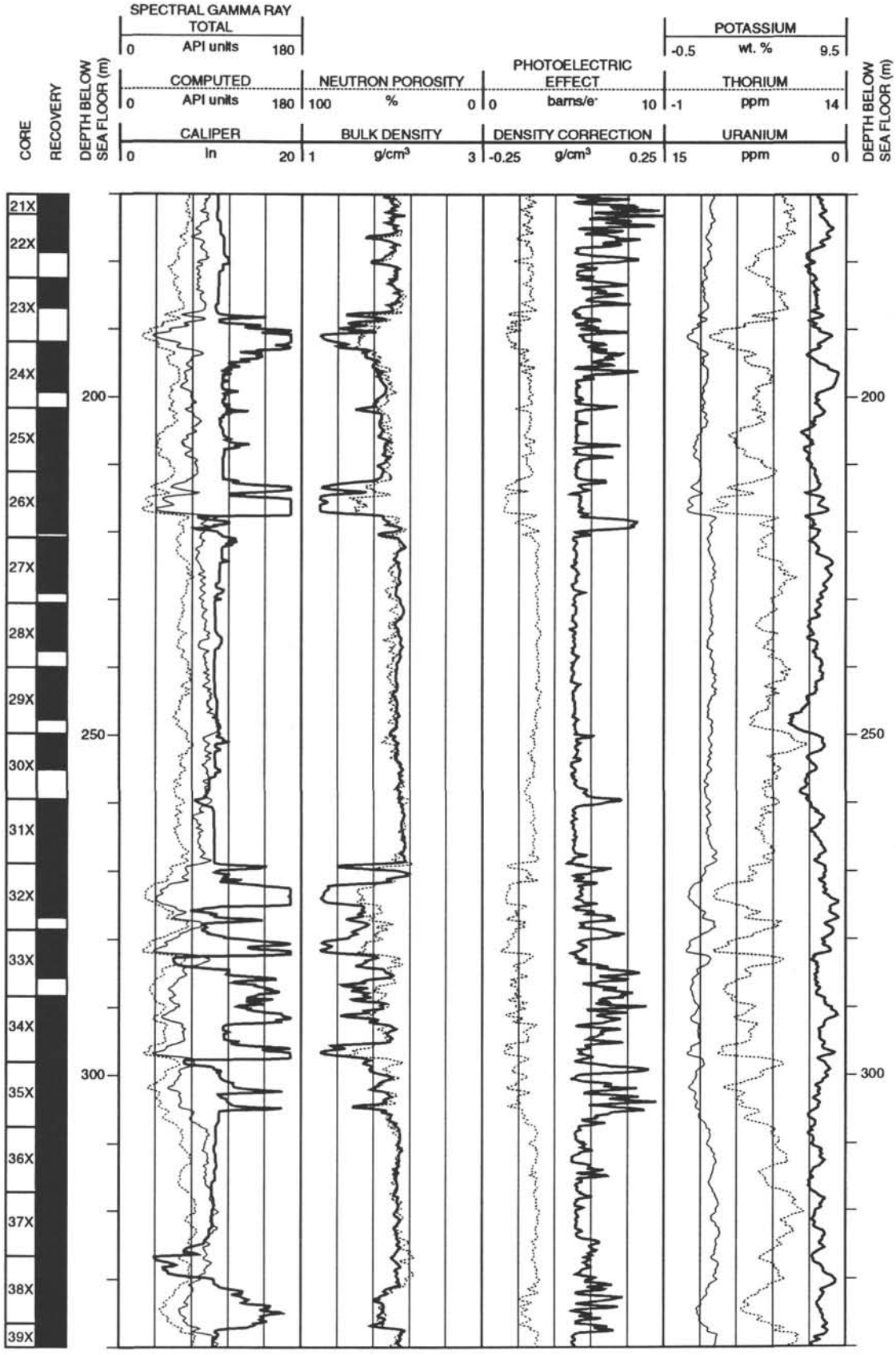

Hole 903A: Density-Porosity-Natural Gamma Ray Log Summary (continued)

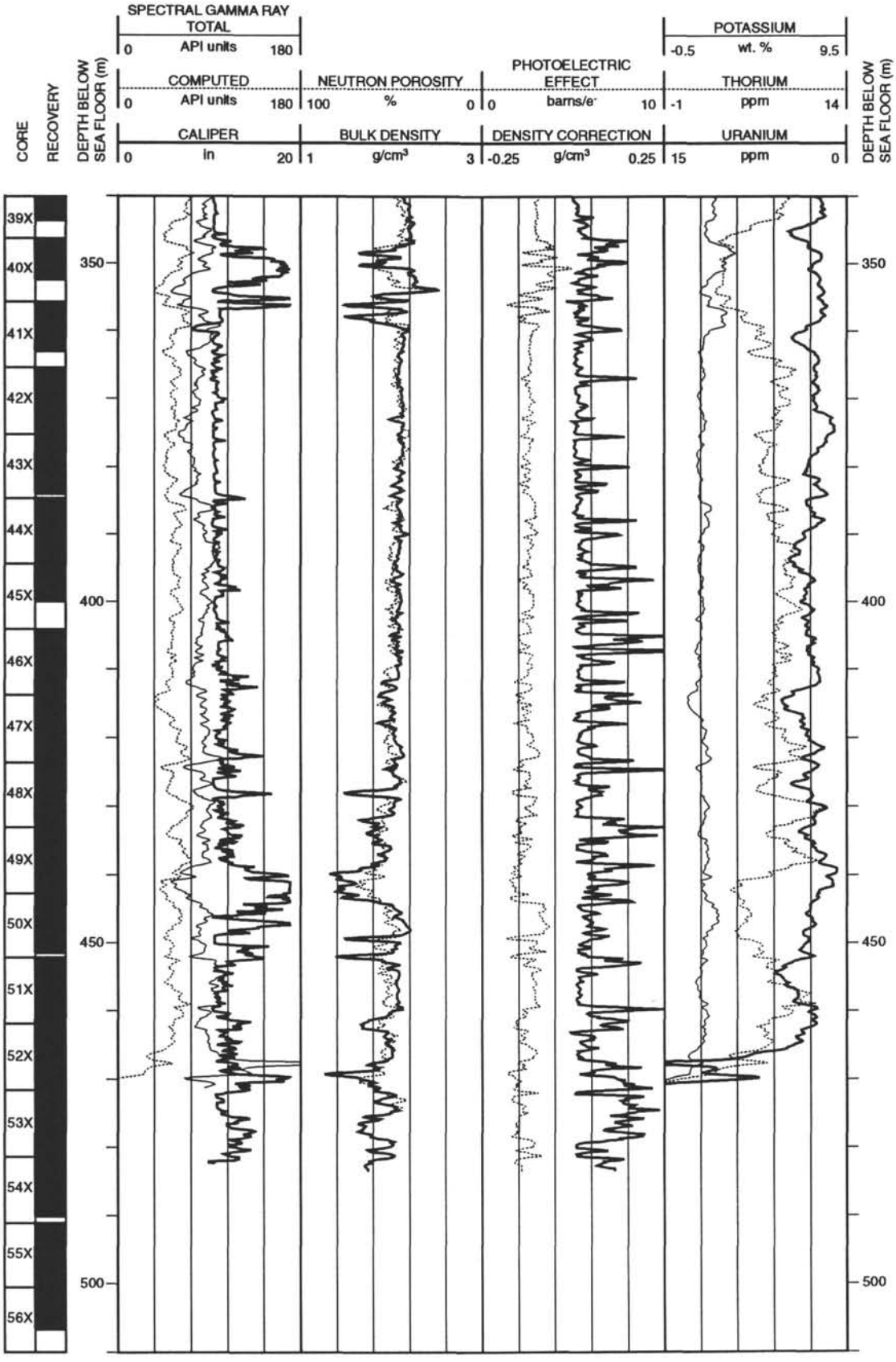

SHORE-BASED LOG PROCESSING

Hole 903C

Bottom felt: 457.5 mbrf (used for depth shift to seafloor)
Total penetration: 1149.7 mbsf
Total core recovered: 323.16 m (60.4%)

Logging Runs

Logging string 1: DIT/DSI/NGT (lower section)
Logging string 2: DIT/DSI/HLDT/CNTG/NGT (middle section)
Logging string 3: DIT/DSI/HLDT/CNTG/NGT (upper section)

Drill Pipe

The following drill-pipe depths are as they appear on the logs after differential depth shift (see **Depth shift** section) and depth shift to the seafloor. As such, there might be a discrepancy with the original depths given by the drillers on board. Possible reasons for depth discrepancies are ship heave and drill-string and/or wireline stretch.

DIT/DSI/NGT: Bottom of drill pipe at ~822.5 mbsf
DIT/DSI/HLDT/CNTG/NGT: Bottom of drill pipe at ~770 mbsf (785 mbsf for NGT)
DIT/DSI/HLDT/CNT/NGT: Bottom of drill pipe at ~472 mbsf

Processing

Depth shift: The DIT/DSI/NGT was used as the reference run for depth shifting the lower section. Run 2 has been interactively depth shifted with reference to SFLU from the DIT/DSI/NGT run, and to the seafloor (– 457.5 m). Run 3 could not be depth shifted because of lack of overlap with any of the previous two runs.
Gamma-ray processing: NGT data have been processed to correct for borehole size and type of drilling fluid.
Acoustic data processing: The DSI (Dipole Sonic Imager) data were processed on the ship's MAXIS unit.

Quality Control

Hole diameter was recorded by the 3-arm mechanical caliper, and by the hydraulic caliper on the HLDT tool (CALI).
Invalid gamma-ray readings were detected from 70 to 73 mbsf on the DIT/DSI/HLDT/CNTG/NGT run (upper section).

Hole 903C: Resistivity-Velocity-Natural Gamma Ray Log Summary

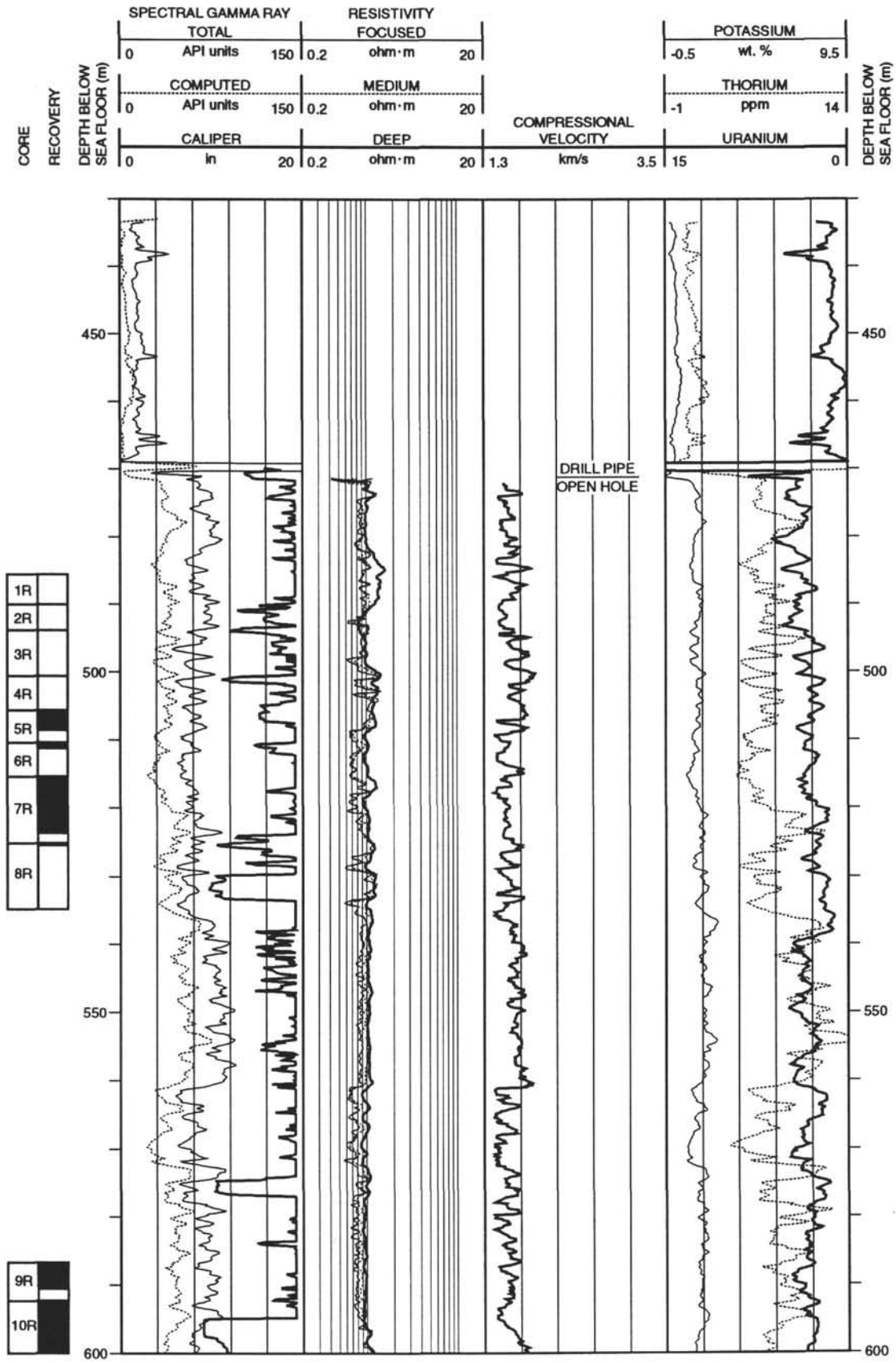

Hole 903C Resistivity-Velocity-Natural Gamma Ray Log Summary (continued)

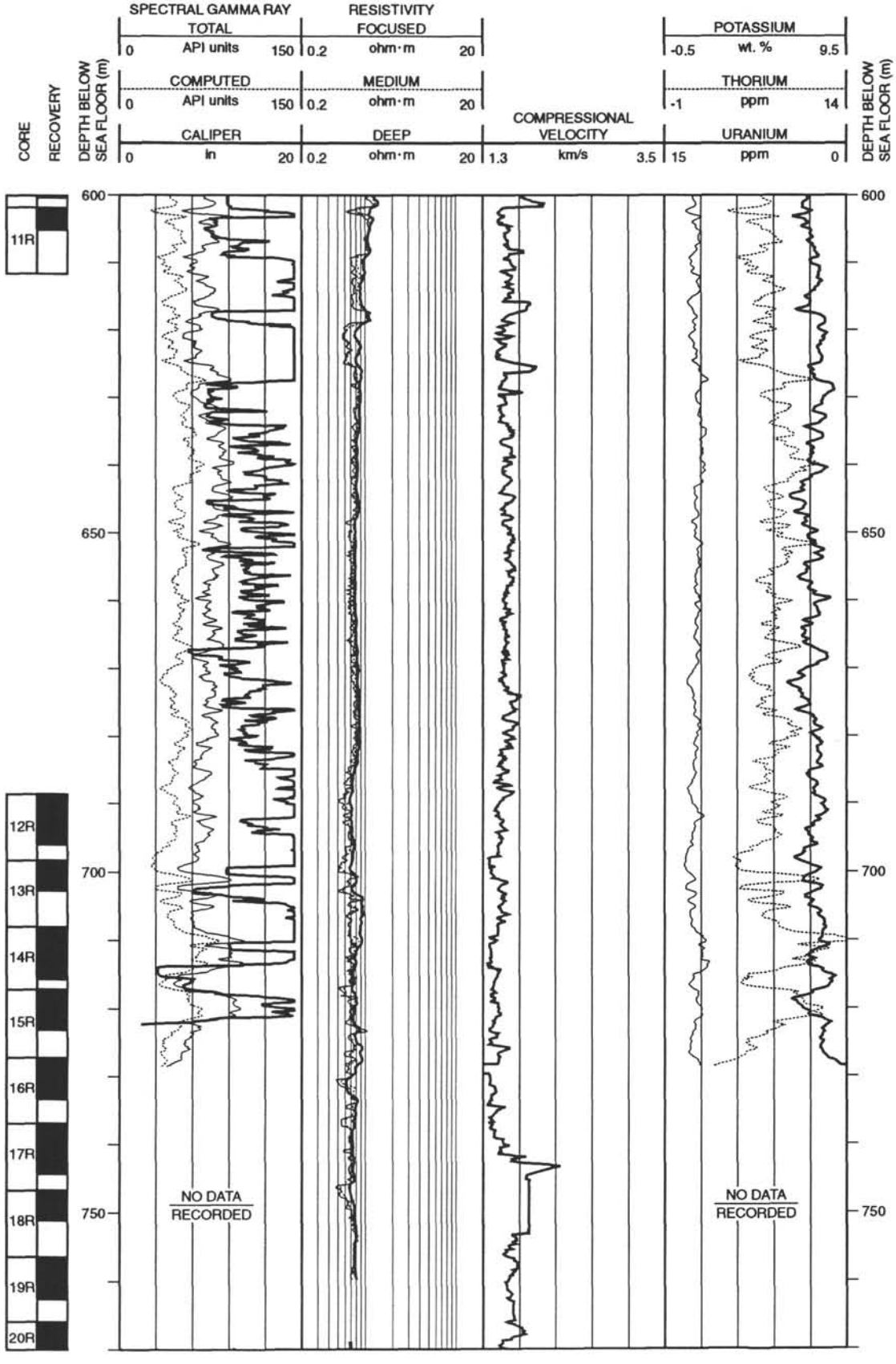

Hole 903C: Resistivity-Velocity-Natural Gamma Ray Log Summary (continued)

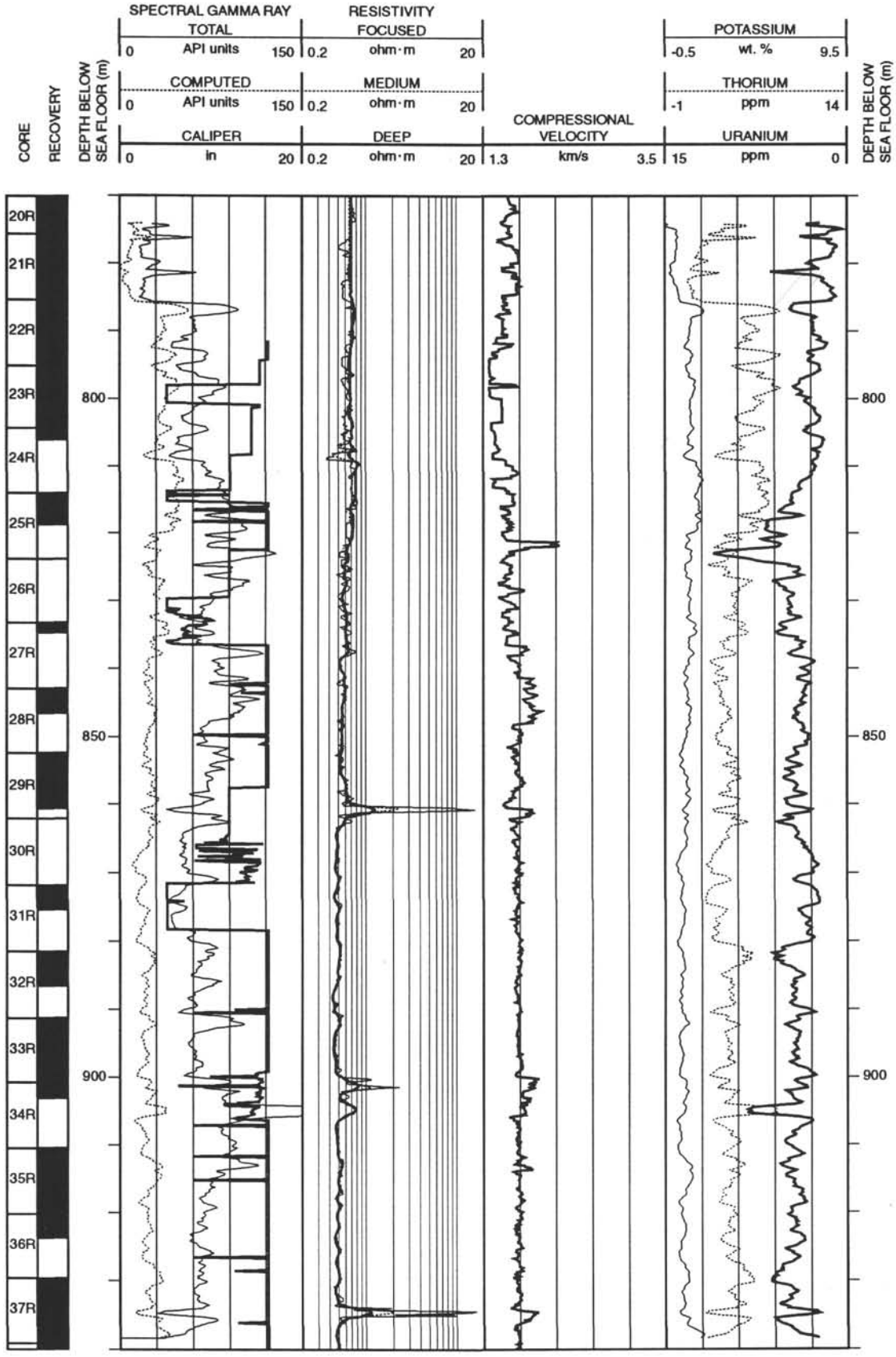

Hole 903C: Resistivity-Velocity-Natural Gamma Ray Log Summary (continued)

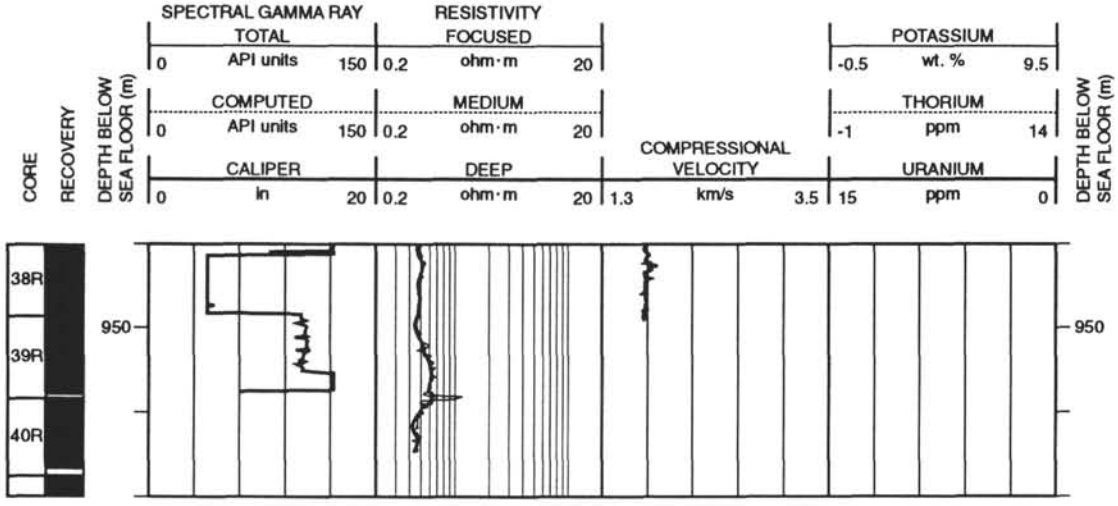

Hole 903C: Density-Porosity-Natural Gamma Ray Log Summary

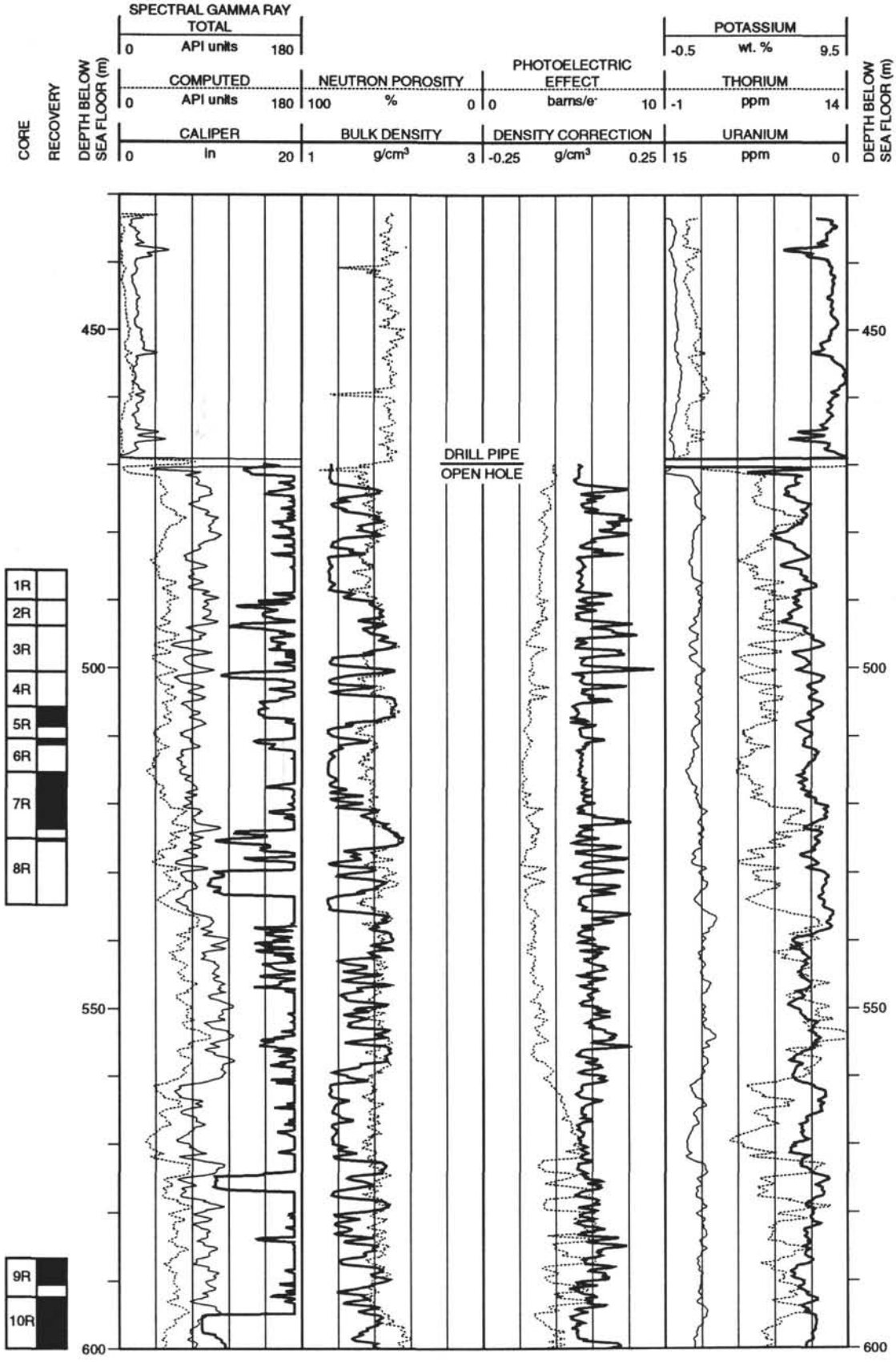

Hole 903C: Density-Porosity-Natural Gamma Ray Log Summary (continued)

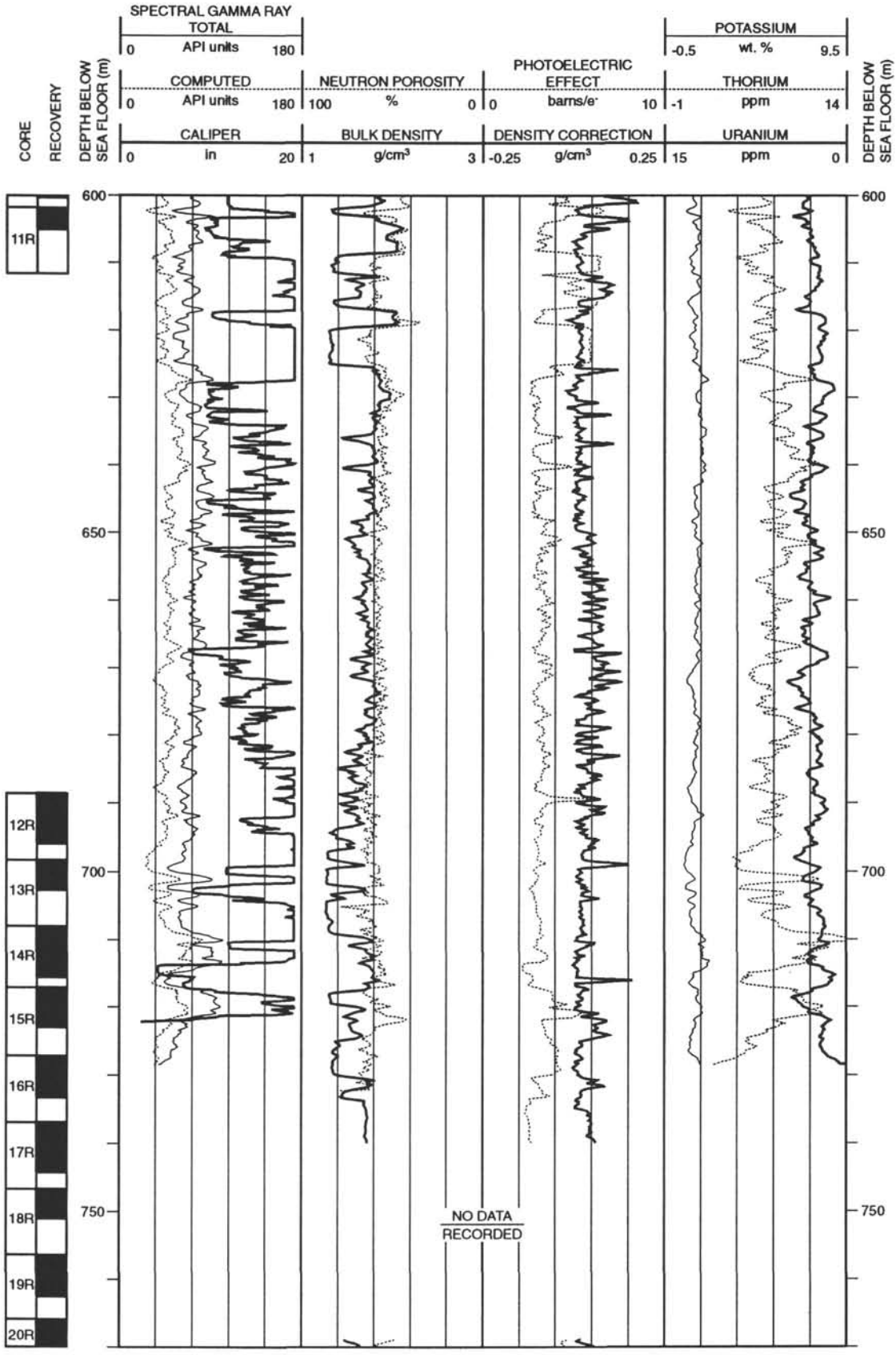

Hole 903C: Density-Porosity-Natural Gamma Ray Log Summary (continued)